# Structural and functional characterization of a metal-sensing sensor histidine kinase ZraS from *Escherichia coli*


*By*

**NILIMA MAHAPATRA**

**LIFE11201904002**

**National Institute of Science Education and Research,**

**Bhubaneshwar**


***A thesis submitted to the***

***Board of Studies in Life Science***

***In partial fulfilment of requirements***

***for the Degree of***

**DOCTOR OF PHILOSOPHY**

***of***

**HOMI BHABHA NATIONAL INSTITUTE**

**July, 2025**

# Homi Bhabha National Institute

## Recommendations of the Viva Voce Committee

As members of the Viva Voce Committee, we certify that we have read the dissertation prepared by Nilima Mahapatra entitled " Structural and functional characterization of a metal sensing sensor histidine kinase ZraS from *Escherichia coli*" and recommend that it may be accepted as fulfilling the thesis requirement for the award of Degree of Doctor of Philosophy.

| | |
|---|---|
| Chairman - Prof. Sharanappa Nembenna | 16/2/2026 |
| Guide - Dr. Rudresh Acharya | 16/02/2026 |
| Examiner – Prof. Saikrishnan Kayarat | 16/02/2026 |
| Member 1 - Dr. Tirumala Kumar Chowdary | 16.02.26. |
| Member 2 - Dr. Ramanujam Srinivasan | 16/02/26 |
| Member 3 – Dr. Dileep Vasudevan | 16/02/26 *Attended online |

---

Final approval and acceptance of this thesis is contingent upon the candidate's submission of the final copies of the thesis to HBNI.

I/We hereby certify that I/we have read this thesis prepared under my/our direction and recommend that it may be accepted as fulfilling the thesis requirement.

**Date:** 16/2/2026

**Place:** Jatni

**Signature**

**Guide**

## STATEMENT BY AUTHOR

This dissertation has been submitted in partial fulfillment of requirements for an advanced degree at Homi Bhabha National Institute (HBNI) and is deposited in the Library to be made available to borrowers under rules of the HBNI.

Brief quotations from this dissertation are allowable without special permission, provided that accurate acknowledgement of source is made. Requests for permission for extended quotation from or reproduction of this manuscript in whole or in part may be granted by the Competent Authority of HBNI when in his or her judgment the proposed use of the material is in the interests of scholarship. In all other instances, however, permission must be obtained from the author.

Nilima Mahapatra

**Nilima Mahapatra**

## DECLARATION

I, hereby declare that the investigation presented in the thesis has been carried out by me. The work is original and has not been submitted earlier as a whole or in part for a degree / diploma at this or any other Institution / University.

Nilima Mahapatra

**Nilima Mahapatra**

# CERTIFICATION OF ACADEMIC INTEGRITY

## Undertaking by the student

1. I Nilima Mahapatra, HBNI Enrolment no. LIFE11201904002 hereby undertake that the Thesis, titled " Structural and functional characterization of a metal-sensing sensor histidine kinase ZraS from *Escherichia coli.*" is prepared by me and is the original work undertaken by me.

2. I also hereby undertake that this document has been duly checked through a plagiarism detection tool and the document is found to be plagiarism free as per the guidelines of the Institute/ UGC.

3. I am aware and undertake that if plagiarism is detected in my thesis at any stage in the future, suitable penalty will be imposed as per the guidelines of the Institute/ UGC.

Nilima Mahapatra 16.02.2026
Signature of the student with date

**Endorsed by the Thesis Supervisor:**

I certify that the thesis written by the researcher is plagiarism free as mentioned above by the student.

Rudresh 16/02/2026
Signature of the Thesis Supervisor with Date and Name: **Dr. Rudresh Acharya**
Designation: Associate professor
Department/Centre: School of Biological Sciences
Name of the CI/OCC: NISER, Bhubaneswar

## List of Publications from the thesis

1. [#] **Mahapatra, N.**, Mahanta, P., Pandey, S., Acharya, R.* (2025) Insights into the conformational dynamics of the cytoplasmic domain of metal-sensing sensor histidine kinase ZraS. *PROTEINS: Structure, Function and Bioinformatics.* http://doi.org/10.1002/prot.26819

2. [#] **Mahapatra, N.**, Acharya, R. Structural and functional characterization of sensor domain of histidine kinase ZraS (Manuscript under preparation).

[#] Pertaining to the thesis work

## Conferences

**Poster presentations:**

International:

1. **Nilima Mahapatra,** Pranjal Mahanta, Shubhant Pandey, Rudresh Acharya, Structural and functional characterization of the cytoplasmic domain of sensor histidine kinase ZraS, 3rd International Conference on Frontiers in Biological Sciences 2023 (5th-7th October 2023 at Rourkela, India).

National:

2. **Nilima Mahapatra,** Shubhant Pandey, Pranjal Mahanta, Rudresh Acharya, Structural and functional characterization of metal-sensing sensor histidine kinase ZraS, 49th National Seminar on Crystallography (28th-30th November 2022 at Jammu, India).

Nilima Mahapatra

**Nilima Mahapatra**

Dedicated to the memory of my grandmother,

**Late Mrs. Indumati Mishra**

Nilima Mahapatra

## ACKNOWLEDGEMENTS

I wish to convey my deep gratitude to my thesis supervisor **Dr. Rudresh Acharya** for his continuous support and constant encouragement throughout my Ph.D. journey. Without his guidance, this thesis would not have been possible. The extent of gratitude I owe to him is immeasurable. I thank my doctoral committee chairman, **Dr. Sharanappa Nembenna**, and members **Dr. Tirumala Kumar Chowdary**, **Dr. Ramanujam Srinivasan** and **Dr. Dileep Vasudevan** for their invaluable guidance throughout my tenure at NISER.

I am highly indebted to my seniors **Dr. Pranjal Mahanta** and **Dr. Shubhant Pandey** for their invaluable support and guidance throughout various stages of my Ph.D. journey. Their encouragement and insights have been instrumental in shaping my research. I would also like to express my sincere gratitude to **Dr. Smitha Mohanlal** for her unwavering encouragement and inspiration which motivated me to persist in the face of adversity.

I am thankful to friends **Shivansh**, **Snehal, Gyan** and my past and present lab members: MS students **Lipsa, Shreya B, Narendra, Shreya S, Vidhi, Vaishnavi, Avra, Ashwin, Satyam, Yadunandan, Anjali, Shivam, Urja, Adisa and Vamsi,** PhD students **Prerana, Ranjita, Hariom, Shoubhik and Karthik** and Postdoc: **Dr. Rakesh** with whom I had many beautiful memories at NISER.

I would like to acknowledge NISER for infrastructure and providing a congenial environment for research and the CSIR, India for providing financial support through the CSIR-NET fellowship.

I want to express my deep and sincere gratitude to my parents **Shri Umesh Chandra Mahapatra** and **Smt. Sarita Mahapatra** and my baby brother **Sourav Mahapatra**, for their love, encouragement, assistance, and support.

Nilima Mahapatra

## ABSTRACT

Sensor histidine kinases (SHKs) or histidine protein kinases (HPKs) are widely distributed stimuli-sensing components of two-component signaling systems (TCSs) present in bacteria, archaea, and lower eukaryotes. SHKs are known to play a vital role in detecting environmental stimuli such as temperature, light, pressure, osmolytes, gases, nutrients, metals, antibiotics, and antimicrobial peptides. They allow organisms to sustain through changes by regulating gene expression and modifying physiological functions by undergoing reversible phosphorylation upon signal detection. Studies on SHKs have been constrained to structural and biochemical information on truncated domains of a few representative members while lacking information on full-length membrane-embedded forms. To uncover the mechanism of intramolecular signal transfer in metal-sensing SHKs, we used X-ray crystallography to determine the crystal structure of the complete cytoplasmic portion of a zinc-sensing SHK ZraS from *Escherichia coli* (EcZraS-CD). The EcZraS-CD structure is resolved at a resolution of 2.49Å. For the first time, we could trap two successive nucleotide-bound intermediate conformers that provide insights into the dynamics of SHK signaling. Our analysis of the conformers reveals reorganization of the dimerization interface in the cytoplasmic four-helix bundle (DHp) caused by segmental helical bending, sliding, and rotation that leads to kinase activation. The findings emphasize on the kink-forming bundle residues that generate helical bending, polar and apolar residue interactions that facilitate sliding motions, and aromatic residue interactions that regulate the directionality of rotation. We also identified a unique linker that undergoes helical bending, aiding the transfer of signal to the cytoplasmic kinase region and the multi-step internal transitions through which the catalytic domain (CA) approaches the DHp for phosphorylation. To further investigate the rate of ATPase activity, we conducted an in vitro real-time kinetics using the pyruvate kinase-lactate dehydrogenase coupled assay. Collectively,

our work provides several important mechanistic insights into the signaling process of metal-sensing SHKs.

Nilima Mahapatra

## CONTENTS

## Chapter 2: Experimental and computational methods

## Chapter 4: Future developments and directions

# SUMMARY

Sensor histidine kinase (SHKs) or histidine protein kinases (HPKs) are membrane associated or cytoplasmic sensory molecules dedicated to cellular signaling. They form integral part of two-component signaling systems (TCSs) along with their cognate response regulators (RRs). SHK-RR pairs are encoded by bacteria, archaea, fungi and lower eukaryotes and play a vital role in detecting environmental stimuli such as temperature, light, pressure, osmolytes, gases, nutrients, metals, antibiotics, and antimicrobial peptides (AMPs). They facilitate organisms to sustain through environmental fluctuations by regulating gene expression and modifying physiological functions by undergoing reversible phosphorylation upon signal detection. The exploration of SHKs is essential to decipher mechanisms underlying bacterial adaptation, developing targeted antimicrobial drugs and repurposing SHKs for applications in synthetic biology such as building custom signaling pathways for environmental sensing and metabolic control. The current studies on SHKs is primarly focused on the structure-function analysis of the truncated domains of a few SHKs. Being highly flexible and unstable in vitro with a multidomain modular architecture, characterization and isolation of these proteins pose a challenge. Investigation of structure, function and organization followed by study of interactions within these domains across various conformers is critical in unravelling the process of signal transduction.

To provide a structural basis for the activation of SHKs, we initiated our work with a few metal-sensing SHKs and stumbled upon ZraS, a zinc sensing SHK from *Escherichia coli* in the process. As purifying the full-length protein turned out to be a hurdle, we moved on to working with numerous variants of the protein including truncated periplasmic, periplasmic and transmembrane, and cytoplasmic regions. We explored the possibility of obtaining apo and ligand-bound conformers for the periplasmic and cytoplasmic regions in order to trap them in multiple states, but were successful in crystallizing them only in their ligand-bound states.

Nonetheless, we determined the crystal structure of the complete cytoplasmic portion of ZraS at a resolution of 2.49Å in two occluded ADP-bound conformers undergoing state transition. This helped elucidate the mechanism of kinase activation through structural comparison of the two intermediate conformers, highlighting reorganization of the dimerization interface driven by helical rearrangements, including segmental bending, sliding, and rotation. This work presented the first structural evidence for the contribution of the DHp base residues and loop in regulating the directionality of bundle rotation during autophosphorylation. We identified a novel linker that aids in the transfer of signal to the cytoplasmic region and the multi-step transitions through which the catalytic domain (CA) approaches the DHp bundle during autophosphorylation. The biochemical analysis helped determine the rate of ATPase activity for the kinase.

Despite sustained efforts, the native periplasmic region proved difficult to crystallize in either the apo or ligand-bound state due to issues with protein stability *in vitro*. The problem was addressed by designing loop truncations, guided by structural comparisons with periplasmic domains of known SHKs with similar topology. One of these variants crystallized and produced low-resolution diffraction that is being enhanced further for structural analysis. To further improve the structural quality and guide construct design, we modelled the loop truncations using Rosetta. Collectively, this thesis work provides important insights into the mechanism of kinase activation in ZraS. Further, it forms the basis for the development of antimicrobials against multi-drug resistant pathogens, designing synthetic/chimeric circuits and biosensors for applications such as bioremediation.

# LIST OF ABBREVIATIONS

| | |
|---|---|
| **ADP** | **A**denosine **di**phosphate |
| **APBS** | **A**daptive **P**oisson-**B**oltzmann **S**olver |
| **ATP** | **A**denosine **tri**phosphate |
| **BME** | **B**eta**m**ercaptoethanol |
| **CA** | **Ca**talytic domain |
| **CAMP** | **Ca**tionic **m**icrobial **p**eptides |
| **CC** | **C**oiled **c**oil |
| **CCS** | **C**o-**c**omponent **s**ystem |
| **DHp** | **D**imerization and **h**istidine **p**hosphoacceptor domain |
| **DISM** | **D**isulfide **iso**merase |
| **DNA** | **D**eoxyribo**n**ucleic **a**cid |
| **DSPK** | **D**ual **s**pecificity **p**rotein **k**inase |
| **DYRK** | **D**ual specificity t**y**rosine phosphorylation **r**egulated **k**inase |
| **ECF** | **E**ctra**c**ytoplasmic **f**unction |
| **ESR** | **E**nvelope **s**tress **r**esponse |
| **GAF** | c**G**MP-specific phosphodiesterase, **A**denylyl cyclases and **F**ormate hydrogenases |
| **HAMP** | **H**istidine kinases, **A**denylyl cyclases, **M**ethyl-accepting chemotaxis proteins and **P**hosphatases |

**HEPES** 4-(2-**H**ydroxy**e**thyl)-1-**p**iperazine**e**thane**s**ulfonic acid

**HGT** **H**orizontal **g**ene **t**ransfer

**HPK** **H**istidine **p**rotein **k**inase

**HPt** **H**istidine-containing **p**hospho**t**ransfer domain

**IM** **I**ntra**m**embrane

**IPTG** **I**so**p**ropyl-D-1-**t**hio**g**alactopyranoside

**ITC** **I**sothermal **t**itration **c**alorimetry

**KD** **K**inase **d**omain

**KIC** **Ki**nematic **c**losure

**LB** **L**uria-**B**ertani

**LDH** **L**actate **de**h**y**drogenase

**LSE** **L**ineage **s**pecific **e**xpansion

**LOV** **L**ight **o**xygen **v**oltage

**MCP** **M**ethyl-accepting **c**hemotaxis **p**rotein

**MCS** **M**ulti-**c**omponent **s**ystem

**MiST** **M**icrobial **s**ignal **t**ransduction **d**atabase

**NAD+** **N**icotinamide **a**denine **d**inucleotide

**NADH** **N**icotinamide **a**denine **d**inucleotide **h**ydrogen

**NTP** **N**ucleoside **tri**p**h**osphate

**OCS** **O**ne-**c**omponent **s**ystem

| | |
|---|---|
| **PAS** | **P**er-**A**rnt-**S**im |
| **PBP** | **P**eriplasmic **b**inding **p**rotein |
| **PDB** | **P**rotein **d**ata **b**ank |
| **PDC** | **P**hoQ-**D**cuS-**C**itA |
| **Pfam** | **P**rotein **fam**ily database |
| **PHY** | **Phy**tochrome |
| **PK** | **P**yruvate **k**inase |
| **PMSF** | **P**henyl**m**ethyl**s**ulfonyl **f**luoride |
| **PNK** | **P**olynucleotide **k**inase |
| **REC** | **Rec**eiver domain |
| **RR** | **R**esponse **r**egulator |
| **SHK** | **S**ensor **h**istidine **k**inase |
| **SLC** | **S**olute **c**arrier |
| **STAC** | **S**olute carriers and **t**wo component signal transduction **a**ssociated **c**omponent |
| **TCS** | **T**wo-**c**omponent **s**ystem |
| **TEV** | **T**obacco **e**tch **v**irus |
| **TM** | **T**rans**m**embrane |
| **Tris** | **Tris**(hydroxymethyl)aminomethane |
| **VFT** | **V**enus **fl**y**t**rap |
| **XDS** | **X**-ray **d**etector **s**oftware |

# LIST OF FIGURES

## Chapter 1



## Chapter 2

# LIST OF TABLES

## Chapter 2

## Chapter 3

# Chapter 1
# Introduction

*Chapter-1*

## 1.1 Bacterial protein kinases

Bacterial protein kinases are enzymes that catalyze transfer of a phosphate group from a nucleoside triphosphate (NTP) to its substrate protein, causing covalent modification of the constituent amino acids. Bacteria are known to possess a wide variety of membrane-bound and cytoplasmic protein kinases regulating cellular metabolism, growth, stress response, and pathogenicity. Based on the type of amino acid modified, they have been classified into Serine/Threonine, Tyrosine/Arginine, Histidine/Aspartic acid and dual-specificity kinases.

### 1.1.1 Serine/Threonine kinases

Bacterial serine and threonine kinases phosphorylate the hydroxyl group of serine and threonine amino acid residues and are grouped into two major groups comprising of Hanks-type serine-threonine kinases and atypical serine-threonine kinases. Hanks-type kinases or eukaryotic-like serine and threonine kinases (eSTKs) such as PknB from *Mycobacterium tuberculosis* are multidomain membrane or cytoplasmic proteins with a catalytic domain containing signature motifs similar to eukaryotic kinases, described by Hanks (Chawla et al., 2014). Atypical serine-threonine kinases (aSTKs) such as CtkA from *Helicobacter pylori* differ from conventional kinases, but share catalytic domain homology with Hank-type kinases, lacking presence of all the Hank motifs (Kim et al., 2010). They phosphorylate their substrates on serine, threonine or tyrosine residues.

### 1.1.2 Tyrosine/Arginine kinases

Bacterial tyrosine kinases (BY-kinases) such as Ptk from *Acinetobacter johnsonii* phosphorylate hydroxyl group of tyrosine residue (Doublet et al., 1999). The BY-kinases do not share sequence homology to their eukaryotic counterparts and are known to possess Walker A and B NTP-binding motifs towards a C-terminal tyrosine-rich region (Grangeasse et al., 2012). Arginine kinases phosphorylate nitrogen at the guanidium cation of the arginine residue.

The phosphorylated arginine acts as a reservoir of energy helping conversion of Adenosine diphosphate (ADP) to Adenosine triphosphate (ATP) upon demand. Though uncommon in bacteria, arginine kinase such as McsB found in *Bacillus subtilis* resemble phosphagen kinases and is involved in protein quality control (Suskiewicz et al., 2019). McsB is regulated by McsA that binds to the kinase domain of the former.

### 1.1.3 Histidine/Aspartic acid kinases

Histidine kinases (HKs) such as CpxA from *Escherichia coli* phosphorylates imidazole nitrogens of the histidine residue. They are integral components of signaling systems possessing conserved kinase domains, but lacking Walker motifs unlike other kinases (T. H. S. Cho et al., 2024; Mechaly et al., 2014). Bacterial aspartate kinases modify aspartic acid residues. Kinase LysC from *Synechocystis sp* containing a Walker A motif, catalyzes phosphorylation at the beta carboxyl group of the aspartic acid residue to produce 4-phospho-L-aspartate that is used during biosynthesis of amino acids such as lysine, threonine, isoleucine and methionine (Robin et al., 2010).

### 1.1.4 Dual-specificity kinases

Dual-specificity kinases are enzymes capable of functioning as both STKs and BY-kinases phosphorylating serine, threonine and tyrosine residues. These kinases are grouped into the typical dual specificity protein kinases (DSPKs) and dual specificity tyrosine phosphorylation-regulated kinases (DYRKs). DSPKs such as PrkG from *Bacillus anthracis* autophosphorylates the hydroxyl groups of serine, threonine and tyrosine residues and is also capable of phosphorylating the same amino acids in its substrates. DYRKs such as PrkD from *Bacillus anthracis* is similar to PrkG phosphorylating serine, threonine and tyrosine residues, though phosphorylation at tyrosine is restricted only to autophosphorylation (Arora et al., 2012).

## 1.2 Signal transduction systems in bacteria

Bacteria are recurrently exposed to rapidly altering internal and external environmental conditions, requiring stimuli detection and adaptation for survival and sustenance. Numerous signal transduction systems are responsible for sensing these cues and regulating their corresponding cellular responses. Detection of cues generated in the external environment (extracellular signaling) and during cell-to-cell communication (intercellular signaling) within a microbial population is sensed by membrane-bound sensors. Internal changes (intracellular signaling) are detected using cytosolic or cytosol-exposed components of the membrane-bound sensors. Bacteria primarily utilise transmembrane signaling systems such as one-component systems (OCSs), two-component systems (TCSs), multi-component systems (MCSs), co-component systems (CCSs) and extracytoplasmic function sigma factors (ECF-σs). Assisting the primary signaling systems are the secondary signaling systems, consisting of membrane transporters with acquired sensory functions **(Figure 1.2.1)**.

### 1.2.1 Primary signaling systems

**1.2.1.1 One-component systems (OCSs) –** One-component signaling systems consists of a single cytosolic or membrane-bound protein with a simple modular architecture encoding two domains: an input sensor domain and an output response domain. They are evolutionarily primitive, comprising of diverse domain combinations and are widely distributed across bacteria and archaea, with a majority of them being soluble cytosolic proteins. CadC is an OCS responding to pH fluctuations in *Escherichia coli*. It has an N-terminal DNA-binding domain containing a helix-turn-helix motif exposed towards the cytoplasm and a C-terminal pH-sensing domain towards the periplasm (Buchner et al., 2015).

**1.2.1.2 Two-component systems (TCSs) -** Two-component signaling systems consists of at least two multi-domain proteins having a slightly intricate modular architecture with separate

sensor and response functions. Environmental cues are sensed by a membrane bound or cytosolic sensor histidine kinase (SHK) that initiates an intracellular response coupled to a cytosolic response regulator (RR). CusS/CusR is a copper-sensing TCS found in *Escherichia coli* regulating metal homeostasis (Rismondo et al., 2023a). Presence of copper and silver stimulates activation of the outer membrane SHK CusS. CusS phosphorylates the cytoplasmic partner CusR that upregulates expression of CusCFBA genes encoding a efflux pump. Reminiscing TCSs are signaling systems that employs more than two proteins, known as multi-component systems (MCSs). Chemotaxis in bacteria is regulated by the CheA/CheY system that comprises of a kinase CheA and a response regulator CheY (Cassidy et al., 2020a; Hess et al., 1988). CheA is indirectly activated upon cue detection at the bacterial surface by methyl accepting chemotaxis proteins (MCPs) and an adapter protein CheW. Sensory perception at the MCPs is further fine-tuned through modifications such as reversible methylation by accessory proteins such as CheB, CheR, CheC and CheD. Bacterial OCSs have evolved to incorporate benefits of sensing multiple internal and external stimuli with controlled regulation of signal transduction in TCSs and MCSs. Ubiquitously distributed across bacteria, archaea, lower eukaryotes and plants, their absence in mammals such as humans is of significance in development of novel antimicrobials.

**1.2.1.3 Co-component systems (CCSs) -** Co-component signaling systems consist of a transmembrane protein with an architecture similar to OCSs possessing a response domain but lacking a functional sensor domain. Signal sensing is facilitated by obligate interaction with a second protein or co-transducer assisting the first component. The co-transducer usually lacks a response domain. VtrA/VtrC heterodimer is a bile-sensing CCS found in *Vibrio parahaemolyticus*. A lipocalin-like periplasmic domain in VtrC binds to bile molecules and transmits the signal to the cytoplasmic DNA-binding domain in VtrA that upregulates the type III secretion system (Kinch et al., 2022).

**1.2.1.4 Extracytoplasmic function σ factors (ECF-σs) -** Extracytoplasmic function σ factors (ECF-σs) are a subfamily of response eliciting components belonging to the σ70 class of proteins. They are located in the cytosol and are negatively regulated by transmembrane components known as anti-σ factors. Cue sensing induces the release of σ factors from their anti-σ factor, activating the signaling cascade. The Fec σ and anti-σ factor pair found in *Escherichia coli* senses the presence of ferric citrate. The binding of ferric citrate to FecA signals the anti-σ factor FecR to initiate σ-factor FecI-mediated transcription of *fecABCDE* transport genes by binding to the β′ subunit of RNA polymerase (Campbell et al., 2003). Carotenogenesis in *Myxococcus xanthus* is regulated by σ factor CarQ bound to anti-σ factor CarR (Browning et al., 2003).

**1.2.2 Secondary signaling systems**

Some membrane-bound transporters possess dual sensor-transporter functions, operating as transceptors and co-sensors (R. Krämer & Jung, 2009; Tetsch & Jung, 2009). Transceptors undergo conformational changes upon direct binding to the environmental cue and activate downstream intracellular effectors to transduce signals. Co-sensors include transporters with functional activity coupled to other signaling systems like TCSs. Both primary and secondary transporters have been observed with acquired secondary functions in bacteria. A high-affinity ammonium transporter AmtB in *Escherichia coli* is blocked by a PII signal transduction protein GlnK. Dissociation of GlnK from AmtB upon uridylylation helps facilitate ammonium flux during deficiency of cellular nitrogen. Deuridylylation of GlnK is regulated by the activity of AmtB, making it a sensing component during signal transduction (Javelle et al., 2004).

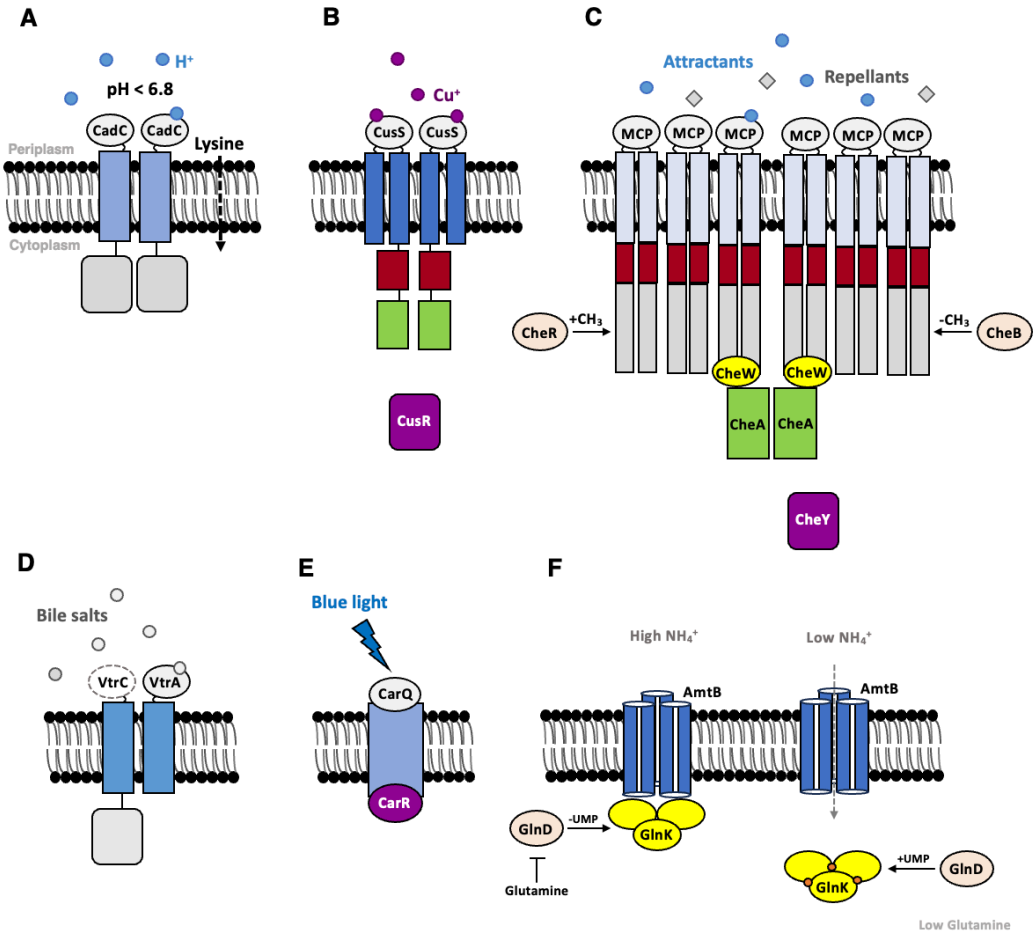


**Figure 1.2.1 Primary and secondary signaling systems in bacteria** (A) CadC found in Vibrio vulnificus is a transmembrane OCS with a periplasmic module sensing pH fluctuations and a cytoplasmic DNA-binding module carrying out regulatory function. (B) SHK CusS of TCS CusRS found in *Escherichia coli* senses presence of copper ions in its periplasmic domain and activates CusR that has a DNA-binding response module. (C) A MCS involved in chemotaxis of *E. coli* comprises of a transmembrane sensor methyl-accepting chemotaxis protein (MCP), a histidine kinase without sensor (CheA), a RR protein lacking response function (CheY). (D) VtrA-VtrC found in *Vibrio parahaemolyticus* is involved in bile salt sensing and activation of type III secretion system 2 (T3SS2). Bile salts bind to the lipocalin-like fold in the periplasmic domain of VtrC, inducing the DNA binding response domain in

VtrA. (E) Light-induced carotenogenesis in *Myxococcus xanthus* is regulated by σ factor CarQ bound to anti-σ factor CarR. CarQ is released from the transmembrane CarR in the presence of blue light. (F) AmtB of *E. coli* is activated in the presence of low levels of ammonium by dissociation of GlnK.

## 1.3 Bacterial stimuli

Bacterial stimuli include signals and factors in the external and internal environment that trigger responses such as cellular signaling, enabling the bacteria to perceive, interpret, and respond to changes in their surroundings, as seen in **Figure 1.3.1** (Armitage, 1992; Evstigneeva et al., 2021; Hegazy & El-Antrawy, 2025; R. Krämer, 2010). The types of stimuli in bacteria as follows:

- **Mechanical stimuli**

Changes in the mechanical forces such as surface tension, deformation and pressure generated during surface adhesions, inside host tissues or in biofilm microenvironments.

- **Physical stimuli**

Changes in parameters such as osmotic pressure, turgor pressure, hydrodynamic forces (in liquid environments), light and temperature.

- **Electromagnetic stimuli**

Includes exposure to variable strengths of electric and magnetic fields, frequencies, and duration of exposure.

- **Biochemical stimuli**

Exposure to biological substances such as molecules from host and other microbial interactions (autoinducers, hormones and antimicrobial peptides) and chemicals such as nutrients or attractants, toxins or repellents, antibiotics, and numerous organic and inorganic compounds. Also includes environmental changes such as pH fluctuations, presence or absence of moisture and gaseous molecules such as oxygen and nitrogen.

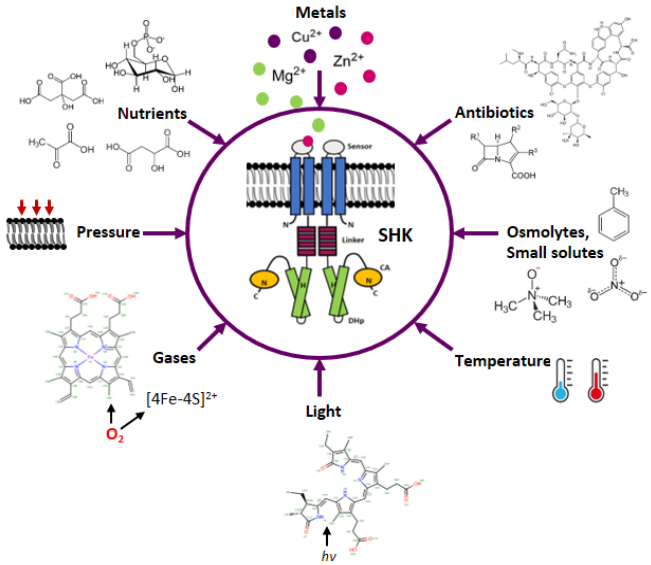


**Figure 1.3.1 Schematic representation of different types of stimuli sensed by SHKs.**

## 1.4 Sensor histidine kinases in bacteria

Sensor histidine kinases (SHKs), synonymously known as histidine protein kinases (HPKs), are signal-sensing components belonging to the two-component systems (TCSs). The two components of a TCS include a stimulus-detecting sensor histidine kinase (SHK) containing a histidine residue and an effector, a response regulator (RR) with an aspartic acid residue. The TCSs carry out signal transduction in response to stimuli such as temperature, light, pressure,

osmolytes, gases, nutrients, metals, antibiotics, and antimicrobial peptides using reversible phosphorylation of conserved residues in SHKs and RRs.

A prototypical SHK is a homodimeric membrane-bound multidomain protein made of multiple modules distributed across periplasmic, transmembrane and cytoplasmic domains (Gao & Stock, 2009; Ishii & Eguchi, 2021a; Jacob-Dubuisson et al., 2018; Stock et al., 2000). The N-terminus of the protein lies towards the cytoplasmic face of the membrane, contiguous with the first transmembrane helix (TM1) that protrudes into the periplasmic space, forming the periplasmic domain and descends as a second transmembrane helix (TM2). The second transmembrane helix furthers into the cytoplasmic domain with one or more linker domains and a kinase core. The RR is a cytoplasmic protein with receiver and effector domains **(Figure 1.4.1).** SHKs have their own specific or cognate RRs, occasionally interacting non-specifically with other RRs during a cross-talk signaling cascade among multiple TCSs.

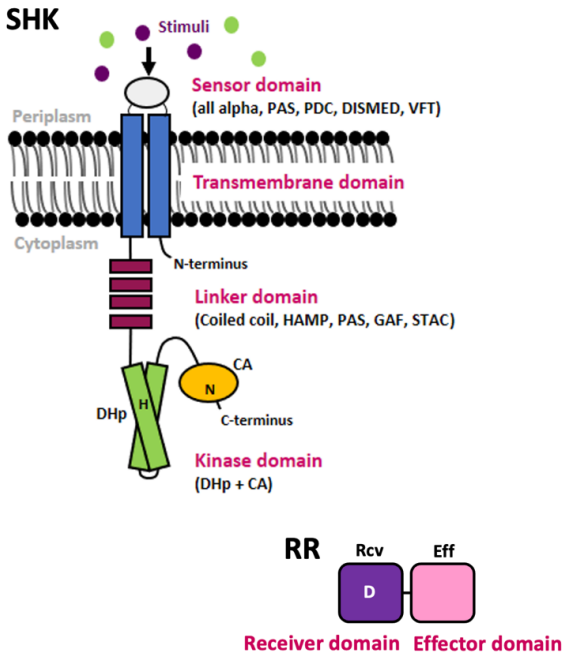

**Figure 1.4.1 Schematic representation of a TCS.** This image shows the types and distribution of domains in the monomeric SHK-RR pair across the periplasmic, transmembrane and cytoplasmic regions.

## 1.5 Sensor histidine kinases in *Escherichia coli*

Signal transduction proteins in *Escherichia coli* have been grouped into OCSs, TCSs, ECF-σs and others in the Microbial Signal Transduction Database (MiST) 4.0 (Gumerov et al., 2024). The TCSs contain nearly 30 SHKs having 24 prototypical kinases (HKs), 5 hybrid histidine kinases (HHKs), and 1 chemosensory kinase. The SHKs are paired with 31 RRs with the SHK-RR pairs mentioned below.

### 1.5.1 Prototypical kinases (HKs) in the TCSs of *E. coli*

- **CreC**

The CreBC system includes the SHK CreC and its RR CreB. This system is known to be a global regulator of genes involved in carbon metabolism, stress responses, and transport processes, which upregulates 9 genes with a 'cre-tag' promoter motif (Avison et al., 2001).

- **BasS**

The BasS-BasR system includes the SHK BasS involved in lipid A modification and resistance to antimicrobial peptides (AMPs), and its cognate RR BasR (Herrera et al., 2010). It is speculated to sense changes in iron levels and cationic microbial peptides (CAMPs). BasR upregulates arnBCADTEF operon involved in lipid A modification, and the TCS enhances survival against polymyxins, colistin and CAMPs (Janssen et al., 2020; Phan et al., 2017).

- **PhoQ**

The PhoQ-PhoP system have been proposed to sense extracellular magnesium and calcium levels along with multiple other types of stimuli such as osmotic shift, pH shift and cationic antimicrobial peptides (CAMPs) (A. Kato et al., 1999; Miyashiro & Goulian, 2007; Regelmann et al., 2002). Activation of SHK PhoQ leads to phosphorylation of PhoP that upregulates genes such as mgtA encoding a magnesium transporter, hdeA and hdeE encoding chaperones that proteins under acidic stress and pagP encoding enzyme that modifies membrane to provide protection against CAMP. It also upregulates operons involved in ion homeostasis, respiration and redox balance.

- **PhoR**

The SHK PhoR detects changes in the levels of extracellular inorganic phosphate (Wanner & Chang, 1987). Upon sensing low levels of phosphate, it activates the cognate RR PhoB through phosphorylation that in turn upregulates the Pho regulon responsible for phosphate uptake and scavenging. The PstSCAB transport system regulates PhoR by binding to it in the presence of high levels of phosphate and dissociating when levels of phosphate is low, thereby activating kinase function. Another protein PhoU, negatively regulates PhoR (Gardner & McCleary, 2019).

- **ZraS**

The ZraS-ZraR system includes SHK ZraS and its cognate RR ZraR, involved in detecting envelope stress, caused due to zinc ions. It helps maintain metal ion homeostasis and protects the cell from metal toxicity (Leonhartsberger et al., 2001; Taher & de Rosny, 2021). A third protein ZraP also forms a part of the operon encoding ZraS and ZraR that acts a periplasmic zinc chaperon and binds to ZraS (Appia-Ayme et al., 2012).

- **CusS**

The SHK CusS is responsible for detecting copper ion stress (Gudipaty & McEvoy, 2014; Rismondo et al., 2023b). Upon detection of metal ions, CusS phosphorylates its cognate RR CusR that induces expression of cusCFBA operon encoding CusCBA efflux system for detoxification and export of excess metal ions (Gudipaty et al., 2012).

- **DcuS**

The DcuS-DcuR system includes the SHK DcuS involved in sensing extracellular C4 carboxylates such as fumarate, and its cognate RR DcuR (Janausch et al., 2002; Zientz et al., 1998). The TCS is active under anaerobic conditions and upregulates expression of C4 carboxylate transporter DcuB.

- **UhpB**

The SHK UhpB is a part of a phosphorelay system including UhpB, UhpC and UhpA (Island & Kadner, 1993). UhpB senses hexose phosphate such as glucose-6-phosphate, indirectly and aids its transport through a transporter UhpT (Verhamme et al., 2001; Weston & Kadner, 1987; Wright et al., 2000). A periplasmic sensor protein, UhpC is known to bind to glucose-6-phosphate and bind to UhpB responsible for its activation. The phosphorylation of UhpB activates its cognate RR UhpA.

- **CpxA**

The CpxA-CpxR system including a SHK CpxA and its cognate RR CpxR, is involved in detection of envelope stress (Keller et al., 2015). It detects signals, such as unfolded proteins, high pH, and binding of the lipoprotein NlpE and activates the CpxR through phosphorylation. CpxP, a periplasmic protein also functions in this cascade as a signal

regulator, potentially inhibiting CpxA from activating the Cpx regulon when proteins are not misfolded (Danese & Silhavy, 1998; Tschauner et al., 2014).

- **GlnL**

The GlnLG system, also known as NtrBC system is involved in nitrogen regulation. GlnL or NtrB detects availability of nitrogen to phosphorylate or dephosphorylate its cognate RR GlnG or NtrC (Kramer & Weiss, 1999). The activation of NtrB is also seen to be regulated by signal transducing PII proteins (Pioszak & Ninfa, 2003).

- **EnvZ**

The SHK-RR pair EnvZ-OmpR are involved in osmoregulation. EnvZ detects changes in osmolarity and phosphorylates its cognate RR OmpR that upregulates outer membrane porins OmpF and OmpC (S. J. Cai & Inouye, 2002). OmpF and OmpC facilitates the diffusion of small molecules, nutrients, and other substances across the membrane.

- **QseC**

The TCS QseC-QseB is involved in multiple processes including bacterial pathogenicity, quorum sensing and antibiotic resistance (Zhu et al., 2023). The SHK QseC detects molecules such as epinephrine, norepinephrine or AI-3 to phosphorylate its cognate RR QseB or non-cognate RRs QseF (GlrR) and KdpE (Hughes et al., 2009). The phosphorylated RRs activates genes involved in flagellar synthesis, type II secretion system and Shiga toxin production.

- **GlrK**

The TCS GlrK-GlrR is involved in regulation of glucose metabolism. The SHK GlrK is activated upon depletion of glucosamine-6-phosphate and phosphorylates its cognate RR GlrR that upregulates glmY. The gene glmY encodes for an enzyme involved in synthesis of

glucosamine-6-phosphate (Göpel et al., 2011). GlrR is phosphorylated by other SHKs such as UhpB, RstB and BaeS (Yamamoto et al., 2005).

- **NarQ**

The NarQ-NarP system is responsible for sensing nitrate and nitrite levels in the surroundings (Noriega et al., 2008; Rabin & Stewart, 1992). NarQ senses the stimuli using its periplasmic domain to activate and phosphorylate its cognate RR NarP or non-cognate RR NarL. NarP activates the operons napF, nrfA, nirB, fdnG mainly encoding nitrate reductases and nitrate-induced formate dehydrogenase used during anaerobic respiration. (Darwin et al., 1998a).

- **NarX**

The NarX-NarL pair is similar to NarQ-NarP, sensing changes in nitrate and nitrite levels (Rabin & Stewart, 1992). The SHK NarX upon activation phosphorylates its cognate RR NarL or non-cognate RR NarP. Though similar to NarP, NarL it has distinct specificity and regulates a different set of target genes. NarL regulates expression of narGHIJ encoding nitrate reductase enzyme complex and narK encoding a nitrate/nitrite antiporter (Darwin et al., 1998b; Rowe et al., 1994).

- **AtoS**

The AtoS-AtoC system is involved in the detection of small molecules such as acetoacetate (Filippou et al., 2008). Phosphorylation of RR AtoC by the SHK AtoS leads to upregulation of the operon atoDAEB necessary for short-chain fatty acid metabolism.

- **RcsC**

The SHK-RR pair RcsC-RcsB belongs to the phosphorelay system RcsC-RcsD-RcsB activated due to envelope stress. Alterations in the outer membrane envelope, damage to peptidoglycan, desiccation, biofilm formation, cell adhesion and osmotic shock is sensed by the SHK RcsC

that phosphorylates RcsD, containing a HPt domain (Rogov et al., 2006). The RcsD finally activates the cognate RR RcsB or RcsA that activates or represses downstream genes involved in capsule synthesis, biofilm regulation and stress mitigation (Ferrières & Clarke, 2003).

- **BaeS**

The BaeS-BaeR system is activated during envelope stress, notably risking the membrane integrity or during accumulation of toxins (heavy metals, antibiotics and metabolites) (Hu et al., 2020; Zoetendal et al., 2008). Autophosphorylation of BaeS and transfer of phosphate group to BaeR results in upregulation of genes such as mdtABC encoding multidrug efflux pumps, acrD encoding aminoglycoside efflux transporter, spy encoding periplasmic chaperone protein involved in envelope stress defence and entS encoding siderophores (Pérez-Palacios et al., 2024; H. Zhang et al., 2019).

- **YpdA**

The YpdA-YpdB system is activated upon nutrient depletion in the bacterial environment as it chooses alternate nutrient sources over depleting carbon sources. The sensor kinase YpdA senses high concentrations of extracellular pyruvate and phosphorylates its cognate RR YpdB before the onset of stationary phase (Behr et al., 2014). YpdB upregulates gene yhjX that encodes a transporter of unknown function (Fried et al., 2013).

- **YehU**

The SHK YehU detects nutrient depletion similar to YpdA, but gets activated in the presence of peptides and amino acids (Behr et al., 2014). The phosphorylated RR YehT upregulates yjiY gene that encodes an amino acid and peptide transporter. The YehU-YehT system negatively regulates expression of gene yhjX controlled by YpdA-YpdB system.

- **YedV**

The YedV-YedW system responds to changes that occur during oxidative stress. YedV senses reactive chlorine species such as hypochlorous acid and hydrogen peroxide (Hajj et al., 2021). The phosphorylation of its cognate RR YedW by activated YedV results in upregulation of operons cyoABCDE, hprRS, hiuH, cusRS and cusCFBA involved in mitigation of oxidative stress. A cross regulation with a non-cognate RR CusS is observed (Urano et al., 2015, 2017).

- **CitA**

The CitA-CitB system is involved in the process of citrate fermentation (Scheu et al., 2012). The SHK CitA activates upon detection of extracellular citrate content and phosphorylates its RR CitB that regulates genes citT encoding a citrate/succinate antiporter and citCDEFXG encoding a citrate lyase.

- **KdpD**

The SHK KdpD detects low external potassium levels and osmotic stress through detection of internal sodium and ammonium ions, following which it phosphorylates its cognate RR KdpE (Epstein, 2015; Laermann et al., 2013). KdpE upregulates the operon kdpFABC involved in potassium uptake with kdpA encoding a membrane protein for potassium transport, kdpB encoding a P-type ATPase that provides energy for potassium uptake, kdpC encoding a chaperone and kdpF encoding a small peptide to stabilise the complex (Schniederberend et al., 2010).

- **RstB**

The RstB-RstA system plays an important role in virulence and evasion of stress (Liu et al., 2019). This system detects stimuli similar to the PhoQ-PhoP system, with its expression partially depending on it. The SHK RstB upon activation, phosphorylates RstA that regulates

genes such as asr involved in acid tolerance response and csgD involved in biofilm regulation (Y. C. Li et al., 2014).

### 1.5.2 Hybrid histidine kinases (HHKs) in the TCSs of *E. coli*

- **ArcB**

The ArcB-ArcA system is involved in the detection of oxygen availability and in monitoring the redox state of the cell. ArcB is activated in anaerobic conditions through the detection of changes in the membrane-bound quinones, such as ubiquinone and menaquinone and phosphorylates ArcA. ArcA upregulates the expression of anaerobic metabolism genes such as ldhA, aceE, adhE, feoABC, gad-mdtEF, gadXW, hyaABCDEF, oppA and represses the expressions of the genes involved in TCA cycle and glyoxalate shunt (Nizam et al., 2009; Park et al., 2013).

- **BarA**

The SHK BarA and RR UvrY are crucial for adaptation to metabolic shifts. BarA detects the presence of acetate and other short chain carboxylic acids (Alvarez et al., 2021). The TCS regulates the csr system upon phosphorylation of the RR UvrY, activating csrB and csrC (Contreras et al., 2023). CsrB and CsrC bind to repress the activity of CsrA, a RNA binding protein derepressing genes involved in gluconeogenesis, glycogen biosynthesis and biofilm formation.

- **RcsC**

The Rcs system, also known as the regulator of capsule synthesis, is a phosphorelay TCS involved in capsule synthesis, biofilm formation and envelope stress response (Z. Li et al., 2024). The phosphorylation of RR RcsB by the SHK RcsC via an intermediate protein RcsD, results in upregulation of operons wza, wzb, wzc and cps encoding capsule biosynthesis, osmB,

osmY, hdeA and gadE involved in stress response, and rprA, bcsA and matAB involved in biofilm formation. RcsB functions as heterodimers with another RR RcsA that lack phosphorylation capability (Ebel & Trempy, 1999).

- **EvgS**

The EvgS-EvgA system plays a major role in acid resistance (Sen et al., 2017). The SHK EvgS detects acidic pH and alkali metals to phosphorylate its RR EvgA, that regulates the expression of genes such as emrXY encoding a efflux pump, mdtEF encoding a multidrug efflux pump, gadE encoding acid resistance regulator, slp encoding a lipoprotein that stabilises the membrane, hdeAB encoding periplasmic chaperones required for survival under acidic conditions and gadAB encoding proteins of the glutamate-dependent acid resistance system (Ma et al., 2004; Nishino et al., 2003).

- **TorS**

The TorS-TorR system is a regulatory system involved in the utilization of trimethylamine-N-oxide (TMAO) under anaerobic conditions and extreme acid stress (Jourlin et al., 1996; G. Li et al., 2022). The SHK TorS detects TMAO or lower pH levels to phosphorylate its RR TorR. During anaerobic conditions, the TorR activates the tor operon to utilise TMAO, but modulates RpoS and acid stress genes alike EvgA.

### 1.5.3 SHKs in the chemosensory systems in *E. coli*

- **CheA**

CheA is the central histidine kinase in chemosensory systems. It lacks the ability to sense signals that is generally carried out by methyl-accepting proteins (MCPs) such as Tar, Tsr, Tap, Aer and Trg. CheA stays docked to the MCP receptor complex and dissociates upon signal sensing to phosphorylate its RRs CheB and CheY (Cassidy et al., 2020b; Muok et al., 2020;

Rowsell et al., 1995). CheB is involved in receptor modulation through regulation of methylation status of the MCPs, while CheY binds to FliM regulating motor functions of the flagella.

## 1.6 Domain organization in sensor histidine kinases

The following modules define the architecture of the SHK in the periplasmic, transmembrane and cytoplasmic regions.

### 1.6.1 Domain architecture in the sensor region

Stimuli sensing regions in SHKs are distributed across the extracellular, transmembrane and cytoplasmic regions, having an all α-helical, all β-stranded or a mixed α and β architecture as seen in **Figure 1.6.1.1** (Cheung & Hendrickson, 2010; Ishii & Eguchi, 2021b). **Extracellular sensor domains** lie in the periplasmic space of Gram negative bacterium. They form functional dimers with ligand-binding sites at the dimerization interface or pockets formed on exposed protomers. Indirect detection of stimuli occurs occasionally in a few domains with the help of accessory protein components instead of direct binding at the sensor. **Transmembrane sensor domains** include the membrane-passing α-helices that detect envelope stress and stimulants inducing disruption in membrane integrity. They are found in a recent class of intra-membrane-sensing histidine kinases (IM-HKs) with an extracellular region of less than 25 amino acids. **Cytoplasmic sensor domains** are located in the cytoplasm and present before the first transmembrane helix or after the second transmembrane helix in prototypical SHKs. Common folds forming sensing domains in SHKs as follows:

- **All α domain**

Sensor domains in kinases such as NarQ, NarX and TorS possess sensor domains made entirely of α-helices. NarQ and NarX sensors are formed by four-helices with the ligand binding site in between the dimerization interface (Cheung & Hendrickson, 2009; Gushchin et al., 2017). TorS sensor comprises of six α-helices arranged in a right-handed membrane proximal four-helix bundle and a left-handed membrane distal four-helix bundle (Moore & Hendrickson, 2009).

- **β-propeller domain**

The β-propeller domains are predominantly all β-strand containing domains found in kinases such as HK3 $BT4673_S$ and HK3 $BT3049_S$. They are made of repeating units of four anti-parallel β-strands with the strands arranged as propeller blades, visibly circulating counter-clockwise around a central pore (Z. Zhang et al., 2014).

- **DISMED 2 domain**

SHKs such as RetS have sensing regions consisting of a β-sandwich fold resembling carbohydrate binding modules in proteins known as DISMED 2(DISM extracellular domain 2) domain (Jing et al., 2010).

- **PAS domain**

PAS (Per-ARNT-Sim) domains are a class of mixed α + β globular folds found in periodic circadian proteins, aryl hydrocarbon nuclear translocator proteins and single-minded proteins. They have a core made of five strands of antiparallel β-sheets surrounded by α-helices associated with covalently or non-covalently bound cofactors such as heme in FixL and are known to sense intracellular stimuli (Gong et al., 2000). Most extracellular PAS folds are classified as Cache domains. A specialized subclass of PAS domains known as LOV (light,

oxygen, voltage) domains are present in the phytochrome modules detecting blue-light similar to kinase YF1 (Diensthuber et al., 2013).

- **PDC domain**

PDC (PhoQ-DcuS-CitA) domains resemble the mixed α + β architecture alike PAS domains consisting of near similar β-core, but differ in their arrangement of α-helices. The PDC domains form extracellular sensors unlike their intracellular PAS counterparts with a central core of five β-strands, flanked by a long N-terminal α-helix with additional loops and helices on either side (Cheung et al., 2008; Cheung & Hendrickson, 2008; Reinelt et al., 2003). The ligand binding occurs at the dimer interface or in grooves formed by exposed regions of an individual protomer. Sensor region in DctB have two PDC domains stacked over one another forming a tandem PDC domain (Cheung & Hendrickson, 2008; Zhou et al., 2008).

- **GAF domain**

GAF domains have a mixed α + β topology present in proteins such as cGMP-specific phosphodiesterase, adenylyl cyclases and formate hydrogenases. They have five or six-stranded antiparallel β-core comparable with PAS domains, having an additional β-strand inserted between the second and the third strands. The GAF domains of DosS and DosT form heme-containing redox sensors that detect changes upon iron and oxygen binding (H. Y. Cho et al., 2011; Podust et al., 2008).

- **PBP-like and VFT domains**

The PBP-like or periplasmic binding protein-like sensors have a bilobed architecture consisting of two mixed α + β domains linked by β-strands adopting a Venus flytrap structure. The domains contain central β-cores with α-helices packed on either side of the core, forming two mobile jaws. The cavity is delimited between the jaws that undergo clamshell motions during

ligand binding. VFT (Venus flytrap) domains, VFT1 and VFT2 in BvgS are homologous to PBP-like domains in $HK29_S$ (Bauer et al., 2015; Dupré et al., 2015; Herrou et al., 2010).

- **PCD domain**

Some entirely cytosolic bacterial phytochromes such as BphP comprise a photosensory core domain that has a sequential tripartite arrangement of PAS, GAF and a PHY domain (Bellini & Papiz, 2012). PHY is a unique phytochrome-associated domain with a mixed α + β architecture similar to the PAS domain with a five β-stranded central scaffold (Wahlgren et al., 2022).

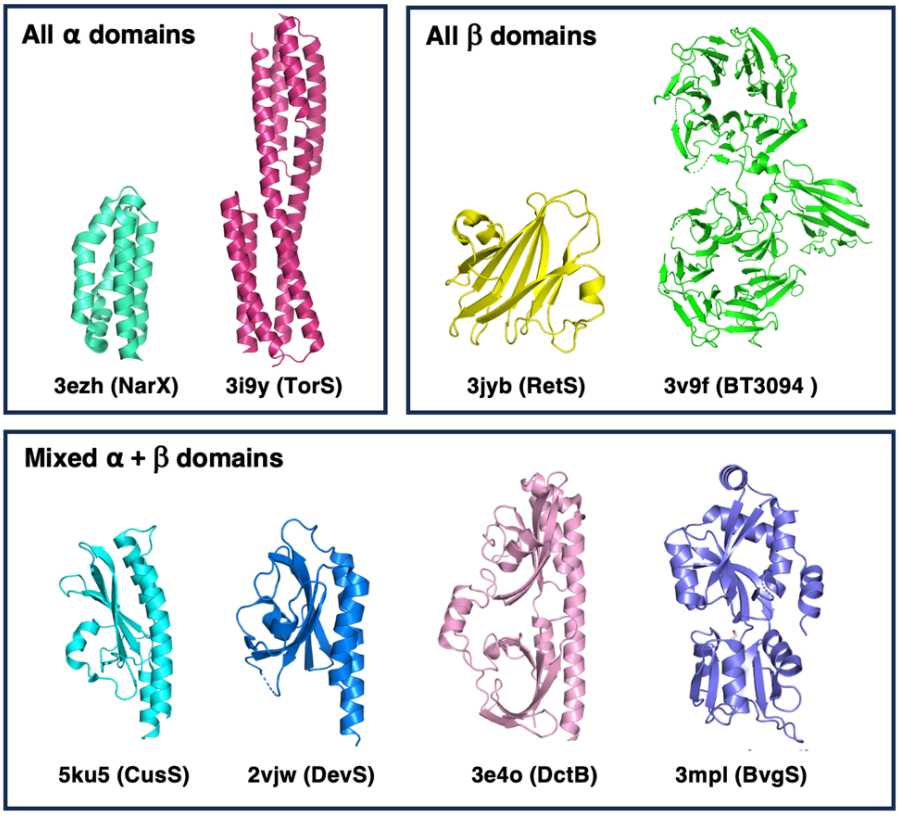


**Figure 1.6.1.1 Sensor domains of SHKs.** The image includes representative members of all α, all β and mixed α + β folds.

### 1.6.2 Domain architecture in the transmembrane region

The transmembrane region (TM) includes a four-stranded coiled coil bundle in its functional state, with each monomer conferring two antiparallel helices TM1 and TM2 (**Figure 1.6.2.1)**. TM region forms a periplasm-cytoplasm domain bridge of an SHK (Diensthuber et al., 2013; Gushchin et al., 2017). In SHKs such as DesK and CbrA, multiple helices are found traversing the membrane region (Almada et al., 2021; Wirtz et al., 2020).

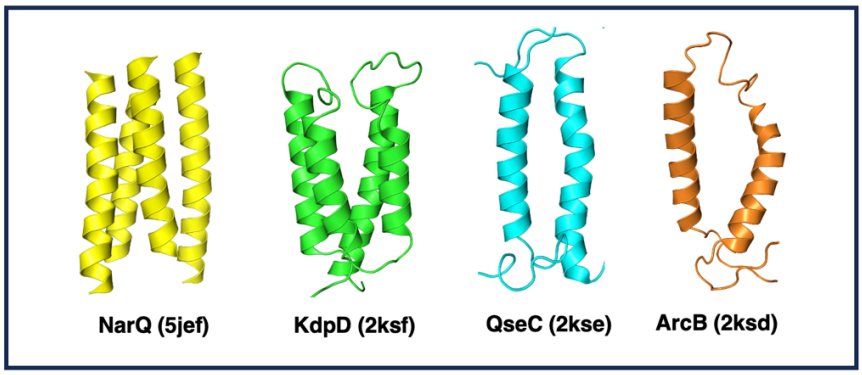


**Figure 1.6.2.1 Transmembrane regions of SHKs.** The image shows helical TM regions of different SHKs. TMs of NarQ and KdpD crystallised as dimers while QseC and ArcB crystallised as monomers.

### 1.6.3 Domain architecture in the cytoplasmic region

#### 1.6.3.1 Linker domain

Linker regions connect TM2 with a kinase domain (KD) in SHKs. One or a combination of many domains including simple α-helices, HAMP (HKs, adenylate cyclases, methyl transferases, and phosphodiesterases), STAC (TCST-Associated Component) or mixed α + β sensing domains PAS and GAF carry out signal transduction as linkers **(Figure 1.6.3.1.1).**

- **α-helices**

Linker regions in some SHKs descend down as a simple α-helix from TM2 connecting the kinase module. The helices may dimerize to form coiled coils as in DesK (Albanesi et al., 2009; Saita et al., 2015). α-helices form extended HAMP connectors known as S or signaling helices in NarQ (Gushchin et al., 2017).

- **HAMP domain**

HAMP domains are helical domains that occur in histidine kinases, adenylyl cyclases, methyl-accepting chemotaxis proteins and phosphatases. They act as linker regions in histidine kinases (CpxA, EnvZ) and chemotaxis receptors (CheA) assembling into a four-helix bundle, with two helices contributed by each monomer (Kishii et al., 2007; Mechaly et al., 2014; Parkinson, 2010). The helices are amphipathic and connected using a connector loop that forms a parallel coiled coil homodimer, allowing conformational reorganization during signal propagation.

- **STAC domain**

SHKs such as CbrA with a dual sensor-transporter activity contains STAC (Solute carriers and two-component signal transduction-associated component) domain connecting the SLC5 transmembrane domain with a cytoplasmic PAS linker and KD (Korycinski et al., 2015).

- **PAS and GAF**

These domains act as both periplasmic domains and constitute linker regions between transmembrane and KDs (Dupré et al., 2013; Podust et al., 2008).

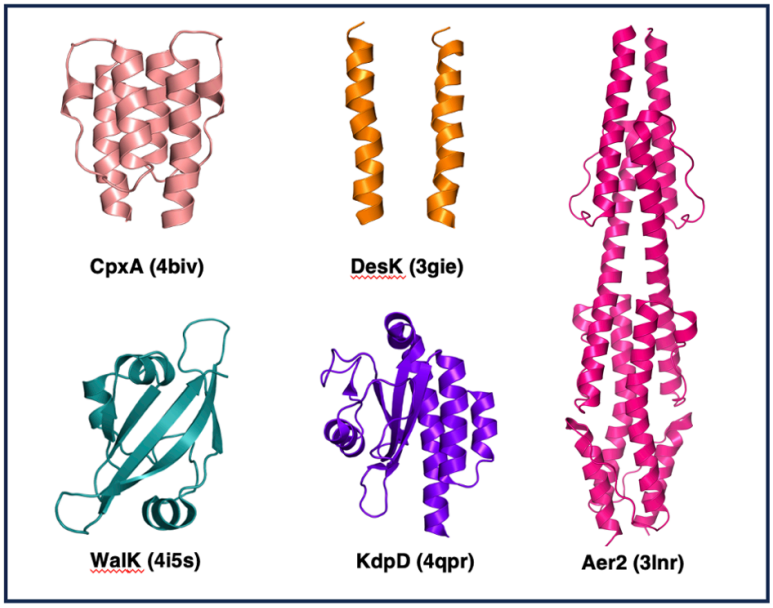


**Figure 1.6.3.1.1 Linker domains of SHKs.** The image shows different types of linker domains such as simple coiled coils, HAMP, tandem HAMP and PAS domains that forms linker regions in SHKs.

### 1.6.3.2 Kinase domain

The kinase domain (KD) in SHKs consists of a dimerization and histidine phosphoacceptor domain (DHp) and a catalytic domain (CA) as seen in **Figure 1.6.3.2.1** (Y. Cai et al., 2017a; Marina et al., 2005; Mechaly et al., 2014; Yoshida et al., 2007).

- **DHp domain**

DHp domains form antiparallel four-helix coiled coil bundles made from two helices of each protomer joined by a connecting loop. The Pfam database groups the bundles into four separate domain families HisKA (PF00512), HisKA_2 (PF07568), HisKA_3 (PF07730), and HWE_HK (PF07536) based on sequence analysis (Mistry et al., 2021). The DHp region possesses a seven-residue consensus or H-box with His-Asp/Glu-Leu/Ile-Lys/Arg-Thr/Asn-Pro-Leu consensus. The His residue of this box undergoes phosphorylation upon stimuli perception.

- **CA domain**

CA domains are compact and globular α/β domains connected to the DHp domain by long unstructured hinge regions. They help bind ATP and bring it to the proximity of the DHp bundle during autophosphorylation. The α/β sandwich fold resembles an ATP-binding Bergarat fold found across members of the GHKL superfamily (Gyrase B, Hsp90, DNA-mismatch-repair enzymes MutL, and histidine protein kinases) (Dutta & Inouye, 2000). The fold has three alpha helices, four beta-strands with N, G1, F and G2 boxes named after conserved Asn, Gly, Phe, and Gly residues respectively. Presence of conserved H, N, G1, F and G2 boxes categorizes these proteins as HPKs. G3 boxes with a conserved glycine residue may be found in continuation with the G2 box.

Some kinases may contain one or more additional domains such as dimerization (Dim), receiver domains (Rec) and histidine-containing phosphotransfer (HPt) that aid in the process of phosphoryl transfer to the response regulator (Bilwes et al., 1999; Brüderlin et al., 2023; M. Kato et al., 1997).

#### 1.6.3.3. Rec

Rec domains have mixed $(\beta/\alpha)_5$ folds similar to domains of the receiver domain of response regulators. They contain five centrally placed parallel β-sheets connected by cross-over helices with a conserved Asp residue, as seen in CckA and are constitutively active unlike their response regulator counterparts (Brüderlin et al., 2023). The γ-phosphate is transferred from the DHp domain to the Rec domain that is further transferred to another His-containing HPt domain.

#### 1.6.3.4. HPt

HPt domains are α-helical modules with six α-helices with four helices forming a bundle (S. K. Chen et al., 2020; M. Kato et al., 1999). They function as monomers (ArcB) or dimers

(Spo0B) and help transfer γ-phosphate through an indirect process instead of direct transfer from the DHp bundle to the response regulator. The active His present in HPt domains acquire phosphate from Rec domain before finally transferring it to the receiver domain of the response regulator.

**1.6.3.5. Dim**

Multi-component kinases chemotactic kinases such as CheA contain distinct domains undergoing dimerization and phosphorylation unlike dual function DHp domains (Bilwes et al., 1999). Dim domain is solely responsible for dimerization with a four-helix bundle architecture lacking phosphorylable His residue.

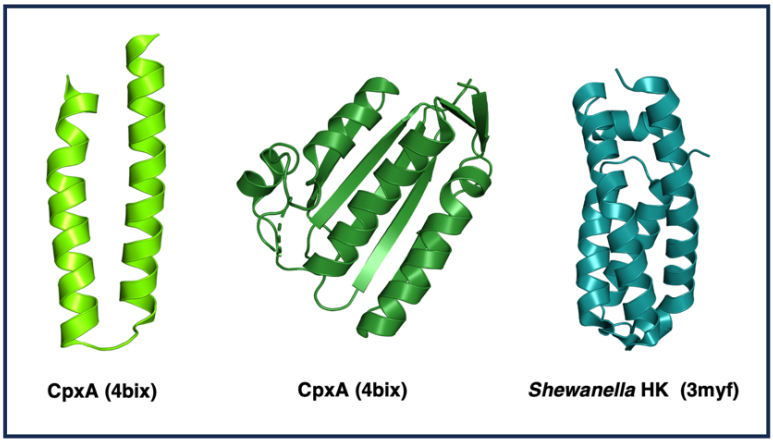


**Figure 1.6.3.2.1 Structures of the kinase and HPt domains.** The image shows the fragment images of kinase domain (DHp and CA) and an Hpt bundle.

**1.6.4. Domain duplication in sensor histidine kinases**

Domain duplication refers to the presence of multiple copies of similar domains in proteins due to causes such as gene duplication, lateral gene transfer, replication slippage, recombination and functional adaptation. Duplication of domains in SHKs is a major evolutionary strategy

that helps these kinases diversify their function and regulation, when occurring between two organisms.

The duplication of regions within the sensor kinases are observed predominantly in the sensing, linker or signal relay regions. It help proteins acquire novel functions, structural stability and functional regulation, though some cases do not have any justified reason for the same. Tandem repetition of PDC domains in the sensing region are found in SHKs such as DctB and DcuS (Cheung & Hendrickson, 2008). Mutational studies on DcuS indicate that deletion or alteration of either PDC domains in DcuS impairs its function and ability to sense stimuli (J. Krämer et al., 2007). The tandem arrangement of may enhance stimuli binding efficiency, amplify signal detection, and improve overall fidelity of the response. PAS containing SHKs such as KinA contains three PAS domains in its linker region, catering to differing functional needs of the protein (Eswaramoorthy & Fujita, 2010; Stephenson & Hoch, 2001). The PAS-A domain is involved in ATP binding, PAS-B domain carries out dimerization and PAS-C domain is involved in formation of dimers or higher oligomers. While most kinases contain a maximum of two or three tandem HAMP domains, an exceptional case of domain duplication is observed for MXAN_6735 from *Myxococcus xanthus* containing 31 HAMP domains in the linker region (Dunin-Horkawicz & Lupas, 2010). The occurrence of multiple HAMP domains possibly enables organisms to fine tune their responses with respect to diverse stimuli types.

## 1.7 Evolution of sensor histidine kinases

Genes encoding SHKs are found across all domains of life but occur abundantly in bacteria (Koonin & Wolf, 2008). TCSs have been hypothesized to have evolved from OCSs. The evolutionary relationship between TCSs and OCSs is apparent in the greater abundance, wider distribution, simpler structure, and broader domain diversity observed in OCSs (Wuichet et al.,

2010). The signaling systems suggest a potential common ancestry or convergent evolution, reflecting the modular nature of component system proteins and the evolutionary pressure to efficiently sense and respond to environmental stimuli. OCSs likely represent the Last Universal Non-Ancestor (LUNA) of TCSs, signifying an ancestral, simpler signaling system from which the more complex TCS architecture may have evolved.

While being prevalent in bacteria, the occurrence of SHKs is rather sparse amongst archaea and eukaryotes. As the cellular evolution of archaea and eukaryotes relied on multiple horizontal gene transfers from bacteria, genes for SHKs may have been acquired during the transfers. In plants, SHK genes were most likely obtained from the chloroplast-forming endosymbiotic cyanobacteria. Eukaryotic SHKs have undergone several evolutionary modifications that distinguish them from their bacterial counterparts, a prominent feature being their integration into signaling networks specific to eukaryotes. A major difference amongst the histidine kinases in prokaryotes and lower eukaryotes is the presence of hybrid kinases (such as HHKs) carrying the γ-phosphate through additional domains absent in a prototypical SHK (Kabbara et al., 2018). The cause of positive selection for hybrid kinases in lower eukaryotes is unknown, but directs towards a need for more intricate regulation of signaling cascades. SHKs are absent in higher eukaryotes such as metazoans and humans.

Bacterial SHKs are known to arise through two evolutionary mechanisms – lineage-specific expansion (LSE) and horizontal gene transfer (HGT) (Alm et al., 2006; Wuichet et al., 2010). Lineage-specific expansion (LSE) includes vertical transfer and duplication of genetic material within a bacterial lineage. LSE is the dominant mechanism of SHK evolution in most bacteria. It leads to the evolution of kinases with potentially new functions, favoring formation of novel domain combinations through domain shuffling. On the other hand, horizontal or lateral gene transfer (HGT) favors the transfer of genetic information across distantly related bacteria, allowing rapid acquisition of functional signaling components. The SHKs obtained in this

process generally conserve their original domain architectures and functionality with few exceptions. HGT is crucial for introducing new SHKs into bacterial genomes, enabling fast expansion of sensory functions without extensive genetic reorganization. The process of vertical transfer and duplications that lead to formation of new SHKs remains poorly understood, whereas horizontal gene transfer occurs via plasmids, phage, conjugative elements, and pathogenicity islands. SHK diversity in bacteria is shaped by constraints on the genome size and environmental complexity. Bacteria living in surroundings with minimal fluctuations encode less number of SHKs compared to ones living in a rapidly changing environment with more diversity in stimuli types.

Following acquisition of genes through vertical or horizontal transfer and gene duplication, TCS components undergo functional diversification. It is accomplished through numerous mechanisms including changes in input or sensor regions, output or RR regions and pathway insulation to avoid unwanted cross-talk with pre-existing pathways (Capra & Laub, 2012). Moreover, TCS components in bacteria are organized as operons containing a paired SHK and RR. This facilitates their duplication or horizontal transfer as intact units. Shuffling between operons is uncommon and fusion events to form hybrid kinases is rare, involving operonic SHK-RR pairs through stop codon mutations or gene fusions.

The changes during functional diversification arise as a result of domain shuffling with unrelated proteins, point mutations and subdomain substitutions. Sensor regions often evolve faster compared to other regions to form SHKs with new sensing capabilities. The output domains of RR modify to gain the ability to interact with new downstream proteins, allowing new signaling pathways to control distinct gene expression profiles. SHKs produced by duplication of the same gene in an organism avoid cross-talk through divergence of specificity determining residues that govern molecular recognition between the kinases and their RRs. The components can accumulate mutations at the interface involved in phosphotransfer with the

residues coevolving to maintain strong interactions within the new SHK-RR pair, while minimizing unintended interactions with other pathways.

## 1.8 Classification of sensor histidine kinases

### 1.8.1 Based on cellular distribution

Based on the location of SHKs inside cells, SHKs have been classified into membrane-bound SHKs and cytoplasmic SHKs **(Figure 1.8.1 A)**.

- **Membrane-bound SHKs**

They have domains spread across extracytoplasmic or periplasmic, transmembrane and cytoplasmic regions. The periplasmic domains of SHKs in Gram-negative bacteria is synonymous with the extracytoplasmic domains of Gram-positive bacteria.

- **Cytoplasmic SHKs**

They are limited to the cytoplasm devoid of any extracytoplasmic, periplasmic and transmembrane regions.

### 1.8.2 Based on multiple sequence alignment

Grebe and Stock (1999) classified SHKs or HPKs into 11 subfamilies (HPK 1-11) based on consensus of conserved regions or boxes obtained from multiple sequence alignment (Grebe & Stock, 1999).

- **HPK1 (PhoR, KdpD)**

SHKs belonging to the HPK1 subfamily have the following H, X, N, D, F, and G-box consensus sequences. ‘x’ and ‘h’ denote variable and hydrophobic amino acids, respectively. The

other letters denote single-letter codes for amino acids. HPK1 has further been classified into HPK1a and HPK1b, with HPK1b containing most HHKs.

H-box: Fhxxh(S/T/A)H(D/E)h(R/K)TPLxxh

X-box: conserved hydrophobic pattern

N-box: (D/N)xxxhxxhhxNLhxNAhxaF(/H/Y)(*S/T)a*

D-box, F-box: hxhxhxDxGxGhxxxxxxxhFxxF

G-box: GGxGLGLxhhxxhhxxxxGxhxhxxxxxxGxxFxhxh

- **HPK2 (EnvZ, BasS)**

SHKs belonging to the HPK2 subfamily resemble EnvZ kinases and have been further divided into HPK2a and HPK2b. The groups HPK2a and HPK2b vary with the presence of Phe or Leu/Met residues before the conserved His. The HPK2b group has a positively charged residue Arg at the third position after the conserved proline of the H-box.

- **HPK3 (PhoQ, CreC)**

The HPK3 subfamily kinases resemble HPK1 and HPK2 kinases and are further distributed into HPK3a-3i. HPK3a lacks a second Phe residue in the F-box. HPK3b has a charged Asn residue preceding the H-box Pro. HPK3c has a typical consensus containing H, N, D, F and G boxes. HPK3e has four Ala residues preceding the His residue in the H-box. HPK8g and 3h have Glu and Asp following the conserved His residue and lack Thr near H-box Pro.

- **HPK4 (ZraS, NtrB)**

SHKs of the HPK4 subfamily contain an Ala residue prior to the conserved His residue and a Gln/Asn residue before the H-box Pro. This family has a PFX-TTK signature motif in the F-box.

- **HPK5 (CitA)**

SHKs of the HPK5 family contain conserved basic amino acids Arg in place of a hydrophobic residue at position four upstream and Asn residue at position four distal to the conserved His residue of the H-box. They lack Phe and Pro residues commonly seen in the H-box region, and the F-box contains only one Phe residue.

- **HPK6 (g2649399)**

These SHKs are mostly found in Archaeoglobus and Halobacteria, containing Arg upstream of the conserved His in H-box.

- **HPK7 (NarQ, NarX)**

SHKs of the HPK7 contain negatively charged residues upstream of the conserved His residue, with a positively charged Arg residue eight positions upstream. His is preceded by an Asp residue with Pro and Phe residues absent from the H-box. The first Asn of the N-box is replaced by a Glu residue.

- **HPK8 (YehU)**

The members of the HPK8 subfamily contain a Pro residue before the conserved His, but lack the downstream Pro and are instead followed by a Phe residue. The N-box has a consensus 'hPxhxhQxhhENAh', and the distance between H and X boxes is reduced.

- **HPK9 (CheA)**

SHKs of the HPK9 subfamily have a distinct domain organization similar to the chemosensory systems. Pro is absent in the H-box region, and the first Asn in the N-box is replaced by a His residue. A second His is found downstream of the first conserved His of the H-box.

- **HPK10 (ComD)**

This subfamily contains SHKs that contain a Tyr residue two residues downstream from the conserved His and lack a H-box Pro. They contain one Asn residue in the N-box and lack the D-box.

- **HPK11 (ExsG)**

The SHKs of HPK11 are mostly found in methanobacters with a unique H-box that differs from all other subfamilies. The conserved His is followed by an Arg and Asn four residues downstream. The first Asn of N-box is replaced by Glu.

### 1.8.3 Based on phylogenetic analysis

Kim and Forst (2001) classified SHKs of bacteria and archaea based on sequence alignment of the transmitter domain, phylogenetic analysis and secondary structure predictions into five major types known as Type I-V as mentioned in **Figure 1.8.1 B** (Kim & Forst, 2001).

### 1.8.4 Based on sensor domain fold

SHKs are classified into multiple groups based on the type of sensor domain folds. A partially published classification mentions HK1-type histidine kinases, which represent the largest and most structurally characterized group of α + β sensors, including PAS, PDC and Cache folds (Z. Zhang & Hendrickson, 2010). Another classification scheme categorizes SHKs into extracytoplasmic, membrane-embedded or cytoplasmic sensor domain containing SHKs based on the location of stimuli sensing region (Cheung & Hendrickson, 2010).

### 1.8.5 Based on transmitter domain organization

The transmitter domain in SHKs comprises a composite structure with the H, N, G1, F and G2 boxes distributed across two distinct domains: a CA domain and a DHp domain, or less commonly a CA domain and an HPt domain involved in phosphate transfer to the RRs. Dutta

et al. (1999) classified the kinases into two classes based on the transmitter domain organization into Class I (EnvZ type) and Class II (CheA type) (Dutta et al., 1999), as seen in **Figure 1.8.1 C**.

- **Class I kinases (NarQ, CpxA and EnvZ)**

They have the H-box containing domain (DHp) adjacent to the ATP-binding domain (CA). Dimerization and phosphorylation of the His residue are both facilitated by a single DHp domain in these kinases.

- **Class II kinases (CheA)**

They have a distantly placed H-box containing domain (HPt) with respect to the ATP-binding domain (CA), arranged as a separate domain. Domains responsible for dimerization and histidine phosphorylation are separated by a Dim domain for dimerization and an HPt domain for phosphorylation.

### 1.8.6 Based on a hierarchical rule system

The MiST 4.0 database classifies SHKs based on the spatial organization of the transmitter and receiver domains, primarily focusing on their signal transduction architecture. The canonical kinases possess the transmitter (DHp and CA) and receiver (Rec) domains in two separate proteins, while hybrid kinases contain fused combinations of both domains (Gumerov et al., 2024; Wuichet et al., 2010). Additionally, hybrid kinases may contain their own response regulators or pseudo-kinases as their downstream signaling partners.

- **Canonical histidine kinases or HKs (EnvZ, CpxA)**

The canonical or prototypical kinases contain a transmitter domain but lacks presence of a fused receiver domain. The γ-phosphate is transferred from the transmitter domain to the receiver domain present in a separate response regulator.

- **Hybrid Histidine Kinases or HHKs (CckA)**

The HHKs contain both the transmitter and receiver domains fused within the same protein. The transmitter domain is found at the N-terminus of the kinase, followed by a receiver domain. These kinases undergo a multi-step phosphorelay, where the γ-phosphate is transferred from the transmitter domain to the receiver domain ($Rec_{inter}$) within the kinase before phosphorylation of the receiver domain ($Rec_{term}$) in the RR.

- **Hybrid Response Regulators or HRRs (LvrA)**

The HRRs also contain both transmitter and receiver domains similar to HHKs. However, they possess a variable domain arrangement, containing an N-terminal receiver domain followed by a transmitter domain. The γ-phosphate is acquired by the receiver domain from an upstream kinase, which is further relayed to the transmitter domain in the HRR before being transferred to a RR.

- **Chemosensory systems (CheA)**

The SHKs involved in chemotaxis are grouped together into a separate group of chemosensory systems along with other accessory proteins involved in the process.

Numerous atypical kinases also stay unclassified under the others group due to the presence of an architecture not found in the above mentioned classes.

### 1.8.7 Based on the phosphotransfer mechanism

SHKs can be orthodox or unorthodox type based on the presence of one or more His residues in the transmitter region, which determines the phosphotransfer mechanism.

- **Orthodox or typical kinases**

Transfer of γ-phosphate during autophosphorylation is direct in orthodox kinases involving Asn of the CA domain to His of the DHp domain and finally to Asp of the RR .

- **Unorthodox or atypical kinases**

Unorthodox kinases are kinases that deviate from the classical model, mostly including hybrid kinases with multiple domains and a multi-step signal transduction mechanism as opposed to single step phosphoryl transfer found in orthodox kinases. The multi-step process includes phosphoryl transfer from Asn of the CA domain to His of the DHp domain, followed by Asp of the Rec domain and His of the HPt, before phosphorylating Asp of the RR.

New SHKs of SLC5/STAC type with solute carrier-like domain with linker STAC (SLC and TCS-Associated Component), such as CrbS and RpuS have not been incorporated into such classification schemes.

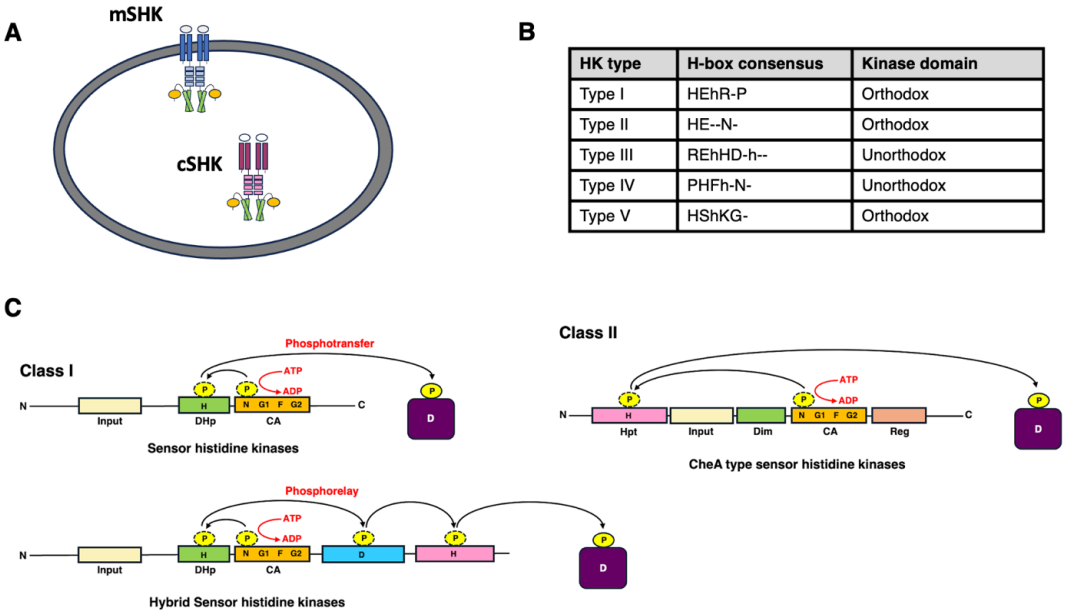


| HK type | H-box consensus | Kinase domain |
|---|---|---|
| Type I | HEhR-P | Orthodox |
| Type II | HE--N- | Orthodox |
| Type III | REhHD-h-- | Unorthodox |
| Type IV | PHFh-N- | Unorthodox |
| Type V | HShKG- | Orthodox |

**Figure 1.8.1 Classification of sensor histidine kinases.** (A) Representation of SHKs based on cellular location. (B) Tabular representation of SHK types based on the phylogenetic analysis. (C) Schematic representation of SHKs based on transmitter domain organization.

## 1.9 Signal transduction in sensor histidine kinases

The mechanism of signal transduction in SHKs proceeds in a three-step process - autophosphorylation, phosphoryl transfer and dephosphorylation including formation of two phosphoprotein intermediates as seen in **Figure 1.9.1** (Bhate et al., 2015; Buschiazzo & Trajtenberg, 2019; Casino et al., 2014; Gao & Stock, 2009; Jacob-Dubuisson et al., 2018; Stock et al., 2000).

### 1.9.1 Autophosphorylation

Signal transduction begins with autophosphorylation or self-phosphorylation of the kinase component of sensor kinases, often triggered by stimuli sensing at the sensor domain. The SHK undergoes formation of HK-His upon reversible phosphorylation, yielding HK-His∼P, although the equilibrium favors an unphosphorylated form. The phosphoryl group for phosphorylation is acquired by hydrolysis of the γ-phosphate group of ATP and transferred to the conserved His residue of the KD, forming a phosphoramidate intermediate. Phosphorylation occurs at either N1 or N3 position of the His imidazole ring, though structural and kinetic analysis predominantly exhibit phosphorylation at N3 for SHKs. The N∼P bond formed is ideally configured for efficient transfer of the phosphoryl group. Under physiological conditions, the ratio of ATP/ADP regulates autophosphorylation, allowing a small fraction of SHKs to get phosphorylated. SHKs exist as a mixed population of unphosphorylated, mono-phosphorylated or hemi-phosphorylated and dephosphorylated species.

The mode of autophosphorylation in SHKs can be classified as cis and trans based on the spatial orientation of the KD during the process. During cis autophosphorylation the kinase phosphorylates its own conserved His residue using the ATP bound within the same monomer in a functional dimer, while it phosphorylates the conserved His residue of the opposite monomer in the dimer in the trans mode.

### 1.9.2 Phosphoryl transfer

The phosphoryl group from HK-His~P is then transferred to a conserved Asp residue in the cognate RR, forming a high-energy acyl phosphate intermediate RR-Asp~P. This enables the RR to drive conformational transitions over long distances in the protein and helps initiate downstream cellular processes such as changes in gene expression or enzymatic activity. The stability of RR-Asp~P complex varies widely, with half-lives ranging from a few seconds to several hours, highlighting differences in the RR structure and function.

### 1.9.3 Dephosphorylation

The final step involves dephosphorylation of the RR, either through spontaneous hydrolysis or due to the phosphatase activity of the corresponding SHK. Most RRs have intrinsic phosphatase activity that actively catalyses the hydrolysis of RR-Asp~P to form RR-Asp. Some RRs lack phosphatase activity and adopt conformations that prevent the phosphoryl group from hydrolysis, causing extended half-lives of RR-Asp~P intermediates. SHKs carry out phosphatase activity, acting as bifunctional enzymes that phosphorylate and dephosphorylate their cognate RRs. This phosphatase activity is essential for resetting and controlling the time duration of signal transduction.

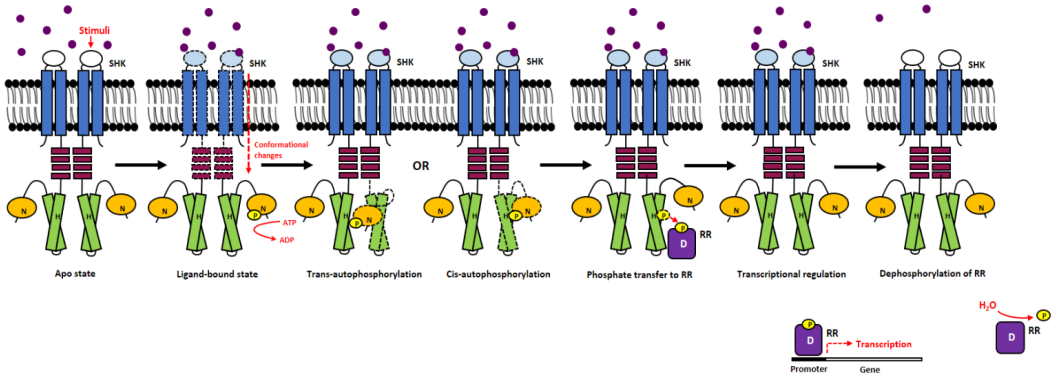


**Figure 1.9.1 Schematic representation of the process of signal transduction in SHKs.** The prototypical SHK detects ligands in the periplasmic domain that induce conformation change

in the protein. The conformational transitions lead to activation of the kinase through autophosphorylation at a conserved His residue in the cytoplasmic KD. The phosphoryl group is then transferred to the conserved Asp residue in the RR acting as a transcription factor, following which the group is hydrolysed to end the cascade.

## 1.10 ZraS: a zinc-sensing HPK4 in enterobacters

ZraS is a membrane-associated SHK that forms a part of the zraPSR operon found in enterobacters. It spans the bacterial inner membrane and possesses a periplasmic sensory domain, a transmembrane region, and a cytoplasmic KD **(Figure 1.10.1 A and B)**. The operon also codes for the cognate RR ZraR and a periplasmic chaperon protein ZraP (Petit-Härtlein et al., 2015; van der Weel et al., 2019). The system is involved in metal sensing, responding to elevated levels of zinc ions and potentially other divalent metal cations in its periplasm exposed sensing region (Leonhartsberger et al., 2001). The results of the study are mentioned in **Figure 1.10.1 C**. The binding of zinc ions at the periplasmic domain of ZraS induces conformational change within the protein, leading to autophosphorylation of the conserved His in the cytoplasmic KD (Taher & de Rosny, 2021). The phosphate is then transferred to ZraR, which eventually upregulates the zra genes. In the absence of zinc, the expression of these genes occur at a basal level with a dimeric ZraP and an inactive ZraS. When the levels of zinc rise, ZraS is activated upon zinc binding and zra operon is upregulated. This results in a higher concentration of ZraP in the periplasm that forms higher oligomeric forms, such as octamers and sequesters zinc ions. By reducing free zinc concentration in the periplasm, the octameric ZraP lowers the activation signal sensed by ZraS that dampens the signal transduction.

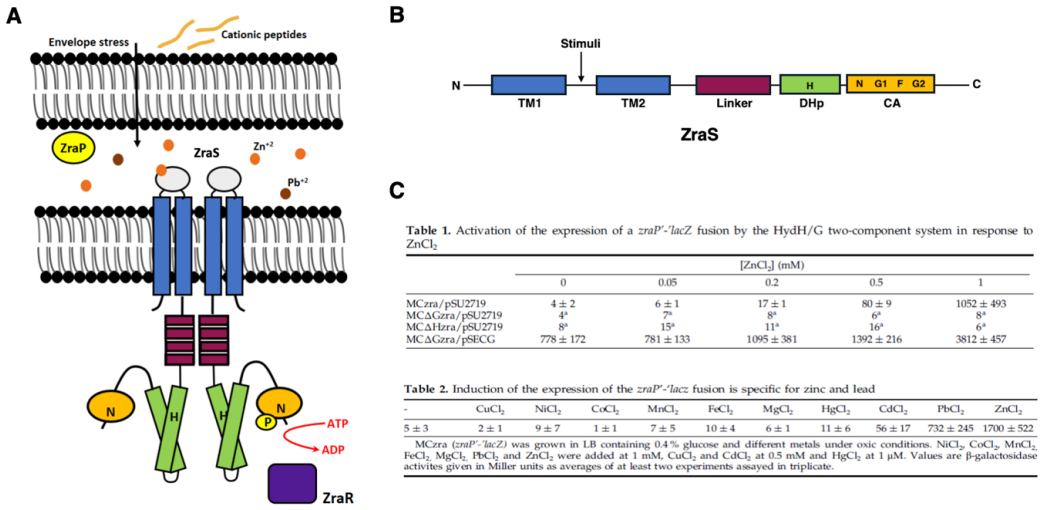


**Table 1.** Activation of the expression of a *zraP'-'lacZ* fusion by the HydH/G two-component system in response to $ZnCl_2$

| | [$ZnCl_2$] (mM) | | | | |
|---|---|---|---|---|---|
| | 0 | 0.05 | 0.2 | 0.5 | 1 |
| MCzra/pSU2719 | 4 ± 2 | 6 ± 1 | 17 ± 1 | 80 ± 9 | 1052 ± 493 |
| MCΔGzra/pSU2719 | 4[a] | 7[a] | 8[a] | 6[a] | 8[a] |
| MCΔHzra/pSU2719 | 8[a] | 15[a] | 11[a] | 16[a] | 6[a] |
| MCΔGzra/pSECG | 778 ± 172 | 781 ± 133 | 1095 ± 381 | 1392 ± 216 | 3812 ± 457 |

**Table 2.** Induction of the expression of the *zraP'-'lacz* fusion is specific for zinc and lead

| - | $CuCl_2$ | $NiCl_2$ | $CoCl_2$ | $MnCl_2$ | $FeCl_2$ | $MgCl_2$ | $HgCl_2$ | $CdCl_2$ | $PbCl_2$ | $ZnCl_2$ |
|---|---|---|---|---|---|---|---|---|---|---|
| 5 ± 3 | 2 ± 1 | 9 ± 7 | 1 ± 1 | 7 ± 5 | 10 ± 4 | 6 ± 1 | 11 ± 6 | 56 ± 17 | 732 ± 245 | 1700 ± 522 |

MCzra (*zraP'-'lacZ*) was grown in LB containing 0.4 % glucose and different metals under oxic conditions. $NiCl_2$, $CoCl_2$, $MnCl_2$, $FeCl_2$, $MgCl_2$, $PbCl_2$ and $ZnCl_2$ were added at 1 mM, $CuCl_2$ and $CdCl_2$ at 0.5 mM and $HgCl_2$ at 1 µM. Values are β-galactosidase activites given in Miller units as averages of at least two experiments assayed in triplicate.

**Figure 1.10.1 The membrane associated SHK ZraS.** (A) and (B) Schematic representation of ZraS from *E. coli*. (C) The results of β-galactosidase assay showing overexpression of ZraP in presence and absence of ZraS and ZraR and presence of different types of divalent metals from a previous study (Leonhartsberger et al., 2001).

## 1.11 Coiled coils and deviation in coiled coil architecture

Coiled coils are commonly occurring structural motifs found in proteins. The coiled coil model was proposed by Francis H. C. Crick (1953) to explain the structure of fibrous proteins such as α-keratin**.** They are formed by the interwinding of two or more alpha helices, resulting in a supercoil. Conventional or ideal coils are made of recurring repeats of seven amino acid residues or heptads (abcdefg). The heptads are distributed across two turns of a helix with a periodicity (n) of 3.5 residues per turn that winds the supercoil in a left-handed manner.

The positions ‘a’ and ‘d’ are occupied by apolar or hydrophobic amino acids, and those of ‘e’ and ‘g’ by charged or polar amino acids **(Figure 1.11.1 A)**. The apolar residues face towards the core and pack together forming a ‘knobs-into-hole’ pattern. The ‘e’ and ‘g’ residues flank

the periphery of the core-forming interhelical salt bridges, thereby adding stability to the coil. Their geometry and packing are described using a set of well-defined parameters that quantify helix orientation, packing, and conformational state. Some of the parameters have been described below **(Figure 1.11.1 C, D)**:

- **Superhelical axis**

Superhelical axis is the geometric centre around which constituent helices wind and forms the basis for defining coiled coil architecture. It acts as the principal reference for all geometric descriptors, with changes reflecting overall bending or structural rearrangement.

- **Superhelical radius ($R_0$)**

Superhelical radius is defined as the distance from the central axis of a coiled coil superhelix to the centre of an individual α-helix. This parameter provides a measure of how tightly the helices are arranged around the superhelical axis.

- **Superhelical pitch (*P*)**

Superhelical pitch describes the axial repeat distance of the superhelix formed by intertwined α-helices in a coiled coil. It reflects the extent of supercoiling that arises from the balance between the intrinsic twist of individual helices and their packing interactions within the assembly.

- **Superhelical pitch angle (α)**

Superhelical pitch angle represents the angle formed between constituent α-helices and the superhelical axis. This parameter reflects the degree of helical winding around the central axis that tends to change with conformational alterations in coils.

- **Crossing angle (Ω)**

Crossing angle or helix-crossing angle is defined as the angle at which two α-helices intersect in space within a coiled coil assembly. This angle is geometrically related to the superhelical pitch and reflects the degree of helix-helix inclination, which directly influences the packing geometry and stability of the interface.

- **Crick angle (ϕ)**

The Crick angle is a geometric parameter that quantifies the rotational orientation of α-helical residues relative to the superhelical axis of the coiled coil assembly. It is defined as the angle between two vectors originating from the individual helix axis ($O_n$), where the first vector connects the helix axis to the central superhelical axis ($C_n$) and the second vector connects the helix axis to the Cα atom of the residue **(Figure 1.11.1 D)**. If a residue faces directly toward the superhelical axis, the Crick angle is 0° (or 360°). Positive and negative Crick angle values typically refer to helix axial rotation deviation or the degree to which an individual helix is rotated around its own axis compared to its expected canonical orientation. When viewed from the N-terminus of a constituent helix, a negative value indicates a counter-clockwise rotation and a positive value indicates a clockwise rotation.

Variations in the Crick angles are known to influence the alignment of hydrophobic and polar residues at the interface that governs the stability and specificity of coiled coil assemblies. It helps understand helical packing. Conformational differences in coiled coils frequently arise from rotational reorientation of the helices around the superhelical axis, leading to minimal translational displacement and small r.m.s.d. variations. Under these conditions, the Crick angle offers a concise and physically meaningful parameter to describe subtle yet functionally important conformational changes.

In a few circumstances, especially involving dynamic and signaling proteins such as dynein, myosin and sensor histidine kinases, the characteristic heptad repeat is interrupted by insertions of one or more amino acid residues. They play a major role in regulating the functionality of the proteins by providing flexibility to acquire conformations otherwise inaccessible to typical α-helical structures. The insertions can be one, three or four residues between the canonical heptad repeats. These amino acids are adjusted along the length of the helix to maintain the structural integrity of the supercoil. A term accommodation index is used as a metric to quantify how a coiled coil domain tolerates insertions without losing characteristic geometry and function (Schmidt et al., 2017). A one-residue, three-residue (stammer) and four-residue (stutter) insertions produce 103º clockwise, 51º anticlockwise and 51º clockwise rotations, respectively. The coiled coils maintain their geometry by shifting the helical phases (**Figure 1.11.1 B)**.

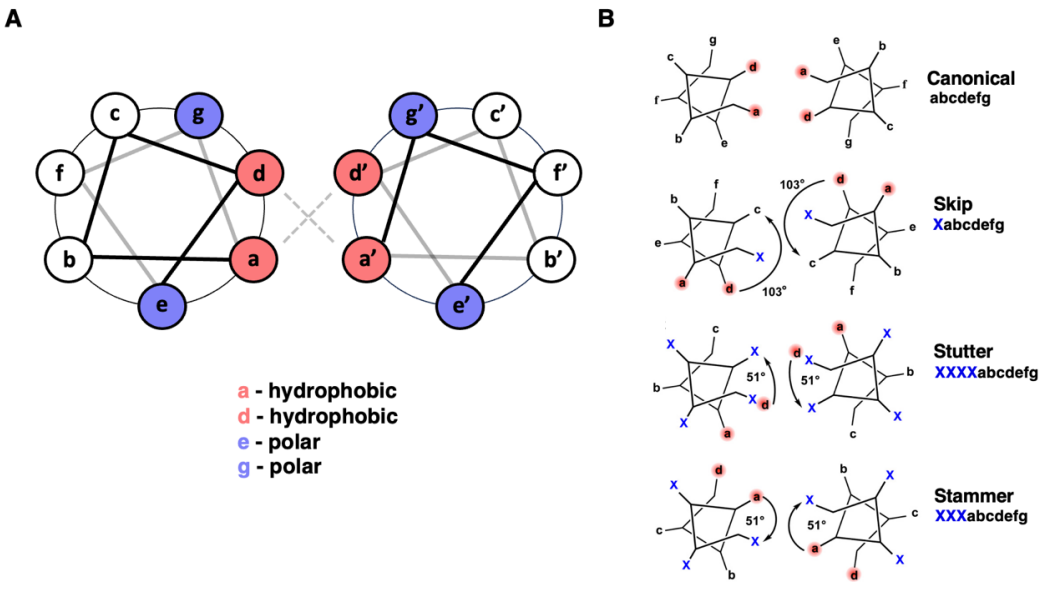

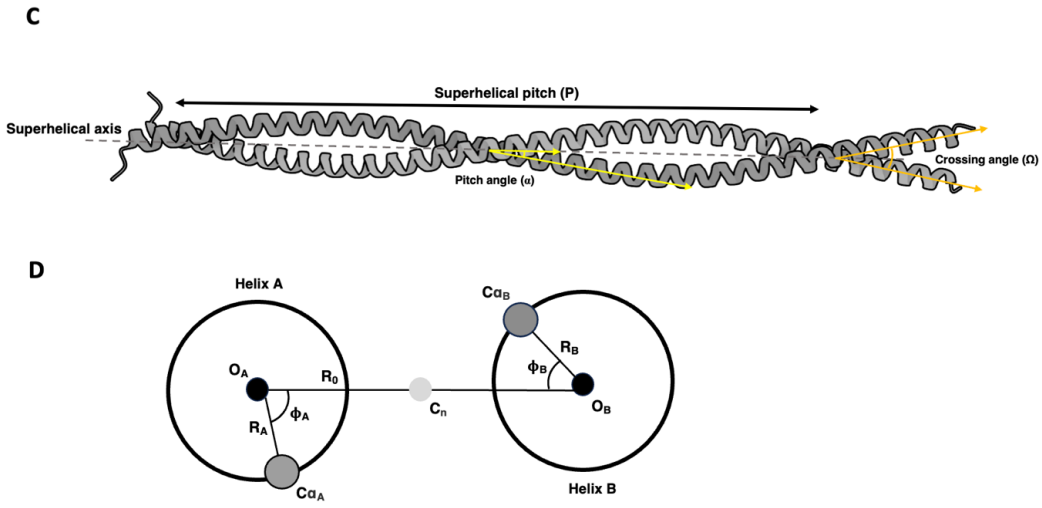


**Figure 1.11.1 Coiled coil and amino acid insertions in coiled coils.** (A) The helical wheel diagram shows the arrangement of amino acids in an ideal coiled coil made up of two helices. The 'a' and 'd' form the hydrophobic core while the residues 'e' and 'g' interact at the periphery forming salt bridges. (B) The image shows the types of amino acid insertions found in coiled coils (Schmidt et al., 2017). (C) and (D) The images depict key structural parameters of a coiled coil superhelix made of helices A and B. The central axis of the assembly is the superhelical axis. $C_n$, $O_A$ and $O_B$ are the centers of the superhelix, helix A and helix B, respectively. $R_o$ is the superhelical radius, $R_A$ and $R_B$ are the radii of helices A and B, respectively. $\phi_A$ and $\phi_B$ denote the Crick angles of two residues in the constituent helices A and B of a coiled coil.

## 1.12 Conclusion

Working with SHKs has been traditionally challenging, evident with the lack of full-length structures, the availability of truncated structures from a few kinases and limited information on their conformational landscape. This can be attributed to their characteristics such as internal

flexibility, dynamic nature, multi-module architecture and sequence diversity. Despite the presence of common structural folds in most kinases, the variability in the arrangement of domains and sequence makes them functionally distinct. Understanding of signal transfer and integration remains largely confined to the studies on truncated domains of a few SHKs, which are unlikely to represent all available SHK classes.

This thesis provides a mechanistic insight into the functioning of the SHKs using structural and functional studies on the truncated domains of ZraS from *E. coli*. Though we were unable to deduce the transmission of the signal from the sensor to the cytoplasmic KD, we succeeded in our attempts to trap the truncated cytoplasmic domain in two different previously unknown conformations. The conformers were ligand-bound and resembled transition states before Michaelis-complex formation. Comparison of the obtained conformers helped deduce the finer structural details, including the modulation of the α-helical KD through helical bending, sliding and rotation, responsible for conformational transition during kinase activation or autophosphorylation. We uncovered a novel linker region and observed an inherent structural bending that may play a role in driving conformational transition. Further, we proposed a model for kinase activation and determined its ATPase activity using a real-time biochemical kinetics study.

The work also focused on studying ligand-binding at the sensor domain of ZraS using structural and functional studies. Given the inability to acquire crystals suitable for diffraction, we resorted to comparative modelling approaches to infer the structural architecture. Our future work aims to determine ligand binding sites through mutational studies, metal binding assays and attempts to modify the obtained crystals for diffraction studies.

# Chapter 2
# Experimental and Computational Methods

*Chapter-2*

## 2.1 Cloning and overexpression of the truncated cytoplasmic domains of ZraS (EcZraS-CD and EcZraS-CD$_{trunc}$)

### 2.1.1 Cloning of the truncated cytoplasmic domains EcZraS-CD and EcZraS-CD$_{trunc}$

The clone for full length ZraS (ZraS-F) was provided by Prof. William DeGrado (University of California, San Francisco). The variants of the truncated cytoplasmic domain ranging from Tyr225–Gly465 (EcZraS-CD) and Asp234–Asn457 (EcZraS-CD$_{trunc}$) were cloned into the plasmid vector pNIC28-Bsa4 with restriction sites NcoI and BamHI. Two sets of primer forward primer 5'-3' AAAAAACCATGGCGTATCTGCGCTCGCGCC and reverse primer 3'-5' TTTTTTGGATCCTCATCCTTGTGGGTCCTTACGC were used for EcZraS-CD and forward primer 5'-3' AAAAAACCATGGCGGATGAAATGAAGCGC and reverse primer 3'-5' TTTTTTGGATCCTCAATTGACCGGAAGCC were used for EcZraS-CD$_{trunc}$. The construct EcZraS-CD was used for the final crystallization trial and enzyme kinetics study following purification and tag cleavage.

The genes of desired length were amplified from the clone ZraS-F using polymerase chain reaction (PCR) with a high-fidelity Q5 polymerase from New England Biolabs (NEB). The protocols used for PCR, including the primer details, reaction mixture and thermocycling conditions has been mentioned in **Tables 2.1.1.1, 2.1.1.2, 2.1.1.3**.

- Meanwhile, the plasmid vector pNIC28-Bsa4 in native form was prepared by transforming it into chemically competent *E. coli* DH5α cells and grown on a Kanamycin-LB Agar plate at 37 ºC and 220 rpm overnight in a shaker incubator. The plasmid vector was isolated by the alkaline lysis method using the miniprep kit from Qiagen.

- The PCR product obtained were conformed visually by running them on a 1% agarose gel **(Figure 2.1.1.1)**. Upon conformation they were purified using the PCR purification kit from Qiagen. The DNA obtained were quantified using a Nanodrop and used for restriction digestion.

- 2 ug of the PCR products obtained for EcZraS-CD, EcZraS-$CD_{trunc}$ and 2 ug of native pNIC28-Bsa4 were used for double digestion using restriction enzymes NcoI and BamHI. The reaction mixture used for double digestion has been mentioned in **Tables 2.1.1.4 and 2.1.1.5**, incubated at 37 ºC for a duration of 1 hour on a dry bath. Post digestion, the products were run on a 0.8 % agarose gel.

- The agarose gel was visualised under a UV transilluminator. The digested PCR products and plasmid vector corresponding to the required molecular weight marker were gel excised with a clean scalpel and subjected to purification using the gel extraction kit from Qiagen.

- The purified double digestion products (EcZraS-CD, EcZraS-$CD_{trunc}$, and plasmid vector pNIC28Bsa4) were quantified using a Nanodrop and used for ligation using Quick ligase from NEB. The reaction mixture used for ligation has been mentioned in **Table 2.1.1.6**. incubated at 25 ºC for 1 hour on a dry bath.

- 2-4 µl of the ligated product was used for transforming 50 ul of *E. coli* DH5α cells and grown on Kanamycin-LB Agar plates, incubated overnight at 37 ºC to allow growth of bacterial colonies.

- Single colonies were selected and screened for the presence of the desired clones. The plasmids from these colonies were subjected to double digestion using NcoI and BamHI, followed by final confirmation using Sanger's sequencing.

**Table 2.1.1.1 Primer details for EcZraS-CD and EcZraS-CD $_{trunc}$**

| Name | Sequence | Length (bp) | GC (%) | Tm (ºC) |
|---|---|---|---|---|
| EcZraS-CD forward | 5' AAAAAACCATGGCGTATCTGCGCTCGCGCC 3' | 30 | 57 | 79 |
| EcZraS-CD reverse | 3' TTTTTTGGATCCTCATCCTTGTGGGTCCTTACGC 5' | 34 | 47 | 74 |
| EcZraS-CD $_{trunc}$ forward | 5' AAAAAACCATGGCGGATGAAATGAAGCGC 3' | 29 | 45 | 72 |
| EcZraS-CD $_{trunc}$ reverse | 3' TTTTTTGGATCCTCAATTGACCGGAAGCC 5' | 29 | 45 | 71 |

**Table 2.1.1.2 PCR reaction mixture for EcZraS-CD and EcZraS-CD $_{trunc}$**

| Components | Volume (µl) |
|---|---|
| 5X Q5 reaction buffer | 10 |
| 10 mM dNTPs | 1 |
| 10 uM forward primer | 2.5 |
| 10 uM reverse primer | 2.5 |
| Template DNA (150 ng/µl ZraS-F) | 1 |
| Q5 DNA polymerase | 0.5 |
| Nuclease free water | 32.5 |
| **Total volume** | **50** |

**Table 2.1.1.3 Thermocycling conditions for EcZraS-CD and EcZraS-CD $_{trunc}$**

| Step | Temperature (ºC) | Duration (min) |
|---|---|---|
| Initial denaturation | 98 | 0:30 |
| 32 cycles | 98 | 0:10 |
| | 71-72 | 0:30 |
| | 72 | 3:30 |
| Final extension | 72 | 2:00 |
| Hold | 4 | ∞ |

**Table 2.1.1.4 Reaction mixture for restriction digestion of EcZraS-CD and EcZraS-$CD_{trunc}$**

| Components | Volume (µl) |
|---|---|
| 10X CutSmart® buffer | 5 |
| PCR product (435ng/µl EcZraS-CD) | 2.5 |
| NcoI | 1 |
| BamHI | 1 |
| Nuclease free water | 40.5 |
| **Total volume** | **50** |

| Components | Volume (µl) |
|---|---|
| 10X CutSmart® buffer | 5 |
| PCR product (122 ng/µl EcZraS-$CD_{trunc}$) | 8.2 |
| NcoI | 1 |
| BamHI | 1 |
| Nuclease free water | 34.8 |
| **Total volume** | **50** |

**Table 2.1.1.5 Reaction mixture for restriction digestion of native pNIC28Bsa4**

| Components | Volume (µl) |
|---|---|
| 10X CutSmart® buffer | 5 |
| 250ng/µl Native pNIC28Bsa4 | 5 |
| NcoI | 1 |
| BamHI | 1 |
| Nuclease free water | 38 |
| **Total volume** | **50** |

**Table 2.1.1.6 Ligation mixture for digested EcZraS-CD and EcZraS-CD$_{trunc}$ and pNIC28Bsa4**

| Components | Volume (µl) |
|---|---|
| 2X Quick ligase buffer | 5 |
| Plasmid vector (6 ng/µl pNIC28Bsa4) | 5 |
| Gene (30 ng/µl EcZraS-CD) | 2 |
| Quick ligase | 1 |
| Nuclease free water | 2 |
| **Total volume** | **15** |

| Components | Volume (µl) |
|---|---|
| 2X Quick ligase buffer | 5 |
| Plasmid vector (6 ng/µl pNIC28Bsa4) | 5 |
| Gene (20 ng/µl EcZraS-CD$_{trunc}$) | 2 |
| Quick ligase | 1 |
| Nuclease free water | 2 |
| **Total volume** | **15** |

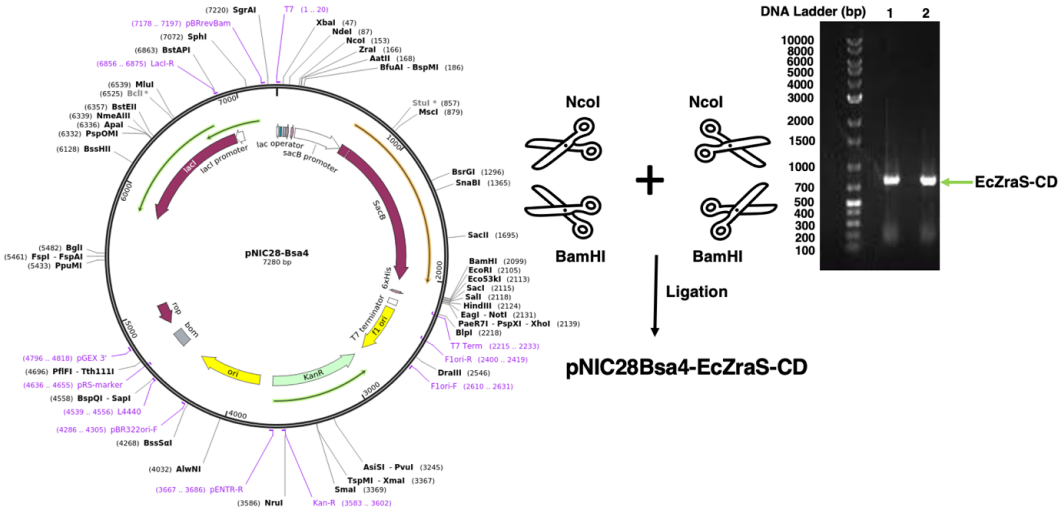

**Figure 2.1.1.1 An overview of the process of gene (EcZraS-CD ~723 bp) insertion into the vector pNIC28Bsa4 (~5334 bp).** Insertion of EcZraS-CD gene into pNIC28Bsa4 required restriction digestion of both the gene and plasmid vector using restriction enzymes followed by ligation. The agarose gel shows the PCR product of EcZraS-CD.

### 2.1.2 Overexpression of the truncated cytoplasmic domains EcZraS-CD and EcZraS-$CD_{trunc}$

Bacterial cultures in a small-scale setup were induced with various concentrations of Isopropyl β- d-1-thiogalactopyranoside (IPTG), post-induction temperatures and OD600 values to optimize the conditions required for protein overexpression. The optimized conditions were then used to scale up the expression required for protein purification. Protocols used for the overexpression and purification of EcZraS-CD and EcZraS-$CD_{trunc}$ were similar. Hence, only EcZraS-CD has been shown.

The steps taken to perform this optimization are as follows:

- 0.5 µl of plasmids for EcZraS-CD and EcZraS-$CD_{trunc}$ were transformed into 50 µl of chemically competent *E. coli* LEMO21(DE3) using the heat-shock method. The chemically competent cells were prepared using the $CaCl_2$-$MgCl_2$ method. Around 750 µl of LB broth was added to the transformed cells and grown for 1 hour in a shaker incubator at 37 ºC and 220 rpm.
- The cells were then harvested by centrifugation at 5000 rpm for 5 minutes and excess broth of nearly 700 µl discarded. The cell pellets obtained were resuspended in the remaining 50 µl of residual broth and spread on Kanamycin + Chloramphenicol-LB Agar plates. It was then incubated overnight at 37 ºC to allow growth of bacterial colonies.

- Bacterial colonies were obtained on the plates after overnight incubation. Each plate was used for picking single isolated colonies and inoculated into 2 ml of LB broth supplemented with 2 µl of Kanamycin (50 mg/ml in autoclaved Milli-Q® water) and 2 µl of Chloramphenicol (25 mg/ml in 100 % ethanol). The colony inoculated broth known as primary culture was incubated overnight in a shaker incubator at 37 ºC and 220 rpm.
- Following 16 hours of growth, around 1 % of the primary culture (500 µl) was used to inoculate two separate bacterial culture flasks containing 50 ml LB broth each, supplemented with 50 µl of Kanamycin and 50 µl of Chloramphenicol.
- The secondary cultures of 50 ml each were incubated in a shaker incubator at 37 ºC and 220 rpm. The $OD_{600}$ was measured at intervals of 1 hour and then after every 30 minutes until the flasks reached the desired OD values of 0.6 in one and 0.8 in another. The flasks were immediately placed on ice bath to avoid any abrupt change in OD values and retard bacterial growth.
- From each 50 ml culture, aliquots of 2 ml each were prepared and labelled as 0.6 UI (uninduced 18 ºC), 0.6 I (0.5 mM IPTG 18 ºC) , 0.6 I (1mM IPTG 18 ºC), 0.6 UI (uninduced 37 ºC), 0.6 I (0.5 mM IPTG 37 ºC) , 0.6 I (1mM IPTG 37 ºC), 0.8 UI (uninduced 18 ºC), 0.8 I (0.5 mM IPTG 18 ºC) , 0.8 I (1mM IPTG 18 ºC), 0.8 UI (uninduced 37 ºC), 0.8 I (0.5 mM IPTG 37 ºC) and 0.8 I (1mM IPTG 37 ºC).
- Except the UI aliquots, all the others were induced at specific IPTG concentrations and placed in the mentioned post induction temperatures. Both the UI and I cultures were allowed to grow for 4 hours at 37 ºC and 16 hours at 18 ºC and 220 rpm.

- The cells in the aliquots were harvested by centrifugation at 5000 rpm for 5 minutes, resuspended in 20 µl of 2X Laemmli's buffer used for sodium dodecyl sulphate-polyacrylamide gel electrophoresis (SDS-PAGE) and heated at 95 ºC for 5 minutes.
- The cell pellet and dye mixture was vortex and heated multiple times to reduce sample viscosity and loaded into the wells of a 12 % SDS-PAGE gel.
- The gel was run up to completion to resolve the constituent protein bands and stained using a staining solution containing Coomassie Brilliant Blue R-250. Based on the results obtained the cultures were scaled up for protein purification using the following condition - 0.8 $OD_{600}$, 0.5 mM IPTG and 18 ºC or 0.8 $OD_{600}$, 0.5 mM IPTG and 37 ºC temperature post-induction **(Figure 2.1.2.1).**

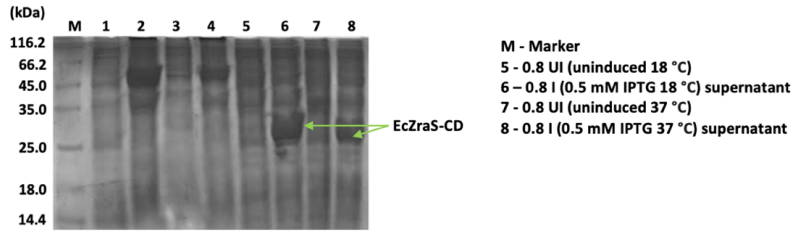


**Figure 2.1.2.1 Overexpression of the truncated cytoplasmic domain EcZraS-CD**. The SDS-PAGE gel shows overexpression profiles of EcZraS-CD at varying temperatures and 0.5mM IPTG concentration at 0.8 $OD_{600}$ as labelled.

## 2.2 Protein purification of EcZraS-CD and EcZraS-$CD_{trunc}$ using affinity chromatography, 6X-His tag removal and size exclusion chromatography.

Poly-histidine tags such as 6X-His tags at the N and C-terminus of a recombinantly expressed protein can facilitate protein purification by using methods of affinity chromatography such as Immobilized Metal Anion Chromatography (IMAC). The plasmid vector pNIC28-Bsa4 used

for the study is a derivative of the commonly used pET28a(+) plasmid, capable of recombinant protein expression, conjugated with a 6X-His tag. EcZraS-CD and EcZraS-$CD_{trunc}$ when overexpressed, are fused with a 6X-His tag towards their N-terminal region, interspersed by a tobacco etch virus (TEV) protease cleavage site. Both EcZraS-CD and EcZraS-$CD_{trunc}$ were purified by a common protocol using a combination of affinity chromatography, 6X-His tag removal and size exclusion chromatography **(Figure 2.2.1).**

### 2.2.1 Affinity chromatography

#### 2.2.1.1 Protein extraction and lysate preparation

Large-scale protein overexpression was carried out using 800 ml of LB broth supplemented with Kanamycin and Chloramphenicol as per the optimised overexpression conditions, and pellets were stored at -80 ºC till further use.

- The protein in the induced pellets was extracted using a combination of mechanical and chemical lysis. The stored pellets were allowed to thaw on ice before protein extraction and purification.
- They were then dissolved in 50 ml hypertonic buffer solution (lysis buffer) containing a final concentration of 1 mM phenylmethanesulfonyl fluoride (PMSF) and 1 mg/ml lysozyme.
- The homogenised suspension of pellet in lysis buffer (100 mM Tris pH 8.0, 500 mM NaCl, 10 % glycerol, and 20 mM imidazole) was subjected to ultra-sonication using a sonicator probe. The sonicator was programmed to operate at an amplitude of 35 %, 15 secs ON & 30 secs OFF cycle for a duration of 25 minutes. The suspension was placed in an ice bath to prevent thermal degradation of the protein during the process.

- The clarified suspension obtained after sonication was subjected to centrifugation at 14000 rpm (23,447 g) for 1 hour at 4 ºC. The presence of a blackish-brown streak in the resulting cell pellet confirmed successful ultrasonication. The supernatant containing protein of interest was decanted from the centrifuged suspension, filtered using a 0.45 µ syringe filter and used for IMAC purification.

**2.2.1.2 IMAC purification using Ni-NTA column**

IMAC purification was carried out using HisTrap FF 5ml columns containing Ni-NTA resin in Fast Protein Liquid Chromatography (FPLC). The nickel ion in the resin binds 6X-His tag, selectively allowing purification of the desired protein. The procedure used for IMAC purification as follows:

- The HisTrap FF 5 ml column was washed with 10 CV of autoclaved Milli-Q® water at a flowrate of 2.5 ml/min to remove resin preservatives such as ethanol and sodium azide, followed by equilibration with 10 CV buffer A (25 mM Tris pH 8.0, 200 mM NaCl, 5 % glycerol, and 20 mM imidazole) at a flowrate of 2.5 ml/min. Autozero of the detector was performed during the equilibration step.
- The supernatant was slowly passed through the column for effective binding at a flowrate of 1 ml/min. The column was then washed with 20-30 CV of buffer A to remove unbound proteins and other impurities at a flowrate of 2.5 ml/min.
- Finally the protein was eluted using a flowrate of 2.5 ml/min and collected in fractions of 4 ml by mixing buffer A (25 mM Tris pH 8.0, 200 mM NaCl, 5 % glycerol, and 20 mM imidazole) and buffer B (25 mM Tris pH 8.0, 200 mM NaCl, 5 % glycerol and 1 M imidazole) to form step gradients (75 mM, 100 mM, 200 mM, 250 mM) and a linear gradient (250 mM-1 M) of imidazole.

- 10 µl of the eluted fractions were mixed with 10 µl of 2X Laemmli's buffer and heated at 95 ºC for 5 minutes. A 12 % SDS-PAGE of eluted fractions and a molecular weight marker was performed to visualise the presence of the desired protein. The desired protein was obtained in fractions eluted between 200-300 mM imidazole concentration.

**2.2.1.3 Desalting and buffer exchange**

Imidazole is a crucial component during the IMAC method of protein purification, but can disrupt the structural integrity of the proteins and render them unfit for use in crystallization trials and functional studies. To alleviate the adverse effect of this salt, buffer exchange or desalting of the protein was performed by the process dialysis. In this process, the imidazole in the protein sample diffuses across the dialyzing membrane from a region of higher concentration (inside the dialysis membrane) to the region of lower concentration (surrounding buffer). The steps involved in buffer exchange as follows:

- The fractions containing the desired protein were clubbed and sealed inside the dialyzing membrane, having a cut-off of 3 kDa. The sealed dialysing membrane with the protein was then placed in a 2 L container with buffer C (50 mM Tris pH 8.0, 200 mM NaCl, 2 mM BME).
- A magnetic bead was dropped into the container, and the whole setup was placed over a magnetic stirrer at 90 rpm in a cold room. The buffer exchange was performed overnight, after which the protein was transferred to a falcon tube and stored at 4 ºC. An alternative process of desalting can be performed using the HiPrep 26/10 desalting column in FPLC.

**2.2.2 6X-His tag removal using tobacco etch virus (TEV) protease**

The process of His tag removal, though not crucial in most cases, can sometimes interfere with crystallization and biochemical assays involving metals. As we were unable to obtain protein

crystals of diffraction quality with the N-terminal 6X-His tag, the tag was removed by incubating the protein with TEV protease after IMAC purification. This was carried out either during the process of dialysis or after the buffer was exchanged. During the process of dialysis, the protease could be added along with the protein into the dialyzing membrane that facilitated tag cleavage overnight. This served a dual function of desalting as well as tag cleavage. The protocol for tag removal as follows:

- The mixture (tagged protein, tagless protein, 6X-His tag and TEV protease) within the dialysing membrane was transferred into a falcon tube after overnight incubation and stored at 4 ºC.
- To separate the tagless protein, the mixture was subjected to IMAC purification using the HisTrap FF 5ml. The column was washed with 10 CV autoclaved Milli-Q® water followed by equilibration with buffer C (50 mM Tris pH 8.0, 200 mM NaCl, 2 mM BME) at a flowrate of 2.5 ml/min.
- The mixture was then passed through the column at a flowrate of 1.5 ml/min, allowing the tagged protein, 6X-His tag and TEV protease containing poly-His residues to bind onto the column. The unbound tagless protein was collected from the flowthrough.
- The flowthrough was concentrated up to 5mg/ml using an ultra-centrifugal filter (cut off 3KDa) and stored at 4 ºC.

**2.2.3 Size exclusion chromatography (SEC)**

To obtain ultra-pure protein for crystallization and biochemical assays, we performed size exclusion chromatography, a technique that separates proteins on the basis of their molecular weight. A persistently faint upper band present in the concentrated fraction of tagless protein was removed in this step.

- SEC was performed in FPLC using the Hi-Load 16/600 Superdex 75 pg column. The column was washed with 4 CV autoclaved Milli-Q® water at a flowrate of 0.8 ml/min to remove resin preservatives such as ethanol and sodium acetate.
- The column was then pre-equilibrated with buffer D (20 mM Tris pH 8.0 and 150 mM NaCl), followed by injection of the concentrated tagless protein. After injection, 1.5 CV of buffer D was passed through the column, and fractions containing protein were collected. Two peaks observed at $A_{280}$ were collected and confirmed using 12 % SDS-PAGE.
- Protein fractions obtained for the higher peak were pooled and concentrated up to 10 mg/ml before screening conditions amenable to crystallization.

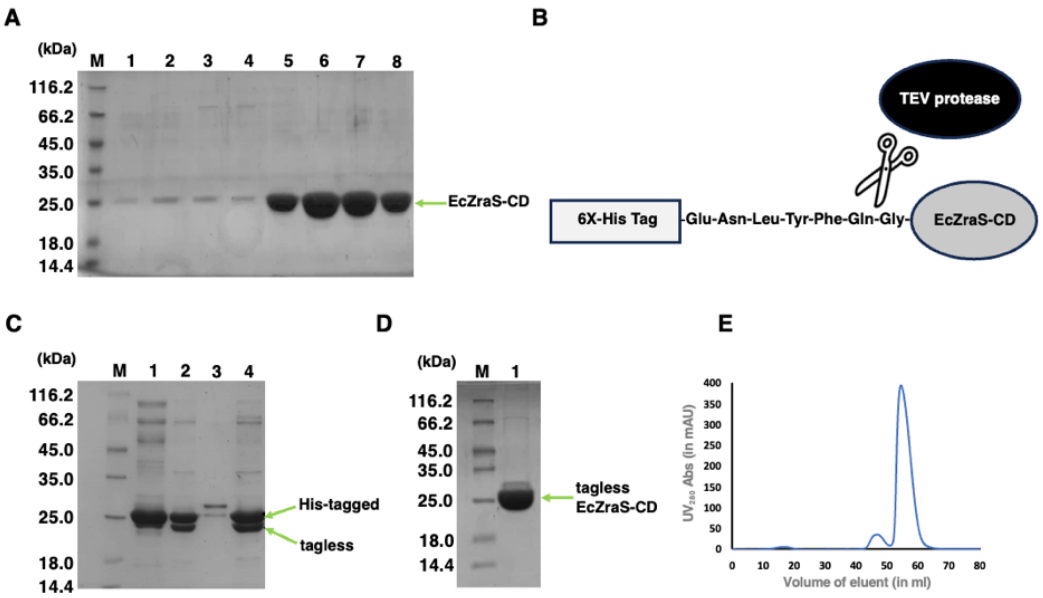


**Figure 2.2.1 An overview of the process of protein purification of EcZraS-CD.** (A) The SDS-PAGE gel shows M, protein marker and 1-8, elution fractions obtained during Ni-NTA chromatography. (B) Schematic representation of the TEC cleavage site between the 6X-His tag and EcZraS-CD. (C) The SDS-PAGE gel shows M, protein marker; 1, concentrated Ni-NTA fraction of EcZraS-CD; 2 and 4, reaction mixture with tagged and tagless EcZraS-CD

and 3, Purified TEV protease used for cleavage reaction setup. (D) The SDS-PAGE gel shows the concentrated protein obtained from peak 2 during SEC. (E) Chromatogram of tagless EcZraS-CD obtained during SEC.

## 2.3 Crystallization of EcZraS-CD and EcZraS-CD$_{trunc}$

Screening for crystallization conditions was performed for His-tagged EcZraS-CD and EcZraS-CD$_{trunc}$ by setting up random trials in commercially available conditions, with protein concentrations ranging 5-10 mg/ml. No crystals were observed for the apo proteins, following which they were incubated with ATP and its analogs to facilitate crystallization. Small microcrystals were obtained that could not be optimised further to obtain diffraction-quality crystals. Hence, optimisation was carried out by cleaving off the N-terminus His tag and re-screening for crystallization. Apo form of the tagless protein was also found to be unamenable to crystallization. The conditions were screened for the tagless protein incubated with ATP and its analogs.

### 2.3.1 Crystallization of EcZraS-CD with ATP and $MgCl_2$

Diffraction quality crystals for EcZraS-CD with 1 mM ATP and 5 mM $MgCl_2$ (incubated for 2 hours before setting up crystallization trials) were obtained in the conditions 0.2 M Ammonium sulfate, 0.1 M HEPES 7.5 or 0.1 M Tris 8.5 and 25 % PEG 3350 (HAMPTON Index HT) after 2 months. The resolution obtained was not good enough for structure solution. To optimise the condition, handmade crystallization grids and additives (HAMPTON Additive screen) were used. The grids were prepared with varying concentrations of ammonium sulphate and PEG, and pH values using Tris 7.0-8.5. The crystals used for final diffraction were obtained in the condition 0.2 M ammonium sulphate, 0.1 M Tris pH 8.5, and 25 % PEG 3350 with

additives sodium citrate and cadmium chloride **(Figure 2.3.1.1)**. The crystals were obtained in a period of 1 to 6 months duration.

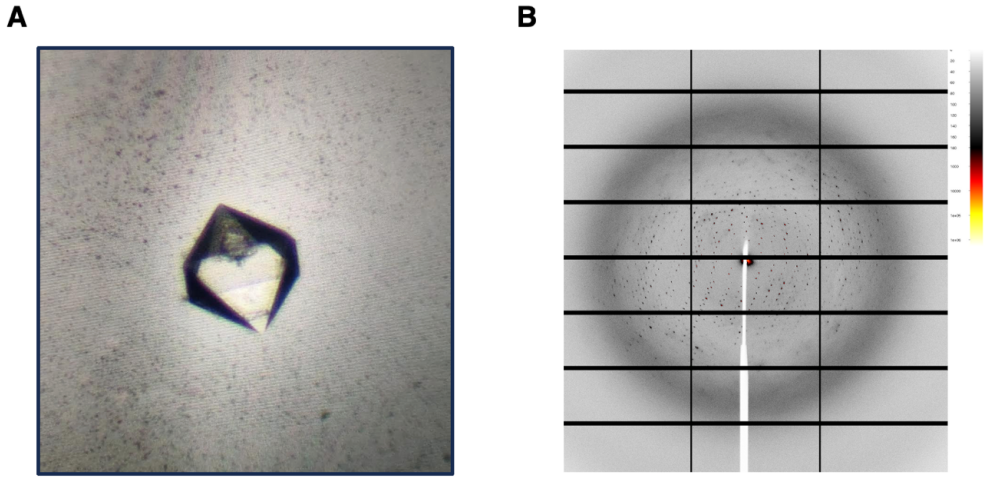


**Figure 2.3.1.1 Crystal and diffraction pattern of EcZraS-CD incubated with ANP and $MgCl_2$.** (A) Crystal of EcZraS-CD incubated with ATP and $MgCl_2$ used for data collection. (B) Image showing diffraction spots for the corresponding crystal of ATP-bound EcZraS-CD.

### 2.3.2 Crystallization of EcZraS-CD with ANP and $MgCl_2$

The non-hydrolyzable analogs of ATP, ANP and ACP are commonly used to help trap kinases in their final autophosphorylation or Michaelis state. Crystallization trials for ANP bound form of the protein with 2 mM ATP and 4 mM $MgCl_2$ (incubated for 4 hours before setting up crystallization trials) were carried out using HAMPTON Index HT. The condition 0.2 M Ammonium sulfate, 0.1 M Tris 8.5 and 25 % PEG 3350 yielded microcrystals which were optimised further using handmade grids with sodium malonate, sodium citrate and potassium sodium tartarate as additives. However, the presence of fused multi-crystals was found during diffraction studies and is being optimized further for data collection **(Figure 2.3.2.1).**

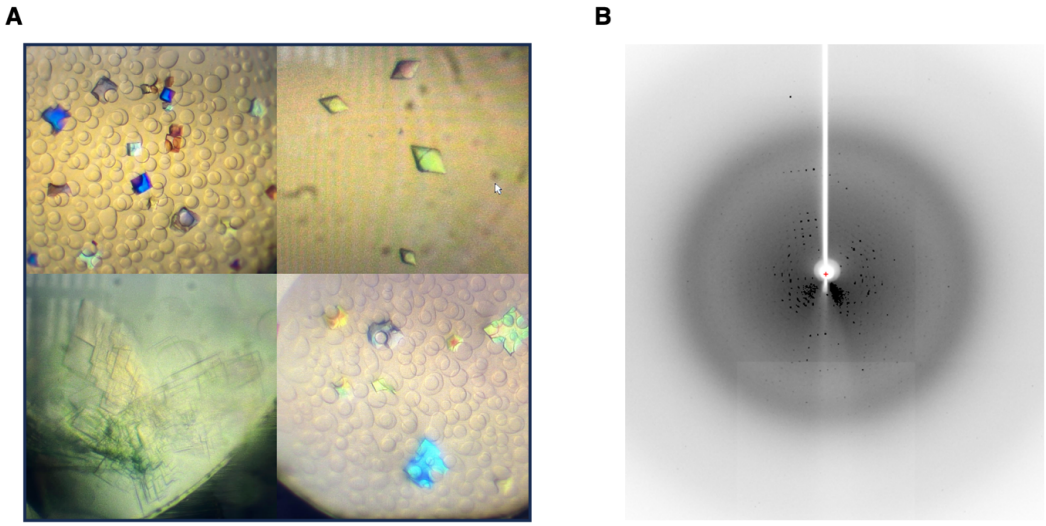


**Figure 2.3.2.1 Crystals and diffraction pattern of EcZraS-CD incubated with ANP and $MgCl_2$.** (A) Crystal obtained in different conditions for EcZraS-CD with ANP and $MgCl_2$ to trap it in Michaelis state. (B) Image showing diffraction spots for a crystal of ANP bound EcZraS-CD.

## 2.4 X-ray diffraction data collection, data processing, structure solution, and refinement

The crystals obtained were briefly soaked in the cryoprotectant (20 % ethylene glycol diluted with the mother liquor) and flash frozen with liquid nitrogen. The initial crystals yielding low-resolution data were diffracted at the NISER home source (BRUKER-PROTEUM X-ray diffractometer), Bhubaneswar. The data collection for the optimised crystals was performed at the European Synchrotron Radiation Facility, Grenoble, at the beamline ID30A. The data collection was carried out with the centered crystal under a stream of liquid nitrogen at a temperature of 100 K to avoid radiation damage and crystal killing.

Multiple crystals were screened for diffraction quality and well-diffracting ones were used for the determination of unit cell parameters. Data collection was carried out for multiple crystals of EcZraS-CD. The maximum recorded resolution for diffraction was 2.49 Å. The raw data images were processed using the X-ray detector software (XDS) (Kabsch, 2010b). Images obtained from data sets were used to harvest for reflection spots (spot finding). The reflection spots were then indexed to determine the unit cell parameters and estimate the type of Bravais lattice (indexing). The reflection spot intensities were determined by profile fitting (integration). The datasets from multiple crystals were scaled using XSCALE (scaling) and assigned space group (space group assignment) (Kabsch, 2010b, 2010a). The data quality was checked and a final scaled and merged output was obtained.

The structure determination was performed by molecular replacement (MR) using PHASER (CCP4 suite), with a poly-Ala model of the AlphaFold-generated CA domain of ZraS as the search template (Jumper et al., 2021; McCoy et al., 2007). The remaining regions of the structure were built manually in Coot, and the resulting model was subsequently subjected to iterative model building and refinement. Refinement was carried out using Phenix (Adams et al., 2010; Emsley & Cowtan, 2004). Refinement strategies included the use of simulated annealing, rigid body, TLS, ADP and real-space refinements. The ligands were placed after tracing the mainchains and sidechains of the protein molecules in the asymmetric unit using the $2F_o$-$F_{calc}$ map. The iterative building and refinement continued until refinement parameters $R_{work}$ converged with $R_{free}$. The workflow has been summarised in **Figure 2.4.1.**

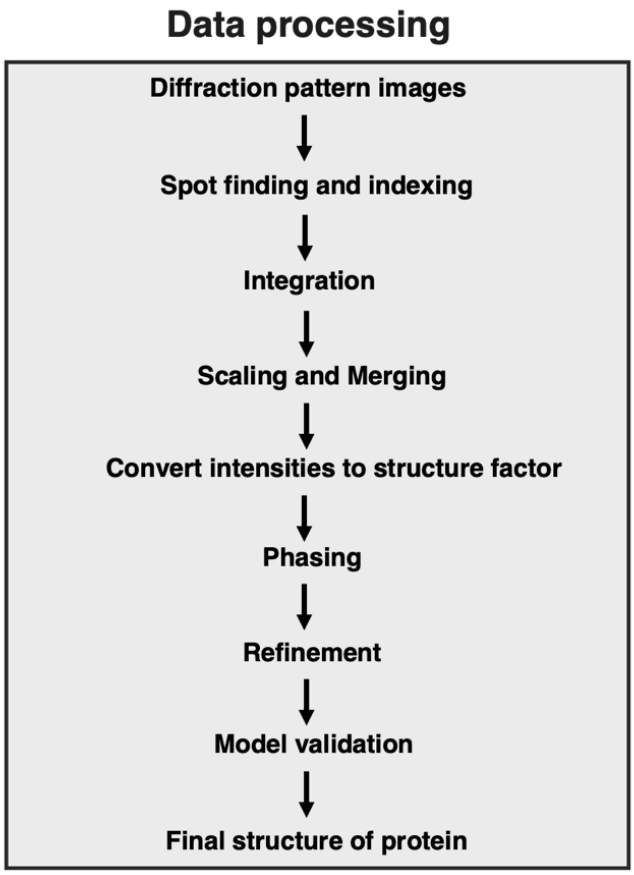


**Figure 2.4.1 An overview of the steps involved in data processing.**

## 2.5 Enzyme kinetics of EcZraS-CD using pyruvate kinase-lactate dehydrogenase (PK-LDH) assay

The study of enzyme kinetics is essential to understand the rate of an enzyme-catalyzed reaction. It aids in our understanding of enzyme function and regulation. The autophosphorylation and phosphatase activity of EcZraS-CD were estimated using a pyruvate kinase-lactate dehydrogenase (PK-LDH) coupled assay. As the detection of ATP or ADP is not feasible spectrophotometrically, this assay couples it with the conversion of Nicotinamide dinucleotide hydrogen (NADH) to Nicotinamide dinucleotide (NAD) in the presence of 2-

phophoenolpyruvate (PEP). NADH has a strong absorbance peak at 340 nm, and the conversion of ATP when coupled with the NADH conversion can be visualised as a gradual decrease in absorbance at 340 nm values. The conversion of ATP to ADP was estimated for EcZraS-CD at varying concentrations of ATP over a time frame to determine its enzyme activity. The protocol used for the coupled assay as follows:

- The tagless protein obtained during SEC was buffer exchanged to 20 mM HEPES 8.0 and 150 mM NaCl using an ultra-centrifugal filter (cut off 3 kDa).
- The reaction mixture for enzyme kinetics was prepared with 145 mM $KCH_3CO_2$, 8 mM $MgCl_2$, 2 mM PEP, 0.16 mM NADH, 4.8 units of PK, 8.1 units of LDH in 50 mM HEPES 8.0. 100X stock of NADH and PEP were prepared fresh before every reaction as mentioned by Lindsley et al. (Lindsley, 2001).
- 100 mM stock of ATP was prepared in 10 mM Tris (9.0). The reaction mixture and NADH was stored in amber coloured containers and removed from 4 ºC only before use.
- The reaction mixture, along with ATP in concentrations of 12.5, 25, 50, 100, 250, 500, 750, 1000 µM were incubated at 25 ºC to allow conversion of ADP contaminants back into ATP.
- Post incubation for 30 mins, the reactions were initiated by the addition of EcZraS-CD to a final concentration of 15 µM. Three sets of the reactions were set up for the mentioned concentrations of ATP against a blank that lacked protein in each case, and absorbance at 340 nm was measured at intervals of 75 seconds for 20 minutes.
- The rate of ATP hydrolysis was calculated using the formula mentioned below, and a plot was made using Graphpad Prism 5.

$$\textbf{Rate of ATP hydrolysis} = \frac{\Delta\,(\textbf{ADP})}{\textbf{Time}} = \frac{\Delta(\textbf{Absorbance at 340 nm})/\Delta\textbf{Time}}{(\textbf{cuvette pathlength in cm})(6.22\ \textbf{mM}^{-1}/\textbf{cm})}$$

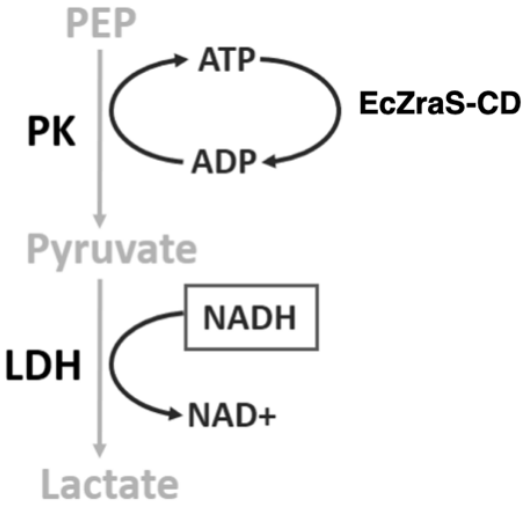


**Figure 2.5.1 Schematic representation of the PK-LDH coupled assay system.** The flow diagram shows the coupling of ATP conversion with the oxidation of NADH during the assay.

## 2.6 Cloning and overexpression of the truncated periplasmic domains of ZraS (EcZraS-SD) and its loop variants (loop 2, loop 3, loop 4 and loop 5)

### 2.6.1 Cloning of the truncated periplasmic domain EcZraS-SD

The truncated periplasmic domain ranging Arg36-Arg199 (EcZraS-SD) was cloned into the plasmid vector pNIC28-Bsa4 with restriction sites NcoI and XhoI. Two sets of forward primer 5'-3' ATATATCCATGGCGCGTGATTATGGGCGGGCAA and reverse primer 3'-5' TATATCTCGAGTCAGCGCTTTTCCCCACTCTGGG were used for molecular cloning. The step-wise protocol was similar to EcZraS-CD as mentioned in section 2.1.1, with changes in the thermocycling conditions, reaction mixtures and restriction enzymes used. The thermocycling conditions and reaction mixtures are mentioned in **Tables 2.6.1.1, 2.6.1.2, 2.6.1.3, 2.6.1.4, 2.6.1.5 and 2.6.1.6. Figure 2.6.1.1** shows the PCR product of EcZraS-SD. The restriction enzymes used were NcoI and XhoI instead of NcoI and BamHI for EcZraS-SD**.**

**Table 2.6.1.1 Primer details for EcZraS-SD**

| Name | Sequence | Length (bp) | GC (%) | Tm (°C) |
|---|---|---|---|---|
| EcZraS-SD forward | 5'ATATATCCATGGCGCGTGATTATGGGCGGGCAAG 3' | 34 | 53 | 78 |
| EcZraS-SD reverse | 3' TATATCTCGAGTCAGCGCTTTTCCCCACTCTGGG 5' | 34 | 53 | 77 |

**Table 2.6.1.2 PCR reaction mixture for EcZraS-SD**

| Components | Volume (µl) |
|---|---|
| 5X Q5 reaction buffer | 10 |
| 10 mM dNTPs | 1 |
| 10 uM forward primer | 2.5 |
| 10 uM reverse primer | 2.5 |
| Template DNA (50 ng/µl EcZraS-SD) | 2.5 |
| Q5 DNA polymerase | 0.5 |
| Nuclease free water | 31 |
| **Total volume** | **50** |

**Table 2.6.1.3 Thermocycling conditions for EcZraS-SD**

| Step | Temperature (°C) | Duration (min) |
|---|---|---|
| Initial denaturation | 98 | 0:30 |
| 32 cycles | 98 | 0:15 |
| | 71 | 0:30 |
| | 72 | 2:50 |
| Final extension | 72 | 2:00 |
| Hold | 4 | ∞ |

**Table 2.6.1.4 Reaction mixture for restriction digestion of EcZraS-SD**

| Components | Volume (µl) |
|---|---|
| 10X CutSmart® buffer | 5 |
| PCR product (500 ng/µl EcZraS-SD) | 2 |
| NcoI | 1 |
| XhoI | 1 |
| Nuclease free water | 41 |
| **Total volume** | **50** |

**Table 2.6.1.5 Reaction mixture for restriction digestion of native pNIC28Bsa4**

| Components | Volume (µl) |
|---|---|
| 10X CutSmart® buffer | 5 |
| 100 ng/µl Native pNIC28Bsa4 | 10 |
| NcoI | 1 |
| XhoI | 1 |
| Nuclease free water | 33 |
| **Total volume** | **50** |

**Table 2.6.1.6 Ligation mixture for digested EcZraS-SD and pNIC28Bsa4**

| Components | Volume (µl) |
|---|---|
| 2X Quick Ligase buffer | 10 |
| Vector (18.5 ng/µl pNIC28Bsa4) | 3 |
| Gene (55.8 ng/µl EcZraS-SD) | 0.45 |
| Quick ligase | 1 |
| Nuclease free water | 5.55 |
| **Total volume** | **20** |

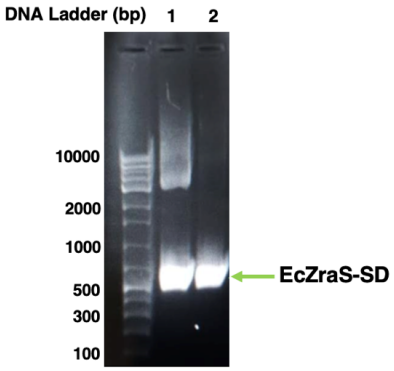


**Figure 2.6.1.1 Agarose gel electrophoresis of the PCR product (~500 bp) of EcZraS-SD.** The lanes 1 and 2 show PCR product obtained for EcZraS-SD.

### 2.6.2 Cloning of the loop variants of EcZraS-SD

The purified protein obtained for EcZraS-SD was observed to be highly unstable. As efforts to stabilise the protein made no difference, the reason behind this instability was explored. Structural superposition of an AlphaFold model of EcZraS-SD with crystal structures of periplasmic domains as templates having similar structural folds was performed (Bittrich et al., 2024; Jumper et al., 2021). The region spanning Phe150-Gln179 was found to form a long loop, absent in other domains **(Figure 2.6.2.1)**. Hence, clones with truncations in the loop region of EcZraS-SD - loop 2, loop 3, loop 4 and loop 5 were designed as shown in **Table 2.6.2.1.**

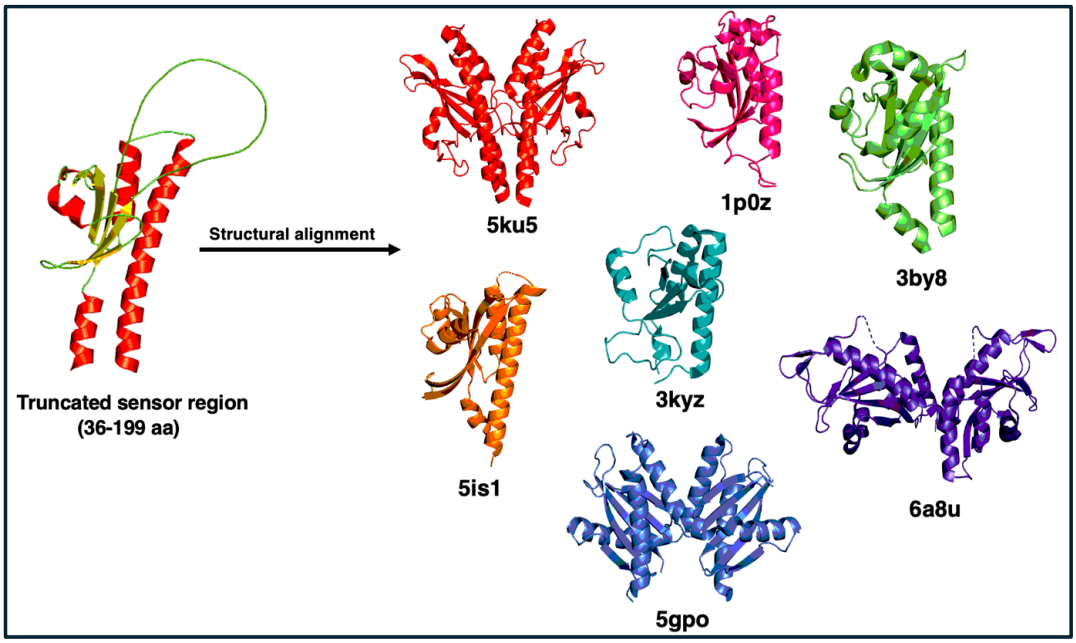


**Figure 2.6.2.1 Representation showing the periplasmic domains used for structural overlap with EcZraS-SD to design the loop truncations.**

**Table 2.6.2.1 Loop variants designed by structural superposition with known sensor templates of similar folds**

| Variant | Sensor | PDB | Truncation | Sequence of loop |
|---|---|---|---|---|
| EcZraS-SD | - | - | - | FQPMSAPWRHGMHNMPRCNGKAVPQVDAQQ |
| Loop 2 | CusS | 5ku5 | S154-V172 | FQPM PQVDAQQ |
| Loop 3 | CitA | 1p0z | P156-V175 | FQPMSA DAQQ |
| Loop 4 | YycG | 5is1 | A155-V175 | FQPMS DAQQ |
| Loop 5 | CzcS | 5gpo | S154-Q174 | FQPM VDAQQ |

The clones of loop 2, loop 3, loop 4 and loop 5 were produced using deletion PCR. Two sets of primers, forward 5'-3' and reverse primers 3'-5', were designed to flank the region to be deleted **(Figure 2.6.2.2 A and Table 2.6.2.2).** The clone of EcZraS-SD was used as template DNA. The thermocycling conditions and reaction mixtures are mentioned in **Tables 2.6.2.3, 2.6.2.4, 2.6.2.5 and 2.6.2.6.**

- Following PCR, 5 µl of the products were run on 1 % agarose gel for visual confirmation of the process **(Figure 2.6.2.2 B).** 45 µl of the remaining products were incubated with 1 µl of DpnI enzyme for 1 hour at 37 ºC on a dry bath to get rid of the parental DNA strands. DpnI was deactivated by heating the mixture at 80 ºC for 20 minutes.
- The mixtures were purified using the PCR purification kit from Qiagen. The DNA obtained were quantified using a Nanodrop and used for 5' end phosphorylation with T4 polynucleotide kinase (T4 PNK) from NEB.
- After preparation of the phosphorylation mixes, the reactions were incubated for 1 hour at 37 ºC on a dry bath. The T4 PNK was heat-deactivated at 65 ºC for 20 minutes to stop the reaction, and PCR purification was performed using the kit method used previously.
- The concentration of phosphorylated DNA for each loop variant was estimated using a Nanodrop, and 100 ng from each was used for ligation. The ligation mixture was prepared and incubated at 25 ºC for 30 minutes, and transformed into *E. coli* DH5α cells.
- Single colonies were picked for plasmid isolation using the miniprep kit from Qiagen and confirmed for deletion by Sanger's sequencing.

**Table 2.6.2.2 Primer details for the loop variants of EcZraS-SD**

| Name | Sequence | Length (bp) | GC (%) | Tm (ºC) |
|---|---|---|---|---|
| Loop 2 forward | 5' CCACAAGTAGATGCACAACAGGC 3' | 23 | 52 | 69 |
| Loop 2 reverse | 3' CATTGGCTGGAACAAACGATAGACC 5' | 25 | 48 | 68 |
| Loop 3 forward | 5' GATGCACAACAGGCTATTTTTATCGCCG 3' | 28 | 46 | 70 |
| Loop 3 reverse | 3' CGCTGACATTGGCTGGAACAAACG 5' | 24 | 54 | 71 |
| Loop 4 forward | 5' GATGCACAACAGGCTATTTTTATCGCCG 3' | 28 | 46 | 70 |

| | | | | |
|---|---|---|---|---|
| Loop 4 reverse | 3’ TGACATTGGCTGGAACAAACGATAGACC 5’ | 28 | 46 | 71 |
| Loop 5 forward | 5’ GTAGATGCACAACAGGCTATTTTTATCGC 3’ | 29 | 41 | 68 |
| Loop 5 reverse | 3’ CATTGGCTGGAACAAACGATAGACC 5’ | 25 | 48 | 68 |

**Table 2.6.2.3 PCR reaction mixture for the loop variants of EcZraS-SD**

| **Components** | **Volume (µl)** |
|---|---|
| 5X Q5 reaction buffer | 10 |
| 10 mM dNTPs | 1 |
| 10 uM forward primer | 2.5 |
| 10 uM reverse primer | 2.5 |
| Template DNA (50 ng/µl EcZraS-SD) | 2.5 |
| Q5 DNA polymerase | 0.5 |
| Nuclease free water | 31 |
| **Total volume** | **50** |

**Table 2.6.2.4 Thermocycling conditions for the loop variants of EcZraS-SD**

| **Step** | **Temperature (ºC)** | **Duration (min)** |
|---|---|---|
| Initial denaturation | 98 | 0:30 |
| 25 cycles | 98 | 0:15 |
| | 69-70 | 0:30 |
| | 72 | 4:20 |
| Final extension | 72 | 2:00 |
| Hold | 4 | ∞ |

**Table 2.6.2.5 5' end phosphorylation mixture of the loop variants of EcZraS-SD**

| Components | Volume (Concentration) |
|---|---|
| T4 PNK | 1 µl (10 units) |
| 10X T4 PNK buffer | 5 µl (1X) |
| 10 mM ATP | 5 µl (1 mM) |
| PCR product (loop variants) | (1-2 µg) |
| Nuclease free water | To make volume up to 50 µl |
| **Total volume** | **50** |

**Table 2.6.2.6 Ligation mixture for the loop variants of EcZraS-SD**

| Components | Volume (Concentration) |
|---|---|
| 2X Quick Ligase buffer | 10 µl (1X) |
| 5' end phosphorylated product (loop variants) | 100 ng |
| Quick Ligase | 1 µl |
| Nuclease free water | To make volume up to 20 µl |
| **Total volume** | **20** |

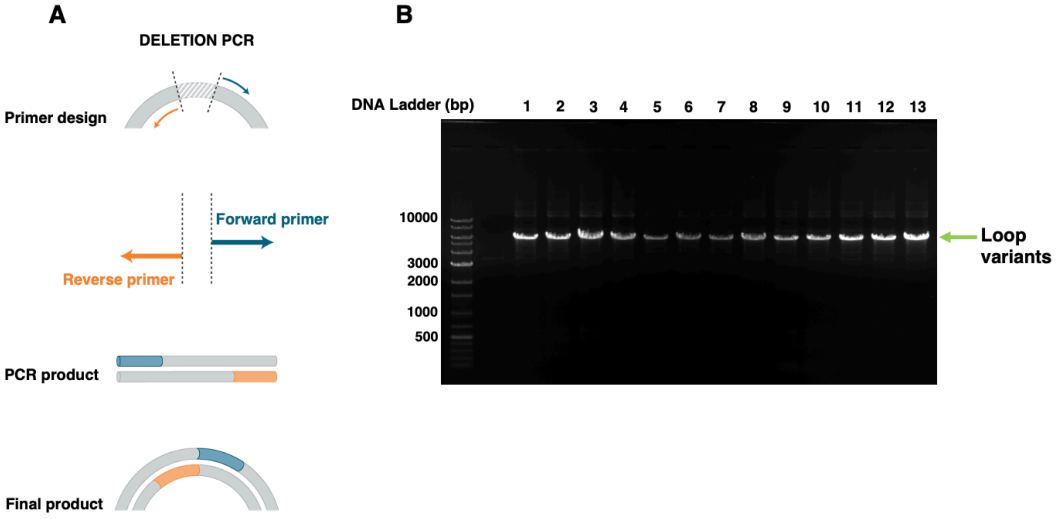


**Figure 2.6.2.2 Primer designing for deletion PCR and agarose gel electrophoresis of the PCR product of the loop variants of EcZraS-SD.** (A) The primers designed for deletion PCR

binds to the region flanking the region chosen for deletion. (B) The agarose gel shows the PCR products of the loop variants of EcZraS-SD. The wells 1-4 show PCR product obtained for loop 2 at annealing temperatures 65.5 ºC, 67 ºC, 69.6 ºC and 72 ºC. Wells 5-7 show PCR product obtained for loop 3 at annealing temperatures 68.1 ºC, 70.8 ºC and 72 ºC. Wells 8-10 show PCR product obtained for loop 4 at annealing temperatures 68.1 ºC, 70.8 ºC and 72 ºC. Wells 11-13 show PCR product obtained for loop 5 at annealing temperatures 67 ºC, 68.1 ºC and 69.6 ºC.

### 2.6.3 Overexpression of the truncated periplasmic domain EcZraS-SD

Overexpression of the protein was optimised using small-scale setup of bacterial cultures induced with varying concentrations of IPTG and temperature. An additional step of checking the solubility of protein in supernatant upon cell lysis was also performed. The protocol to perform this optimisation as follows:

- 0.8 µl of plasmid for EcZraS-SD was transformed into 50 µl of chemically competent *E. coli* LEMO21(DE3) using the heat-shock method and allowed to grow overnight on a Kanamycin + Chloramphenicol-LB Agar plate.
- Bacterial colonies were observed after overnight incubation. Single colonies were picked to prepare primary culture using 2 ml of LB broth supplemented with 2 µl of Kanamycin (50 mg/ml in autoclaved Milli-Q® water) and 2 µl of Chloramphenicol (25 mg/ml in 100 % ethanol), incubated overnight in a shaker incubator at 37 ºC and 220 rpm.
- 1 % primary culture (500 µl) was used to inoculate a bacterial culture flask containing 50 ml LB broth, supplemented with 50 µl of Kanamycin and 50 µl of Chloramphenicol. The secondary culture was incubated in a shaker incubator at 37 ºC and 220 rpm till the $OD_{600}$ reached a value of 0.8.

- From each 50 ml culture, aliquots of 2 ml each were prepared and labelled as 0.8 UI (uninduced 37 ºC), 0.8 I (0.5 mM IPTG 37 ºC), 0.8 I (1 mM IPTG 37 ºC), 0.8 UI (uninduced 25 ºC), 0.8 I (0.5 mM IPTG 25 ºC), 0.8 I (1 mM IPTG 25 ºC), 0.8 UI (uninduced 18 ºC), 0.8 I (0.5 mM IPTG 18 ºC), 0.8 I (1 mM IPTG 18 ºC). 37 ºC, 25 ºC and 18 ºC refers to post-induction temperatures used for incubation.

- The aliquots at 37 ºC were incubated for 4 hours, 25 ºC for 8 hours and 18 ºC for 16 hours. The cells were then harvested by centrifugation at 5000 rpm for 5 minutes. The pellets were dissolved in 20 µl of 2X Laemmli's buffer, heated at 95 ºC for 5 minutes and vortexed before loading into a 15% SDS-PAGE gel for visualisation of overexpression.

- In a second batch of experiments, solubility of the sample in supernatant during lysis was checked for temperatures 18 ºC and 37 ºC. The cell pellets obtained for 0.8 I (0.5 mM IPTG 37 ºC) and 0.8 I (0.5 mM IPTG 18 ºC) were dissolved in 600 µl of buffer (20 mM Tris 8.0 and 200 mM NaCl). The suspensions were subjected to ultra-sonication at an amplitude of 35 %, 5 secs ON & 10 secs OFF cycle for a duration of 10 minutes.

- The lysate was centrifuged at 14000 rpm (23,447 g) for 30 minutes at 4 ºC. Supernatant and pellets were separated for 0.8 I (0.5 mM IPTG 37 ºC) and 0.8 I (0.5 mM IPTG 18 ºC) and visualised on a 15% SDS-PAGE gel. Based on the results obtained the cultures were scaled up for protein purification using the following condition - 0.8 $OD_{600}$, 0.5 mM IPTG and 18 ºC temperature post-induction.

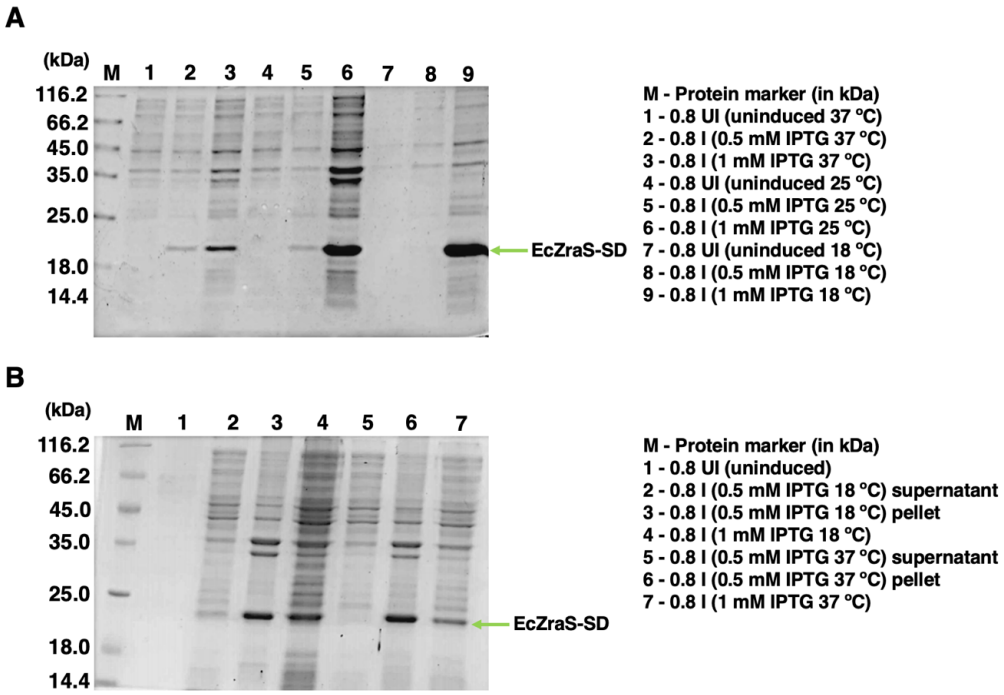


**Figure 2.6.3.1 Overexpression and solublization of the truncated periplasmic domain EcZraS-SD.** (A) The SDS-PAGE gel shows overexpression profiles of EcZraS-SD at varying temperature and IPTG concentrations at 0.8 $OD_{600}$ as labelled. (B) The SDS-PAGE gel shows the distribution of EcZraS-SD in the supernatant and pellet fractions after lysis at varying temperatures as labelled. The supernatant fractions were used for protein purification.

### 2.6.4 Overexpression of the loop variants of EcZraS-SD

- The loop variants of EcZraS-SD were induced with varying concentration of IPTG at 0.8 $OD_{600}$ in temperatures 18 ºC and 37 ºC. Based on the results obtained the cultures were scaled up for protein purification using the following condition - 0.8 $OD_{600}$, 0.5 mM IPTG and 18 ºC temperature post-induction.

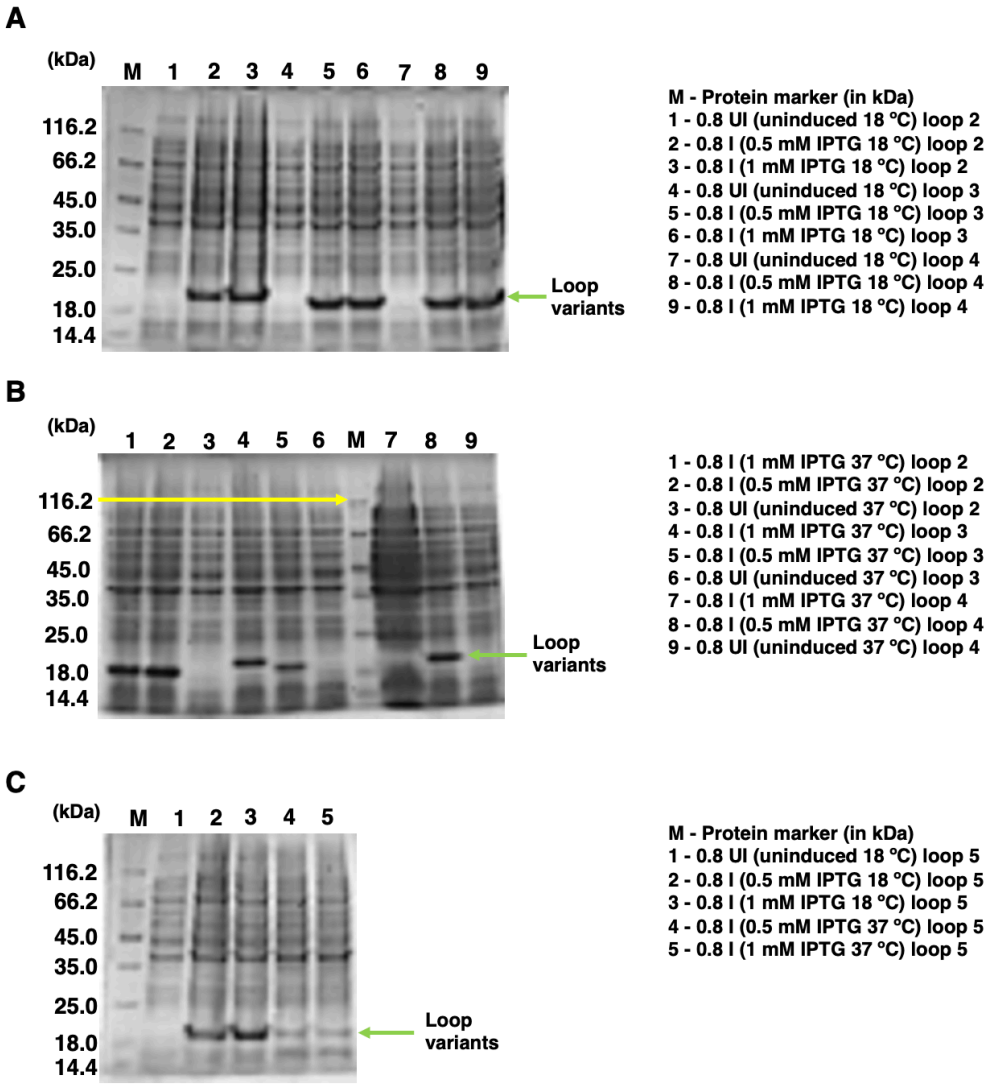


**Figure 2.6.4.1 Overexpression of the loop variants of EcZraS-SD.** (A) The SDS-PAGE gel shows the overexpression profiles of loop 2, loop 3 and loop 4 at 18 ºC and varying IPTG concentrations at 0.8 $OD_{600}$ as labelled. (B) The SDS-PAGE gel shows the overexpression profiles of loop 2, loop 3 and loop 4 at 37 ºC and varying IPTG concentrations at 0.8 $OD_{600}$ as labelled. (C) The SDS-PAGE gel shows the overexpression profile of loop 5 at 18 ºC and 37 ºC with varying IPTG concentrations at 0.8 $OD_{600}$ as labelled.

## 2.7 Protein purification of native EcZraS-SD and its loop variants using affinity chromatography, 6X-His tag removal and size exclusion chromatography

The protein purification for EcZraS-SD and its loop variants was similar to EcZraS-CD and carried out in a three step process involving affinity chromatography, 6X-His tag removal and size exclusion chromatography as described under section 2.2. The composition of buffer D was changed to 20 mM Tris pH 8.0 and 200 mM NaCl for SEC and ultra-pure protein obtained was concentrated up to 11 mg/ml.

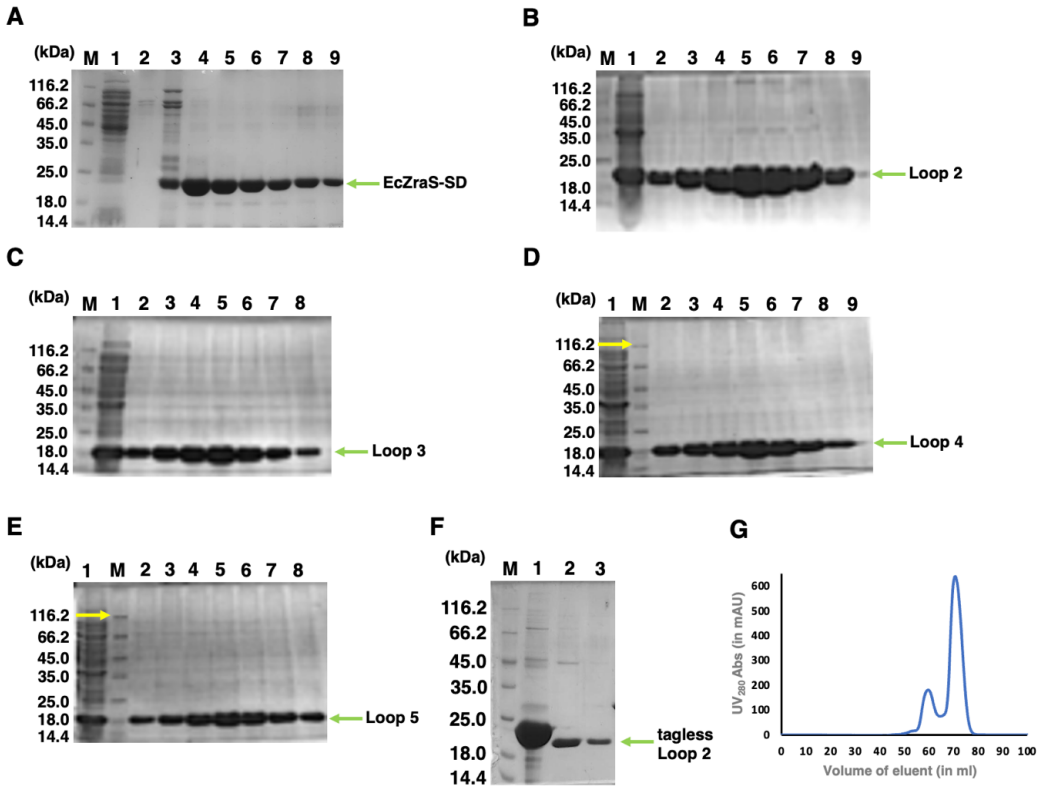


**Figure 2.7.1 An overview of the process of protein purification of EcZraS-SD and its loop variants.** (A-E) The SDS-PAGE gels shows M, protein marker and 1-8 or 1-9, elution fractions obtained during Ni-NTA chromatography of EcZraS-SD, loop 2, loop 3, loop 4 and loop 5. (F)

The SDS-PAGE gel shows M, protein marker; 1, concentrated tagless protein of loop 2; 2 and 3, tagless SEC fractions of 2$^{nd}$ peak of loop 2. (G) Chromatogram of tagless loop 2 obtained during SEC.

## 2.8 Crystallization of EcZraS-SD and its loop variants

Screening for crystallization conditions was performed for His-tagged and tagless EcZraS-SD by setting up random trials in commercially available conditions, with protein concentrations ranging 3-4 mg/ml. Screening with higher concentrations was not feasible due to heavy precipitation. The protein was buffer exchanged into buffers of pH ranges 4.5-9.0 and varying concentrations of salts in subsequent trials, but was found to be unamenable for crystallisation.

Hence the loop truncations were designed for the study to improve stability and enhance crystallization capability of the molecule. Both His-tagged and tagless proteins were screened in apo and ligand bound forms. Small crystals of tagless loop 2 incubated with zinc chloride, cadmium chloride and cobalt chloride were obtained. The crystals diffracted up to a resolution of 7 Å. Further optimisations will be necessary to obtain high-resolution data for structure solution.

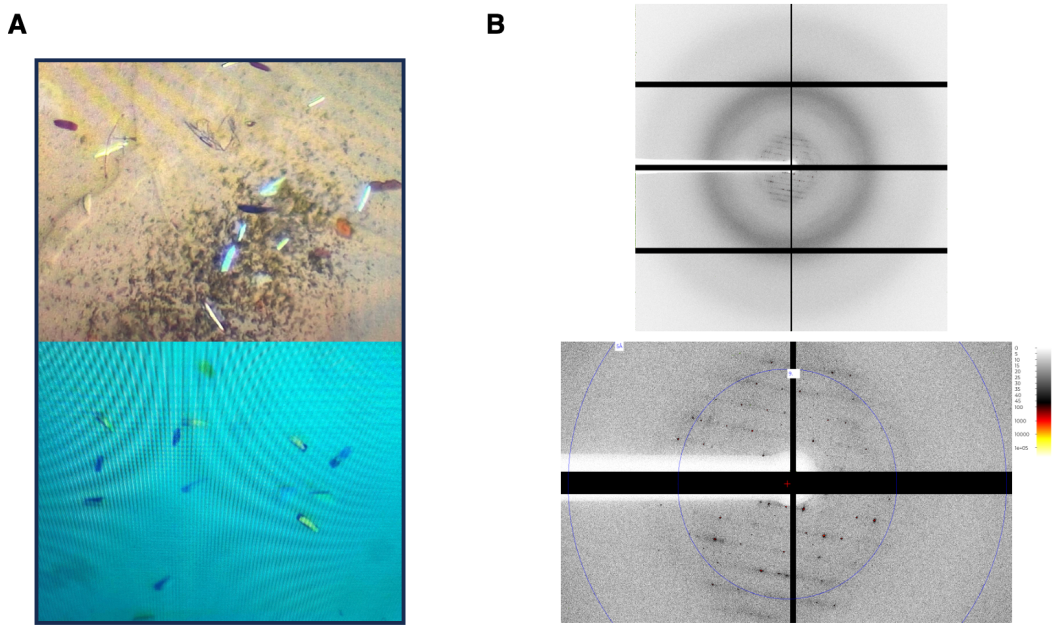


**Figure 2.8.1 Crystals and diffraction pattern of loop 2 incubated with $CdCl_2$ and $CoCl_2$.**

## 2.9 Comparative modelling of loop variants of EcZraS-SD using Rosetta

As crystallisation of EcZraS-SD and its variants posed a challenge, the sensor domain and its variants were modelled using loop modelling protocols in Rosetta 3.0. The loops were modelled using the generalised kinematic closure (KIC) algorithms. During a kinematic closure protocol, the possible conformations of a chain of atoms fixed at both ends in a molecule are determined, such that they satisfy geometrical constraints including bond angles, bond lengths and dihedral angles. The procedure used for modelling the variants as follows:

- The model for the periplasmic domain of ZraS was obtained from AlphaFold and modified to make the template for loop modelling.
- A short loop file was made mentioning the starting and ending positions of the loop along with the cut positions, followed by the use of loop model application the KIC protocol in Rosetta. The score function used was REF2015.

- Outputs obtained were stored as .pdb files that could be accessed using PyMol and used for further analysis with reference to each other and the other template.

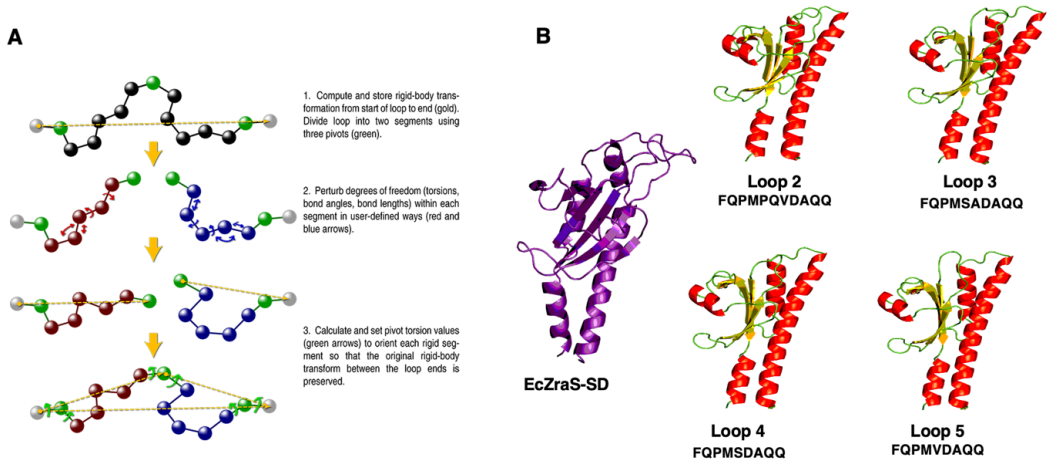


**Figure 2.9.1 Modelling of loop variants using Rosetta.** (A) This image represents the generalised procedure for loop modelling using the kinematic closure algorithm in Rosetta (cite the reference here and say the image is taken from this article; check for permission to use the figure. (B) This image shows the cartoon representation of monomeric EcZraS-SD with the modelled loop variants.

## 2.10 Modelling of full length structure of ZraS using AlphaFold

The full length structure of ZraS was modelled using AlphaFold. The SHK was initially divided into two segments, one segment containing the periplasmic, TM and linker domain followed by the second segment containing the linker and the kinase domain to obtain two apo form dimers. The dimers were them overlapped structurally to obtain the full length protein.

# Chapter 3

# Structural and biochemical characterisation of the cytoplasmic domain of ZraS (EcZraS-CD)

*Chapter-3*

## 3.1 Introduction

This chapter highlights the structural basis of signal transduction in the SHK ZraS through analysis of the crystal structures of its cytoplasmic domain (EcZraS-CD). The cytoplasmic stretch was purified and crystallised as mentioned in section 2.2 and 2.3 respectively. Two dimers were trapped in the asymmetric unit of the crystal in distinct conformations bound to ADP and $Mg^{2+}$. The structure revealed functional homodimer of the stretch including a kinase domain (KD) and a α-helical linker domain. The dimers were analysed to determine the conformational transitions involved in state switching. It demonstrated involvement of numerous transitions such as helical rotation, bending or scissoring, registry shifts, and variable accommodation of amino acid insertions during the process. This work also proposed the structural basis for regulation of directionality (trans phosphorylation) and interdomain allostery during autophosphorylation. The bundle rotation was found to be linked with differential interactions of bundle base and loop residues. Overall, the findings helped elucidate the coordinated nature of information transfer among different domains and helped elucidate the mechanism of kinase activation via multiple intermediate conformers in a multi-step process.

## 3.2 Three-dimensional structure of the cytoplasmic domain of EcZraS-CD in a ligand-bound form

The structure of EcZraS-CD, ranging residues Tyr225-Thr459, was crystallized using the methods mentioned in section 2.3.1. Phases were obtained by molecular replacement (MR) using a polyalanine model of the CA domain derived from the AlphaFold (Jumper et al., 2021) structure of ZraS, and the resulting model was subsequently refined to a resolution of 2.49 Å

using Phenix (Adams et al., 2010; Emsley & Cowtan, 2004)**.** The data collection and refinement table has been mentioned in **Table 3.2.1**.

The asymmetric unit of the crystal contained four chains (cA-cD) that arranged into two parallel homodimers: dimer AB and dimer CD. The constituent chains were bound to one molecule of ADP and $Mg^{2+}$ each. The overall cytoplasmic stretch of ZraS includes a linker region from residues Tyr225–Ala250 and a kinase domain (KD) from residues Gly251–Thr459, comprising of a dimerization and histidine phosphoacceptor bundle (DHp) and two catalytic and ATP-binding domains (CAs) shown in **Figure 3.2.1 B**. The linker helices Lα1 (cA/cC) and Lα1' (cB/cD) assembles into a parallel bundle, forming a continuous helical axis connecting the transmembrane helices TM2/TM2' with the of the DHp bundle in the KD. The DHp domain comprises of two helices, helix-1 [hα1 (cA/cC)/hα1' (cB/cD)] and helix-2 [hα2 (cA/cC)/hα2′ (cB/cD)] arranged into helix–turn–helix motifs connected by base loops. The helices orient in an antiparallel manner forming a four-helix bundle. The conserved phosphorylable His 254 is located on helix-1 (hα1/ hα1') of the DHp bundle with each bundle housing two such residues. The second helix, helix-2 (hα2/ hα2') connects the DHp bundle to the CA domain on either sides using hinges spanning residues Val305-Leu312. The CA domain features a compact structure with a mixed α/β fold topology containing three alpha helices (α1-α3) and seven beta sheets (β1- β7). Three alpha helices (α1, α2 and α3) and five antiparallel β sheets (β2, β4, β5, β6, and β7) of the CA domain assemble to form a bilayer structure resembling a sandwich. The ligand is housed inside the sandwich-like structure inside a groove formed towards one edge of the domain.

The sequence motifs present in the KD region of EcZraS-CD aligns closely with those found in members of the GHKL superfamily (Gyrases, Hsp90, Histidine kinases and MutL). These regions H, N, G1, F, G2, and G3 boxes are denoted after single-letter codes of the conserved His, Asn, Phe, and Gly residues, present in their sequence consensus (Bhate et al., 2015; Bilwes

et al., 1999; Marina et al., 2005). The H-box is located in the upper half of the DHp helices hα1/hα1', with the N, G1, F, G2, and G3 boxes embedded within the ligand-binding cleft of the CA domain. Multiple sequence alignments of these conserved motifs place ZraS in the HPK4 subfamily **(Figure 3.2.2)**. It marks similarity with kinases such as NtrB and FleS, possessing a TTK motif in the ATP lid loop region, with a distinctive feature being the presence of Ala253 and Gln258 directly preceding His254 and the presence of Pro259 in the H-box (Grebe & Stock, 1999).

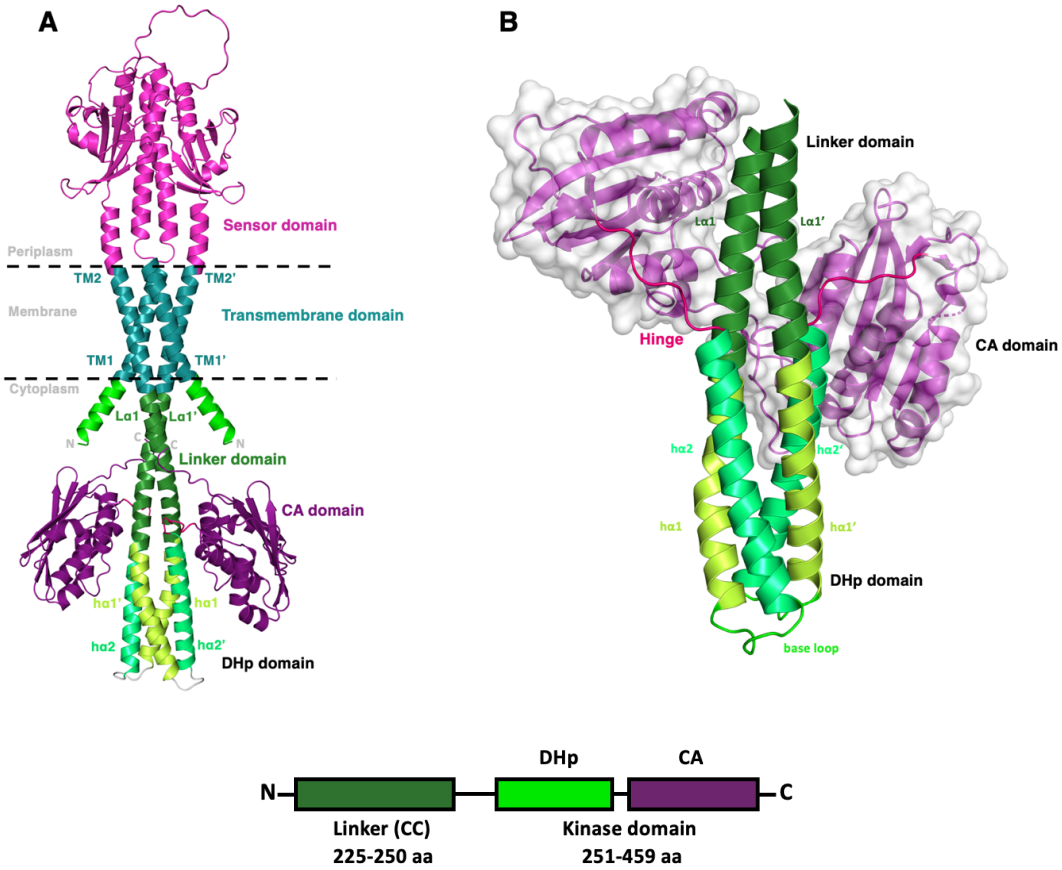

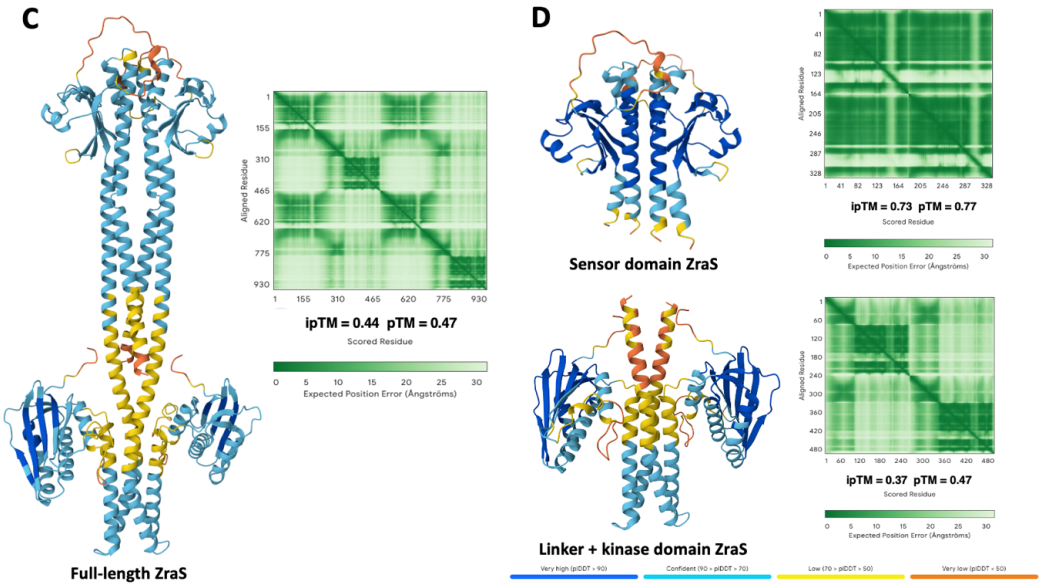


**Figure 3.2.1 Full-length model and truncated crystal structure of the cytoplasmic domain of EcZraS.** (A) AlphaFold model of the apo form of full-length ZraS (EcZraS-F) displaying domain distributions across periplasmic (light magenta), transmembrane (deep teal), and cytoplasmic regions (forest, limon, lime green, and deep purple) (Jumper et al., 2021). (B) Three-dimensional structure of ligand-bound EcZraS-CD. The overall structure of the cytoplasmic region features a simple linker domain (forest) and a kinase domain comprising the DHp and CA domains. The DHp region (limon and lime green) is connected to the CA domains (deep purple) using hinges (hot pink). (C) and (D) Image showing full-length and truncated sensor and kinase domains of ZraS, with pLDDT score-based colouring and their pAE scores. The dimer interface confidence (ipTM) and global fold confidence (pTM) for each generated structure have been mentioned.

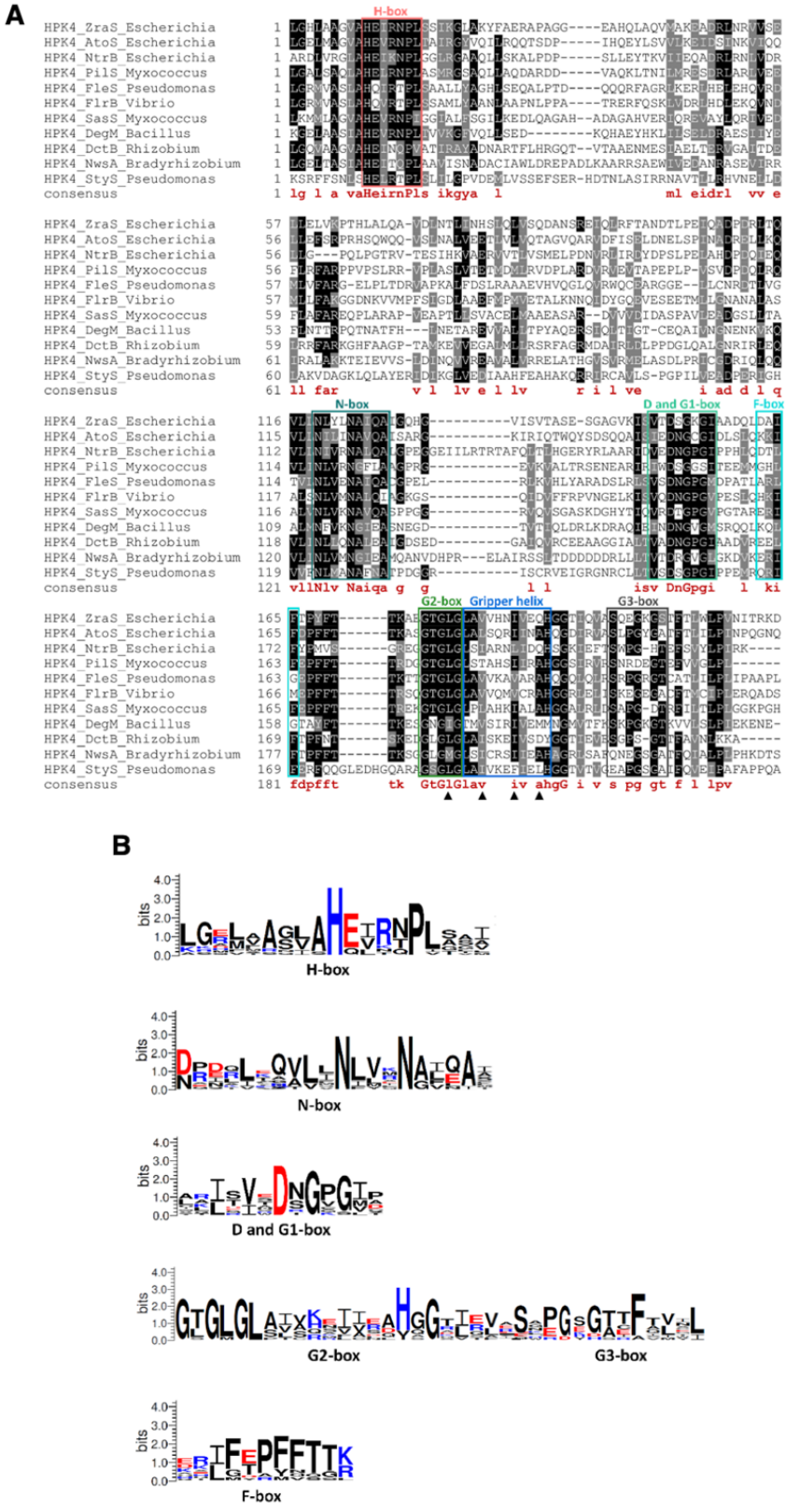
A
H-box
N-box
D and G1-box
F-box
G2-box
Gripper helix
G3-box
B
H-box
N-box
D and G1-box
G2-box
G3-box
F-box
bits

**Figure 3.2.2 Multiple sequence alignment and sequence consensus of conserved domains of EcZraS-CD.** (A) Sequence alignment showing conserved regions of KD region of sensor histidine kinases belonging to HPK4 family (Thompson et al., 1994). Sequence consensus are represented in maroon. Black triangles represent residues forming sticky fingers that help CA domain bind to the DHp bundle. (B) Logo depicting sequence consensus in H, N, F, G1, G2 and G3 boxes of HPK4 family representatives used in A (Crooks et al., 2004).

**Table 3.2.1 Data collection and refinement statistics of EcZraS-CD**

| **Data Collection Statistics** | |
|---|---|
| Protein | EcZraS-CD (**PDB: 9JFJ**) |
| Radiation source | ESRF, Grenoble, France |
| Beamline | ID30A |
| Wavelength (Å) | 0.96546 |
| Processing software | XDS |
| Unit cell parameter | a = 127.87 Å, b = 121.79 Å, c = 88.43 Å<br>α = 90.0°, β = 126.0°, γ = 90.0° |
| Space group | C2 |
| Resolution range (Å) | 46.36-2.49 (2.59-2.49) * |
| $R_{merge}$ | 0.1637 (0.6929) |
| Total reflections | 38311 (4257) |
| I/σ(I) | 5.57 (0.72) |
| Completeness (%) | 99.9 (99.9) |
| Multiplicity | 5.96 (4.53) |
| CC 1/2 | 0.994 (0.727) |
| **Data Refinement Statistics** | |
| Refinement program | Phenix |
| $R_{work}/R_{free}$ | 0.2609/0.2819 |
| $\Delta R = \lvert R_{work} - R_{free} \rvert$ | 0.021 |
| Matthews Coefficient $V_m$(Å$^3$/Da) | 2.65 |
| Number of molecules/asymmetric unit (Z′) [monomer] | 4 |
| Solvent content (%) | 53.6 |
| **Number of atoms** | |
| Proteins | 6722 |
| Ligands or ions | 112 |
| **B-factors** | |
| Wilson B-factor (Å$^2$) | 65.9 |
| Overall B-factor (Å$^2$) | 94.7 |
| Proteins (Å$^2$) | 94.6 |
| Ligand (Å$^2$) | 99.6 |
| **RMSD from ideal values** | |
| rms bond length (Å) | 0.01 |
| rms bond angle (°) | 1.49 |
| **Ramachandran regions (%)** | |
| Favored | 98.5 |
| Allowed | 1.5 |
| Outliers | 0 |

$R_{work} = \sum||F_O|-|F_C||/\sum|F_O|$. $R_{free}$ is the $R_{work}$ value for 5% of the reflections excluded from the refinement.

$R_{merge} = \sum|I - \langle I \rangle|/\sum I$. (*) Values in parentheses are for the highest resolution shell.

## 3.3 The ligand binding pocket of EcZraS-CD

The ligand binding pocket of EcZraS-CD is formed between helices α2 and α3, bound laterally by the sheets β6 and β7. The pocket is lined by residues from the N, G1, F, G2, and G3-boxes **(Figure 3.3.1 B and 3.3.2 A)**. The sequence consensus for each of the boxes of ZraS has been mentioned in **Figure 3.3.1 B**. It harbours both ADP and $Mg^{2+}$ guarded by the lid loop, positioned between the F-box and G2-box. It acts as a flexible gate extending toward the base of the pocket, responsible for accommodating the ligand. The G1-box (green cyan) forms the floor of the pocket, while the G2-box (forest), the Gripper region (marine), and the N-box (deep teal) together line the ceiling. The two phosphate groups of ADP lie adjacent to the G2-box flanking one side of the pocket, while the opposite end delimited by the N-box. The rear boundary is lined by residues from the G1-box, parts of the G3-box (gray40), and the F-box (cyan).

The ADP moiety is accommodated inside the pocket using multiple direct and indirect interactions with residues lining the pocket that aid collectively position the nucleotide inside the groove **(Figure 3.3.2 B)**. The binding groove accommodating the adenine ring of the ADP is formed by residues Asp395, Ser448, Gly399, and Gly397. The amino group at the N6 position of the adenine ring forms a hydrogen bond with Asp395 from the G1-box. A positively charged residue Lys416 stabilises the ring by long range cation- π interaction spanning a distance of 5.5–6.5 Å. The side-chain hydroxyl oxygen atoms and main-chain nitrogen atoms of the residues Thr414, Thr415, and Lys416 interact with the 2′ and 3′ hydroxyl groups of the ribose sugar. Thr420 of the ATP lid loop and Leu424 of the G2-box interacts with the α- and β-phosphate oxygen atoms of ADP. The F-box residues Phe409 and Phe413 located in the vicinity, flanking one side of the pocket forms indirect contact with the ADP. Coordination of the $Mg^{2+}$ is mediated by oxygen atoms from the conserved Asn367 of the N-box and phosphate groups of ADP. Despite the presence of positive electron density, the lack of a high resolution

structure prevented explicit modeling of water placed in close co-ordination of $Mg^{2+}$ fulfilling its regular octahedral co-ordination. The CA domain of EcZraS-CD shares 35% sequence identity with CckA having a highly conserved ligand-binding pocket and the characteristic TTK motif in the lid loop region **(Figure 3.3.3)**. However it lacks presence of any cyclic di-GMP binding residues present in CckA (Dubey et al., 2016).

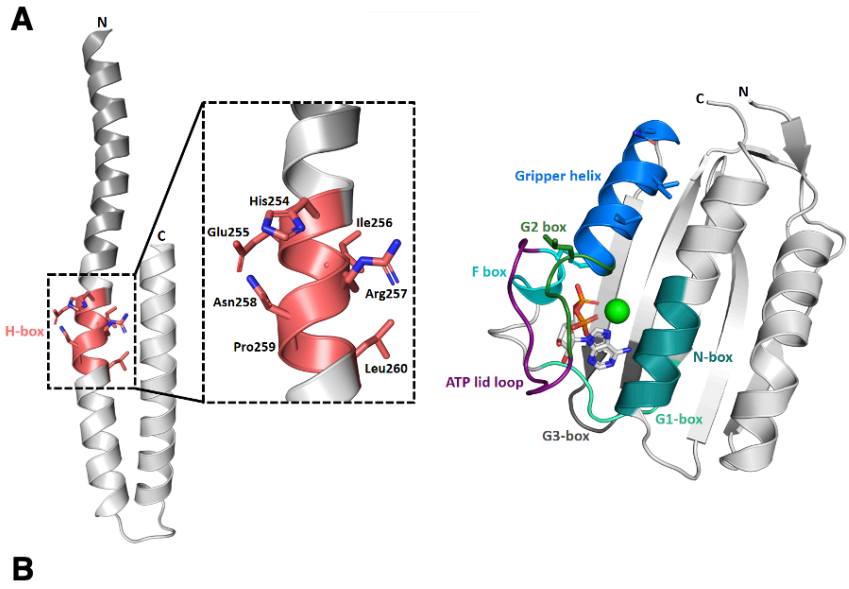


| Box | Sequence | Conserved residues | Location |
|---|---|---|---|
| H (His) | HEIRNPL | His254 | hα1 of DHp |
| N (Asn) | NLYLNAIQA | Asn367 | α2 of CA |
| D (Asp) and G1 (Gly) | VTDSGKGI | Asp395, Gly397, Gly399 | βE and adjacent loop of CA |
| F-box (Phe) | DAIF | Phe409 | α4 of CA |
| G2-box (Gly) | GTGLG | Gly419, Gly421, Gly423 | Loop adjacent to α3 of CA |
| G3-box (Gly) | SQEGKGS | Gly447 | βF, βG and βF-βG loop of CA |

**Figure 3.3.1 Conserved boxes and sequence consensus of EcZraS-CD.** (A) and (B) The cartoon and stick representation shows the H-box residues (deep salmon) in the DHp helix hα1, N (deep teal), G1 (green cyan), F (cyan), G2 (forest), G3 (gray50) boxes and the ATP lid (deep purple) in the CA domain. Hydrophobic residues of gripper region (marine) and Phe of F-box, are also shown in stick representation. The ligand ADP (gray90) is shown as a stick and $Mg^{2+}$ (green) as a sphere.

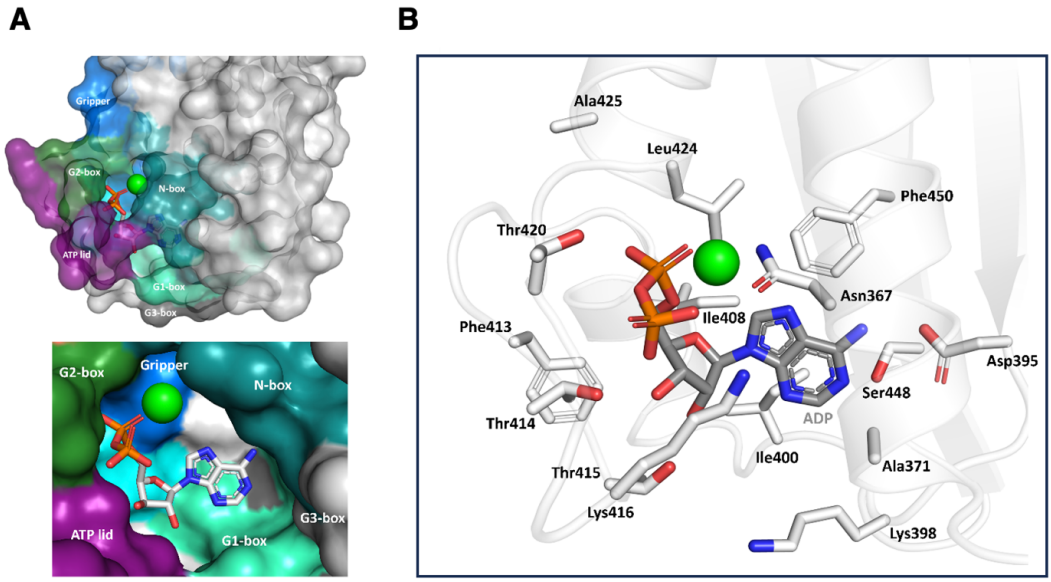


**Figure 3.3.2 Ligand binding pocket of EcZraS-CD.** (A) The surface representation of the ligand-binding pocket lined by residues from N (deep teal), G1 (green cyan), F (cyan), G2 (forest), and G3 (gray50) boxes in EcZraS-CD (B) This image shows ADP (gray50) and $Mg^{2+}$ (green) inside the ligand binding pocket. The interacting residues have been shown in stick representation.

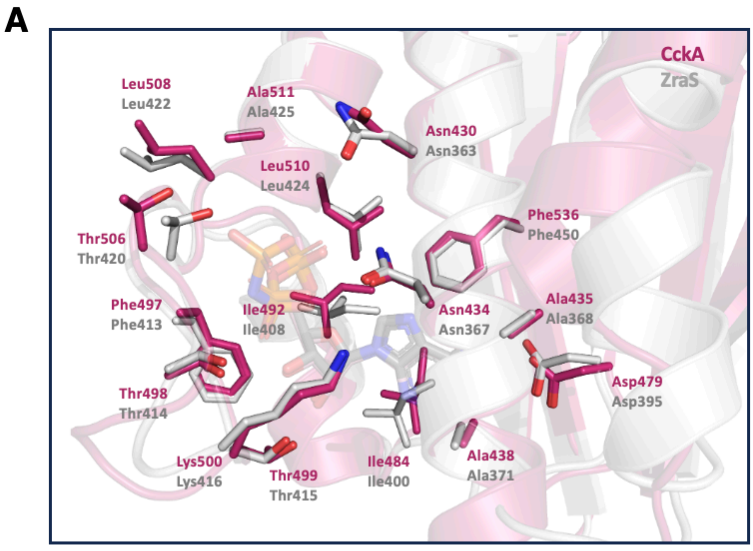

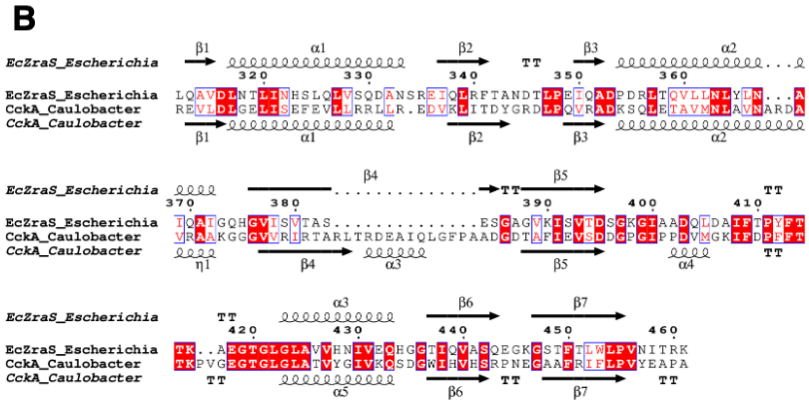


**Figure 3.3.3 Structural comparison of the CA domain of EcZraS-CD with CckA.** (A) This image shows the conserved residues enclosing the ligand binding pocket in the CA domain of ZraS (gray90) and CckA (hotpink). (B) Structural alignment of the CA domain of ZraS with the CA domain of CckA.

## 3.4 Dynamics of the ATP lid loop region of EcZraS-CD

The 14-residue ATP lid loop stretches from residues Thr410–Gly423, bordered by helix α3 of the G2-box and helix α4 of the F-box. It is anchored by the conserved hydrophobic residues Phe409 of helix α4 and Leu424 of helix α3 at the ends. The Phe409 residue fits into a hydrophobic patch typical to SHKs comprising Ile408, Leu424, and Ile438. The relatively shorter loop shows a distinct intermediate orientation unlike the long loops of PhoQ (1id0) directed toward the core or that of EnvZ (1bxd) directed away from the core as seen in **Figure 3.4.1 A** (Ferris et al., 2014; Marina et al., 2001)**.** Due to its short length the lid loop remains in a mid-position, enclosing the ligand-binding pocket upon association with the DHp domain. This shift in loop conformation favoring nucleotide association through DHp interaction has been noted in other sensor kinases. Though no significant structural rearrangement was observed in the loop, the residue Lys416 displayed an altered interaction with the ADP moiety in the proximally placed CA domain as opposed to the distally placed CA domain **(Figure**

**3.4.1 C)**. The effective length of the loop is adjusted by local unwinding of helices α3 and α4. Unlike the disordered loop structures found in the nucleotide-free NR(II) (1r62) and CpxA (4bix), the lid loop of EcZraS-CD maintains an ordered conformation with the residues Gly419, Gly421, and Gly423 of the G2-box regulating its flexibility (Mechaly et al., 2014; Song et al., 2004). The SHKs CheA (1i58) and KinB (3d36) show additional secondary structures in their lid loop regions absent in EcZraS-CD **(Figure 3.4.1 B)** (Bick et al., 2009; Bilwes et al., 1999)**.**

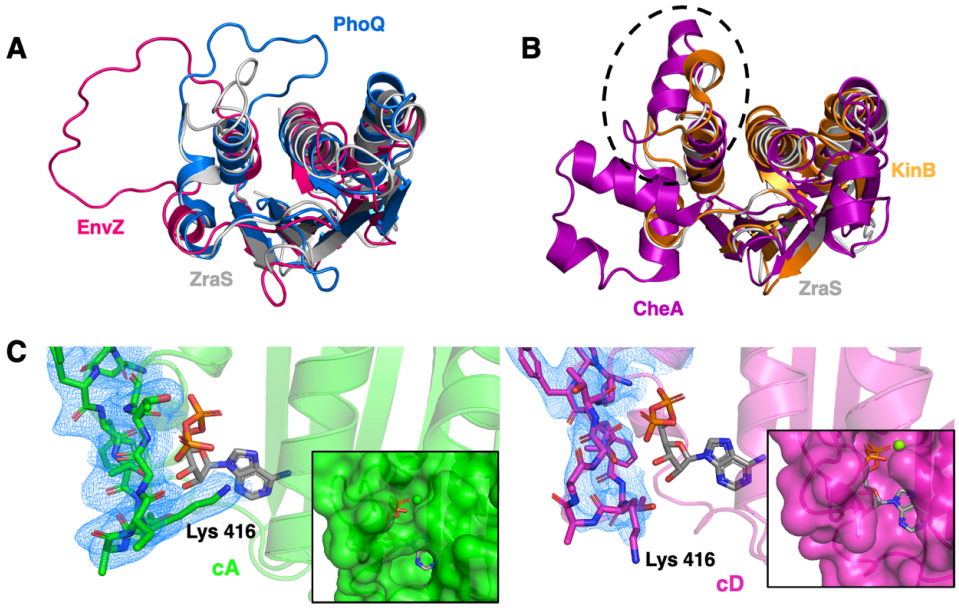


**Figure 3.4.1 ATP lid loop of EcZraS-CD.** (A) This image shows the structural overlap of the lid loop region of EnvZ (hotpink) in an open-state and PhoQ (marine) in a closed-state with EcZraS-CD (gray90). (B) Comparison of ATP lid loop of EcZraS-CD with CheA (purple) and KinB (orange). (C) This image shows interaction of Lys416 with the adenine ring of ADP in the chains cA and cD. Interaction was only observed for cA, containing a proximally located CA domain. The 2Fo-Fc map has been contoured at 1.0 σ.

## 3.5 The asymmetric ligand-bound structures of EcZraS-CD

Structural overlap of the ligand-bound dimers of EcZraS-CD – dimer AB (chains cA and cB) and dimer CD (chains cC and cD) yielded an r.m.s. deviation value of 2.3 Å **(Figure 3.7.2 A)**. The chains cA and cC exhibit near similar conformations having an r.m.s. deviation value of 1.0 Å, while cB has a disposition similar to cD with an r.m.s. deviation of 0.6 Å. Though the overall fold appears to be conserved based on the r.m.s. deviation values, the 1.0 Å value between cA and cC suggests minor structural differences. A close structural analysis indicated rotation of the CA domain of cC by an angle of nearly 20° and change in residues ranging Val305–Leu310 as compared to cA **(Figure 3.5.1 C)** (Veevers & Hayward, 2019)**.** A subtle helical bending was observed in the base region of the chains cA and cC, possible attributed to titling of DHp helices **(Figure 3.5.1 B)**. Moreover, we were unable to trace residues Ala274–Ala276 corresponding to the base loop region in cC of dimer CD.

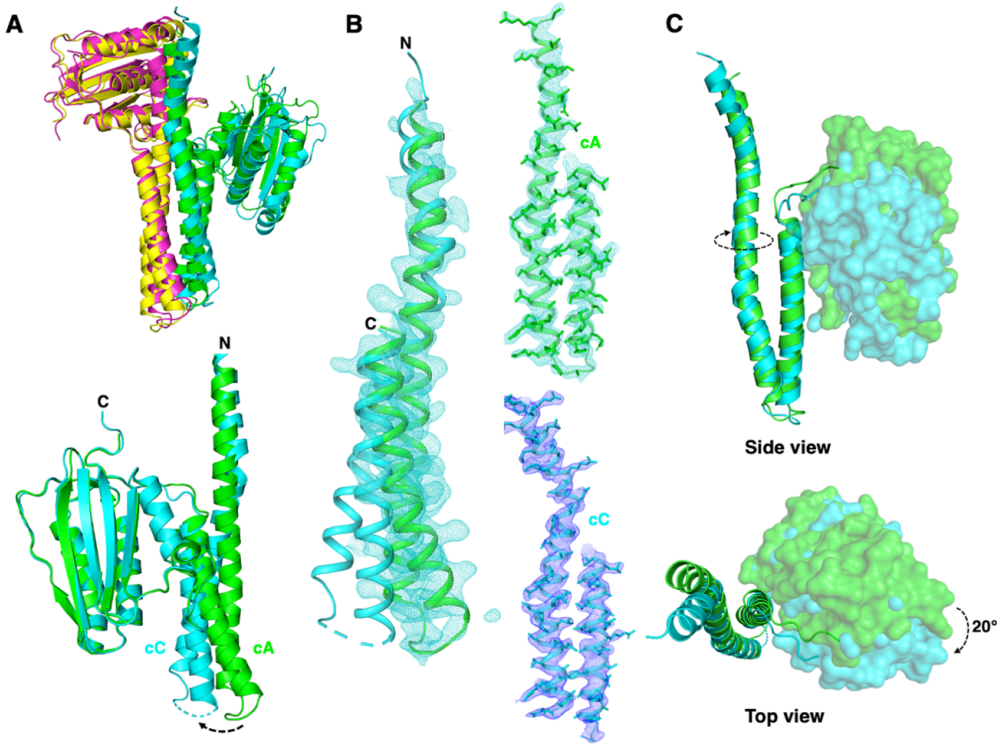

**Figure 3.5.1 Structural overlap of the asymmetric ligand-bound dimers of EcZraS-CD.** (A) This image shows the cartoon representation of the structural superposition of dimers AB and CD. (B) The image highlights the bending of the DHp helix of cC in comparison to cA, along with their 2Fo-Fc maps contoured at 1.0 σ. (C) The CA domain of cC has been shown to be rotated by an angle of 20°.

Ligand binding in EcZraS-CD induced an asymmetric arrangement of the CA domains across the central bundle, positioning the CA domains in different planes. The CA domains of dimer AB and CD were separated by 36.8 Å and 39.4 Å apart, forming angles of 112.9° and 127.26 respectively, while the ligand-bound forms had an asymmetric disposition. The apo model of EcZraS-F, a dimer XY consisting of chains cX and cY was seen to have coplanar CA domains 52 Å apart, forming an angle of 180° **(Figure 3.5.2 A)**. One CA domain in EcZraS-CD dimers rotated outwards, with the other located in proximity to the bundle. The Cα–Cα distances between His254 of DHp and Asn367 of the CA domain of the opposing protomers in dimers AB and CD averaged 23 Å and 36.5 Å, with exact distances being 23.9 and 36.7 Å for dimer AB, and 22.2 and 36.1 Å for dimer CD **(Figure 3.5.2 D)**. The helices hα1 and hα1′ in the ligand-bound structures exhibit bending angles ranging from 11°-26° near Pro259 in the H-box **(Figure 3.5.2 B)**. An additional bend near the N-terminus of DHp toward the linker Lα1 was observed in chain C of dimer CD. The monomers of EcZraS-F show a uniform Cα–Cα distance between His254 and Asn367 of nearly 22.4 Å and a bend of approximately 17.5° near Pro259 for both hα1 and hα1′ **(Figure 3.5.2 B and D)**. The His–Asn Cα distance-based structural clustering of the cytoplasmic domains of SHKs reflects the functional distinctions linked to CA-DHp symmetry (Bhate et al., 2015).

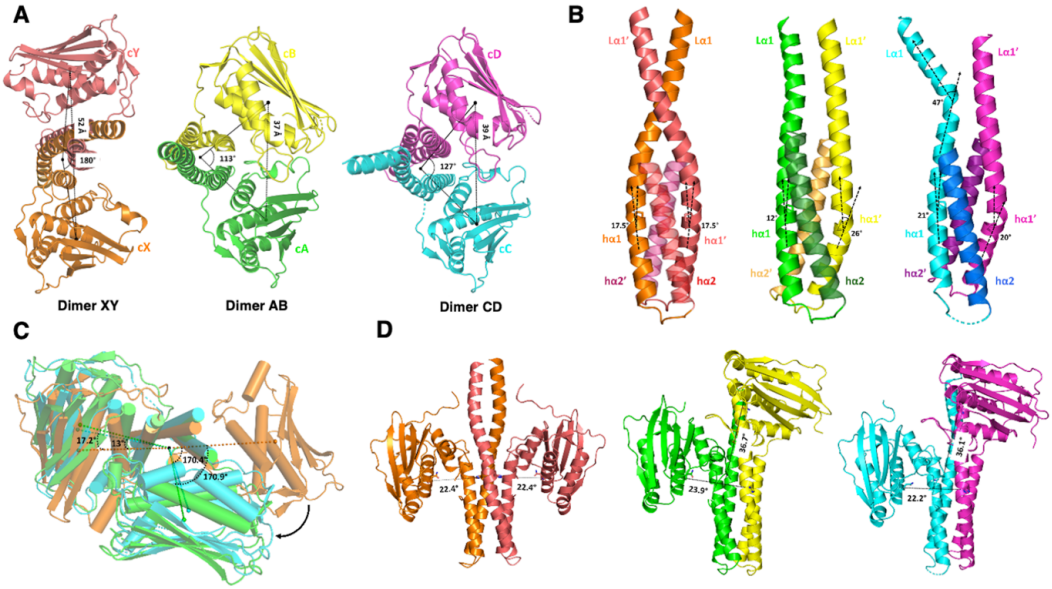


**Figure 3.5.2 Angles and distances of the apo and ligand-bound dimers of ZraS.** (A) Angles and inter-domain distances between the CA domains of apo and ligand-bound dimers of EcZraS-CD. (B) Helix bending angles at Pro259 of helix hα1 (orange) and hα1' (deep salmon) of dimer XY, helix hα1 (green) and hα1' (yellow) of dimer AB, and helix hα1 (cyan) and hα1' (light magenta) of dimer CD. (C) The structural superposition of dimer XY (orange), dimer AB (green), and dimer CD (cyan) demonstrates the angular rotation of the CA domain upon ligand binding. (D) The distances between His254 in the DHp bundles and Asn367 in the CA domains of the opposite protomers in dimer XY, dimer AB and dimer CD.

Apo and ADP-bound phosphatase-active structures show symmetric conformations with the CA domains oriented outward in an open state. ATP and its non-hydrolyzable analog bound kinase-active structures show relatively asymmetric conformations, with one CA domain associated proximally with the bundle in a closed conformation and the other oriented away in an open conformation. The structures of CpxA (4cb0) and phosphorylated DesK (5ium) show CA domains positioned asymmetrically inhibited by steric hindrance with only one domain in a closed conformation (Mechaly et al., 2014; Trajtenberg et al., 2016). Closed-state

conformations are associated with DHp helical bending observed in WalK (25.7° at Pro396) and CovS (25° at Pro222) (Y. Cai et al., 2017b; Wang et al., 2013). WalK is also speculated to possess intermediate autophosphorylation states characterized by coordinated small-angle bending of the DHp helices. The proximally placed CA domain and the DHp bundle in the ADP-bound dimers of EcZraS-CD are positioned 20–30 Å apart. The conformation acquired is consistent with other ADP-bound SHK structures, but far exceeds the distance of 10–15 Å required for forming a closed autophosphorylation complex (Bhate et al., 2015). The asymmetry seen in the crystal structures, including a pronounced helical bending and varied CA domain positioning, indicates the existence of two intermediate states nearing a kinase-active conformation.

## 3.6 Coiled coil architecture in helical backbone of EcZraS-CD

The DHp bundles are categorized into four main domains: HisKA (PF00512), HisKA_2 (PF07568), HisKA_3 (PF07730), and HWE (PF07536) based on sequence conservation and their structural position according to the Pfam database (Mistry et al., 2021). EcZraS-CD contains an H-box sequence of His–Glu–Ile–Arg–Asn–Pro–Leu, categorizing it as a member of the HisKA domain family. The HisKA bundles consist of two helix–turn–helix motifs arranged in an antiparallel manner. Both the turns of these bundles are positioned at one end with the N and C-termini extending out from the other.

The structural analysis of the DHp bundle from apo model of EcZraS-F (dimer XY) using TWISTER and SamCC Turbo (manual mode) helped reveal the coiled coil arrangement in the domain (Strelkov & Burkhard, 2002; Szczepaniak et al., 2021). The heptad repeats spanning Ala253–Phe270 and Leu301–Ala284 in both chains of the dimer were identified. The helices were found to assemble into heterotetrametric structures containing a hydrophobic core

composed of 'a' and 'd' positions. These residues project out along the length of the helices interdigitating with diagonally opposing helices resulting in formation of alternating ad layers. It gives out an appearance of knobs housed inside cavities formed by adjacent knobs, a knobs-into-holes arrangement **(Figure 3.6.1 A)**. The position 'a' is occupied by smaller residues such as Ala or occasional occurrence of Leu or Val and 'd' by large hydrophobic residues such as Leu, Ile, and Met. The bundle displays a staggered pattern of ad layers as opposed to parallel layers found in typical coiled coils with helices hα2 and hα2' translated downward by half a helical turn in comparison to hα1 and hα1'.This shift results in an alternating arrangement of knobs in the inner core formed by 'd' residues, majorly Ile in hα1/hα1' and Leu in hα2/hα2' of the ad layers adL1-adL6 **(Figure 3.6.1 B and C)**. The 'd' residues face towards the core accommodating into the pockets formed by the sidechains of peripheral 'a' residues **(Figure 3.6.1 D)**.

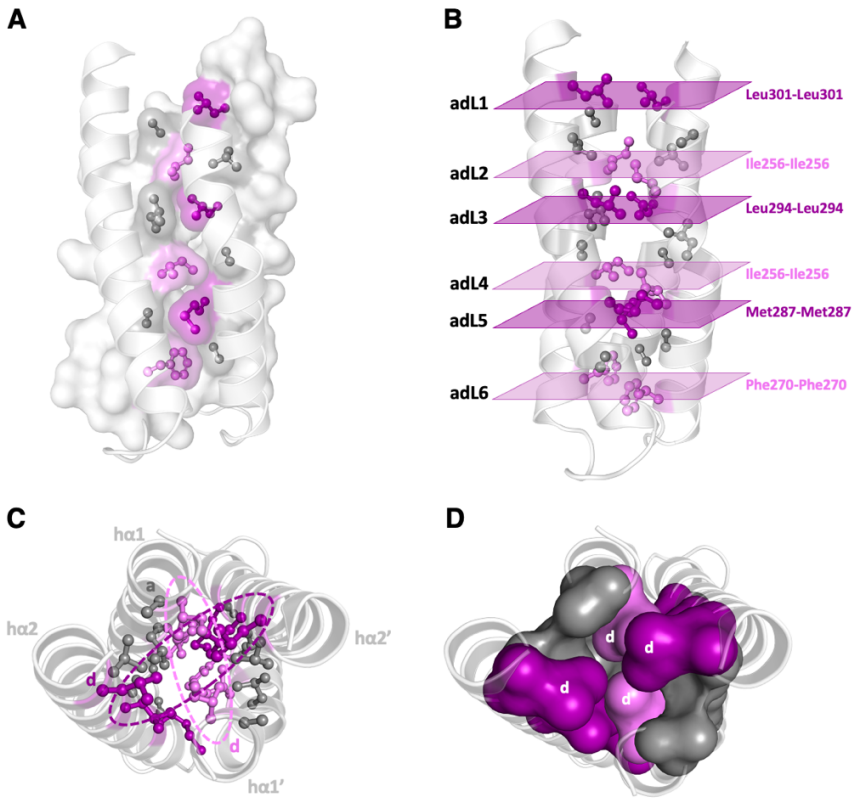

**Figure 3.6.1 Coiled coil packing at the DHp bundle of EcZraS-CD.** (A) The image shows the knobs-into-holes architecture of the DHp bundle. Knobs are formed by the side chains of 'a' (gray50) and 'd' (purple and violet) packed into grooves formed between ridges of neighbouring helices along the dimer interface. (B) The alternating residue layers labelled as adL1–adL6 at position "d" from helix-1 (purple) and helix-2 (violet), forming the inner core of DHp bundle. (C) The top view of the bundle shows the distribution of "a" and "d" residues forming the a and d layers. (D) The surface representation depicts the "d" residues (violet and purple) forming the inner core and "a" residues (gray50) lining its periphery.

## 3.7 A rotary switch mechanism in DHp helices facilitates the transition between alternative structural conformations

The diversity of the DHp domains in SHKs reflects their ability to support various signaling needs. The formation of precise dimer interfaces and structural alignment are essential for kinase function and any disruption in the bundle due to mutations or deletions hinder their autophosphorylation, phosphate transfer, and phosphatase activities (Capra et al., 2010; Qin et al., 2003).

TWISTER revealed a similar distribution of heptads in the bundles of the dimer AB and CD. However, as a result of ligand-induced variations in the local structure, SamCC Turbo was unable to detect the corresponding residue stretches automatically. The stretches were defined manually using dimer XY as a reference to analyze the layering and helical geometry. The layering pattern in EcZraS-CD remained unchanged with evident variations in the Crick angle deviation values **(Figure 3.7.1 A,B and Tables 3.7.1-3.7.3).** Differences in these values between dimers AB and CD indicate altered core packing driven by helical rotation. Further, measurement of other helical parameters - axial shift and radius also signifies bundle rotation

**(Figure 3.7.1 C, D and Tables 3.7.4-3.7.7).** The deviation in r.m.s. values in the mid-section of the DHp bundle were found to be minimal **(Figure 3.7.2).**

Repeated scanning of the linker stretch of the dimers AB and CD using TWISTER revealed the presence of a four-residue insertion (stutter) among the heptads of the linker helices Lα1/Lα1' and DHp helices hα1/hα1' **(Table 3.7.8).** Insertions are known to aid conformation shifts in multiple kinases. They are accommodated along the entire length of the helices, allowing in repacking of the central bundle during signal transfer from the TM to the KD domain. Stutters introduce a non-heptad pattern among the heptads that disrupts the regular knobs-into-holes packing of 'a' and 'd' residues (Schmidt et al., 2017). The dimers AB and CD have 'd' residues forming two kinds of contacts, either a centrally placed tip-to-tip interaction or an extended lateral interaction enclosing the central bundle. A 'd' residue from layer adL5 – Met287 can be seen to exhibit altered packing, forming a lateral association with Ala267 in dimer AB and a tip-to-tip association with Met287 from the opposite protomer in dimer CD **(Figure 3.7.3).** The changes in residue packing at the DHp interface of the dimers involve repositioning of the knobs into holes, causing alterations in the core packing during conformational transition. Other helical residue interactions within the DHp bundle are illustrated in **Figure 3.7.4.**

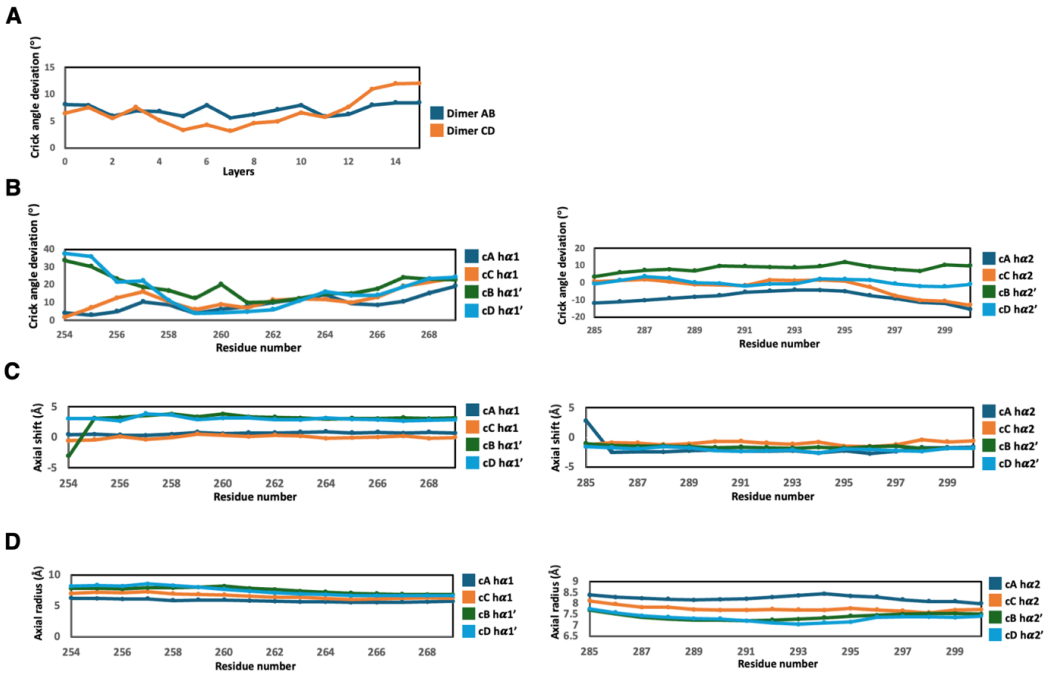


**Figure 3.7.1 Graphical representation of coiled coil parameters derived using SamCC-Turbo.** (A) Line graph representation of the data in Table 3.7.1. The variation in Crick angle deviation values (°) suggests reorganisation of the DHp core packing upon rotation of constituent helices in the bundle. (B) Line graph representation of the data in Tables 3.7.2 and 3.7.3. The displacement of Crick angle deviation (°) per residue in cA and cB is relatively large as compared to that of cC and cD. (C) Line graph representation of the data in Tables 3.7.4 and 3.7.5. The plot shows the axial shift (Å) per residue observed in cA and cB of dimer AB, compared to that of the corresponding chains cC and cD of dimer CD. (D) Line graph representation of the data present in Tables 3.7.6 and 3.7.7.

**A**

**r.m.s.d. values for EcZraS-CD chains**

| Chains | cC | cD |
|---|---|---|
| cA | 1.022 | 3.070 |
| cB | 2.430 | 0.580 |

**B**

**r.m.s.d. values for the DHp residue windows**

| cA | 254-260 | 261-267 | 268-274 | 275-281 | 282-288 | 289-295 | 296-302 |
|---|---|---|---|---|---|---|---|
| cA | 0 | 0 | 0 | 0 | 0 | 0 | 0 |
| cB | 0.428 | 0.229 | 0.126 | 0.277 | 0.200 | 0.151 | 0.193 |
| cC | 0.293 | 0.188 | - | - | 0.228 | 0.099 | 0.141 |
| cD | 0.718 | 0.200 | 0.187 | 0.418 | 0.198 | 0.144 | 0.155 |

**C**

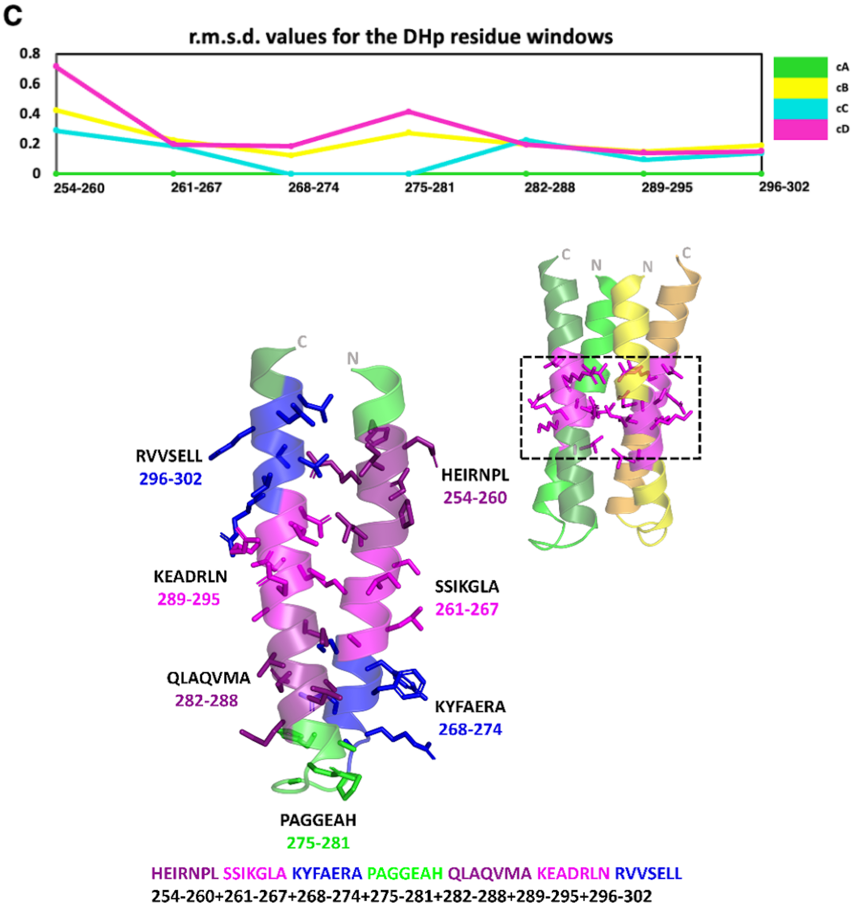


**Figure 3.7.2 R.m.s. deviation (Å) values of EcZraS-CD.** (A) R.m.s. deviation (Å) values calculated using superpose (PyMol) for the chains of dimers AB and CD. (B) R.m.s. deviation (Å) values calculated using Pair_fit algorithm (PyMol) for the 7 residue windows of DHp

domains in dimers AB and CD. Reference used is chain cA. (C) Graphical representation of the r.m.s. deviation (Å) values obtained in using Pair_fit. Pair_fit values for the region 268-274 and 275-281 in cC could not be obtained due to chain break.

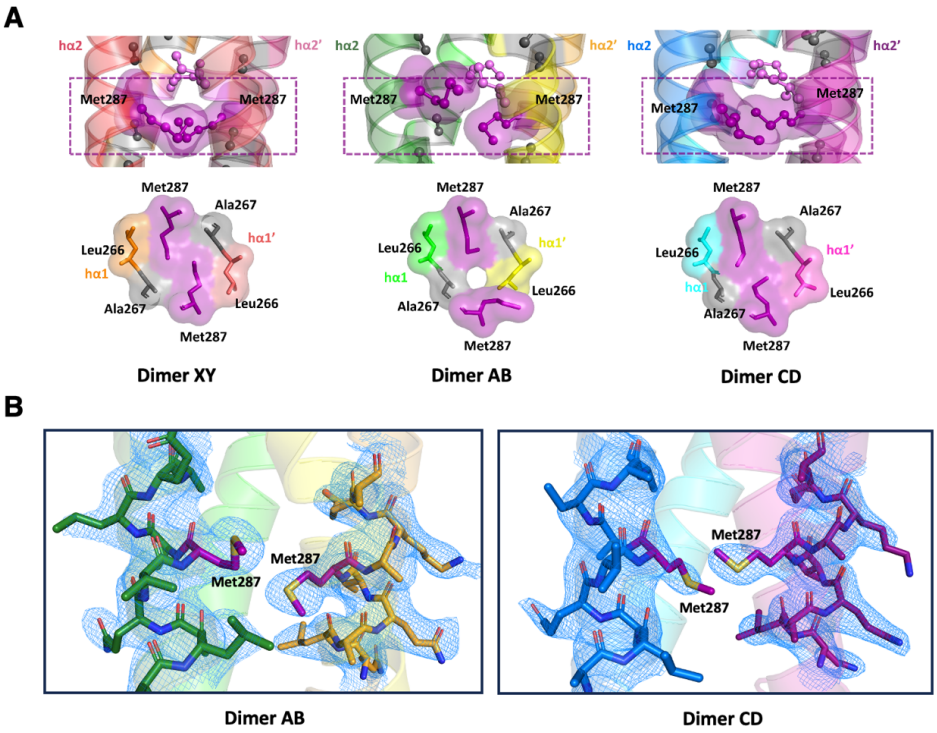


**Figure 3.7.3 Reorganization of interactions at the coiled coil interface.** (A) This image shows the side and top views of Met287-Met278 interaction in the layer adL5 of the apo and ligand-bound dimers. (B) The 2Fo-Fc electron density map contoured at 1.0 σ showing Met287-Met287 interactions in dimers AB and CD.

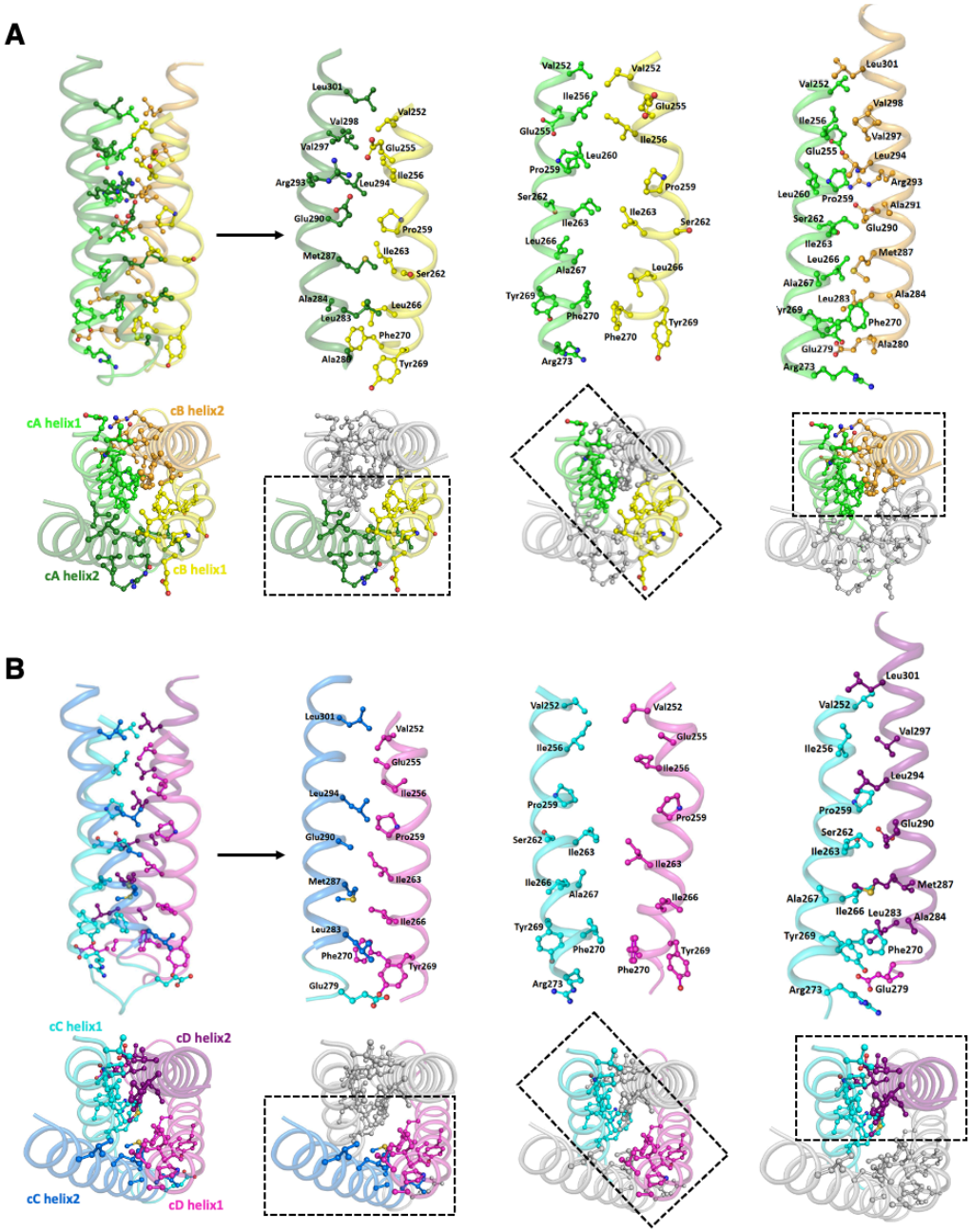


**Figure 3.7.4 Residue interactions at the dimer interface of the DHp bundle in dimers AB and CD.** (A) This image shows the DHp helical interfaces of dimer AB. (B) This image shows the DHp helical interfaces of dimer CD. The chains of dimers AB and CD have been represented as cA hα1 (green), cA hα2 (forest), cB hα1' (yellow), cB hα2' (brightorange), cC

hα1 (cyan), cC hα2 (marine), cD hα1' (magenta) and cD hα2' (deeppurple). The residues have been shown in ball and stick representation.

**Table 3.7.1 Crick angle deviation values per layer of EcZraS-CD DHp (°)** Tabular representation of average Crick angle deviation (°) values for the residue layers, calculated using SamCC-Turbo for the dimers AB and CD. "Layers" are the residue layers predicted according to SamCC-Turbo and "ad Layers" include the identified layers with a and d residues.

| ad layers | Layers | Dimer AB | Dimer CD |
|---|---|---|---|
| | 0 | 8.13 | 6.45 |
| | 1 | 7.99 | 7.56 |
| **adL2** | 2 | 5.99 | 5.58 |
| | 3 | 6.94 | 7.6 |
| | 4 | 6.87 | 5.2 |
| | 5 | 5.92 | 3.34 |
| **adL3** | 6 | 7.99 | 4.3 |
| | 7 | 5.6 | 3.18 |
| | 8 | 6.25 | 4.62 |
| **adL4** | 9 | 7.16 | 4.99 |
| | 10 | 7.99 | 6.58 |
| | 11 | 5.87 | 5.77 |
| | 12 | 6.3 | 7.66 |
| **adL5** | 13 | 8.02 | 10.96 |
| | 14 | 8.47 | 12.03 |
| | 15 | 8.47 | 12.05 |

**Table 3.7.2 Crick angle deviation (°) values per residue of EcZraS-CD DHp helix-1 (254-269)** Tabular representation of the Crick angle deviation (°) values of the residues in the DHp helix-1 calculated using SamCC-Turbo.

| Residue no. | cA hα1 | cC hα1 | cB hα1' | cD hα1' |
|---|---|---|---|---|
| **254** | 4.36 | 1.98 | 33.72 | 37.62 |
| **255** | 3.1 | 7.14 | 30.37 | 35.93 |
| **256** | 5.19 | 12.73 | 23.27 | 21.68 |
| **257** | 10.51 | 16.27 | 18.7 | 22.32 |
| **258** | 8.77 | 10.58 | 16.73 | 11.23 |
| **259** | 4.06 | 6.17 | 12.46 | 4.07 |
| **260** | 6.32 | 9.06 | 20.25 | 4.39 |
| **261** | 7.6 | 7 | 10.02 | 5.02 |
| **262** | 10.05 | 11.55 | 10.61 | 6.12 |
| **263** | 12.07 | 12.2 | 12.39 | 11.06 |
| **264** | 14.51 | 11.84 | 15.08 | 16.05 |
| **265** | 9.58 | 9.97 | 15.04 | 14.12 |
| **266** | 8.6 | 13.12 | 17.73 | 14.17 |
| **267** | 10.74 | 19.33 | 24.16 | 18.94 |
| **268** | 15.44 | 21.63 | 23.32 | 23.54 |
| **269** | 19.24 | 23.77 | 22.82 | 24.27 |

**Table 3.7.3 Crick angle deviation (°) values per residue of EcZraS-CD DHp helix-2 (285-300)** Tabular representation of the Crick angle deviation (°) values of the residues in the DHp helix-2 calculated using SamCC-Turbo.

| Residue no. | cA h$\alpha$2 | cC h$\alpha$2 | cB h$\alpha$2' | cD h$\alpha$2' |
|---|---|---|---|---|
| **285** | -11.76 | 0.71 | 3.57 | -0.54 |
| **286** | -10.87 | 1.49 | 5.99 | 1.45 |
| **287** | -10.08 | 1.92 | 7.26 | 3.63 |
| **288** | -8.91 | 0.65 | 7.79 | 2.72 |
| **289** | -8.17 | -1.08 | 7.03 | 0.08 |
| **290** | -7.4 | -1.14 | 9.78 | -0.43 |
| **291** | -5.41 | -1.53 | 9.58 | -1.76 |
| **292** | -4.68 | 1.56 | 9.03 | -0.74 |
| **293** | -4.13 | 1.19 | 8.92 | -0.49 |
| **294** | -4.23 | 1.58 | 9.63 | 2.17 |
| **295** | -4.89 | 1.04 | 12.05 | 2.07 |
| **296** | -7.41 | -2.56 | 9.39 | 1.56 |
| **297** | -9.16 | -7.58 | 7.73 | -0.6 |
| **298** | -11.32 | -10.09 | 6.81 | -2.01 |
| **299** | -11.87 | -10.7 | 10.35 | -2.13 |
| **300** | -15.37 | -12.91 | 9.82 | -0.9 |

**Table 3.7.4 Axial shift (Å) values per residue of EcZraS-CD DHp helix-1 (254-269)** Tabular representation of the axial shift values (Å) of the residues in the DHp helix-1 calculated using SamCC-Turbo.

| Residue no. | cA h$\alpha$1 | cC h$\alpha$1 | cB h$\alpha$1' | cD h$\alpha$1' |
|---|---|---|---|---|
| **254** | 0.44 | -0.57 | -3.08 | 3.03 |
| **255** | 0.47 | -0.43 | 3.11 | 3.07 |
| **256** | 0.35 | 0.08 | 3.23 | 2.68 |
| **257** | 0.29 | -0.38 | 3.59 | 3.85 |
| **258** | 0.49 | -0.05 | 3.83 | 3.69 |
| **259** | 0.79 | 0.54 | 3.33 | 2.92 |
| **260** | 0.55 | 0.32 | 3.81 | 3.14 |
| **261** | 0.73 | 0.1 | 3.32 | 3.18 |
| **262** | 0.73 | 0.32 | 3.27 | 2.9 |
| **263** | 0.8 | 0.19 | 3.13 | 2.84 |
| **264** | 0.92 | -0.21 | 3 | 3.16 |
| **265** | 0.7 | -0.08 | 3.11 | 2.94 |
| **266** | 0.83 | -0.01 | 3.03 | 2.86 |
| **267** | 0.69 | 0.19 | 3.19 | 2.67 |
| **268** | 0.79 | -0.18 | 3.07 | 2.83 |
| **269** | 0.67 | -0.03 | 3.16 | 2.87 |

**Table 3.7.5 Axial shift (Å) values per residue of EcZraS-CD DHp helix-2 (285-300)** Tabular representation of the axial shift (Å) values of the residues in the DHp helix-2 calculated using SamCC-Turbo.

| Residue no. | cA h$\alpha$2 | cC h$\alpha$2 | cB h$\alpha$2' | cD h$\alpha$2' |
|---|---|---|---|---|
| **285** | 2.8 | -1.26 | -1.03 | -1.59 |
| **286** | -2.49 | -0.91 | -1.38 | -1.74 |
| **287** | -2.4 | -0.95 | -1.47 | -1.91 |
| **288** | -2.44 | -1.25 | -1.42 | -1.6 |
| **289** | -2.28 | -1.08 | -1.52 | -1.79 |
| **290** | -2.19 | -0.71 | -1.73 | -2.24 |
| **291** | -2.32 | -0.66 | -1.61 | -2.37 |
| **292** | -2.3 | -0.94 | -1.71 | -2.28 |
| **293** | -2.25 | -1.16 | -1.8 | -2.12 |
| **294** | -2.66 | -0.81 | -1.7 | -2.64 |
| **295** | -2.27 | -1.5 | -1.84 | -1.96 |
| **296** | -2.75 | -1.55 | -1.57 | -2.09 |
| **297** | -2.38 | -1.23 | -1.5 | -2.23 |
| **298** | -1.74 | -0.4 | -1.84 | -2.36 |
| **299** | -1.75 | -0.75 | -1.83 | -1.89 |
| **300** | -1.63 | -0.62 | -1.88 | -1.84 |

**Table 3.7.6 Axial radius (Å) values per residue of EcZraS-CD DHp helix-1 (254-269)**

Tabular representation of the axial radius (Å) values of the residues in the DHp helix-1 calculated using SamCC-Turbo.

| Residue no. | cA h$\alpha$1 | cC h$\alpha$1 | cB h$\alpha$1' | cD h$\alpha$1' |
|---|---|---|---|---|
| **254** | 6.23 | 7.02 | 7.85 | 8.22 |
| **255** | 6.22 | 7.2 | 7.86 | 8.34 |
| **256** | 6.11 | 7.18 | 7.75 | 8.22 |
| **257** | 6.15 | 7.31 | 7.91 | 8.57 |
| **258** | 5.88 | 6.98 | 7.95 | 8.3 |
| **259** | 5.98 | 6.91 | 8.03 | 8.03 |
| **260** | 5.98 | 6.79 | 8.19 | 7.72 |
| **261** | 5.86 | 6.59 | 7.84 | 7.39 |
| **262** | 5.76 | 6.43 | 7.64 | 7.1 |
| **263** | 5.66 | 6.37 | 7.4 | 6.93 |
| **264** | 5.65 | 6.22 | 7.24 | 6.83 |
| **265** | 5.58 | 6.09 | 7.05 | 6.67 |
| **266** | 5.58 | 6.16 | 6.96 | 6.64 |
| **267** | 5.6 | 6.25 | 6.9 | 6.67 |
| **268** | 5.66 | 6.28 | 6.83 | 6.66 |
| **269** | 5.77 | 6.26 | 6.83 | 6.68 |

**Table 3.7.7 Axial radius (Å) values per residue of EcZraS-CD DHp helix-2 (285-300)**

Tabular representation of the axial radius (Å) values of the residues in the DHp helix-2 measured using SamCC-Turbo.

| Residue no. | cA h$\alpha$2 | cC h$\alpha$2 | cB h$\alpha$2' | cD h$\alpha$2' |
|---|---|---|---|---|
| **285** | 8.38 | 8.11 | 7.69 | 7.74 |
| **286** | 8.28 | 7.95 | 7.52 | 7.57 |
| **287** | 8.23 | 7.82 | 7.36 | 7.43 |
| **288** | 8.19 | 7.82 | 7.29 | 7.36 |
| **289** | 8.15 | 7.71 | 7.23 | 7.3 |
| **290** | 8.18 | 7.68 | 7.23 | 7.28 |
| **291** | 8.2 | 7.69 | 7.2 | 7.19 |
| **292** | 8.28 | 7.73 | 7.23 | 7.11 |
| **293** | 8.36 | 7.7 | 7.27 | 7.04 |
| **294** | 8.44 | 7.68 | 7.33 | 7.11 |
| **295** | 8.33 | 7.76 | 7.42 | 7.14 |
| **296** | 8.29 | 7.7 | 7.45 | 7.36 |
| **297** | 8.16 | 7.65 | 7.5 | 7.39 |
| **298** | 8.08 | 7.57 | 7.53 | 7.38 |
| **299** | 8.08 | 7.68 | 7.53 | 7.35 |
| **300** | 7.98 | 7.71 | 7.51 | 7.41 |

**Table 3.7.8 Prediction of heptad repeats in linker and DHp helix-1 of EcZraS-CD** Tabular representation of the heptad positions predicted using the program TWISTER. The region predicted to be the stutter is highlighted in yellow.

| Residue no. | Residue | Dimer AB | Dimer CD |
|---|---|---|---|
| **226** | L | | f |
| **227** | R | | g |
| **228** | S | | a |
| **229** | R | | b |
| **230** | Q | c | c |
| **231** | L | d | a |
| **232** | L | e | b |
| **233** | Q | f | c |
| **234** | D | g | d |
| **235** | E | a | e |
| **236** | M | b | f |
| **237** | K | c | g |
| **238** | R | d | d |
| **239** | K | e | e |
| **240** | E | f | f |
| **241** | K | g | g |
| **242** | L | a | a |
| **243** | V | b | b |
| **244** | A | c | c |
| **245** | L | d | d |
| **246** | G | e | e |
| **247** | H | f | f |
| **248** | L | g | g |
| **249** | **A** | **a** | **a** |

| | | | |
|---|---|---|---|
| **250** | **A** | **b** | **b** |
| **251** | **G** | **c** | **c** |
| **252** | **V** | **z** | **z** |
| **253** | A | a | a |
| **254** | H | b | b |
| **255** | E | c | c |
| **256** | I | d | d |
| **257** | R | e | e |
| **258** | N | f | f |
| **259** | P | g | g |
| **260** | L | a | a |
| **261** | S | b | b |
| **262** | S | c | c |
| **263** | I | d | d |
| **264** | K | e | e |
| **265** | G | f | f |
| **266** | L | g | g |
| **267** | A | a | a |
| **268** | K | b | b |
| **269** | Y | c | c |
| **270** | F | d | d |

## 3.8 Balance between polar and hydrophobic residue interactions result in rearrangement of the ad layers of the DHp bundle

The hydrophobic residues forming the core interface of the DHp bundle of EcZraS-CD stabilise the four-helix bundle. The periphery of the core is flanked by “c” and “g” residues forming interfaces between hα1–hα2’ and hα1’–hα2. A layering rearrangement in the core is observed

in dimers AB and CD upon variable interaction of polar "c" and "g" residues like Glu255, Ser262, and Glu290 **(Figure 3.8.1 A and B).** These residues hinder a rigid core packing, facilitating structural flexibility, a prerequisite for bundle dynamics. The protomers of dimers AB and CD show differential interactions at the peripheral interfaces between hα1–hα2' and hα1'–hα2. The c-c and g-g interactions occur predominantly at the hα1'–hα2 interface located closer to the adjacent CA domain, in contrast to the c-g pairing observed at the distant hα1–hα2' interface. This shift in interaction pattern, as seen in dimer AB signifies a change in helical registry **(Figure 3.8.1 C).** Gomez et al. demonstrated the role of both core and peripheral interactions in determining the mechanical stability and flexibility of coiled coils (Gomez et al., 2019). The coiled coil stalk of the motor protein dynein undergoes translational movement guided by the interplay between hydrophobic and electrostatic forces at the superhelical core and peripheral interfaces.

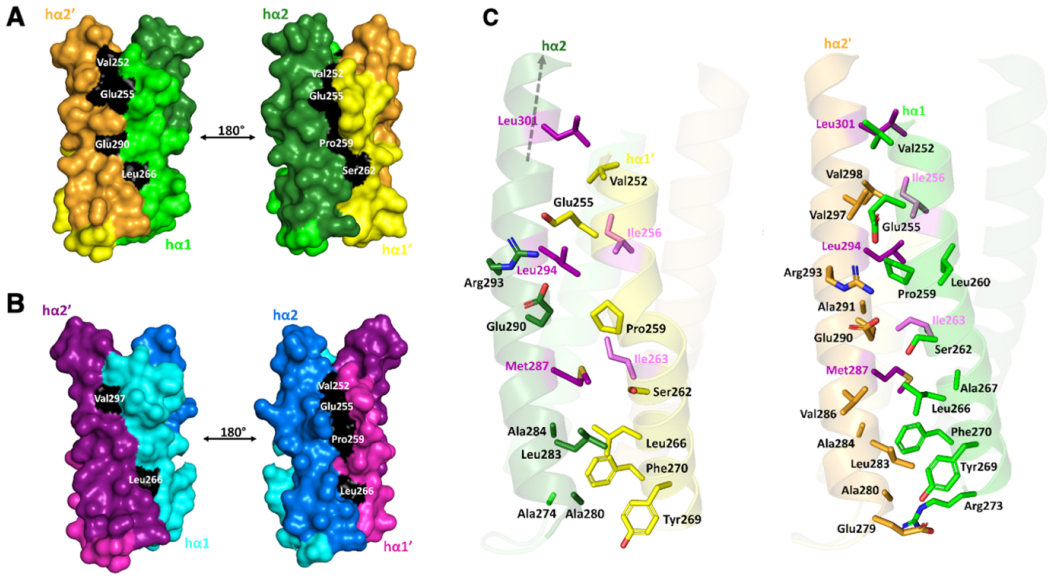


**Figure 3.8.1 Helical interface interactions of the DHp domain in dimers AB and CD.** (A) and (B) "c" and "g" residues of DHp hα1-hα2' and hα1'-hα2 of dimer AB and CD interacting directly with the inner core forming "d" residues. This aids in the reorganization of the coiled

coil layers. (C) Differential residue interactions on either side of the bundle between helices hα1'-hα2 and hα1-hα2' in dimer AB.

## 3.9 Directionality of kinase rotation is governed by interactions involving base aromatic and loop residues

The modes of autophosphorylation in SHKs – cis (left-handed) and trans (right-handed) require precise coordination of the CA domain motions across its central bundle. It is speculated to be mediated by structural alterations at the bundle base (Ashenberg et al., 2013; Casino et al., 2014). In vitro phosphorylation studies in *E. coli* show ZraS is a trans-acting kinase, but the structural basis underlying the mechanism remains elusive (Yamamoto et al., 2005). The asymmetric dimers AB and CD exhibit a distal CA domain having a pronounced vertical shift and rotation of approximately 170°, absent in the proximal CA domain **(Figure 3.5.2 C).** The hydrophobic core of the DHp bundle contains a localized cluster of aromatic residues such as Tyr and Phe, in the base of helices hα1 and hα1'. The side chains of the base Phe270 residues extend into the bundle core with solvent-exposed Tyr269 residues flanking either sides of each homodimer. The Phe270 residues from cA hα1 and cB hα1' are arranged in a parallel-displaced orientation 4.8 Å apart. Comparison of the spatial positions of Tyr269 and Phe270 shows Tyr269 to be 5.0 Å away from Phe270 in cA, while being 5.7 Å in cB **(Figure 3.9.1 A).** Further, Tyr 269 residues display variable interactions with the base of the bundle and the adjacent loop bordering Glu279 residues. It results in the formation of resulting in two interface patterns, between the helix pairs hα1–hα2' and hα1'–hα2, where only Tyr269 of cA interacts with Glu279 from cB **(Figure 3.9.1 B).** A similar conformation is observed for dimer CD, confirming the presence of an adaptable π–π stacking in Tyr269–Phe270 and electrostatic coupling between Tyr269-Glu279 across the bundle base. It potentially introduced a torsional

stress that facilitates bundle rotation. The absence of electron density of the base loop in cB suggests the dynamic nature of the bundle base.

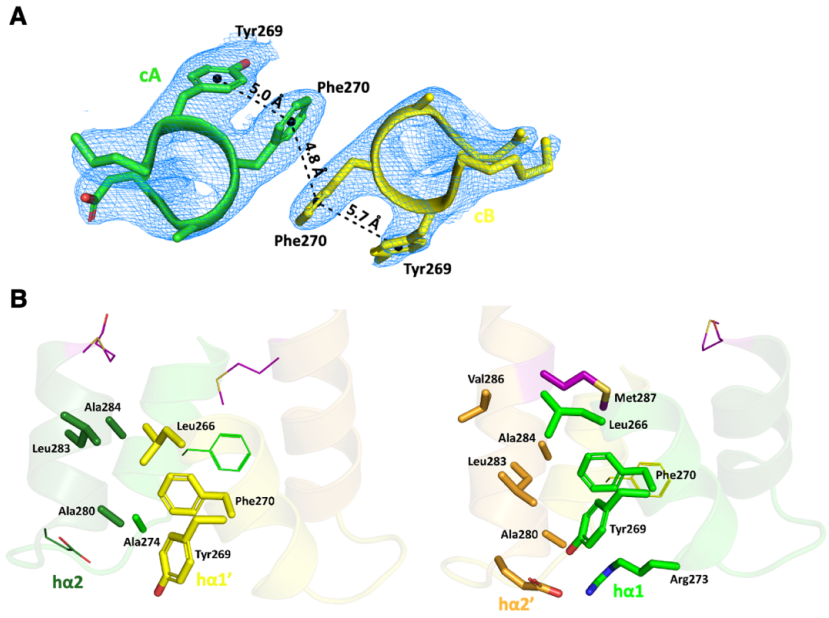


**Figure 3.9.1 Interactions at the DHp bundle base of dimer AB.** (A) 2Fo-Fc map contoured 1.0 σ showing the distance between aromatic amino acid residues Tyr269 and Phe270 of chains cA and cB. (B) Bundle base interactions regulating rotation. Interacting residues are shown in stick representation, and non-interacting residues are shown in line representation.

## 3.10 Helical bending and scissoring in the DHp bundle of EcZraS-CD

The α-helix destabilizing residues such as Pro and Gly are frequently found in dynamic proteins and regions requiring structural flexibility (Barlow & Thornton, 1988; Chou & Pasman, 1974; Reiersen & Rees, 2001). The H-box Pro259 of EcZraS-CD induces a noticeable kink in the helical backbone of DHp bundle. The region containing Pro259 shows minimal distortion in both dimers AB and CD but vary in their extent of helical bending before and after the residue.

The angles of bending for hα1 and hα1' of dimer AB were observed to be 12° and 26°, and those of hα1 and hα1' of dimer CD to be ~21° and 20° **(Figure 3.5.2 B)**.

Helices found in both membrane-associated and aqueous environments, such as those present in GPCRs, SHKs, motor protein stalks, and ion channel gating elements utilize kinks or hinges to support their biological functions (Can et al., 2019; Hauser et al., 2021; Wang et al., 2013; Woolfson et al., 1991). Most SHKs majorly rely on Pro-induced kinks but a few SHKs, such as DesK (3gig), feature a Gly-induced kink (Albanesi et al., 2009). Studies on VicK demonstrated abolition of phosphatase activity upon replacement of Pro with Ala and restoration by mutation to Gly. This highlights the crucial function of hinge-forming residues in conformational switching.

## 3.11 A unique α-helical linker facilitates signal relay to the DHp bundle

The N-terminal helical extension of the KD forms a linker segment that connects it to the membrane-spanning helix TM2. Unlike typical linkers with complex topology and tertiary structures, the linker of EcZraS-CD has a simple helical structure differing from well-characterized α-helical linkers such as the S and Jα-helices (Stewart & Chen, 2010). Sequence-based analysis using psi-BLAST, pLM-BLAST, PLM Search, and multiple sequence alignments with known S-helices failed to identify available homologs for the linker. The pattern for coiled coil heptads could not be detected using SamCC Turbo. Use of TWISTER helped detect both canonical and non-canonical heptads in the region interspersed by an amino acid insertion (stutter).

The 'a' and 'd' positions of the linker region are predominantly occupied by hydrophobic residues, with an occasional presence of polar residues at position 'a'. The linker and DHp helices lack presence of a defined boundary lying juxtaposed on one another, resulting in a

continuous coiled coil. The presence of polar clusters Arg227-Gln230 (RSRQ) and Gln233-Met236 (QDEM) reduced the stability of the coiled coil, promoting structural plasticity. Comparison of dimers AB and CD reveals differences in the linker interface interactions during signaling, evident with bending of cC of dimer CD through ~47° **(Figure 3.11.1)**. This bending is likely caused by polar residues such as Arg238 and Asp234.

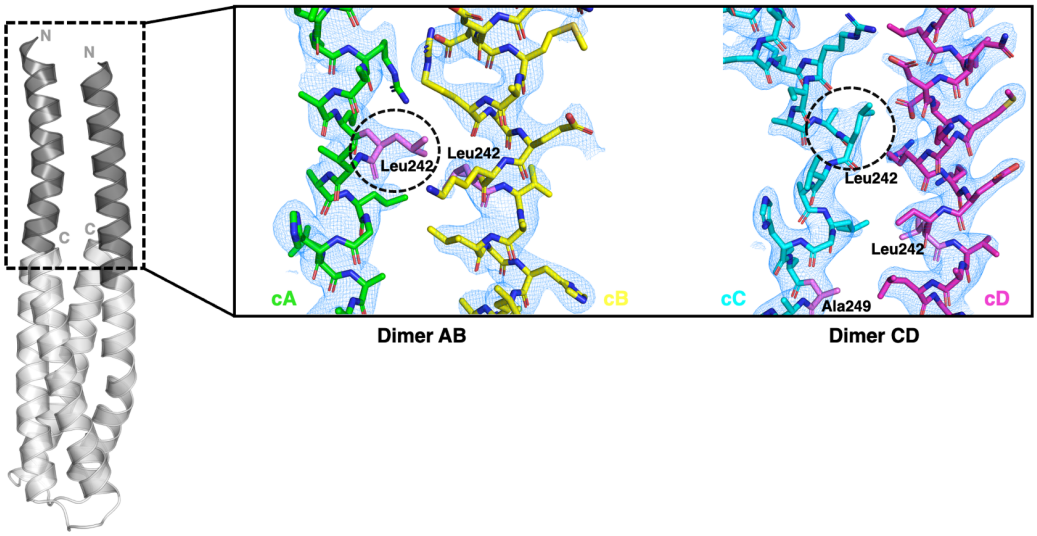


**Figure 3.11.1 Residue interactions at the linker interface of dimers AB and CD.** The disruption in the layering arrangement of the residues in the linker region is caused due to intervention by polar clusters. The 'd' residues interacting at the interface are labelled in violet. 2Fo-Fc maps for each dimer are contoured at 1.0 σ. The dotted circles highlight the position of Leu242, a residue where the bending initiates in the chains cA and cC.

## 3.12 CA-DHp interface of the ligand-bound dimers of EcZraS-CD

The CA domains of cA and cC of EcZraS-CD form CA–DHp interfaces with hα1 helices of cB and cD, respectively **(Figure 3.12.1 A)**. Tyr 412, a lid loop residue located on the proximally placed CA domain, interacts with residues Leu248, Gly251, and Val252 on the

DHp helices of the opposite protomer in both the dimers AB and CD. Pro411 of cA and cC interacts with Tyr412 and Leu248 of the opposing CA domains in cB and cD. However, no detectable interactions were observed between residues of the CA domain and phosphorylable His254 found in previously known Michaelis complexes (Casino et al., 2014; Mechaly et al., 2014). The electrostatic surface potential analysis indicated the interaction to be driven by charge complementarity between a positively charged region on the CA domain and a negatively charged region on the DHp bundle **(Figure 3.12.1 B)**.

The dimer AB displayed additional CA-CA interactions, not observed in dimer CD. These contacts may play a crucial role in the functional co-ordination and inter-domain allosteric regulation in SHKs, enabling conformational changes in one domain to influence the other during autophosphorylation. Further, the lack of direct interaction between CA domain residues and His254 of the DHp bundle supports a step-wise transition to the final autophosphorylation complex through formation of several contact interfaces between the domains or the multi-step transition hypothesis.

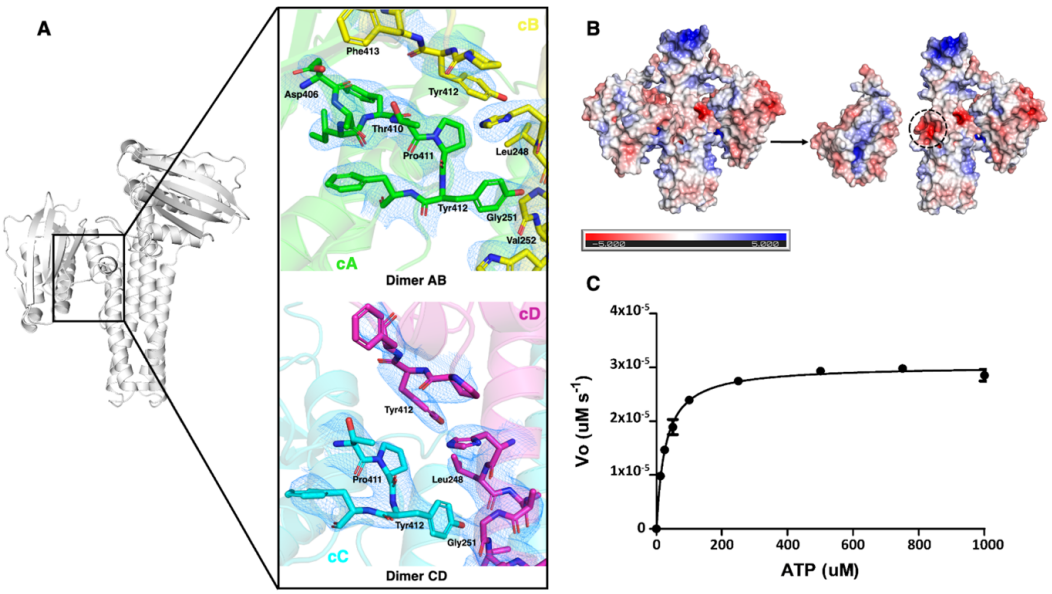

**Figure 3.12.1 CA-DHp interface for the ligand-bound dimers and rate kinetics of EcZraS-CD.** (A) The image shows interacting residues in stick representation at the CA-DHp interface of the dimers AB and CD. (B) The electrostatic surface potential representation of the CA and DHp interfaces. The nucleotide binding pocket has a highly positive electrostatic potential while the corresponding interacting surface of DHp bundle has a highly negative electrostatic potential. (C) The Michaelis-Menten curve showing ATP dependence on initial velocities of autophosphorylation. It has been used to calculate the rate of ATPase activity of EcZraS-CD.

## 3.13 Crystal packing of EcZraS-CD

The molecules of EcZraS-CD (cA, cB, cC and cD) are arranged into a monoclinic system with a C2 space group. In the unit cell, the molecules are related by equivalent points: **1. x,y,z; 2. -x, y, -z; 3.x+1/2, y+1/2, z; and 4. ½-x, y+1/2, -z.** The asymmetric unit comprises four chains arranged as two homodimers AB and CD. The homodimers related by a NCS (Non-crystallographic symmetry) two-fold, which results in antiparallel orientation between AB and CD dimers. The Matthews coefficient, $V_m$ = 2.65 (Å$^3$/Da), Table 3.2.1 suggests a solvent content of 53.6%, with the rest of the unit cell (46.4%) occupied by the EcZraS. These numbers are suggestive of soft packing of EcZraS in the crystal lattice. In the following section, we will discuss about the crystal packing and how the symmetry-related molecules are stabilized in the packing.

Interface analysis of the constituent chains using Protein Interfaces, Surfaces and Assemblies (PISA) (Krissinel & Henrick, 2007) shows 4 significant interfaces formed between the chains cA-cB, cC-cD, cA-cC and cB-cD with buried surface area (BSA) values of 1882, 1664.1, 1795.1 and 932 Å$^2$, and free energy of interaction (ΔG) values of -40.1, -39.6, -20.5 and -7 kcal/mol, respectively **(Appendix A).** This suggests the presence of biological interfaces

between cA-cB and cC-cD. The interface cB-cD likely forms a crystal contact with a small buried surface area and a free energy of interaction value. The cA–cC interface possesses a relatively higher number of hydrogen bonds in comparison with cA–cB and cC–cD interfaces. However, the cA–cB and cC–cD interfaces are predominantly hydrophobic in nature, consistent with the canonical dimerization mode observed in sensor histidine kinases and other biologically relevant helical bundle assemblies (Bhate et al., 2015; Kalinowska et al., 2017). The absence of characteristic hydrophobic packing at the cA–cC interface and the presence of a symmetry relationship suggest that the interface likely arises from a crystallographic screw-axis operation rather than from a physiological interaction. Further, the interatomic contacts between the constituent chains and their symmetry mates are shown in **Figure 3.13.1** and **Appendix B**, highlighting hydrogen-bond and salt-bridge interactions (Agirre et al., 2023).

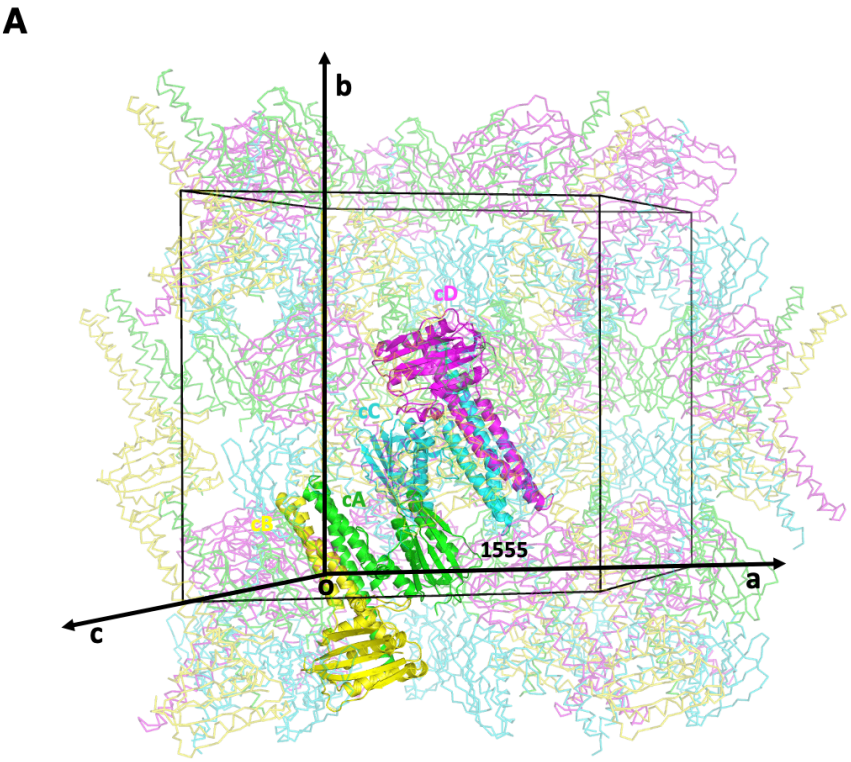


In 1555, 1 stands for the symmetry operator and 555 stands for translation across x,y and z. Translation along x,y,z is 0,0,0 respectively.

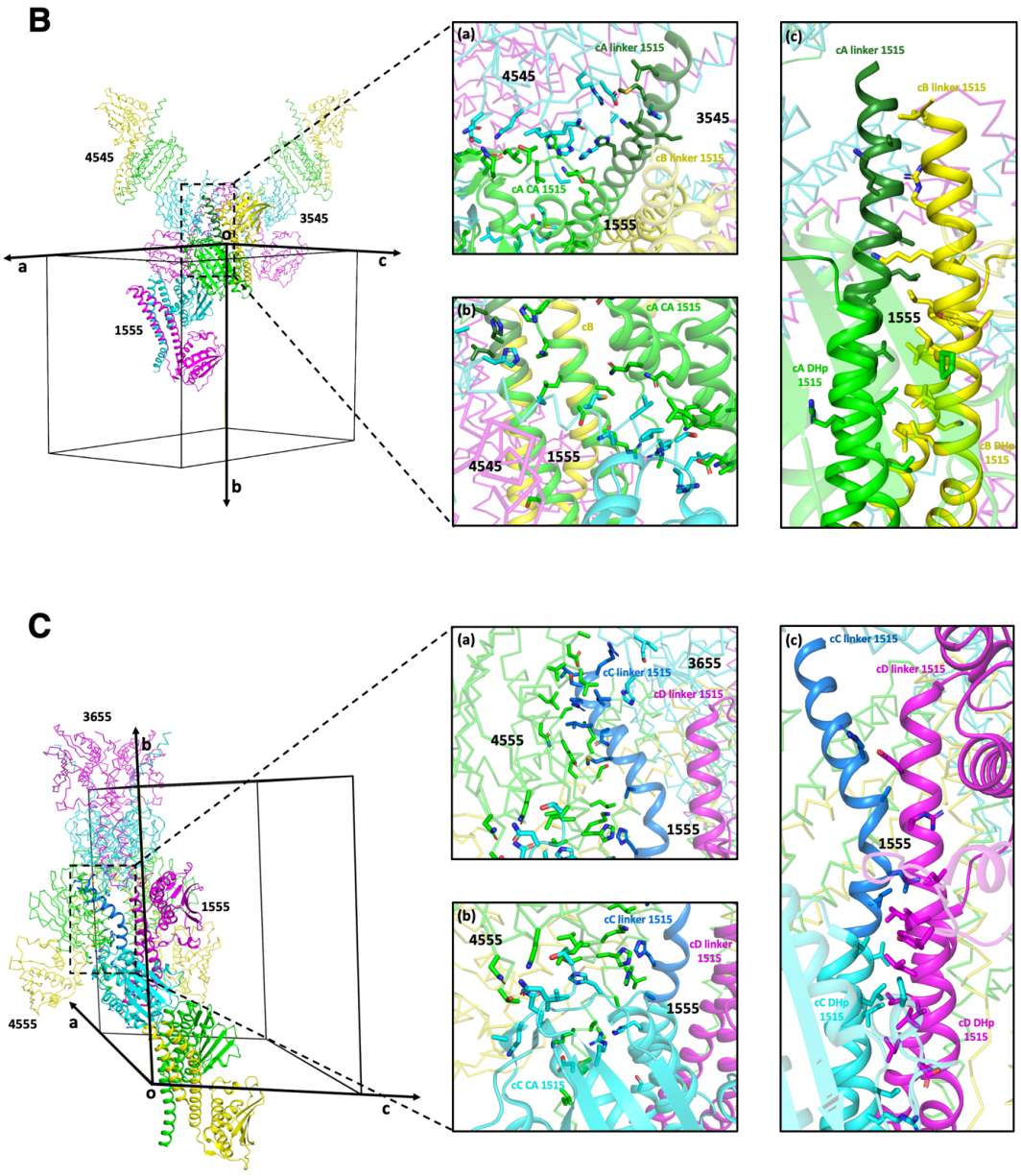


**Figure 3.13.1 Crystal packing: Packing of EcZraS-CD with symmetry mates.** (A) Arrangement of symmetry mates of EcZraS-CD inside the unit cell. The image shows how cA, cB, cC and cD of EcZraS-CD dimers AB and CD pack inside a crystal lattice. 1555 refers to the set of two antiparallel homodimers AB and CD of EcZraS-CD at the origin (0,0,0) of the unit cell, without any translation. 3545,3655,4545, 4555 denote the symmetry operator and

translations used to generate the respective symmetry mates. (B) The image shows interactions between the linker region (cartoon, forest) and the CA domain (cartoon, green) of cA, with symmetry mates shown in ribbon representation with chains cA (green), cB (yellow), cC (cyan) and cD (magenta) in (a) and (b). (c) shows interaction between the linker regions of cA and cB of dimer AB. (C) The image shows interactions between the linker region (cartoon, marine) and the CA domain (cartoon, cyan) of cC, with symmetry mates shown in ribbon representation with chains cA (green), cB (yellow), cC (cyan) and cD (magenta) in (a) and (b). (c) shows interaction between the linker regions of cC and cD of dimer CD.

## 3.14 Kinetic characterization of EcZraS-CD

To determine the ATPase activity of EcZraS-CD, a coupled assay system as mentioned in section 2.5 was performed. The data plot obtained followed the conventional Michaelis-Menten kinetics curve **(Figure 3.12.1 C).** The $K_m$ and $V_{max}$ values were determined to be 27.31 and $3.032 \times 10^{-5}$ μM/s with an enzyme concentration of 15 μM.

## 3.15 Conclusion

The transfer of signal across multidomain proteins such as SHKs is indeed an intricate and elaborate process requiring concerted and well-orchestrated changes of both interdomain and intradomain nature. To navigate through a multitude of confers, they rely on numerous intermediate states that undergo gradual structural rearrangements in a step-wise manner. As shown in **Figure 3.15.1**, the transition of ZraS from an inactive apo to a ligand-bound state occurs through numerous intermediate conformers. The dimers AB and CD represent two such successive intermediate conformers before formation of the final Michaelis or

autophosphorylation complex. Structural comparison suggested rearrangement of the dimerization interface of the bundle through helicity shifts, rotational movement, bending, scissoring and amino acid insertion. Further studies capturing additional conformations will be necessary to determine an even more precise sequence of events leading to signal transfer.

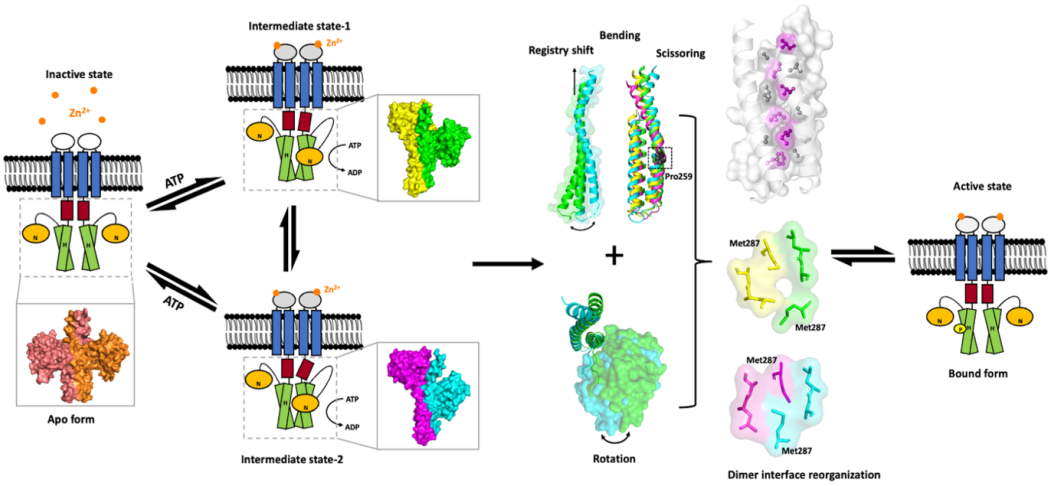


**Figure 3.15.1 Schematic representation of autokinase activation of EcZraS-CD.** The cytoplasmic domain of ZraS illustrates transition from an inactive apo form to an active ligand-bound form that is mediated through intermediate conformers, state-1 (dimer AB) and state-2 (dimer CD). Conformational transition in the cytoplasmic region is facilitated through dimer interface reorganization driven by helical bending, scissoring, registry shift, and domain rotation.

# Chapter 4
# Future development and directions

*Chapter-4*

## 4.1 Trapping EcZraS-CD in its active histidine phosphorylating state

Studying the association of the CA and DHp domains in an ATP-bound state formed during autophosphorylation prior to γ-phosphate transfer to the conserved His residue is essential to understand the process of kinase activation and overall signal transfer. Due to the hydrolysis of the γ-phosphate of ATP and the labile nature of N~P bond in HK-His~P, the structure of a handful of HKs has been captured in their final autophosphorylation state. To trap additional conformations nearing the final state, EcZraS-CD can be co-crystallised with non-hydrolyzable analogs of ATP - AMP-PNP or ANP and ATP-γ-S. The structural comparison of conformers obtained can be compared to the known structures, to further validate and gain additional insights into conformational transitions required for autokinase activation.

## 4.2 Understanding the mechanism of zinc binding in the periplasmic domain

The periplasmic domain, EcZraS-SD of ZraS is speculated to sense zinc ions. But the binding site and geometry of binding remain uncertain. To determine the metal-binding site, mutational studies of zinc-binding residues such as His, Cys, Glu, Asp may be considered. The wild-type and mutant proteins can be subjected to techniques such as PAR (4-(2-Pyridylazo)resorcinol) assay, followed by ITC (Isothermal titration calorimetry) or fluorescence spectrometry to test for zinc binding sites. Additionally, metal-induced oligomerisation may be tested using techniques such as size exclusion chromatography (SEC) or analytical ultracentrifugation (AUC).

## 4.3 Understanding interactions between ZraS and ZraP

The periplasmic zinc chaperon binds with the periplasmic domain of ZraS to regulate the signaling cascade. This binding is known to activate a negative feedback pathway to inhibit ZraS. However, the interaction between ZraS and ZraP remains elusive of any structural or biochemical analysis. Protein-protein interaction studies between ZraS and ZraP through co-immunoprecipitation, bacterial two-hybrid assay or ITC can be performed to check for their association in the presence and absence of zinc or zinc mimetics. Further, such assays can also be performed with loop variants to check for the effect of loop truncation on the binding efficiency of the signaling partners.

## 4.4 Applications of sensor histidine kinases

SHKs have emerged as essential tools serving a wide range of applications such as understanding adaptation and evolution of organisms, development of novel antimicrobials, biosensors and repurposing chimeric or synthetic signaling circuits.

### 4.4.1 Understanding the mechanism of signal transduction

The TCSs are one of the most widely known stimuli sensors distributed across the microbial membranes. The primary application of studying SHKs is to understand the process of signal transduction within these systems. The SHKs are bifunctional switches transitioning through multiples intermediate states acting as either kinases or phosphatases. Studies on SHKs can enhance our understanding of stimuli detection, conformational switching between kinase and phosphatase states, followed by signal transfer from the SHK to its cognate partner RR.

### 4.4.2 Understanding the process of microbial evolution

Though the core kinase module remains fairly conserved across all the SHKs, structural modifications through domain duplications, fusions and shuffling has often been found to result in formation of new SHKs. With their modular domain architecture, sequence and functional diversity, comparative analysis of amino acid sequence, domain arrangements, functions and presence across multiple domains of life can aid study of microbial evolution. They can be subjected to the process of directed evolution modifying their abilities to sense stimuli or elicit an output response.

### 4.4.3 Development of novel antimicrobials

Resistance to antibiotics and antimicrobials is a raising concern in the global health sector. With more and more pathogens becoming resistant to newly developed drugs, the need of the hour is to search for new druggable targets. The absence of SHKs in humans, enhances their potential of being used as drug targets. Such targets could include SHKs involved in regulating crucial metabolic pathways, biofilm formation, or those aiding antimicrobial sensing in microbes, leading to degradation and efflux of drugs. Recent studies have identified numerous small molecules such as benzothiazole, thiazolidione, luteolin, waldiomycin, signermycin, that can be used to inhibit different domains of SHKs (Ahsan et al., 2024; H. Chen et al., 2022; Igarashi et al., 2013; Wilke et al., 2015).

### 4.4.4 Development of biosensors

SHKs in microorganisms can be repurposed to aid the process of bioremediation. The extracellular periplasmic domains can be engineered to detect environmental pollutants such as heavy metals, nitrogenous and phosphorous-containing wastes, hydrocarbons and other organic compounds. They can also be modified to detect metabolites, drugs and inflammatory compounds, used for the diagnosis of medical conditions.

### 4.4.5 Development of artificial signaling circuits

The modular arrangement of domains in SHKs provides an additional benefit, recombining them to design artificial signaling circuits. Domains from two or more SHKs can be fused to produce chimeric proteins, allowing activation of signaling cascades through different sets of stimuli or producing a response that differs from the naturally existing one. SHKs can be modified to build entirely new signaling circuits responding to a specific stimulus used for reprogramming cellular behaviour, metabolism and production of desired biomolecules. SHKs of plant bacteria can be modified to respond to plant-specific signals, improving nutrient uptake and disease resistance. Synthetic systems in human cells could respond to disease-specific signals and help release therapeutic agents such as antibodies, interferons, cytokines etc. Further, drug delivery in targeted environments can be achieved by engineering SHKs in microbial or cell-based drug carriers to release drugs (low or high pH).

With the multitude of applications and considering its broad potential in biotechnology and medicine, understanding the structure and function of SHKs remains crucial.

# Appendix

# APPENDIX A: PISA analysis

## Table A1 PISA interface table for EcZraS-CD

| Serial no. | Int type | Monomer1 | Monomer2 | Symmetry Operation | BSA (Å²) | ΔG (kcal/mol) | Nhb | Nsb | Nds |
|---|---|---|---|---|---|---|---|---|---|
| 1 | 1 | B | A | X,Y,Z | 1882 | -40.1 | 1 | 1 | 0 |
| 2 | 2 | A | C | -X+1/2,Y-1/2,-Z | 1795.1 | -20.5 | 8 | 1 | 0 |
| 3 | 3 | C | D | X,Y,Z | 1664.1 | -39.6 | 4 | 4 | 0 |
| 4 | 4 | B | D | X-1/2,Y-1/2,Z | 932 | -7 | 7 | 0 | 0 |
| 5 | 5f | [ADP]C:801 | C | X,Y,Z | 392.1 | -5.9 | 14 | 0 | 0 |
| 6 | 6f | [ADP]A:801 | A | X,Y,Z | 381.4 | -5.8 | 13 | 0 | 0 |
| 7 | 7f | [ADP]D:801 | D | X,Y,Z | 375.7 | -4.9 | 10 | 0 | 0 |
| 8 | 8f | [ADP]B:801 | B | X,Y,Z | 368.8 | -5.7 | 11 | 0 | 0 |
| 9 | 9 | C | D | -X+1/2,Y-1/2,-Z | 352.9 | -0.8 | 4 | 0 | 0 |
| 10 | 10 | C | D | -X+1,Y,-Z | 315.6 | -3.7 | 0 | 0 | 0 |
| 11 | 11 | B | A | -X,Y,-Z | 307.6 | -3 | 0 | 1 | 0 |
| 12 | 12 | B | A | -X+1/2,Y-1/2,-Z+1 | 227.8 | -0.4 | 0 | 1 | 0 |
| 13 | 13 | C | B | -X,Y,-Z | 211.9 | -0.6 | 3 | 0 | 0 |
| 14 | 14x | C | C | -X+1/2,Y-1/2,-Z | 163.4 | 0.7 | 4 | 0 | 0 |
| 15 | 15 | C | A | X,Y,Z | 142.2 | -3.4 | 0 | 0 | 0 |
| 16 | 16 | B | B | -X,Y,-Z | 101.8 | 0.2 | 0 | 2 | 0 |
| 17 | 16 | D | D | -X+1,Y,-Z | 99.3 | 0.8 | 0 | 2 | 0 |
| 18 | 17 | A | A | -X+1,Y,-Z+1 | 74.2 | 0.8 | 0 | 0 | 0 |
| 19 | 18f | [MG]A:800 | A | X,Y,Z | 46 | -5.4 | 0 | 0 | 0 |
| 20 | 19f | [MG]C:800 | C | X,Y,Z | 44.3 | -5 | 0 | 0 | 0 |
| 21 | 20f | [MG]B:800 | B | X,Y,Z | 41 | -5 | 0 | 0 | 0 |
| 22 | 20f | [MG]D:800 | D | X,Y,Z | 40.4 | -4.4 | 0 | 0 | 0 |
| 23 | 21 | A | D | X-1/2,Y-1/2,Z | 40.9 | -0.3 | 0 | 0 | 0 |
| 24 | 22 | C | C | -X+1,Y,-Z | 40.1 | -1.2 | 0 | 0 | 0 |
| 25 | 23 | A | A | -X,Y,-Z | 39.4 | -1.3 | 0 | 0 | 0 |
| 26 | 24f | [ADP]D:801 | [MG]D:800 | X,Y,Z | 37.3 | -6.4 | 0 | 0 | 0 |
| 27 | 24f | [ADP]B:801 | [MG]B:800 | X,Y,Z | 36.1 | -5.9 | 0 | 0 | 0 |
| 28 | 24f | [ADP]C:801 | [MG]C:800 | X,Y,Z | 35.7 | -5.7 | 0 | 0 | 0 |
| 29 | 24f | [ADP]A:801 | [MG]A:800 | X,Y,Z | 34.6 | -5.4 | 0 | 0 | 0 |
| 30 | 25 | D | D | -X+1,Y,-Z+1 | 6.3 | 0.1 | 0 | 0 | 0 |
| 31 | 26 | C | A | -X,Y,-Z | 5.9 | 0 | 0 | 0 | 0 |

Int type – Interface type, f - fixed or ligand-related interface, x - crystal contact interface, BSA – buried surface area, DeltaG - free energy of interaction, Nhb - number of hydrogen bonds across the interface, Nsb - number of salt bridges, Nds - number of disulfide bonds.

# APPENDIX B: Interaction of EcZraS-CD dimers with symmetry mates

## Table B1 Inter-atomic contact distances between symmetry-related molecules and chains cA of dimer AB of EcZraS-CD

| Source residue | Source residue no. | Source atom | Target residue | Target residue no. | Target atom | Distance | Unit cell translation | X | Y | Z |
|---|---|---|---|---|---|---|---|---|---|---|
| Leu | 232A | CD1 | Asp | 355C | OD1 | 3.53 | -1B | -X+1/2 | Y+1/2 | -Z |
| Met | 236A | SD | Asp | 355C | OD2 | 2.98 | -1B | -X+1/2 | Y+1/2 | -Z |
| Met | 236A | SD | Asp | 355C | CB | 3.4 | -1B | -X+1/2 | Y+1/2 | -Z |
| Met | 236A | SD | Asp | 355C | CG | 3.18 | -1B | -X+1/2 | Y+1/2 | -Z |
| Met | 236A | CE | Arg | 356C | CZ | 3.64 | -1B | -X+1/2 | Y+1/2 | -Z |
| Met | 236A | CE | Arg | 356C | NH1 | 2.95 | -1B | -X+1/2 | Y+1/2 | -Z |
| Lys | 239A | NZ | Asp | 355C | OD2 | 2.5 | -1B | -X+1/2 | Y+1/2 | -Z |
| Lys | 239A | NZ | Asp | 355C | CG | 3.67 | -1B | -X+1/2 | Y+1/2 | -Z |
| Glu | 240A | C | His | 254C | NE2 | 3.37 | -1B | -X+1/2 | Y+1/2 | -Z |
| Glu | 240A | O | His | 254C | NE2 | 3.57 | -1B | -X+1/2 | Y+1/2 | -Z |
| Glu | 240A | CB | His | 254C | NE2 | 3.44 | -1B | -X+1/2 | Y+1/2 | -Z |
| Lys | 241A | N | His | 254C | CE1 | 3.64 | -1B | -X+1/2 | Y+1/2 | -Z |
| Lys | 241A | N | His | 254C | NE2 | 3.37 | -1B | -X+1/2 | Y+1/2 | -Z |
| Lys | 241A | CA | His | 254C | CE1 | 3.38 | -1B | -X+1/2 | Y+1/2 | -Z |
| Lys | 241A | CA | His | 254C | NE2 | 3.62 | -1B | -X+1/2 | Y+1/2 | -Z |
| Ala | 244A | CB | His | 254C | CG | 3.61 | -1B | -X+1/2 | Y+1/2 | -Z |
| His | 247A | O | His | 247C | CB | 3.69 | -1B | -X+1/2 | Y+1/2 | -Z |
| His | 247A | CB | His | 247C | O | 3.55 | -1B | -X+1/2 | Y+1/2 | -Z |
| His | 247A | CG | His | 247C | ND1 | 3.69 | -1B | -X+1/2 | Y+1/2 | -Z |
| His | 247A | CD2 | His | 247C | CG | 3.59 | -1B | -X+1/2 | Y+1/2 | -Z |
| His | 247A | CD2 | His | 247C | ND1 | 2.56 | -1B | -X+1/2 | Y+1/2 | -Z |
| His | 247A | CD2 | His | 247C | CE1 | 3.35 | -1B | -X+1/2 | Y+1/2 | -Z |
| His | 247A | ND1 | Ala | 250C | CB | 3.51 | -1B | -X+1/2 | Y+1/2 | -Z |
| His | 247A | NE2 | His | 247C | ND1 | 3.28 | -1B | -X+1/2 | Y+1/2 | -Z |
| Leu | 248A | CG | Gly | 251C | CA | 3.55 | -1B | -X+1/2 | Y+1/2 | -Z |
| Leu | 248A | CD2 | Gly | 251C | CA | 3.61 | -1B | -X+1/2 | Y+1/2 | -Z |
| Ser | 262A | CA | Val | 286B | CG2 | 3.63 | | -X | Y | -Z |
| Gly | 265A | N | Gln | 282B | OE1 | 3.46 | | -X | Y | -Z |
| Gly | 265A | CA | Gln | 282B | OE1 | 3.5 | | -X | Y | -Z |

| | | | | | | | | | | |
|---|---|---|---|---|---|---|---|---|---|---|
| Tyr | 269A | CA | Glu | 279B | OE1 | 3.68 | | -X | Y | -Z |
| Tyr | 269A | CB | Glu | 279B | OE1 | 3.52 | | -X | Y | -Z |
| Tyr | 269A | CD1 | Glu | 279B | OE1 | 3.29 | | -X | Y | -Z |
| Arg | 296A | CG | Gln | 233C | CD | 3.5 | -1B | -X+1/2 | Y+1/2 | -Z |
| Arg | 296A | CD | Arg | 229C | NH1 | 3.43 | -1B | -X+1/2 | Y+1/2 | -Z |
| Arg | 296A | NE | Arg | 229C | NH1 | 3.08 | -1B | -X+1/2 | Y+1/2 | -Z |
| Arg | 296A | CZ | Arg | 229C | NH1 | 2.85 | -1B | -X+1/2 | Y+1/2 | -Z |
| Arg | 296A | NH1 | Arg | 229C | CZ | 3.43 | -1B | -X+1/2 | Y+1/2 | -Z |
| Arg | 296A | NH1 | Arg | 229C | NH1 | 2.9 | -1B | -X+1/2 | Y+1/2 | -Z |
| Arg | 296A | NH1 | Arg | 229C | NH2 | 3.65 | -1B | -X+1/2 | Y+1/2 | -Z |
| Arg | 296A | NH2 | Arg | 229C | NH1 | 3.42 | -1B | -X+1/2 | Y+1/2 | -Z |
| Ser | 299A | C | Met | 236C | CE | 3.21 | -1B | -X+1/2 | Y+1/2 | -Z |
| Ser | 299A | O | Met | 236C | CE | 3.4 | -1B | -X+1/2 | Y+1/2 | -Z |
| Ser | 299A | CB | Met | 236C | CE | 3.45 | -1B | -X+1/2 | Y+1/2 | -Z |
| Ser | 299A | OG | Gln | 233C | NE2 | 3.62 | -1B | -X+1/2 | Y+1/2 | -Z |
| Glu | 300A | N | Met | 236C | CE | 3.22 | -1B | -X+1/2 | Y+1/2 | -Z |
| Glu | 300A | CA | Met | 236C | CE | 3.19 | -1B | -X+1/2 | Y+1/2 | -Z |
| Leu | 302A | CD2 | Glu | 240C | CG | 3.1 | -1B | -X+1/2 | Y+1/2 | -Z |
| Lys | 306A | CD | His | 247C | CE1 | 3.29 | -1B | -X+1/2 | Y+1/2 | -Z |
| Lys | 306A | CD | His | 247C | NE2 | 2.77 | -1B | -X+1/2 | Y+1/2 | -Z |
| Thr | 308A | O | His | 309C | CB | 2.59 | -1B | -X+1/2 | Y+1/2 | -Z |
| Thr | 308A | O | His | 309C | ND1 | 3.06 | -1B | -X+1/2 | Y+1/2 | -Z |
| Thr | 308A | O | His | 309C | CG | 2.65 | -1B | -X+1/2 | Y+1/2 | -Z |
| Thr | 308A | O | His | 309C | CD2 | 3.33 | -1B | -X+1/2 | Y+1/2 | -Z |
| Thr | 308A | O | His | 309C | CG | 2.65 | -1B | -X+1/2 | Y+1/2 | -Z |
| Thr | 308A | O | His | 309C | CD2 | 3.33 | -1B | -X+1/2 | Y+1/2 | -Z |
| Thr | 308A | CG2 | His | 309C | CE1 | 3.31 | -1B | -X+1/2 | Y+1/2 | -Z |
| Thr | 308A | CG2 | His | 309C | NE2 | 3.66 | -1B | -X+1/2 | Y+1/2 | -Z |
| His | 309A | CA | His | 309C | CD2 | 3.54 | -1B | -X+1/2 | Y+1/2 | -Z |
| Leu | 310A | N | His | 309C | CD2 | 3.28 | -1B | -X+1/2 | Y+1/2 | -Z |
| Leu | 310A | N | His | 309C | NE2 | 3.65 | -1B | -X+1/2 | Y+1/2 | -Z |
| Leu | 312A | CD2 | Leu | 312C | CD2 | 3.5 | -1B | -X+1/2 | Y+1/2 | -Z |
| Gln | 313A | CA | Thr | 459C | CG2 | 3.61 | -1B | -X+1/2 | Y+1/2 | -Z |
| Gln | 313A | C | Thr | 459C | CG2 | 3.5 | -1B | -X+1/2 | Y+1/2 | -Z |
| Ala | 314A | N | Thr | 459C | CG2 | 3.4 | -1B | -X+1/2 | Y+1/2 | -Z |

| | | | | | | | | | | |
|---|---|---|---|---|---|---|---|---|---|---|
| Leu | 327A | CD2 | Leu | 231C | CD2 | 3.35 | -1B | -X+1/2 | Y+1/2 | -Z |
| Val | 328A | CA | Ser | 228C | OG | 3.64 | -1B | -X+1/2 | Y+1/2 | -Z |
| Val | 328A | CG1 | Ser | 228C | OG | 3.49 | -1B | -X+1/2 | Y+1/2 | -Z |
| Gln | 330A | CB | Arg | 227C | NH2 | 3.41 | -1B | -X+1/2 | Y+1/2 | -Z |
| Asp | 331A | CG | Arg | 227C | N | 3.47 | -1B | -X+1/2 | Y+1/2 | -Z |
| Asp | 331A | CG | Leu | 226C | CD2 | 3.56 | -1B | -X+1/2 | Y+1/2 | -Z |
| Asp | 331A | OD2 | Arg | 227C | N | 2.56 | -1B | -X+1/2 | Y+1/2 | -Z |
| Asp | 331A | OD2 | Ser | 228C | N | 2.91 | -1B | -X+1/2 | Y+1/2 | -Z |
| Asp | 331A | OD2 | Leu | 226C | CA | 3.15 | -1B | -X+1/2 | Y+1/2 | -Z |
| Asp | 331A | OD2 | Leu | 226C | C | 3.1 | -1B | -X+1/2 | Y+1/2 | -Z |
| Asp | 331A | OD2 | Leu | 226C | CB | 2.81 | -1B | -X+1/2 | Y+1/2 | -Z |
| Asp | 331A | OD2 | Leu | 226C | CG | 3.61 | -1B | -X+1/2 | Y+1/2 | -Z |
| Asp | 331A | OD2 | Leu | 226C | CD2 | 3.39 | -1B | -X+1/2 | Y+1/2 | -Z |
| Asp | 331A | OD2 | Leu | 228C | OG | 3.65 | -1B | -X+1/2 | Y+1/2 | -Z |
| Asp | 331A | OD2 | Arg | 227C | CB | 3.68 | -1B | -X+1/2 | Y+1/2 | -Z |
| Arg | 335A | NE | Leu | 226C | CD2 | 3.61 | -1B | -X+1/2 | Y+1/2 | -Z |
| Arg | 335A | NH2 | Leu | 226C | CD1 | 3.3 | -1B | -X+1/2 | Y+1/2 | -Z |
| Arg | 335A | NH2 | Leu | 226C | CG | 3.65 | -1B | -X+1/2 | Y+1/2 | -Z |
| Gln | 351A | CG | Thr | 459C | OG1 | 3.16 | -1B | -X+1/2 | Y+1/2 | -Z |
| Gln | 351A | CD | Gln | 351C | NE2 | 3.64 | -1B | -X+1/2 | Y+1/2 | -Z |
| Gln | 351A | CD | Thr | 459C | OG1 | 3.44 | -1B | -X+1/2 | Y+1/2 | -Z |
| Gln | 351A | NE2 | Gln | 351C | NE2 | 3.05 | -1B | -X+1/2 | Y+1/2 | -Z |
| Gln | 351A | NE2 | Gln | 351C | OE1 | 3.65 | -1B | -X+1/2 | Y+1/2 | -Z |
| Gln | 351A | NE2 | Asn | 457C | CG | 3.62 | -1B | -X+1/2 | Y+1/2 | -Z |
| Gln | 351A | NE2 | Asn | 457C | OD1 | 3.69 | -1B | -X+1/2 | Y+1/2 | -Z |
| Gln | 351A | NE2 | Thr | 459C | OG1 | 3.16 | -1B | -X+1/2 | Y+1/2 | -Z |
| Gln | 351A | OE1 | Gln | 351C | NE2 | 3.42 | -1B | -X+1/2 | Y+1/2 | -Z |
| Gln | 351A | OE1 | Gln | 351C | OE1 | 3.56 | -1B | -X+1/2 | Y+1/2 | -Z |
| Gln | 359A | NE2 | Met | 236C | SD | 3.51 | -1B | -X+1/2 | Y+1/2 | -Z |
| Asn | 363A | OD1 | Leu | 232C | CD1 | 3.51 | -1B | -X+1/2 | Y+1/2 | -Z |
| Leu | 366A | CD1 | Arg | 229C | CG | 3.35 | -1B | -X+1/2 | Y+1/2 | -Z |
| Leu | 366A | CD2 | Arg | 229C | CG | 3.35 | -1B | -X+1/2 | Y+1/2 | -Z |
| Gln | 370A | O | Thr | 346B | CG2 | 3.06 | +1C | -X+1/2 | Y+1/2 | -Z |
| Ala | 371A | C | Thr | 346B | CG2 | 3.44 | +1C | -X+1/2 | Y+1/2 | -Z |
| Ala | 371A | O | Thr | 346B | CG2 | 2.68 | +1C | -X+1/2 | Y+1/2 | -Z |

| | | | | | | | | | | |
|---|---|---|---|---|---|---|---|---|---|---|
| Ala | 371A | O | Thr | 346B | CB | 3.4 | +1C | -X+1/2 | Y+1/2 | -Z |
| Gly | 373A | CA | Thr | 346B | OG1 | 3.42 | +1C | -X+1/2 | Y+1/2 | -Z |
| Gln | 374A | OE1 | Glu | 384B | O | 3.5 | +1C | -X+1/2 | Y+1/2 | -Z |
| Gln | 374A | OE1 | Glu | 384B | CB | 3.69 | +1C | -X+1/2 | Y+1/2 | -Z |
| His | 375A | CB | Glu | 384B | OE1 | 3.48 | +1C | -X+1/2 | Y+1/2 | -Z |
| His | 375A | CG | Glu | 384B | OE1 | 3.18 | +1C | -X+1/2 | Y+1/2 | -Z |
| His | 375A | ND1 | Glu | 384B | CD | 3.27 | +1C | -X+1/2 | Y+1/2 | -Z |
| His | 375A | ND1 | Glu | 384B | OE1 | 2.58 | +1C | -X+1/2 | Y+1/2 | -Z |
| His | 375A | CE1 | Glu | 384B | OE1 | 3.36 | +1C | -X+1/2 | Y+1/2 | -Z |
| His | 375A | CE1 | Gly | 386B | O | 3.44 | +1C | -X+1/2 | Y+1/2 | -Z |
| His | 375A | NE2 | Gly | 386B | O | 3.35 | +1C | -X+1/2 | Y+1/2 | -Z |
| Lys | 398A | CE | Asp | 345B | C | 3.4 | +1C | -X+1/2 | Y+1/2 | -Z |
| Lys | 398A | NZ | Asp | 345B | CB | 3.12 | +1C | -X+1/2 | Y+1/2 | -Z |
| Glu | 418A | O | Arg | 229C | NH2 | 3.68 | -1B | -X+1/2 | Y+1/2 | -Z |
| Asn | 457A | CG | Gln | 351C | NE2 | 3.34 | -1B | -X+1/2 | Y+1/2 | -Z |
| Asn | 457A | ND2 | Gln | 351C | NE2 | 3.11 | -1B | -X+1/2 | Y+1/2 | -Z |
| Asn | 457A | ND2 | Asn | 457C | OD1 | 3.56 | -1B | -X+1/2 | Y+1/2 | -Z |
| Asn | 457A | OD1 | Gln | 351C | NE2 | 2.88 | -1B | -X+1/2 | Y+1/2 | -Z |
| Thr | 459A | CG2 | Leu | 312C | O | 3.52 | -1B | -X+1/2 | Y+1/2 | -Z |
| Thr | 459A | CG2 | Leu | 312C | C | 3.46 | -1B | -X+1/2 | Y+1/2 | -Z |
| Thr | 459A | CG2 | Gln | 312C | N | 3.33 | -1B | -X+1/2 | Y+1/2 | -Z |
| Thr | 459A | CG2 | Gln | 313C | CA | 3.19 | -1B | -X+1/2 | Y+1/2 | -Z |
| Thr | 459A | CG2 | Gln | 313C | C | 3.66 | -1B | -X+1/2 | Y+1/2 | -Z |
| Thr | 459A | OG1 | Gln | 351C | CG | 3.28 | -1B | -X+1/2 | Y+1/2 | -Z |

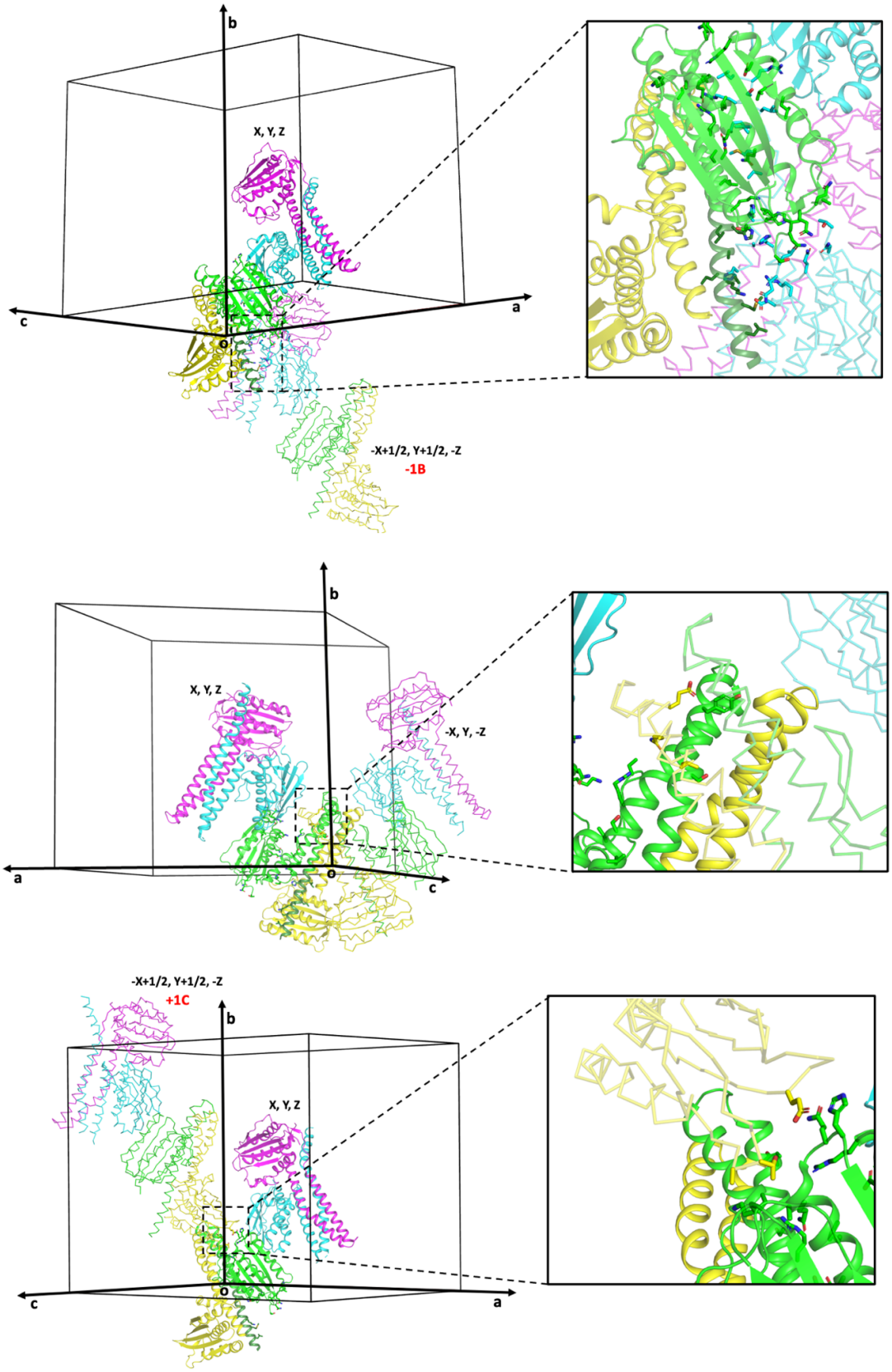


**Figure B1 Interaction of chain cA of EcZraS dimer AB with symmetry mates.**

**Table B2 Inter-atomic contact distances between symmetry-related molecules and chains cB of dimer AB of EcZraS-CD**

| Source residue | Source residue no. | Source atom | Target residue | Target residue no. | Target atom | Distance | Unit cell translation | X | Y | Z |
|---|---|---|---|---|---|---|---|---|---|---|
| Arg | 257B | CB | His | 309D | CE1 | 3.62 | -1A-1B | X+1/2 | Y+1/2 | Z |
| Arg | 257B | CG | His | 309D | CE1 | 2.84 | -1A-1B | X+1/2 | Y+1/2 | Z |
| Arg | 257B | CD | His | 309D | CE1 | 3.46 | -1A-1B | X+1/2 | Y+1/2 | Z |
| Ser | 261B | CA | Leu | 310D | O | 3.19 | -1A-1B | X+1/2 | Y+1/2 | Z |
| Ser | 261B | O | Leu | 310D | O | 3.45 | -1A-1B | X+1/2 | Y+1/2 | Z |
| Ser | 261B | CB | Leu | 310D | O | 2.78 | -1A-1B | X+1/2 | Y+1/2 | Z |
| Ser | 261B | OG | Leu | 312D | CG | 3.65 | -1A-1B | X+1/2 | Y+1/2 | Z |
| Ser | 261B | OG | Leu | 312D | CD1 | 3.36 | -1A-1B | X+1/2 | Y+1/2 | Z |
| Lys | 264B | C | Ala | 311D | CB | 3.65 | -1A-1B | X+1/2 | Y+1/2 | Z |
| Lys | 264B | CE | His | 309D | O | 3.56 | -1A-1B | X+1/2 | Y+1/2 | Z |
| Lys | 264B | NZ | His | 309D | O | 2.66 | -1A-1B | X+1/2 | Y+1/2 | Z |
| Gly | 265B | N | Ala | 311D | CA | 3.47 | -1A-1B | X+1/2 | Y+1/2 | Z |
| Gly | 265B | CA | Ala | 311D | C | 3.69 | -1A-1B | X+1/2 | Y+1/2 | Z |
| Gly | 265B | CA | Ala | 311D | CB | 3.47 | -1A-1B | X+1/2 | Y+1/2 | Z |
| Gly | 265B | O | Gln | 313D | CG | 3.58 | -1A-1B | X+1/2 | Y+1/2 | Z |
| Lys | 268B | CD | Ala | 224D | O | 3.47 | -1A-1B | X+1/2 | Y+1/2 | Z |
| Lys | 268B | CD | Gln | 313D | NE2 | 3.47 | -1A-1B | X+1/2 | Y+1/2 | Z |
| Lys | 268B | CE | Asp | 355D | OD2 | 3.28 | -1A-1B | X+1/2 | Y+1/2 | Z |
| Lys | 268B | CE | Ala | 224D | O | 3.08 | -1A-1B | X+1/2 | Y+1/2 | Z |
| Tyr | 269B | CB | Gln | 313D | OE1 | 3.66 | -1A-1B | X+1/2 | Y+1/2 | Z |
| Ala | 271B | O | Arg | 340C | NH2 | 3.09 | | -X | Y | -Z |
| Glu | 272B | CA | Arg | 340C | NH2 | 3.51 | | -X | Y | -Z |
| Glu | 272B | C | Thr | 342C | CG2 | 3.52 | | -X | Y | -Z |
| Glu | 272B | C | Arg | 340C | NH2 | 3.45 | | -X | Y | -Z |
| Glu | 272B | O | Arg | 340C | CZ | 3.69 | | -X | Y | -Z |
| Glu | 272B | O | Thr | 342C | CG2 | 3.53 | | -X | Y | -Z |
| Glu | 272B | O | Arg | 340C | NH2 | 2.8 | | -X | Y | -Z |
| Glu | 272B | CB | Ala | 224D | CB | 3.25 | -1A-1B | X+1/2 | Y+1/2 | Z |
| Glu | 272B | CB | Thr | 342C | CG2 | 3.44 | | -X | Y | -Z |
| Glu | 272B | CG | Ala | 224D | CB | 3.52 | -1A-1B | X+1/2 | Y+1/2 | Z |

| | | | | | | | | | | |
|---|---|---|---|---|---|---|---|---|---|---|
| Glu | 272B | CG | Thr | 342C | CG2 | 2.89 | | -X | Y | -Z |
| Glu | 272B | OE1 | Tyr | 225D | O | 3.5 | -1A-1B | X+1/2 | Y+1/2 | Z |
| Arg | 273B | CA | Thr | 342C | OG1 | 3.64 | | -X | Y | -Z |
| Arg | 274B | O | Arg | 340C | NH1 | 3.67 | | -X | Y | -Z |
| Arg | 274B | O | Arg | 340C | NH2 | 3.11 | | -X | Y | -Z |
| Glu | 279B | OE1 | Tyr | 269A | CA | 3.68 | | -X | Y | -Z |
| Glu | 279B | OE1 | Tyr | 269A | CB | 3.52 | | -X | Y | -Z |
| Glu | 279B | OE1 | Tyr | 269A | CD1 | 3.29 | | -X | Y | -Z |
| Gln | 282B | NE2 | Lys | 264A | CE | 3.41 | | -X | Y | -Z |
| Gln | 282B | OE1 | Gly | 265A | N | 3.46 | | -X | Y | -Z |
| Gln | 282B | OE1 | Gly | 265A | CA | 3.5 | | -X | Y | -Z |
| Val | 286B | CG2 | Ser | 262A | CA | 3.63 | | -X | Y | -Z |
| Arg | 293B | CD | Arg | 293B | NH1 | 3.43 | | -X | Y | -Z |
| Arg | 293B | NE | Arg | 293B | CZ | 3.48 | | -X | Y | -Z |
| Arg | 293B | NE | Arg | 293B | NH1 | 3.68 | | -X | Y | -Z |
| Arg | 293B | NH1 | Arg | 293B | NE | 3.68 | | -X | Y | -Z |
| Arg | 293B | NH1 | Arg | 293B | CD | 3.43 | | -X | Y | -Z |
| Asn | 295B | CG | His | 309D | NE2 | 3.57 | -1A-1B | X+1/2 | Y+1/2 | Z |
| Asn | 295B | ND2 | His | 309D | CD2 | 3.51 | -1A-1B | X+1/2 | Y+1/2 | Z |
| Asn | 295B | ND2 | His | 309D | NE2 | 3.63 | -1A-1B | X+1/2 | Y+1/2 | Z |
| Asn | 295B | OD1 | His | 309D | CE1 | 3.63 | -1A-1B | X+1/2 | Y+1/2 | Z |
| Asn | 295B | OD1 | His | 309D | NE2 | 3.25 | -1A-1B | X+1/2 | Y+1/2 | Z |
| Glu | 303B | OE1 | Ser | 299D | CB | 3.43 | -1A-1B | X+1/2 | Y+1/2 | Z |
| Glu | 303B | OE1 | Ser | 299D | OG | 2.97 | -1A-1B | X+1/2 | Y+1/2 | Z |
| Glu | 303B | OE2 | Glu | 303D | CG | 3.65 | -1A-1B | X+1/2 | Y+1/2 | Z |
| His | 309B | C | Lys | 264D | NZ | 3.51 | -1A-1B | X+1/2 | Y+1/2 | Z |
| His | 309B | O | Lys | 264D | NZ | 2.51 | -1A-1B | X+1/2 | Y+1/2 | Z |
| His | 309B | CE1 | Asn | 295D | CB | 3.66 | -1A-1B | X+1/2 | Y+1/2 | Z |
| Leu | 310B | C | Ser | 261D | CB | 3.69 | -1A-1B | X+1/2 | Y+1/2 | Z |
| Leu | 310B | O | Ser | 261D | CB | 2.52 | -1A-1B | X+1/2 | Y+1/2 | Z |
| Leu | 310B | O | Ser | 261D | O | 3.44 | -1A-1B | X+1/2 | Y+1/2 | Z |
| Leu | 310B | O | Ser | 261D | CA | 2.99 | -1A-1B | X+1/2 | Y+1/2 | Z |
| Leu | 310B | O | Ser | 261D | C | 3.66 | -1A-1B | X+1/2 | Y+1/2 | Z |
| Ala | 311B | CA | Ser | 261D | O | 3.64 | -1A-1B | X+1/2 | Y+1/2 | Z |
| Ala | 311B | C | Ser | 261D | O | 3.49 | -1A-1B | X+1/2 | Y+1/2 | Z |

| | | | | | | | | | | |
|---|---|---|---|---|---|---|---|---|---|---|
| Leu | 312B | N | Ser | 261D | O | 2.66 | -1A-1B | X+1/2 | Y+1/2 | Z |
| Leu | 312B | N | Ser | 261D | C | 3.52 | -1A-1B | X+1/2 | Y+1/2 | Z |
| Leu | 312B | CA | Ser | 261D | O | 3.51 | -1A-1B | X+1/2 | Y+1/2 | Z |
| Leu | 312B | O | Ser | 262D | CA | 3.6 | -1A-1B | X+1/2 | Y+1/2 | Z |
| Leu | 312B | O | Ser | 261D | O | 3.38 | -1A-1B | X+1/2 | Y+1/2 | Z |
| Leu | 312B | O | Ser | 262D | O | 3.61 | -1A-1B | X+1/2 | Y+1/2 | Z |
| Leu | 312B | O | Ser | 265D | CA | 3.27 | -1A-1B | X+1/2 | Y+1/2 | Z |
| Leu | 312B | CB | Ser | 261D | OG | 3.58 | -1A-1B | X+1/2 | Y+1/2 | Z |
| Leu | 312B | CB | Ser | 261D | O | 3.67 | -1A-1B | X+1/2 | Y+1/2 | Z |
| Leu | 312B | CG | Ser | 261D | CB | 3.59 | -1A-1B | X+1/2 | Y+1/2 | Z |
| Leu | 312B | CG | Ser | 261D | OG | 3.22 | -1A-1B | X+1/2 | Y+1/2 | Z |
| Leu | 312B | CD1 | Ser | 261D | CB | 3.62 | -1A-1B | X+1/2 | Y+1/2 | Z |
| Leu | 312B | CD1 | Ser | 261D | OG | 2.73 | -1A-1B | X+1/2 | Y+1/2 | Z |
| Gln | 313B | NE2 | Gly | 265D | O | 3.4 | -1A-1B | X+1/2 | Y+1/2 | Z |
| Asp | 345B | CB | Lys | 398A | CE | 3.4 | -1B+1C | X+1/2 | Y+1/2 | Z |
| Asp | 345B | CB | Lys | 398A | NZ | 3.12 | -1B+1C | X+1/2 | Y+1/2 | Z |
| Thr | 346B | CB | Ala | 371A | O | 3.4 | -1B+1C | X+1/2 | Y+1/2 | Z |
| Thr | 346B | CG2 | Ala | 371A | C | 3.44 | -1B+1C | X+1/2 | Y+1/2 | Z |
| Thr | 346B | CG2 | Ala | 371A | O | 2.68 | -1B+1C | X+1/2 | Y+1/2 | Z |
| Thr | 346B | CG2 | Gln | 370A | O | 3.06 | -1B+1C | X+1/2 | Y+1/2 | Z |
| Thr | 346B | OG1 | Gly | 373A | CA | 3.42 | -1B+1C | X+1/2 | Y+1/2 | Z |
| Glu | 384B | O | Gln | 374A | OE1 | 3.5 | -1B+1C | X+1/2 | Y+1/2 | Z |
| Glu | 384B | CB | Gln | 374A | OE1 | 3.69 | -1B+1C | X+1/2 | Y+1/2 | Z |
| Glu | 384B | CD | His | 375A | ND1 | 3.27 | -1B+1C | X+1/2 | Y+1/2 | Z |
| Glu | 384B | OE1 | His | 375A | CB | 3.48 | -1B+1C | X+1/2 | Y+1/2 | Z |
| Glu | 384B | OE1 | His | 375A | CG | 3.18 | -1B+1C | X+1/2 | Y+1/2 | Z |
| Glu | 384B | OE1 | His | 375A | ND1 | 2.58 | -1B+1C | X+1/2 | Y+1/2 | Z |
| Glu | 384B | OE1 | His | 375A | CE1 | 3.36 | -1B+1C | X+1/2 | Y+1/2 | Z |
| Gly | 386B | O | His | 375A | CE1 | 3.44 | -1B+1C | X+1/2 | Y+1/2 | Z |
| Gly | 386B | O | His | 375A | NE2 | 3.35 | -1B+1C | X+1/2 | Y+1/2 | Z |

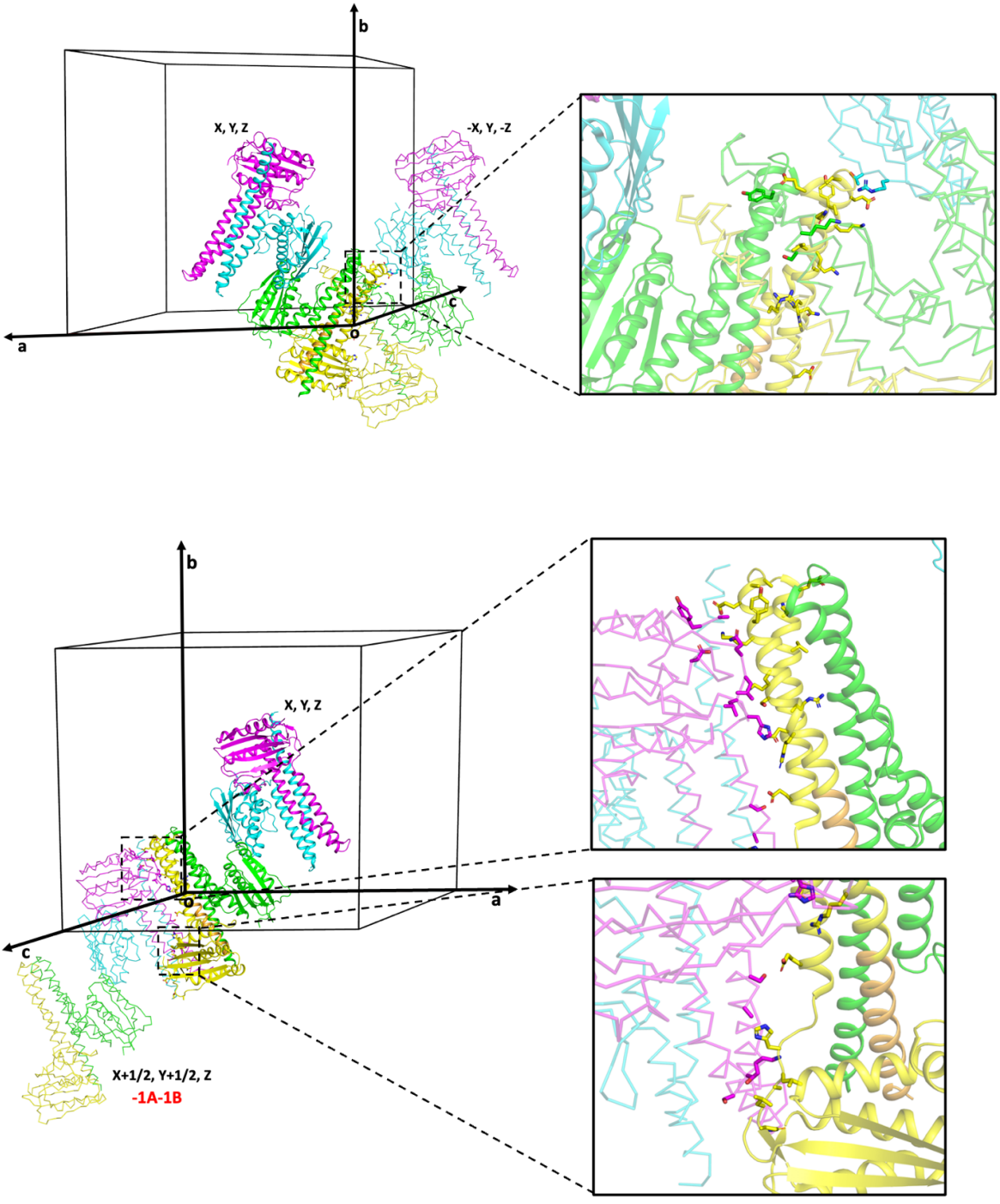
b
X, Y, Z
-X, Y, -Z
c
o
a
b
X, Y, Z
o
a
c
X+1/2, Y+1/2, Z
-1A-1B

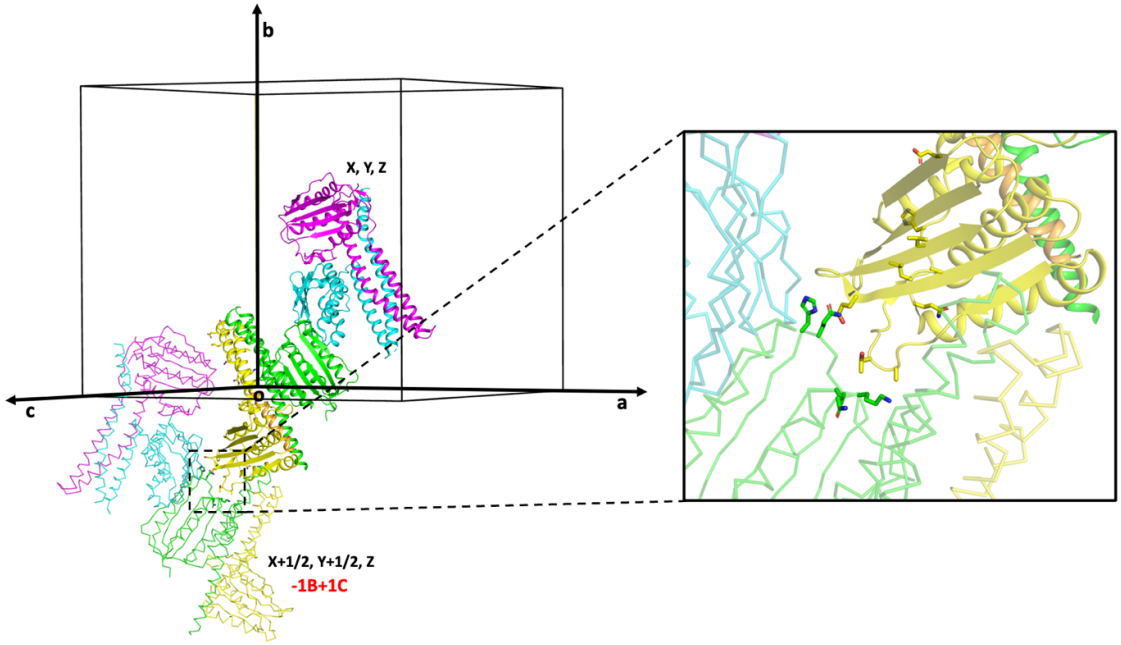


**Figure B2 Interaction of chain cB of EcZraS dimer AB with symmetry mates.**

**Table B3 Inter-atomic contact distances between symmetry-related molecules and chains cC of dimer CD of EcZraS-CD**

| Source residue | Source residue no. | Source atom | Target residue | Target residue no. | Target atom | Distance | Unit cell translation | X | Y | Z |
|---|---|---|---|---|---|---|---|---|---|---|
| Leu | 226C | CA | Asp | 331A | OD2 | 3.15 | | -X+1/2 | Y+1/2 | -Z |
| Leu | 226C | C | Asp | 331A | OD2 | 3.1 | | -X+1/2 | Y+1/2 | -Z |
| Leu | 226C | C | Asp | 331A | OD2 | 2.81 | | -X+1/2 | Y+1/2 | -Z |
| Leu | 226C | CG | Asp | 331A | OD2 | 3.61 | | -X+1/2 | Y+1/2 | -Z |
| Leu | 226C | CG | Arg | 335A | NH2 | 3.65 | | -X+1/2 | Y+1/2 | -Z |
| Leu | 226C | CD1 | Arg | 335A | NH2 | 3.3 | | -X+1/2 | Y+1/2 | -Z |
| Leu | 226C | CD2 | Asp | 331A | CG | 3.56 | | -X+1/2 | Y+1/2 | -Z |
| Leu | 226C | CD2 | Asp | 331A | OD2 | 3.39 | | -X+1/2 | Y+1/2 | -Z |
| Leu | 226C | CD2 | Arg | 335A | NE | 3.61 | | -X+1/2 | Y+1/2 | -Z |
| Arg | 227C | N | Asp | 331A | CG | 3.47 | | -X+1/2 | Y+1/2 | -Z |
| Arg | 227C | N | Asp | 331A | OD2 | 2.56 | | -X+1/2 | Y+1/2 | -Z |
| Arg | 227C | CA | Asp | 331A | OD2 | 3.44 | | -X+1/2 | Y+1/2 | -Z |
| Arg | 227C | C | Asp | 331A | OD2 | 3.65 | | -X+1/2 | Y+1/2 | -Z |
| Arg | 227C | CB | Asp | 331A | OD2 | 3.68 | | -X+1/2 | Y+1/2 | -Z |
| Arg | 227C | CG | Gly | 445C | O | 3.02 | | -X+1/2 | Y+1/2 | -Z |

| | | | | | | | | | | |
|---|---|---|---|---|---|---|---|---|---|---|
| Arg | 227C | CG | Gly | 445C | O | 3.69 | | -X+1/2 | Y+1/2 | -Z |
| Arg | 227C | CD | Ser | 396C | O | 2.92 | | -X+1/2 | Y+1/2 | -Z |
| Arg | 227C | NE | Ser | 396C | O | 3.32 | | -X+1/2 | Y+1/2 | -Z |
| Arg | 227C | CZ | Ile | 372C | O | 3.59 | | -X+1/2 | Y+1/2 | -Z |
| Arg | 227C | CZ | Ser | 396C | O | 3.54 | | -X+1/2 | Y+1/2 | -Z |
| Arg | 227C | NH1 | Ile | 372C | O | 3.11 | | -X+1/2 | Y+1/2 | -Z |
| Arg | 227C | NH1 | His | 375C | O | 3.59 | | -X+1/2 | Y+1/2 | -Z |
| Arg | 227C | NH1 | Ser | 396C | O | 3.37 | | -X+1/2 | Y+1/2 | -Z |
| Arg | 227C | NH2 | Gln | 330A | CB | 3.41 | | -X+1/2 | Y+1/2 | -Z |
| Arg | 227C | NH2 | Ile | 372C | O | 3.21 | | -X+1/2 | Y+1/2 | -Z |
| Ser | 228C | N | Asp | 331A | OD2 | 2.91 | | -X+1/2 | Y+1/2 | -Z |
| Ser | 228C | OG | Val | 328A | CA | 3.64 | | -X+1/2 | Y+1/2 | -Z |
| Ser | 228C | OG | Val | 328A | CG1 | 3.49 | | -X+1/2 | Y+1/2 | -Z |
| Ser | 228C | OG | Asp | 331A | OD2 | 3.65 | | -X+1/2 | Y+1/2 | -Z |
| Arg | 229C | CG | Leu | 366A | CD2 | 3.35 | | -X+1/2 | Y+1/2 | -Z |
| Arg | 229C | CG | Leu | 366A | CD1 | 3.35 | | -X+1/2 | Y+1/2 | -Z |
| Arg | 229C | NH1 | Arg | 296A | CD | 3.43 | | -X+1/2 | Y+1/2 | -Z |
| Arg | 229C | NH1 | Arg | 296A | NE | 3.08 | | -X+1/2 | Y+1/2 | -Z |
| Arg | 229C | NH1 | Arg | 296A | CZ | 2.85 | | -X+1/2 | Y+1/2 | -Z |
| Arg | 229C | NH1 | Arg | 296A | NH1 | 2.9 | | -X+1/2 | Y+1/2 | -Z |
| Arg | 229C | NH1 | Arg | 296A | NH2 | 3.42 | | -X+1/2 | Y+1/2 | -Z |
| Arg | 229C | NH2 | Glu | 418A | O | 3.68 | | -X+1/2 | Y+1/2 | -Z |
| Arg | 229C | NH2 | Arg | 296A | NH1 | 3.65 | | -X+1/2 | Y+1/2 | -Z |
| Leu | 231C | CD1 | His | 375C | CB | 3.68 | | -X+1/2 | Y+1/2 | -Z |
| Leu | 231C | CD2 | Leu | 327A | CD2 | 3.35 | | -X+1/2 | Y+1/2 | -Z |
| Leu | 232C | CD1 | Asn | 363A | OD1 | 3.51 | | -X+1/2 | Y+1/2 | -Z |
| Gln | 233C | CD | Arg | 296A | CG | 3.5 | | -X+1/2 | Y+1/2 | -Z |
| Gln | 233C | NE2 | Ser | 299A | OG | 3.62 | | -X+1/2 | Y+1/2 | -Z |
| Met | 236C | CE | Gln | 359A | NE2 | 3.51 | | -X+1/2 | Y+1/2 | -Z |
| Met | 236C | CE | Glu | 300A | CG | 3.19 | | -X+1/2 | Y+1/2 | -Z |
| Met | 236C | CE | Ser | 299A | C | 3.21 | | -X+1/2 | Y+1/2 | -Z |
| Met | 236C | CE | Ser | 299A | O | 3.4 | | -X+1/2 | Y+1/2 | -Z |
| Met | 236C | CE | Glu | 300A | N | 3.22 | | -X+1/2 | Y+1/2 | -Z |
| Met | 236C | CE | Glu | 300A | CA | 3.47 | | -X+1/2 | Y+1/2 | -Z |
| Met | 236C | CE | Ser | 299A | CB | 3.45 | | -X+1/2 | Y+1/2 | -Z |

| | | | | | | | | | | |
|---|---|---|---|---|---|---|---|---|---|---|
| Glu | 240C | CG | Leu | 302A | CD2 | 3.1 | | -X+1/2 | Y+1/2 | -Z |
| His | 247C | O | His | 247A | CB | 3.55 | | -X+1/2 | Y+1/2 | -Z |
| His | 247C | CB | His | 247A | O | 3.69 | | -X+1/2 | Y+1/2 | -Z |
| His | 247C | CG | His | 247A | CD2 | 3.59 | | -X+1/2 | Y+1/2 | -Z |
| His | 247C | ND1 | His | 247A | CG | 3.69 | | -X+1/2 | Y+1/2 | -Z |
| His | 247C | ND1 | His | 247A | CD2 | 2.56 | | -X+1/2 | Y+1/2 | -Z |
| His | 247C | ND1 | His | 247A | NE2 | 3.28 | | -X+1/2 | Y+1/2 | -Z |
| His | 247C | CE1 | His | 247A | CD2 | 3.35 | | -X+1/2 | Y+1/2 | -Z |
| His | 247C | CE1 | Lys | 306A | CD | 3.29 | | -X+1/2 | Y+1/2 | -Z |
| His | 247C | NE2 | Lys | 306A | CD | 2.77 | | -X+1/2 | Y+1/2 | -Z |
| Ala | 250C | CB | His | 247A | ND1 | 3.51 | | -X+1/2 | Y+1/2 | -Z |
| Gly | 251C | CA | Leu | 248A | CG | 3.55 | | -X+1/2 | Y+1/2 | -Z |
| Gly | 251C | CA | Leu | 248A | CD2 | 3.61 | | -X+1/2 | Y+1/2 | -Z |
| His | 254C | CG | Ala | 244A | CB | 3.61 | | -X+1/2 | Y+1/2 | -Z |
| His | 254C | CE1 | Lys | 241A | N | 3.64 | | -X+1/2 | Y+1/2 | -Z |
| His | 254C | CE1 | Lys | 241A | CA | 3.38 | | -X+1/2 | Y+1/2 | -Z |
| His | 254C | NE2 | Glu | 240A | CB | 3.44 | | -X+1/2 | Y+1/2 | -Z |
| His | 254C | NE2 | Glu | 240A | C | 3.37 | | -X+1/2 | Y+1/2 | -Z |
| His | 254C | NE2 | Lys | 241A | N | 3.37 | | -X+1/2 | Y+1/2 | -Z |
| His | 254C | NE2 | Lys | 241A | CA | 3.62 | | -X+1/2 | Y+1/2 | -Z |
| His | 254C | NE2 | Glu | 240A | O | 3.57 | | -X+1/2 | Y+1/2 | -Z |
| Ser | 262C | CA | Val | 286D | CG2 | 3.51 | +1A | -X | Y | -Z |
| Ser | 262C | OG | Val | 286D | CG1 | 3.53 | +1A | -X | Y | -Z |
| Gly | 265C | CA | Gln | 282D | OE1 | 3.35 | +1A | -X | Y | -Z |
| Tyr | 269C | CD1 | Glu | 279D | OE2 | 3.13 | +1A | -X | Y | -Z |
| Glu | 272C | CB | Glu | 279D | OE1 | 3.58 | +1A | -X | Y | -Z |
| His | 309C | CB | Thr | 308A | O | 2.59 | | -X+1/2 | Y+1/2 | -Z |
| His | 309C | CG | Thr | 308A | C | 3.5 | | -X+1/2 | Y+1/2 | -Z |
| His | 309C | CG | Thr | 308A | O | 2.65 | | -X+1/2 | Y+1/2 | -Z |
| His | 309C | CD2 | Thr | 308A | O | 3.33 | | -X+1/2 | Y+1/2 | -Z |
| His | 309C | CD2 | His | 309A | CA | 3.54 | | -X+1/2 | Y+1/2 | -Z |
| His | 309C | CD2 | Leu | 310A | N | 3.28 | | -X+1/2 | Y+1/2 | -Z |
| His | 309C | ND1 | Thr | 308A | O | 3.06 | | -X+1/2 | Y+1/2 | -Z |
| His | 309C | CE1 | Thr | 308A | CG2 | 3.31 | | -X+1/2 | Y+1/2 | -Z |
| His | 309C | NE2 | Thr | 306A | CG2 | 3.66 | | -X+1/2 | Y+1/2 | -Z |

| | | | | | | | | | | |
|---|---|---|---|---|---|---|---|---|---|---|
| His | 309C | NE2 | Leu | 310A | N | 3.65 | | -X+1/2 | Y+1/2 | -Z |
| Leu | 312C | C | Thr | 459A | CG2 | 3.46 | | -X+1/2 | Y+1/2 | -Z |
| Leu | 312C | O | Thr | 459A | CG2 | 3.52 | | -X+1/2 | Y+1/2 | -Z |
| Leu | 312C | CD2 | Leu | 312A | CD2 | 3.5 | | -X+1/2 | Y+1/2 | -Z |
| Gln | 313C | N | Thr | 459A | CG2 | 3.33 | | -X+1/2 | Y+1/2 | -Z |
| Gln | 313C | CA | Thr | 459A | CG2 | 3.19 | | -X+1/2 | Y+1/2 | -Z |
| Gln | 313C | C | Thr | 459A | CG2 | 3.66 | | -X+1/2 | Y+1/2 | -Z |
| Asn | 322C | OD1 | Arg | 227D | NH2 | 3.09 | -1B | -X+1/2 | Y+1/2 | -Z |
| Asn | 322C | OD1 | Tyr | 225D | OH | 3.59 | -1B | -X+1/2 | Y+1/2 | -Z |
| Gln | 330C | CG | Gln | 330D | OE1 | 2.99 | -1B | -X+1/2 | Y+1/2 | -Z |
| Gln | 330C | CD | Gln | 330D | OE1 | 3.27 | -1B | -X+1/2 | Y+1/2 | -Z |
| Gln | 330C | NE2 | Gln | 330D | CD | 3.68 | -1B | -X+1/2 | Y+1/2 | -Z |
| Gln | 330C | NE2 | Gln | 330D | OE1 | 3.31 | -1B | -X+1/2 | Y+1/2 | -Z |
| Asn | 333C | ND2 | Arg | 229D | CB | 3.54 | -1B | -X+1/2 | Y+1/2 | -Z |
| Leu | 339C | O | Arg | 227D | CN | 3.65 | -1B | -X+1/2 | Y+1/2 | -Z |
| Leu | 339C | O | Arg | 227D | CD | 3.61 | -1B | -X+1/2 | Y+1/2 | -Z |
| Arg | 340C | CZ | Glu | 272B | O | 3.69 | | -X | Y | -Z |
| Arg | 340C | NH1 | Ala | 274B | O | 3.67 | | -X | Y | -Z |
| Arg | 340C | NH2 | Ala | 271B | O | 3.09 | | -X | Y | -Z |
| Arg | 340C | NH2 | Glu | 272B | CA | 3.51 | | -X | Y | -Z |
| Arg | 340C | NH2 | Glu | 272B | CA | 3.45 | | -X | Y | -Z |
| Arg | 340C | NH2 | Glu | 272B | O | 2.8 | | -X | Y | -Z |
| Arg | 340C | NH2 | Ala | 274B | O | 3.11 | | -X | Y | -Z |
| Phe | 341C | N | Arg | 227D | NH1 | 3.48 | -1B | -X+1/2 | Y+1/2 | -Z |
| Phe | 341C | O | Arg | 227D | CZ | 3.47 | -1B | -X+1/2 | Y+1/2 | -Z |
| Phe | 341C | O | Arg | 227D | NH1 | 3.17 | -1B | -X+1/2 | Y+1/2 | -Z |
| Phe | 341C | O | Arg | 227D | NH2 | 3.06 | -1B | -X+1/2 | Y+1/2 | -Z |
| Thr | 342C | CG2 | Glu | 272B | C | 3.52 | | -X | Y | -Z |
| Thr | 342C | CG2 | Glu | 272B | O | 3.53 | | -X | Y | -Z |
| Thr | 342C | CG2 | Glu | 272B | CB | 3.44 | | -X | Y | -Z |
| Thr | 342C | CG2 | Glu | 272B | CG | 2.89 | | -X | Y | -Z |
| Thr | 342C | OG1 | Arg | 273B | CA | 3.64 | | -X | Y | -Z |
| Gln | 351C | CG | Thr | 459A | OG1 | 3.28 | | -X+1/2 | Y+1/2 | -Z |
| Gln | 351C | NE2 | Asn | 457A | ND2 | 3.11 | | -X+1/2 | Y+1/2 | -Z |
| Gln | 351C | NE2 | Gln | 351A | NE2 | 3.05 | | -X+1/2 | Y+1/2 | -Z |

| | | | | | | | | | | |
|---|---|---|---|---|---|---|---|---|---|---|
| Gln | 351C | NE2 | Asn | 457A | CG | 3.34 | | -X+1/2 | Y+1/2 | -Z |
| Gln | 351C | NE2 | Asn | 457A | OD1 | 2.88 | | -X+1/2 | Y+1/2 | -Z |
| Gln | 351C | NE2 | Gln | 351A | CD | 3.64 | | -X+1/2 | Y+1/2 | -Z |
| Gln | 351C | NE2 | Gln | 351A | OE1 | 3.42 | | -X+1/2 | Y+1/2 | -Z |
| Gln | 351C | OE1 | Gln | 351A | NE2 | 3.65 | | -X+1/2 | Y+1/2 | -Z |
| Gln | 351C | OE1 | Gln | 351A | OE1 | 3.56 | | -X+1/2 | Y+1/2 | -Z |
| Asp | 355C | CG | Met | 236A | SD | 3.18 | | -X+1/2 | Y+1/2 | -Z |
| Asp | 355C | CG | Lys | 239A | NZ | 3.67 | | -X+1/2 | Y+1/2 | -Z |
| Asp | 355C | OD1 | Leu | 232A | CD1 | 3.53 | | -X+1/2 | Y+1/2 | -Z |
| Asp | 355C | OD2 | Met | 236A | SD | 2.98 | | -X+1/2 | Y+1/2 | -Z |
| Asp | 355C | OD2 | Lys | 239A | NZ | 2.5 | | -X+1/2 | Y+1/2 | -Z |
| Arg | 356C | CZ | Met | 236A | CE | 3.64 | | -X+1/2 | Y+1/2 | -Z |
| Arg | 356C | NH1 | Met | 236A | CE | 2.95 | | -X+1/2 | Y+1/2 | -Z |
| Ile | 372C | O | Arg | 227C | CZ | 3.59 | -1B | -X+1/2 | Y+1/2 | -Z |
| Ile | 372C | O | Arg | 227C | NH1 | 3.11 | -1B | -X+1/2 | Y+1/2 | -Z |
| Ile | 372C | O | Arg | 227C | NH2 | 3.21 | -1B | -X+1/2 | Y+1/2 | -Z |
| His | 375C | O | Arg | 227C | NH1 | 3.59 | -1B | -X+1/2 | Y+1/2 | -Z |
| His | 375C | CB | Leu | 231C | CD1 | 3.68 | -1B | -X+1/2 | Y+1/2 | -Z |
| Ser | 396C | O | Arg | 227C | CD | 2.92 | -1B | -X+1/2 | Y+1/2 | -Z |
| Ser | 396C | O | Arg | 227C | NE | 3.32 | -1B | -X+1/2 | Y+1/2 | -Z |
| Ser | 396C | O | Arg | 227C | CZ | 3.54 | -1B | -X+1/2 | Y+1/2 | -Z |
| Ser | 396C | O | Arg | 227C | NH1 | 3.37 | -1B | -X+1/2 | Y+1/2 | -Z |
| Gly | 445C | O | Arg | 227C | CG | 3.02 | -1B | -X+1/2 | Y+1/2 | -Z |
| Gly | 445C | O | Arg | 227C | CD | 3.69 | -1B | -X+1/2 | Y+1/2 | -Z |
| Asn | 457C | CG | Gln | 351A | NE2 | 3.62 | | -X+1/2 | Y+1/2 | -Z |
| Asn | 457C | OD1 | Asn | 457A | ND2 | 3.56 | | -X+1/2 | Y+1/2 | -Z |
| Asn | 457C | OD1 | Gln | 351A | NE2 | 3.69 | | -X+1/2 | Y+1/2 | -Z |
| Thr | 459C | CG2 | Gln | 313A | C | 3.5 | | -X+1/2 | Y+1/2 | -Z |
| Thr | 459C | CG2 | Ala | 314A | N | 3.4 | | -X+1/2 | Y+1/2 | -Z |
| Thr | 459C | CG2 | Gln | 313A | CA | 3.61 | | -X+1/2 | Y+1/2 | -Z |
| Thr | 459C | OG1 | Gln | 351A | NE2 | 3.16 | | -X+1/2 | Y+1/2 | -Z |
| Thr | 459C | OG1 | Gln | 351A | CG | 3.16 | | -X+1/2 | Y+1/2 | -Z |
| Thr | 459C | OG1 | GLn | 351A | CD | 3.44 | | -X+1/2 | Y+1/2 | -Z |

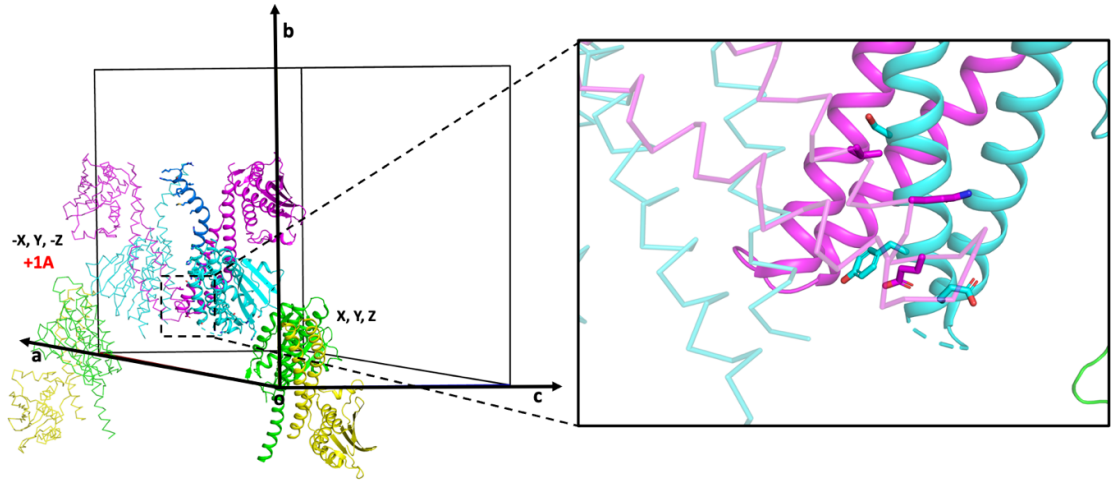
b
-X, Y, -Z
+1A
X, Y, Z
a
o
c

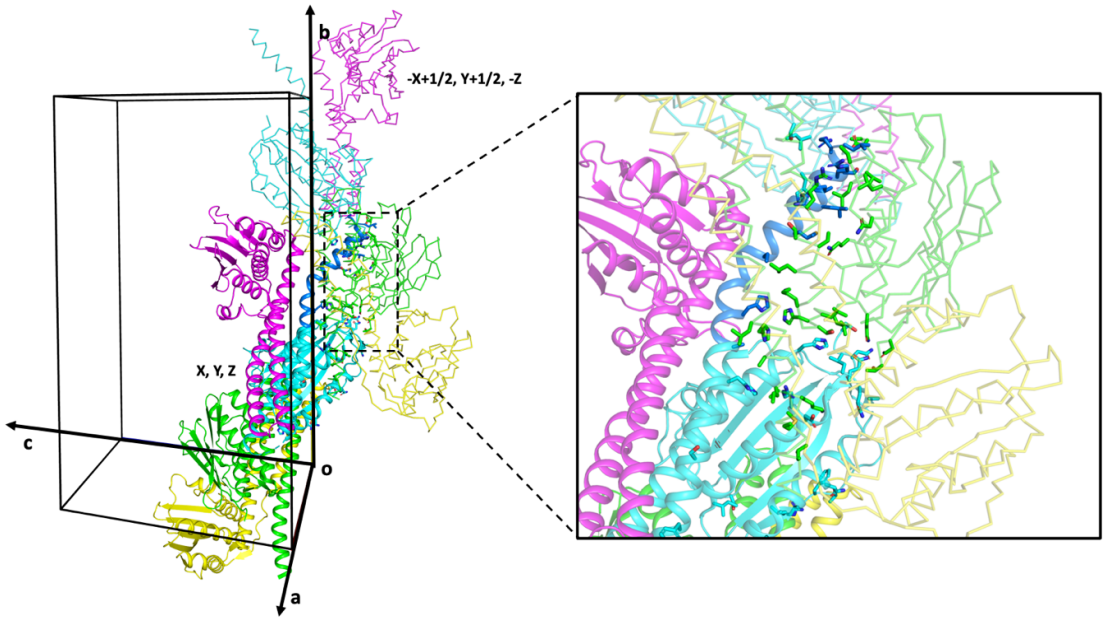
b
-X+1/2, Y+1/2, -Z
X, Y, Z
c
o
a

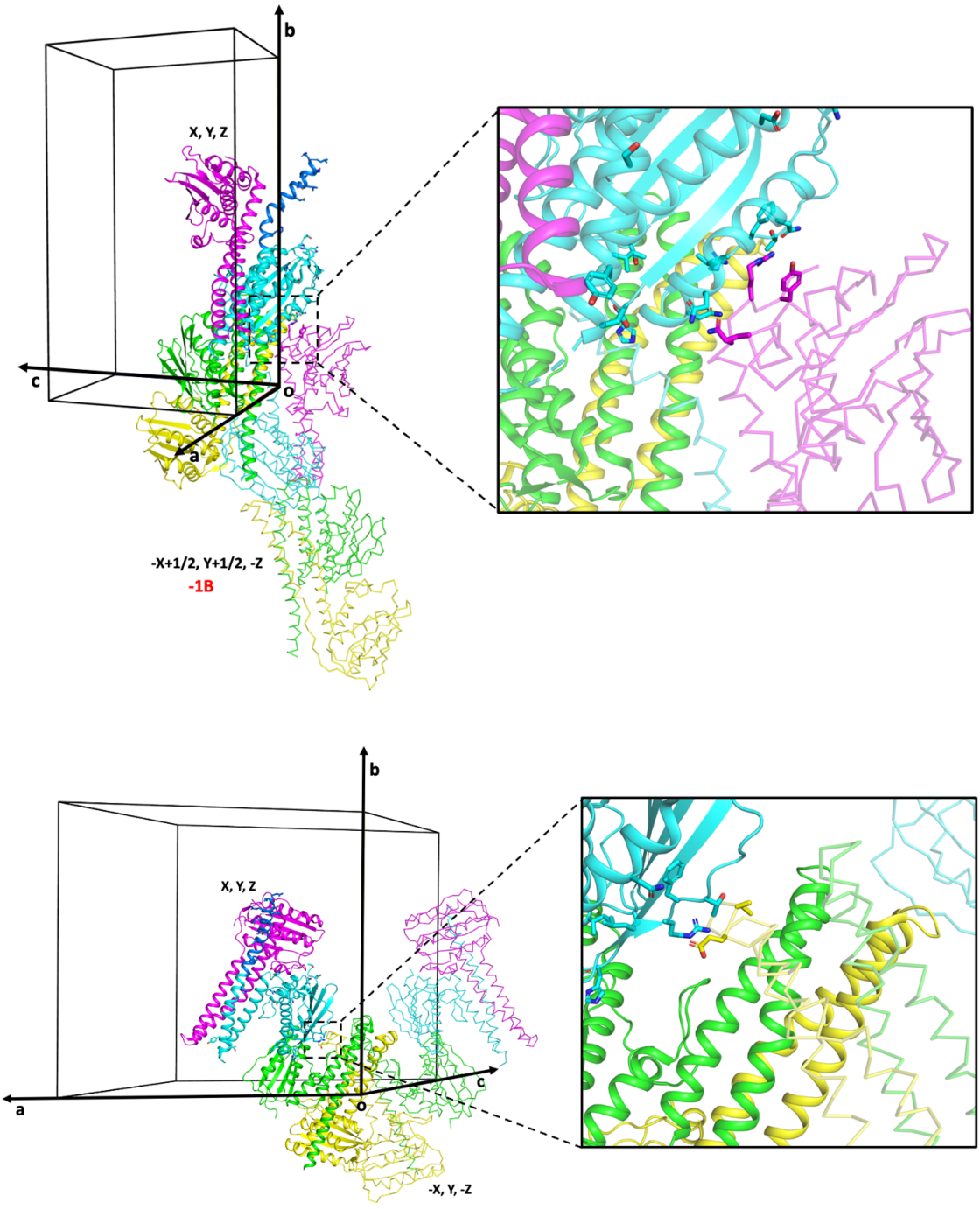


**Figure B3 Interaction of chain cC of EcZraS dimer CD with symmetry mates.**

**Table B4 Inter-atomic contact distances between symmetry-related molecules and chains cD of dimer CD of EcZraS-CD.**

| Source residue | Source residue no. | Source atom | Target residue | Target residue no. | Target atom | Distance | Unit cell translation | X | Y | Z |
|---|---|---|---|---|---|---|---|---|---|---|
| Ala | 224D | O | Lys | 268B | CD | 3.47 | | X+1/2 | Y+1/2 | Z |
| Ala | 224D | O | Lys | 268B | CE | 3.08 | | X+1/2 | Y+1/2 | Z |
| Ala | 224D | CB | Glu | 272B | CB | 3.25 | | X+1/2 | Y+1/2 | Z |
| Ala | 224D | CB | Glu | 272B | CG | 3.52 | | X+1/2 | Y+1/2 | Z |
| Tyr | 225D | O | Glu | 272B | OE1 | 3.5 | | X+1/2 | Y+1/2 | Z |
| Tyr | 225D | OH | Asn | 322C | OD1 | 3.59 | | -X+1/2 | Y+1/2 | -Z |
| Arg | 227D | CB | Leu | 339C | O | 3.65 | | -X+1/2 | Y+1/2 | -Z |
| Arg | 227D | CB | Leu | 339C | O | 3.65 | | -X+1/2 | Y+1/2 | -Z |
| Arg | 227D | CD | Leu | 339C | O | 3.61 | | -X+1/2 | Y+1/2 | -Z |
| Arg | 227D | CZ | Phe | 341C | O | 3.47 | | -X+1/2 | Y+1/2 | -Z |
| Arg | 227D | NH1 | Phe | 341C | N | 3.48 | | -X+1/2 | Y+1/2 | -Z |
| Arg | 227D | NH1 | Phe | 341C | O | 3.17 | | -X+1/2 | Y+1/2 | -Z |
| Arg | 227D | NH2 | Asn | 322C | OD1 | 3.09 | | -X+1/2 | Y+1/2 | -Z |
| Arg | 227D | NH2 | Phe | 341C | O | 3.06 | | -X+1/2 | Y+1/2 | -Z |
| Arg | 229D | CB | Asn | 333C | ND2 | 3.54 | | -X+1/2 | Y+1/2 | -Z |
| Ser | 261D | CA | Leu | 310B | O | 2.99 | | X+1/2 | Y+1/2 | Z |
| Ser | 261D | C | Leu | 310B | O | 3.66 | | X+1/2 | Y+1/2 | Z |
| Ser | 261D | C | Leu | 312B | N | 3.52 | | X+1/2 | Y+1/2 | Z |
| Ser | 261D | O | Leu | 312B | O | 3.38 | | X+1/2 | Y+1/2 | Z |
| Ser | 261D | O | Leu | 312B | CA | 3.51 | | X+1/2 | Y+1/2 | Z |
| Ser | 261D | O | Leu | 312B | CB | 3.67 | | X+1/2 | Y+1/2 | Z |
| Ser | 261D | O | Leu | 310B | O | 3.44 | | X+1/2 | Y+1/2 | Z |
| Ser | 261D | O | Ala | 311B | CA | 3.64 | | X+1/2 | Y+1/2 | Z |
| Ser | 261D | O | Ala | 311B | C | 3.49 | | X+1/2 | Y+1/2 | Z |
| Ser | 261D | O | Leu | 312B | N | 2.66 | | X+1/2 | Y+1/2 | Z |
| Ser | 261D | CB | Leu | 312B | CG | 3.59 | | X+1/2 | Y+1/2 | Z |
| Ser | 261D | CB | Leu | 312B | CD1 | 3.62 | | X+1/2 | Y+1/2 | Z |
| Ser | 261D | CB | Leu | 310B | C | 3.69 | | X+1/2 | Y+1/2 | Z |
| Ser | 261D | CB | Leu | 310B | O | 2.52 | | X+1/2 | Y+1/2 | Z |
| Ser | 261D | OG | Leu | 312B | CB | 3.58 | | X+1/2 | Y+1/2 | Z |
| Ser | 261D | OG | Leu | 312B | CG | 3.22 | | X+1/2 | Y+1/2 | Z |

| | | | | | | | | | | |
|---|---|---|---|---|---|---|---|---|---|---|
| Ser | 261D | OG | Leu | 312B | CD1 | 2.73 | | X+1/2 | Y+1/2 | Z |
| Ser | 262D | CA | Leu | 312B | O | 3.6 | | X+1/2 | Y+1/2 | Z |
| Ser | 262D | O | Leu | 312B | O | 3.61 | | X+1/2 | Y+1/2 | Z |
| Lys | 264D | NZ | His | 309B | O | 2.51 | | X+1/2 | Y+1/2 | Z |
| Lys | 264D | NZ | His | 309B | C | 3.51 | | X+1/2 | Y+1/2 | Z |
| Gly | 265D | CA | Leu | 312B | O | 3.27 | | X+1/2 | Y+1/2 | Z |
| Gly | 265D | O | Gln | 313B | NE2 | 3.4 | | X+1/2 | Y+1/2 | Z |
| Glu | 279D | OE1 | Glu | 272C | CB | 3.58 | +1A | -X | Y | -Z |
| Glu | 279D | OE2 | Tyr | 269C | CD1 | 3.13 | +1A | -X | Y | -Z |
| Gln | 282D | OE1 | Gly | 265C | CA | 3.35 | +1A | -X | Y | -Z |
| Val | 286D | CG1 | Ser | 262C | OG | 3.53 | +1A | -X | Y | -Z |
| Val | 286D | CG2 | Ser | 262C | CA | 3.51 | +1A | -X | Y | -Z |
| Glu | 290D | OE2 | Arg | 293D | NH2 | 3.51 | +1A | -X | Y | -Z |
| Arg | 293D | NH2 | Glu | 290D | OE2 | 3.51 | +1A | -X | Y | -Z |
| Asn | 295D | CB | His | 309B | CE1 | 3.66 | | X+1/2 | Y+1/2 | Z |
| Ser | 299D | CB | Glu | 303B | OE1 | 3.43 | | X+1/2 | Y+1/2 | Z |
| Glu | 303D | CG | Glu | 303B | OE2 | 3.65 | | X+1/2 | Y+1/2 | Z |
| His | 309D | O | Lys | 264B | CE | 3.56 | | X+1/2 | Y+1/2 | Z |
| His | 309D | O | Lys | 264B | NZ | 2.66 | | X+1/2 | Y+1/2 | Z |
| His | 309D | CD2 | Asn | 295B | ND2 | 3.51 | | X+1/2 | Y+1/2 | Z |
| His | 309D | CE1 | Arg | 257B | CG | 2.84 | | X+1/2 | Y+1/2 | Z |
| His | 309D | CE1 | Arg | 257B | CD | 3.46 | | X+1/2 | Y+1/2 | Z |
| His | 309D | CE1 | Asn | 295B | OD1 | 3.63 | | X+1/2 | Y+1/2 | Z |
| His | 309D | CE1 | Arg | 257B | CB | 3.62 | | X+1/2 | Y+1/2 | Z |
| His | 309D | NE2 | Asn | 295B | ND2 | 3.63 | | X+1/2 | Y+1/2 | Z |
| His | 309D | NE2 | Asn | 295B | CG | 3.57 | | X+1/2 | Y+1/2 | Z |
| His | 309D | NE2 | Asn | 295B | OD1 | 3.25 | | X+1/2 | Y+1/2 | Z |
| Leu | 310D | O | Ser | 261B | CA | 3.19 | | X+1/2 | Y+1/2 | Z |
| Leu | 310D | O | Ser | 261B | O | 3.45 | | X+1/2 | Y+1/2 | Z |
| Leu | 310D | O | Ser | 261B | CB | 2.78 | | X+1/2 | Y+1/2 | Z |
| Ala | 311D | CA | Gly | 265B | N | 3.47 | | X+1/2 | Y+1/2 | Z |
| Ala | 311D | C | Gly | 265B | CA | 3.69 | | X+1/2 | Y+1/2 | Z |
| Ala | 311D | CB | Lys | 264B | C | 3.65 | | X+1/2 | Y+1/2 | Z |
| Ala | 311D | CB | Gly | 265B | N | 3.48 | | X+1/2 | Y+1/2 | Z |
| Ala | 311D | CB | Gly | 265B | CA | 3.47 | | X+1/2 | Y+1/2 | Z |

| | | | | | | | | | | |
|---|---|---|---|---|---|---|---|---|---|---|
| Leu | 312D | N | Ser | 261B | O | 3.15 | | X+1/2 | Y+1/2 | Z |
| Leu | 312D | CG | Ser | 261B | OG | 3.65 | | X+1/2 | Y+1/2 | Z |
| Leu | 312D | CD1 | Ser | 261B | OG | 3.36 | | X+1/2 | Y+1/2 | Z |
| Gln | 313D | CG | Gly | 265B | O | 3.58 | | X+1/2 | Y+1/2 | Z |
| Gln | 313D | NE2 | Lys | 268B | CD | 3.47 | | X+1/2 | Y+1/2 | Z |
| Gln | 313D | OE1 | Tyr | 269B | CB | 3.66 | | X+1/2 | Y+1/2 | Z |
| Gln | 330D | CD | Gln | 330C | NE2 | 3.68 | | -X+1/2 | Y+1/2 | -Z |
| Gln | 330D | OE1 | Gln | 330C | CD | 3.27 | | -X+1/2 | Y+1/2 | -Z |
| Gln | 330D | OE1 | Gln | 330C | NE2 | 3.31 | | -X+1/2 | Y+1/2 | -Z |
| Gln | 330D | OE1 | Gln | 330C | CG | 2.99 | | -X+1/2 | Y+1/2 | -Z |
| Asp | 355D | OD2 | Lys | 268B | CE | 3.28 | | X+1/2 | Y+1/2 | Z |

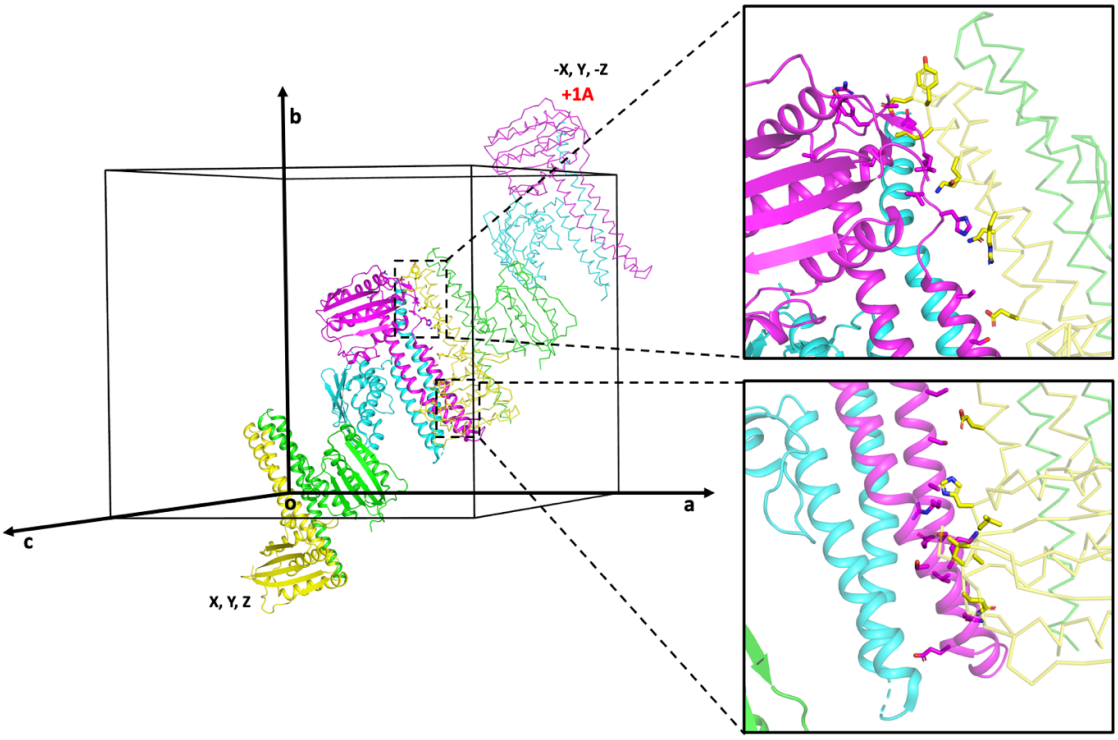

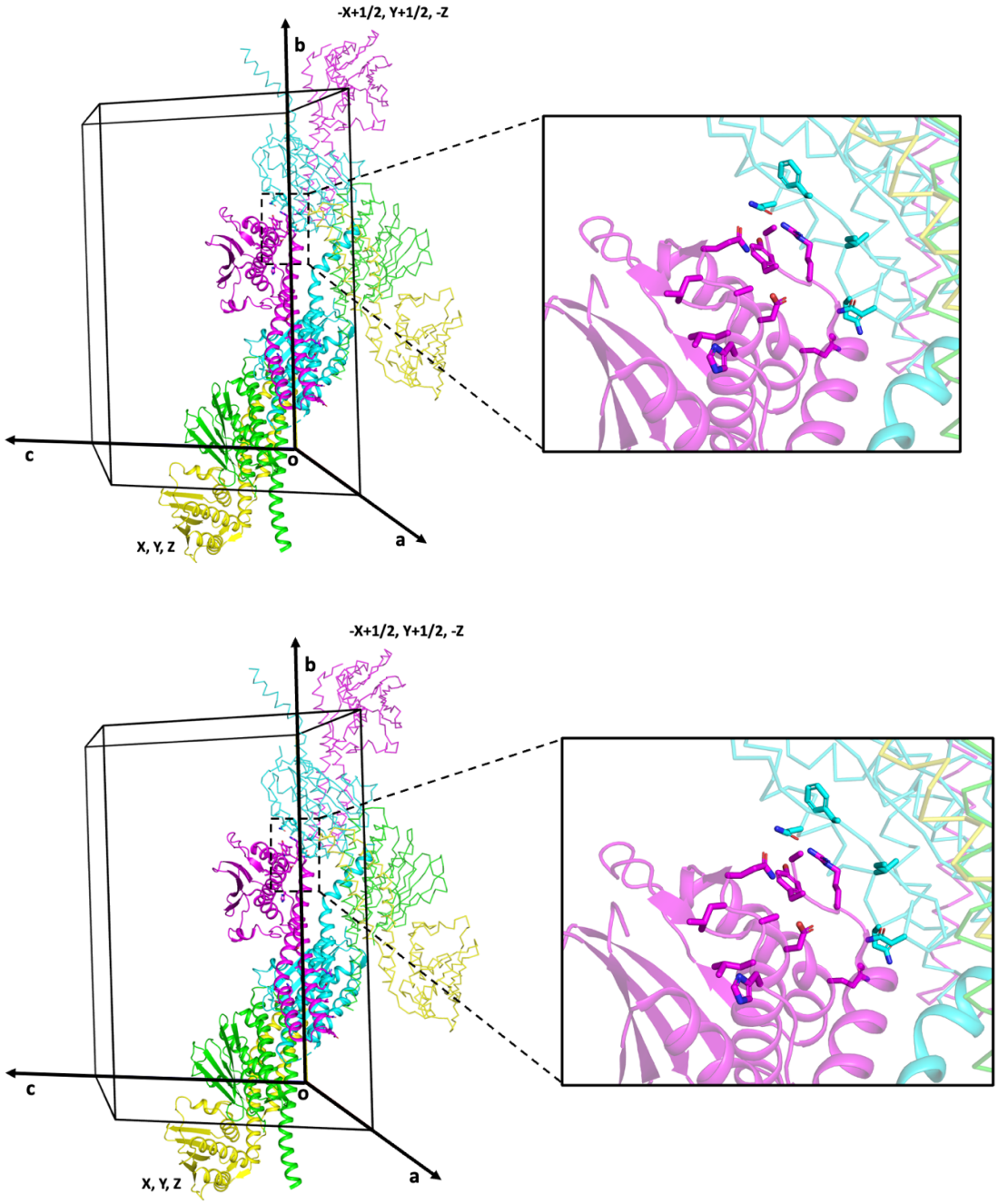


**Figure B4 Interaction of chain cD of EcZraS dimer CD with symmetry mates.**

# BIBLIOGRAPHY

Adams, P. D., Afonine, P. V., Bunkóczi, G., Chen, V. B., Davis, I. W., Echols, N., Headd, J. J., Hung, L. W., Kapral, G. J., Grosse-Kunstleve, R. W., McCoy, A. J., Moriarty, N. W., Oeffner, R., Read, R. J., Richardson, D. C., Richardson, J. S., Terwilliger, T. C., & Zwart, P. H. (2010). PHENIX: a comprehensive Python-based system for macromolecular structure solution. *Acta Crystallographica. Section D, Biological Crystallography*, *66*(Pt 2), 213–221. https://doi.org/10.1107/S0907444909052925

Agirre, J., Atanasova, M., Bagdonas, H., Ballard, C. B., Baslé, A., Beilsten-Edmands, J., Borges, R. J., Brown, D. G., Burgos-Mármol, J. J., Berrisford, J. M., Bond, P. S., Caballero, I., Catapano, L., Chojnowski, G., Cook, A. G., Cowtan, K. D., Croll, T. I., Debreczeni, J., Devenish, N. E., … Yamashita, K. (2023). The CCP4 suite: integrative software for macromolecular crystallography. *Urn:Issn:2059-7983*, *79*(6), 449–461. https://doi.org/10.1107/S2059798323003595

Ahsan, R., Kifayat, S., Pooniya, K. K., Kularia, S., Adimalla, B. S., Sanapalli, B. K. R., Sanapalli, V., & Sigalapalli, D. K. (2024). Bacterial Histidine Kinase and the Development of Its Inhibitors in the 21st Century. *Antibiotics 2024, Vol. 13, Page 576*, *13*(7), 576. https://doi.org/10.3390/ANTIBIOTICS13070576

Albanesi, D., Martín, M., Trajtenberg, F., Mansilla, M. C., Haouz, A., Alzari, P. M., De Mendoza, D., & Buschiazzo, A. (2009). Structural plasticity and catalysis regulation of a thermosensor histidine kinase. *Proceedings of the National Academy of Sciences of the United States of America*, *106*(38), 16185–16190. https://doi.org/10.1073/PNAS.0906699106

Alm, E., Huang, K., & Arkin, A. (2006). The Evolution of Two-Component Systems in Bacteria Reveals Different Strategies for Niche Adaptation. *PLOS Computational Biology*, *2*(11), e143. https://doi.org/10.1371/JOURNAL.PCBI.0020143

Almada, J. C., Bortolotti, A., Ruysschaert, J. M., de Mendoza, D., Inda, M. E., & Cybulski, L. E. (2021). Interhelical h-bonds modulate the activity of a polytopic transmembrane kinase. *Biomolecules*, *11*(7), 938. https://doi.org/10.3390/BIOM11070938/S1

Alvarez, A. F., Rodríguez, C., González-Chávez, R., & Georgellis, D. (2021). The Escherichia coli two-component signal sensor BarA binds protonated acetate via a conserved hydrophobic-binding pocket. *The Journal of Biological Chemistry*, *297*(6), 101383. https://doi.org/10.1016/J.JBC.2021.101383

Appia-Ayme, C., Hall, A., Patrick, E., Rajadurai, S., Clarke, T. A., & Rowley, G. (2012). ZraP is a periplasmic molecular chaperone and a repressor of the zinc-responsive two-component regulator ZraSR. *The Biochemical Journal*, *442*(1), 85–93. https://doi.org/10.1042/BJ20111639

Armitage, J. P. (1992). Behavioral responses in bacteria. *Annual Review of Physiology*, *54*(Volume 54,), 683–714. https://doi.org/10.1146/ANNUREV.PH.54.030192.003343/CITE/REFWORKS

Arora, G., Sajid, A., Arulanandh, M. D., Singhal, A., Mattoo, A. R., Pomerantsev, A. P., Leppla, S. H., Maiti, S., & Singh, Y. (2012). Unveiling the novel dual specificity protein kinases in Bacillus anthracis: identification of the first prokaryotic dual specificity tyrosine phosphorylation-regulated kinase (DYRK)-like kinase. *The Journal of Biological Chemistry*, *287*(32), 26749–26763. https://doi.org/10.1074/JBC.M112.351304

Ashenberg, O., Keating, A. E., & Laub, M. T. (2013). Helix bundle loops determine whether histidine kinases autophosphorylate in cis or in trans. *Journal of Molecular Biology*, *425*(7), 1198–1209. https://doi.org/10.1016/J.JMB.2013.01.011

Avison, M. B., Horton, R. E., Walsh, T. R., & Bennett, P. M. (2001). Escherichia coli CreBC is a global regulator of gene expression that responds to growth in minimal media. *The Journal of Biological Chemistry*, *276*(29), 26955–26961. https://doi.org/10.1074/JBC.M011186200

Barlow, D. J., & Thornton, J. M. (1988). Helix geometry in proteins. *Journal of Molecular Biology*, *201*(3), 601–619. https://doi.org/10.1016/0022-2836(88)90641-9

Bauer, W. J., Luthra, A., Zhu, G., Radolf, J. D., Malkowski, M. G., & Caimano, M. J. (2015). Structural characterization and modeling of the Borrelia burgdorferi hybrid histidine kinase Hk1 periplasmic sensor: A system for sensing small molecules associated with tick feeding. *Journal of Structural Biology*, *192*(1), 48–58. https://doi.org/10.1016/J.JSB.2015.08.013

Behr, S., Fried, L., & Jung, K. (2014). Identification of a novel nutrient-sensing histidine kinase/response regulator network in Escherichia coli. *Journal of Bacteriology*, *196*(11), 2023–2029. https://doi.org/10.1128/JB.01554-14

Bellini, D., & Papiz, M. Z. (2012). Structure of a Bacteriophytochrome and Light-Stimulated Protomer Swapping with a Gene Repressor. *Structure*, *20*(8), 1436–1446. https://doi.org/10.1016/J.STR.2012.06.002

Bhate, M. A. P., Molnar, K. A. S., Goulian, M., & Degrado, W. F. (2015). Signal Transduction in Histidine Kinases: Insights from New Structures. *Structure*, *23*(6), 981–994. https://doi.org/10.1016/J.STR.2015.04.002

Bick, M. J., Lamour, V., Rajashankar, K. R., Gordiyenko, Y., Robinson, C. V., & Darst, S. A. (2009). How to switch off a histidine kinase: crystal structure of Geobacillus

stearothermophilus KinB with the inhibitor Sda. *Journal of Molecular Biology*, *386*(1), 163–177. https://doi.org/10.1016/J.JMB.2008.12.006

Bilwes, A. M., Alex, L. A., Crane, B. R., & Simon, M. I. (1999). Structure of CheA, a Signal-Transducing Histidine Kinase. *Cell*, *96*(1), 131–141. https://doi.org/10.1016/S0092-8674(00)80966-6

Bittrich, S., Segura, J., Duarte, J. M., Burley, S. K., & Rose, Y. (2024). RCSB protein Data Bank: exploring protein 3D similarities via comprehensive structural alignments. *Bioinformatics*, *40*(6). https://doi.org/10.1093/BIOINFORMATICS/BTAE370

Browning, D. F., Whitworth, D. E., & Hodgson, D. A. (2003). Light-induced carotenogenesis in Myxococcus xanthus: Functional characterization of the ECF sigma factor CarQ and antisigma factor CarR. *Molecular Microbiology*, *48*(1), 237–251. https://doi.org/10.1046/J.1365-2958.2003.03431.X

Brüderlin, M., Böhm, R., Fadel, F., Hiller, S., Schirmer, T., & Dubey, B. N. (2023). Structural features discriminating hybrid histidine kinase Rec domains from response regulator homologs. *Nature Communications 2023 14:1*, *14*(1), 1–15. https://doi.org/10.1038/s41467-023-36597-8

Buchner, S., Schlundt, A., Lassak, J., Sattler, M., & Jung, K. (2015). Structural and Functional Analysis of the Signal-Transducing Linker in the pH-Responsive One-Component System CadC of Escherichia coli. *Journal of Molecular Biology*, *427*(15), 2548–2561. https://doi.org/10.1016/J.JMB.2015.05.001

Buschiazzo, A., & Trajtenberg, F. (2019). Two-component sensing and regulation: How do histidine kinases talk with response regulators at the molecular level? *Annual Review of Microbiology*, *73*(Volume 73, 2019), 507–528. https://doi.org/10.1146/ANNUREV-MICRO-091018-054627/1

Cai, S. J., & Inouye, M. (2002). EnvZ-OmpR interaction and osmoregulation in Escherichia coli. *The Journal of Biological Chemistry*, *277*(27), 24155–24161. https://doi.org/10.1074/JBC.M110715200

Cai, Y., Su, M., Ahmad, A., Hu, X., Sang, J., Kong, L., Chen, X., Wang, C., Shuai, J., & Han, A. (2017a). Conformational dynamics of the essential sensor histidine kinase WalK. *Acta Crystallographica Section D: Structural Biology*, *73*(10), 793–803. https://doi.org/10.1107/S2059798317013043/DI5014SUP1.PDF

Cai, Y., Su, M., Ahmad, A., Hu, X., Sang, J., Kong, L., Chen, X., Wang, C., Shuai, J., & Han, A. (2017b). Conformational dynamics of the essential sensor histidine kinase WalK. *Acta Crystallographica Section D: Structural Biology*, *73*(10), 793–803. https://doi.org/10.1107/S2059798317013043/DI5014SUP1.PDF

Campbell, E. A., Tupy, J. L., Gruber, T. M., Wang, S., Sharp, M. M., Gross, C. A., & Darst, S. A. (2003). Crystal Structure of Escherichia coli σE with the Cytoplasmic Domain of Its Anti-σ RseA. *Molecular Cell*, *11*(4), 1067–1078. https://doi.org/10.1016/S1097-2765(03)00148-5

Can, S., Lacey, S., Gur, M., Carter, A. P., & Yildiz, A. (2019). Directionality of dynein is controlled by the angle and length of its stalk. *Nature*, *566*(7744), 407–410. https://doi.org/10.1038/S41586-019-0914-Z

Capra, E. J., & Laub, M. T. (2012). Evolution of two-component signal transduction systems. *Annual Review of Microbiology*, *66*(Volume 66, 2012), 325–347. https://doi.org/10.1146/ANNUREV-MICRO-092611-150039/CITE/REFWORKS

Capra, E. J., Perchuk, B. S., Lubin, E. A., Ashenberg, O., Skerker, J. M., & Laub, M. T. (2010). Systematic dissection and trajectory-scanning mutagenesis of the molecular interface that ensures specificity of two-component signaling pathways. *PLoS Genetics*, *6*(11). https://doi.org/10.1371/JOURNAL.PGEN.1001220

Casino, P., Miguel-Romero, L., & Marina, A. (2014). Visualizing autophosphorylation in histidine kinases. *Nature Communications 2014 5:1*, *5*(1), 1–12. https://doi.org/10.1038/ncomms4258

Cassidy, C. K., Himes, B. A., Sun, D., Ma, J., Zhao, G., Parkinson, J. S., Stansfeld, P. J., Luthey-Schulten, Z., & Zhang, P. (2020a). Structure and dynamics of the E. coli chemotaxis core signaling complex by cryo-electron tomography and molecular simulations. *Communications Biology 2020 3:1*, *3*(1), 1–10. https://doi.org/10.1038/s42003-019-0748-0

Cassidy, C. K., Himes, B. A., Sun, D., Ma, J., Zhao, G., Parkinson, J. S., Stansfeld, P. J., Luthey-Schulten, Z., & Zhang, P. (2020b). Structure and dynamics of the E. coli chemotaxis core signaling complex by cryo-electron tomography and molecular simulations. *Communications Biology 2020 3:1*, *3*(1), 1–10. https://doi.org/10.1038/s42003-019-0748-0

Chawla, Y., Upadhyay, S., Khan, S., Nagarajan, S. N., Forti, F., & Nandicoori, V. K. (2014). Protein Kinase B (PknB) of Mycobacterium tuberculosis Is Essential for Growth of the Pathogen in Vitro as well as for Survival within the Host. *The Journal of Biological Chemistry*, *289*(20), 13858. https://doi.org/10.1074/JBC.M114.563536

Chen, H., Yu, C., Wu, H., Li, G., Li, C., Hong, W., Yang, X., Wang, H., & You, X. (2022). Recent Advances in Histidine Kinase-Targeted Antimicrobial Agents. *Frontiers in Chemistry*, *10*, 866392. https://doi.org/10.3389/FCHEM.2022.866392/XML/NLM

Chen, S. K., Guan, H. H., Wu, P. H., Lin, L. T., Wu, M. C., Chang, H. Y., Chen, N. C., Lin, C. C., Chuankhayan, P., Huang, Y. C., Lin, P. J., & Chen, C. J. (2020). Structural insights into the histidine-containing phosphotransfer protein and receiver domain of sensor histidine kinase suggest a complex model in the two-component regulatory system in Pseudomonas aeruginosa. *IUCrJ*, *7*(5), 934–948. https://doi.org/10.1107/S2052252520009665/LZ5039SUP1.PDF

Cheung, J., Bingman, C. A., Reyngold, M., Hendrickson, W. A., & Waldburger, C. D. (2008). Crystal structure of a functional dimer of the PhoQ sensor domain. *Journal of Biological Chemistry*, *283*(20), 13762–13770. https://doi.org/10.1074/JBC.M710592200

Cheung, J., & Hendrickson, W. A. (2008). Crystal structures of C4-dicarboxylate ligand complexes with sensor domains of histidine kinases DcuS and DctB. *Journal of Biological Chemistry*, *283*(44), 30256–30265. https://doi.org/10.1074/jbc.M805253200

Cheung, J., & Hendrickson, W. A. (2009). Structural Analysis of Ligand Stimulation of the Histidine Kinase NarX. *Structure*, *17*(2), 190–201. https://doi.org/10.1016/J.STR.2008.12.013/ASSET/E02D97DC-B392-41CB-9582-B76CC911D40D/MAIN.ASSETS/GR8.JPG

Cheung, J., & Hendrickson, W. A. (2010). Sensor Domains of Two-Component Regulatory Systems. *Current Opinion in Microbiology*, *13*(2), 116. https://doi.org/10.1016/J.MIB.2010.01.016

Cho, H. Y., Cho, H. J., Kim, M. H., & Kang, B. S. (2011). Blockage of the channel to heme by the E87 side chain in the GAF domain of Mycobacterium tuberculosis DosS confers the unique sensitivity of DosS to oxygen. *FEBS Letters*, *585*(12), 1873–1878. https://doi.org/10.1016/J.FEBSLET.2011.04.050

Cho, T. H. S., Murray, C., Malpica, R., Margain-Quevedo, R., Thede, G. L., Lu, J., Edwards, R. A., Glover, J. N. M., & Raivio, T. L. (2024). The sensor of the bacterial histidine kinase CpxA is a novel dimer of extracytoplasmic Per-ARNT-Sim domains. *Journal of Biological Chemistry*, *300*(5), 107265. https://doi.org/10.1016/J.JBC.2024.107265/ATTACHMENT/A96D89C9-86C1-4703-B1EA-3575B7852824/MMC1.PDF

Chou, P. Y., & Pasman, G. D. (1974). Conformational parameters for amino acids in helical, beta-sheet, and random coil regions calculated from proteins. *Biochemistry*, *13*(2), 211–222. https://doi.org/10.1021/BI00699A001

Contreras, F. U., Camacho, M. I., Pannuri, A., Romeo, T., Alvarez, A. F., & Georgellis, D. (2023). Spatiotemporal regulation of the BarA/UvrY two-component signaling system. *Journal of Biological Chemistry*, *299*(6), 104835. https://doi.org/10.1016/J.JBC.2023.104835

Crooks, G. E., Hon, G., Chandonia, J. M., & Brenner, S. E. (2004). WebLogo: A Sequence Logo Generator. *Genome Research*, *14*(6), 1188–1190. https://doi.org/10.1101/GR.849004

Danese, P. N., & Silhavy, T. J. (1998). CpxP, a stress-combative member of the Cpx regulon. *Journal of Bacteriology*, *180*(4), 831–839. https://doi.org/10.1128/JB.180.4.831-839.1998

Darwin, A. J., Ziegelhoffer, E. C., Kiley, P. J., & Stewart, V. (1998a). Fnr, NarP, and NarL Regulation of Escherichia coli K-12 napF (Periplasmic Nitrate Reductase) Operon Transcription In Vitro. *Journal of Bacteriology*, *180*(16), 4192. https://doi.org/10.1128/JB.180.16.4192-4198.1998

Darwin, A. J., Ziegelhoffer, E. C., Kiley, P. J., & Stewart, V. (1998b). Fnr, NarP, and NarL regulation of Escherichia coli K-12 napF (periplasmic nitrate reductase) operon transcription in vitro. *Journal of Bacteriology*, *180*(16), 4192–4198. https://doi.org/10.1128/jb.180.16.4192-4198.1998

Diensthuber, R. P., Bommer, M., Gleichmann, T., & Möglich, A. (2013). Full-Length Structure of a Sensor Histidine Kinase Pinpoints Coaxial Coiled Coils as Signal Transducers and Modulators. *Structure*, *21*(7), 1127–1136. https://doi.org/10.1016/J.STR.2013.04.024

Doublet, P., Vincent, C., Grangeasse, C., Cozzone, A. J., & Duclos, B. (1999). On the binding of ATP to the autophosphorylating protein, Ptk, of the bacterium Acinetobacter johnsonii. *FEBS Letters*, *445*(1), 137–143. https://doi.org/10.1016/S0014-5793(99)00111-8

Dubey, B. N., Lori, C., Ozaki, S., Fucile, G., Plaza-Menacho, I., Jenal, U., & Schirmer, T. (2016). Cyclic di-GMP mediates a histidine kinase/phosphatase switch by noncovalent domain cross-linking. *Science Advances*, *2*(9). https://doi.org/10.1126/SCIADV.1600823

Dunin-Horkawicz, S., & Lupas, A. N. (2010). Comprehensive Analysis of HAMP Domains: Implications for Transmembrane Signal Transduction. *Journal of Molecular Biology*, *397*(5), 1156–1174. https://doi.org/10.1016/J.JMB.2010.02.031

Dupré, E., Herrou, J., Lensink, M. F., Wintjens, R., Vagin, A., Lebedev, A., Crosson, S., Villeret, V., Locht, C., Antoine, R., & Jacob-Dubuisson, F. (2015). Virulence regulation with Venus flytrap domains: structure and function of the periplasmic moiety of the sensor-kinase BvgS. *PLoS Pathogens*, *11*(3), 1–21. https://doi.org/10.1371/JOURNAL.PPAT.1004700

Dupré, E., Wohlkonig, A., Herrou, J., Locht, C., Jacob-Dubuisson, F., & Antoine, R. (2013). Characterization of the PAS domain in the sensor-kinase BvgS: Mechanical role in signal transmission. *BMC Microbiology*, *13*(1), 1–12. https://doi.org/10.1186/1471-2180-13-172/FIGURES/6

Dutta, R., & Inouye, M. (2000). GHKL, an emergent ATPase/kinase superfamily. *Trends in Biochemical Sciences*, *25*(1), 24–28. https://doi.org/10.1016/S0968-0004(99)01503-0

Dutta, R., Qin, L., & Inouye, M. (1999). Histidine kinases: diversity of domain organization. *Molecular Microbiology*, *34*(4), 633–640. https://doi.org/10.1046/J.1365-2958.1999.01646.X

Ebel, W., & Trempy, J. E. (1999). Escherichia coli RcsA, a positive activator of colanic acid capsular polysaccharide synthesis, functions To activate its own expression. *Journal of Bacteriology*, *181*(2), 577–584. https://doi.org/10.1128/JB.181.2.577-584.1999

Emsley, P., & Cowtan, K. (2004). Coot: model-building tools for molecular graphics. *Acta Crystallographica. Section D, Biological Crystallography*, *60*(Pt 12 Pt 1), 2126–2132. https://doi.org/10.1107/S0907444904019158

Epstein, W. (2015). The KdpD Sensor Kinase of Escherichia coli Responds to Several Distinct Signals To Turn on Expression of the Kdp Transport System. *Journal of Bacteriology*, *198*(2), 212. https://doi.org/10.1128/JB.00602-15

Eswaramoorthy, P., & Fujita, M. (2010). Systematic Domain Deletion Analysis of the Major Sporulation Kinase in Bacillus subtilis. *Journal of Bacteriology*, *192*(6), 1744. https://doi.org/10.1128/JB.01481-09

Evstigneeva, S. S., Telesheva, E. M., Mokeev, D. I., Borisov, I. V., Petrova, L. P., & Shelud'ko, A. V. (2021). Response of Bacteria to Mechanical Stimuli. *Microbiology (Russian Federation)*, *90*(5), 558–568. https://doi.org/10.1134/S0026261721050052/METRICS

Ferrières, L., & Clarke, D. J. (2003). The RcsC sensor kinase is required for normal biofilm formation in Escherichia coli K-12 and controls the expression of a regulon in response to growth on a solid surface. *Molecular Microbiology*, *50*(5), 1665–1682. https://doi.org/10.1046/J.1365-2958.2003.03815.X

Ferris, H. U., Coles, M., Lupas, A. N., & Hartmann, M. D. (2014). Crystallographic snapshot of the Escherichia coli EnvZ histidine kinase in an active conformation. *Journal of Structural Biology*, *186*(3), 376–379. https://doi.org/10.1016/J.JSB.2014.03.014

Filippou, P. S., Kasemian, L. D., Panagiotidis, C. A., & Kyriakidis, D. A. (2008). Functional characterization of the histidine kinase of the E. coli two-component signal transduction system AtoS–AtoC. *Biochimica et Biophysica Acta (BBA) - General Subjects*, *1780*(9), 1023–1031. https://doi.org/10.1016/J.BBAGEN.2008.05.002

Fried, L., Behr, S., & Jung, K. (2013). Identification of a Target Gene and Activating Stimulus for the YpdA/YpdB Histidine Kinase/Response Regulator System in Escherichia coli. *Journal of Bacteriology*, *195*(4), 807. https://doi.org/10.1128/JB.02051-12

Gao, R., & Stock, A. M. (2009). Biological Insights from Structures of Two-Component Proteins. *Annual Review of Microbiology*, *63*, 133. https://doi.org/10.1146/ANNUREV.MICRO.091208.073214

Gardner, S. G., & McCleary, W. R. (2019). Control of the phoBR Regulon in Escherichia coli. *EcoSal Plus*, *8*(2), 10.1128/ecosalplus.ESP-0006–2019. https://doi.org/10.1128/ECOSALPLUS.ESP-0006-2019

Gomez, D., Gavrilov, Y., & Levy, Y. (2019). Sliding Mechanism at a Coiled-Coil Interface. *Biophysical Journal*, *116*(7), 1228–1238. https://doi.org/10.1016/J.BPJ.2019.02.026

Gong, W., Hao, B., & Chan, M. K. (2000). New mechanistic insights from structural studies of the oxygen-sensing domain of Bradyrhizobium japonicum FixL. *Biochemistry*, *39*(14), 3955–3962. https://doi.org/10.1021/BI992346W

Göpel, Y., Lüttmann, D., Heroven, A. K., Reichenbach, B., Dersch, P., & Görke, B. (2011). Common and divergent features in transcriptional control of the homologous small RNAs GlmY and GlmZ in Enterobacteriaceae. *Nucleic Acids Research*, *39*(4), 1294–1309. https://doi.org/10.1093/NAR/GKQ986

Grangeasse, C., Nessler, S., & Mijakovic, I. (2012). Bacterial tyrosine kinases: evolution, biological function and structural insights. *Philosophical Transactions of the Royal Society B: Biological Sciences*, *367*(1602), 2640. https://doi.org/10.1098/RSTB.2011.0424

Grebe, T. W., & Stock, J. B. (1999). The Histidine Protein Kinase Superfamily. *Advances in Microbial Physiology*, *41*, 139–227. https://doi.org/10.1016/S0065-2911(08)60167-8

Gudipaty, S. A., Larsen, A. S., Rensing, C., & Mcevoy, M. M. (2012). Regulation of Cu(I)/Ag(I) efflux genes in Escherichia coli by the sensor kinase CusS. *FEMS Microbiology Letters*, *330*(1), 30–37. https://doi.org/10.1111/J.1574-6968.2012.02529.X

Gudipaty, S. A., & McEvoy, M. M. (2014). The histidine kinase CusS senses silver ions through direct binding by its sensor domain. *Biochimica et Biophysica Acta*, *1844*(9), 1656. https://doi.org/10.1016/J.BBAPAP.2014.06.001

Gumerov, V. M., Ulrich, L. E., & Zhulin, I. B. (2024). MiST 4.0: a new release of the microbial signal transduction database, now with a metagenomic component. *Nucleic Acids Research*, *52*(D1), D647–D653. https://doi.org/10.1093/NAR/GKAD847

Gushchin, I., Melnikov, I., Polovinkin, V., Ishchenko, A., Yuzhakova, A., Buslaev, P., Bourenkov, G., Grudinin, S., Round, E., Balandin, T., Borshchevskiy, V., Willbold, D., Leonard, G., Büldt, G., Popov, A., & Gordeliy, V. (2017). Mechanism of transmembrane signaling by sensor histidine kinases. *Science*, *356*(6342). https://doi.org/10.1126/SCIENCE.AAH6345

Hajj, S. El, Henry, C., Vergnes, A., Loiseau, L., Brasseur, G., Barré, R., Aussel, L., & Ezraty, B. (2021). HypVW is an HOCl-Sensing Two Component System in Escherichia coli. *BioRxiv*, 2021.09.09.459708. https://doi.org/10.1101/2021.09.09.459708

Hauser, A. S., Kooistra, A. J., Munk, C., Heydenreich, F. M., Veprintsev, D. B., Bouvier, M., Babu, M. M., & Gloriam, D. E. (2021). GPCR activation mechanisms across classes and

macro/microscales. *Nature Structural & Molecular Biology 2021 28:11*, *28*(11), 879–888. https://doi.org/10.1038/s41594-021-00674-7

Hegazy, E. A., & El-Antrawy, M. A. (2025). Impact of high frequency electromagnetic radiation on bacterial survival and antibiotic activity in exposed bacteria. *Scientific Reports 2025 15:1*, *15*(1), 1–9. https://doi.org/10.1038/s41598-025-90599-8

Herrera, C. M., Hankins, J. V., & Trent, M. S. (2010). Activation of PmrA inhibits LpxT-dependent phosphorylation of lipid A promoting resistance to antimicrobial peptides. *Molecular Microbiology*, *76*(6), 1444. https://doi.org/10.1111/J.1365-2958.2010.07150.X

Herrou, J., Bompard, C., Wintjens, R., Dupré, E., Willery, E., Villeret, V., Locht, C., Antoine, R., & Jacob-Dubuisson, F. (2010). Periplasmic domain of the sensor-kinase BvgS reveals a new paradigm for the Venus flytrap mechanism. *Proceedings of the National Academy of Sciences of the United States of America*, *107*(40), 17351–17355. https://doi.org/10.1073/PNAS.1006267107

Hess, J. F., Bourret, R. B., & Simon, M. I. (1988). Histidine phosphorylation and phosphoryl group transfer in bacterial chemotaxis. *Nature 1988 336:6195*, *336*(6195), 139–143. https://doi.org/10.1038/336139a0

Hu, L., Wang, C., Lu, W., Lu, H., Chen, H., & Tan, C. (2020). BaeSR activates type VI secretion system expression in porcine extra-intestinal pathogenic Escherichia coli to enhance bacterial resistance to zinc stress. *Microbial Pathogenesis*, *147*, 104357. https://doi.org/10.1016/J.MICPATH.2020.104357

Hughes, D. T., Clarke, M. B., Yamamoto, K., Rasko, D. A., & Sperandio, V. (2009). The QseC Adrenergic Signaling Cascade in Enterohemorrhagic E. coli (EHEC). *PLoS Pathogens*, *5*(8), e1000553. https://doi.org/10.1371/JOURNAL.PPAT.1000553

Igarashi, M., Watanabe, T., Hashida, T., Umekita, M., Hatano, M., Yanagida, Y., Kino, H., Kimura, T., Kinoshita, N., Inoue, K., Sawa, R., Nishimura, Y., Utsumi, R., & Nomoto, A. (2013). Waldiomycin, a novel WalK-histidine kinase inhibitor from Streptomyces sp. MK844-mF10. *The Journal of Antibiotics 2013 66:8*, *66*(8), 459–464. https://doi.org/10.1038/ja.2013.33

Ishii, E., & Eguchi, Y. (2021a). Diversity in Sensing and Signaling of Bacterial Sensor Histidine Kinases. *Biomolecules*, *11*(10), 1524. https://doi.org/10.3390/BIOM11101524

Ishii, E., & Eguchi, Y. (2021b). Diversity in Sensing and Signaling of Bacterial Sensor Histidine Kinases. *Biomolecules*, *11*(10), 1524. https://doi.org/10.3390/BIOM11101524

Island, M. D., & Kadner, R. J. (1993). Interplay between the membrane-associated UhpB and UhpC regulatory proteins. *Journal of Bacteriology*, *175*(16), 5028–5034. https://doi.org/10.1128/JB.175.16.5028-5034.1993

Jacob-Dubuisson, F., Mechaly, A., Betton, J. M., & Antoine, R. (2018). Structural insights into the signalling mechanisms of two-component systems. *Nature Reviews. Microbiology*, *16*(10), 585–593. https://doi.org/10.1038/S41579-018-0055-7

Janausch, I. G., Garcia-Moreno, I., & Unden, G. (2002). Function of DcuS from Escherichia coli as a Fumarate-stimulated Histidine Protein Kinase in Vitro. *Journal of Biological Chemistry*, *277*(42), 39809–39814. https://doi.org/10.1074/JBC.M204482200

Janssen, A. B., Bartholomew, T. L., Marciszewska, N. P., Bonten, M. J. M., Willems, R. J. L., Bengoechea, J. A., & van Schaik, W. (2020). Nonclonal Emergence of Colistin Resistance Associated with Mutations in the BasRS Two-Component System in Escherichia coli Bloodstream Isolates. *MSphere*, *5*(2), e00143-20. https://doi.org/10.1128/MSPHERE.00143-20

Javelle, A., Severi, E., Thornton, J., & Merrick, M. (2004). Ammonium sensing in Escherichia coli: Role of the ammonium transporter Amtb and AmtB-GlnK complex formation. *Journal of Biological Chemistry*, *279*(10), 8530–8538. https://doi.org/10.1074/JBC.M312399200/ASSET/C80C1119-77EA-4864-806F-2399EA1D51BF/MAIN.ASSETS/GR7.JPG

Jing, X., Jaw, J., Robinson, H. H., & Schubot, F. D. (2010). Crystal structure and oligomeric state of the Ret S signaling kinase sensory domain. *Proteins: Structure, Function and Bioinformatics*, *78*(7), 1631–1640. https://doi.org/10.1002/PROT.22679

Jourlin, C., Bengrine, A., Chippaux, M., & Méjean, V. (1996). An unorthodox sensor protein (TorS) mediates the induction of the tor structural genes in response to trimethylamine N-oxide in Escherichia coli. *Molecular Microbiology*, *20*(6), 1297–1306. https://doi.org/10.1111/J.1365-2958.1996.TB02648.X

Jumper, J., Evans, R., Pritzel, A., Green, T., Figurnov, M., Ronneberger, O., Tunyasuvunakool, K., Bates, R., Žídek, A., Potapenko, A., Bridgland, A., Meyer, C., Kohl, S. A. A., Ballard, A. J., Cowie, A., Romera-Paredes, B., Nikolov, S., Jain, R., Adler, J., … Hassabis, D. (2021). Highly accurate protein structure prediction with AlphaFold. *Nature*, *596*(7873), 583–589. https://doi.org/10.1038/S41586-021-03819-2

Kabbara, S., Herivaux, A., De Bernonville, T. D., Courdavault, V., Clastre, M., Gastebois, A., Osman, M., Hamze, M., Mark Cock, J., Schaap, P., & Papon, N. (2018). Diversity and Evolution of Sensor Histidine Kinases in Eukaryotes. *Genome Biology and Evolution*, *11*(1), 86. https://doi.org/10.1093/GBE/EVY213

Kabsch, W. (2010a). Integration, scaling, space-group assignment and post-refinement. *Acta Crystallographica Section D: Biological Crystallography*, *66*(2), 133–144. https://doi.org/10.1107/S0907444909047374

Kabsch, W. (2010b). XDS. *Acta Crystallographica. Section D, Biological Crystallography*, *66*(Pt 2), 125–132. https://doi.org/10.1107/S0907444909047337

Kalinowska, B., Banach, M., Wiśniowski, Z., Konieczny, L., & Roterman, I. (2017). Is the hydrophobic core a universal structural element in proteins? *Journal of Molecular Modeling*, *23*(7), 205. https://doi.org/10.1007/S00894-017-3367-Z

Kato, A., Tanabe, H., & Utsumi, R. (1999). Molecular characterization of the PhoP-PhoQ two-component system in Escherichia coli K-12: Identification of extracellular Mg2+-responsive promoters. *Journal of Bacteriology*, *181*(17), 5516–5520. https://doi.org/10.1128/JB.181.17.5516-5520.1999/ASSET/B6E6F83C-1E3F-4E4C-981F-58C4AEC84D6F/ASSETS/GRAPHIC/JB1790328004.JPEG

Kato, M., Mizuno, T., Shimizu, T., & Hakoshima, T. (1997). Insights into Multistep Phosphorelay from the Crystal Structure of the C-Terminal HPt Domain of ArcB. *Cell*, *88*(5), 717–723. https://doi.org/10.1016/S0092-8674(00)81914-5

Kato, M., Mizuno, T., Shimizu, T., & Hakoshima, T. (1999). Refined structure of the histidine-containing phosphotransfer (HPt) domain of the anaerobic sensor kinase ArcB from Escherichia coli at 1.57 Å resolution. *Urn:Issn:0907-4449*, *55*(11), 1842–1849. https://doi.org/10.1107/S0907444999010392

Keller, R., Ariöz, C., Hansmeier, N., Stenberg-Bruzell, F., Burstedt, M., Vikström, D., Kelly, A., Wieslander, Å., Daley, D. O., & Hunke, S. (2015). The Escherichia coli Envelope Stress Sensor CpxA Responds to Changes in Lipid Bilayer Properties. *Biochemistry*, *54*(23), 3670–3676. https://doi.org/10.1021/ACS.BIOCHEM.5B00242/SUPPL_FILE/BI5B00242_SI_001.PDF

Kim, D. J., & Forst, S. (2001). Genomic analysis of the histidine kinase family in bacteria and archaea. *Microbiology*, *147*(5), 1197–1212. https://doi.org/10.1099/00221287-147-5-1197/CITE/REFWORKS

Kim, D. J., Park, K. S., Kim, J. H., Yang, S. H., Yoon, J. Y., Han, B. G., Kim, H. S., Lee, S. J., Jang, J. Y., Kim, K. H., Kim, M. J., Song, J. S., Kim, H. J., Park, C. M., Lee, S. K., Il Lee, B., & Suh, S. W. (2010). Helicobacter pylori proinflammatory protein upregulates NF-κB as a cell-translocating Ser/Thr kinase. *Proceedings of the National Academy of Sciences of the United States of America*, *107*(50), 21418–21423. https://doi.org/10.1073/PNAS.1010153107/SUPPL_FILE/PNAS.1010153107_SI.PDF

Kinch, L. N., Cong, Q., Jaishankar, J., & Orth, K. (2022). Co-component signal transduction systems: Fast-evolving virulence regulation cassettes discovered in enteric bacteria. *Proceedings of the National Academy of Sciences of the United States of America*, *119*(24), e2203176119. https://doi.org/10.1073/PNAS.2203176119/SUPPL_FILE/PNAS.2203176119.SAPP.PDF

Kishii, R., Falzon, L., Yoshida, T., Kobayashi, H., & Inouye, M. (2007). Structural and functional studies of the HAMP domain of EnvZ, an osmosensing transmembrane histidine kinase in Escherichia coli. *The Journal of Biological Chemistry*, *282*(36), 26401–26408. https://doi.org/10.1074/JBC.M701342200

Koonin, E. V., & Wolf, Y. I. (2008). Genomics of bacteria and archaea: the emerging dynamic view of the prokaryotic world. *Nucleic Acids Research*, *36*(21), 6688. https://doi.org/10.1093/NAR/GKN668

Korycinski, M., Albrecht, R., Ursinus, A., Hartmann, M. D., Coles, M., Martin, J., Dunin-Horkawicz, S., & Lupas, A. N. (2015). STAC--A New Domain Associated with Transmembrane Solute Transport and Two-Component Signal Transduction Systems.

*Journal of Molecular Biology*, *427*(20), 3327–3339. https://doi.org/10.1016/J.JMB.2015.08.017

Kramer, G., & Weiss, V. (1999). Functional dissection of the transmitter module of the histidine kinase NtrB in Escherichia coli. *Proceedings of the National Academy of Sciences of the United States of America*, *96*(2), 604–609. https://doi.org/10.1073/pnas.96.2.604

Krämer, J., Fischer, J. D., Zientz, E., Vijayan, V., Griesinger, C., Lupas, A., & Unden, G. (2007). Citrate sensing by the C4-dicarboxylate/citrate sensor kinase DcuS of Escherichia coli: Binding site and conversion of DcuS to a C 4-dicarboxylate- or citrate-specific sensor. *Journal of Bacteriology*, *189*(11), 4290–4298. https://doi.org/10.1128/JB.00168-07/ASSET/7059DD18-6963-4D76-835D-615987006B30/ASSETS/GRAPHIC/ZJB0110768120005.JPEG

Krämer, R. (2010). Bacterial stimulus perception and signal transduction: Response to osmotic stress. *Chemical Record*, *10*(4), 217–229. https://doi.org/10.1002/TCR.201000005

Krämer, R., & Jung, K. (2009). *Bacterial signaling*. https://books.google.com/books?hl=en&lr=&id=3LlvtppJ5kkC&oi=fnd&pg=PR5&ots=xnEbUsRkoT&sig=-OYYe9ErDXRYBkPCCBBMXCwNN_0

Krissinel, E., & Henrick, K. (2007). Inference of macromolecular assemblies from crystalline state. *Journal of Molecular Biology*, *372*(3), 774–797. https://doi.org/10.1016/J.JMB.2007.05.022

Laermann, V., Ćudić, E., Kipschull, K., Zimmann, P., & Altendorf, K. (2013). The sensor kinase KdpD of Escherichia coli senses external K+. *Molecular Microbiology*, *88*(6), 1194–1204. https://doi.org/10.1111/MMI.12251

Leonhartsberger, S., Huber, A., Lottspeich, F., & Böck, A. (2001). The hydH/G genes from Escherichia coli code for a zinc and lead responsive two-component regulatory system. *Journal of Molecular Biology*, *307*(1), 93–105. https://doi.org/10.1006/JMBI.2000.4451

Li, G., Morigen, & Yao, Y. (2022). TorR/TorS Two-Component system resists extreme acid environment by regulating the key response factor RpoS in Escherichia coli. *Gene*, *821*, 146295. https://doi.org/10.1016/J.GENE.2022.146295

Li, Y. C., Chang, C. K., Chang, C. F., Cheng, Y. H., Fang, P. J., Yu, T., Chen, S. C., Li, Y. C., Hsiao, C. D., & Huang, T. H. (2014). Structural dynamics of the two-component response regulator RstA in recognition of promoter DNA element. *Nucleic Acids Research*, *42*(13), 8777–8788. https://doi.org/10.1093/NAR/GKU572

Li, Z., Zhu, Y., Zhang, W., & Mu, W. (2024). Rcs signal transduction system in Escherichia coli: Composition, related functions, regulatory mechanism, and applications. *Microbiological Research*, *285*, 127783. https://doi.org/10.1016/J.MICRES.2024.127783

Lindsley, J. E. (2001). Use of a real-time, coupled assay to measure the ATPase activity of DNA topoisomerase II. *Methods in Molecular Biology (Clifton, N.J.)*, *95*, 57–64. https://doi.org/10.1385/1-59259-057-8:57

Liu, Y., Li, S., Li, W., Wang, P., Ding, P., Li, L., Wang, J., Yang, P., Wang, Q., Xu, T., Xiong, Y., & Yang, B. (2019). RstA, a two-component response regulator, plays important roles in multiple virulence-associated processes in enterohemorrhagic Escherichia coli O157:H7. *Gut Pathogens*, *11*(1), 1–11. https://doi.org/10.1186/S13099-019-0335-4/FIGURES/6

Ma, Z., Masuda, N., & Foster, J. W. (2004). Characterization of EvgAS-YdeO-GadE branched regulatory circuit governing glutamate-dependent acid resistance in Escherichia coli. *Journal of Bacteriology*, *186*(21), 7378–7389. https://doi.org/10.1128/JB.186.21.7378-7389.2004

Marina, A., Mott, C., Auyzenberg, A., Hendrickson, W. A., & Waldburger, C. D. (2001). Structural and mutational analysis of the PhoQ histidine kinase catalytic domain. Insight into the reaction mechanism. *Journal of Biological Chemistry*, *276*(44), 41182–41190. https://doi.org/10.1074/JBC.M106080200/ASSET/DBFF36B6-8E0B-4D0A-9BF2-61F15E5FF0BB/MAIN.ASSETS/GR5.JPG

Marina, A., Waldburger, C. D., & Hendrickson, W. A. (2005). Structure of the entire cytoplasmic portion of a sensor histidine-kinase protein. *EMBO Journal*, *24*(24), 4247–4259. https://doi.org/10.1038/SJ.EMBOJ.7600886/SUPPL_FILE/EMBJ7600886-SUP-0001.PDF

McCoy, A. J., Grosse-Kunstleve, R. W., Adams, P. D., Winn, M. D., Storoni, L. C., & Read, R. J. (2007). Phaser crystallographic software. *Journal of Applied Crystallography*, *40*(Pt 4), 658–674. https://doi.org/10.1107/S0021889807021206

Mechaly, A. E., Sassoon, N., Betton, J. M., & Alzari, P. M. (2014). Segmental Helical Motions and Dynamical Asymmetry Modulate Histidine Kinase Autophosphorylation. *PLOS Biology*, *12*(1), e1001776. https://doi.org/10.1371/JOURNAL.PBIO.1001776

Mistry, J., Chuguransky, S., Williams, L., Qureshi, M., Salazar, G. A., Sonnhammer, E. L. L., Tosatto, S. C. E., Paladin, L., Raj, S., Richardson, L. J., Finn, R. D., & Bateman, A. (2021). Pfam: The protein families database in 2021. *Nucleic Acids Research*, *49*(D1), D412–D419. https://doi.org/10.1093/nar/gkaa913

Miyashiro, T., & Goulian, M. (2007). Stimulus-dependent differential regulation in the Escherichia coli PhoQ-PhoP system. *Proceedings of the National Academy of Sciences of the United States of America*, *104*(41), 16305–16310. https://doi.org/10.1073/PNAS.0700025104/SUPPL_FILE/00025SITEXT.PDF

Moore, J. O., & Hendrickson, W. A. (2009). Structural Analysis of Sensor Domains from the TMAO-Responsive Histidine Kinase Receptor TorS. *Structure*, *17*(9), 1195–1204.

https://doi.org/10.1016/J.STR.2009.07.015/ASSET/A89E1770-F781-4454-B804-75EFD508CC2F/MAIN.ASSETS/GR6.JPG

Muok, A. R., Briegel, A., & Crane, B. R. (2020). Regulation of the chemotaxis histidine kinase CheA: A structural perspective. *Biochimica et Biophysica Acta (BBA) - Biomembranes*, *1862*(1), 183030. https://doi.org/10.1016/J.BBAMEM.2019.183030

Nishino, K., Inazumi, Y., & Yamaguchi, A. (2003). Global Analysis of Genes Regulated by EvgA of the Two-Component Regulatory System in Escherichia coli. *Journal of Bacteriology*, *185*(8), 2667. https://doi.org/10.1128/JB.185.8.2667-2672.2003

Nizam, S. A., Zhu, J., Ho, P. Y., & Shimizu, K. (2009). Effects of arcA and arcB genes knockout on the metabolism in Escherichia coli under aerobic condition. *Biochemical Engineering Journal*, *44*(2–3), 240–250. https://doi.org/10.1016/J.BEJ.2008.12.017

Noriega, C. E., Schmidt, R., Gray, M. J., Chen, L. L., & Stewart, V. (2008). Autophosphorylation and dephosphorylation by soluble forms of the nitrate-responsive sensors NarX and NarQ from Escherichia coli K-12. *Journal of Bacteriology*, *190*(11), 3869–3876. https://doi.org/10.1128/JB.00092-08/ASSET/83AD3E44-9B93-442F-9BA6-7C5BE35CA74A/ASSETS/GRAPHIC/ZJB0110878480006.JPEG

Park, D. M., Akhtar, M. S., Ansari, A. Z., Landick, R., & Kiley, P. J. (2013). The Bacterial Response Regulator ArcA Uses a Diverse Binding Site Architecture to Regulate Carbon Oxidation Globally. *PLoS Genetics*, *9*(10), e1003839. https://doi.org/10.1371/JOURNAL.PGEN.1003839

Parkinson, J. S. (2010). Signaling mechanisms of HAMP domains in chemoreceptors and sensor kinases. *Annual Review of Microbiology*, *64*, 101–122. https://doi.org/10.1146/ANNUREV.MICRO.112408.134215

Pérez-Palacios, P., Rodríguez-Ochoa, J. L., Velázquez-Escudero, A., Rodríguez-Baño, J., Rodríguez-Martínez, J. M., Pascual, Á., & Docobo-Pérez, F. (2024). Implications of two-component systems EnvZ/OmpR and BaeS/BaeR in in vitro temocillin resistance in Escherichia coli. *Journal of Antimicrobial Chemotherapy*, *79*(3), 641. https://doi.org/10.1093/JAC/DKAE021

Petit-Härtlein, I., Rome, K., De Rosny, E., Molton, F., Duboc, C., Gueguen, E., Rodrigue, A., & Covès, J. (2015). Biophysical and physiological characterization of ZraP from Escherichia coli, the periplasmic accessory protein of the atypical ZraSR two-component system. *The Biochemical Journal*, *472*(2), 205–216. https://doi.org/10.1042/BJ20150827

Phan, M. D., Nhu, N. T. K., Achard, M. E. S., Forde, B. M., Hong, K. W., Chong, T. M., Yin, W. F., Chan, K. G., West, N. P., Walker, M. J., Paterson, D. L., Beatson, S. A., & Schembri, M. A. (2017). Modifications in the pmrB gene are the primary mechanism for the development of chromosomally encoded resistance to polymyxins in uropathogenic Escherichia coli. *The Journal of Antimicrobial Chemotherapy*, *72*(10), 2729–2736. https://doi.org/10.1093/JAC/DKX204

Pioszak, A. A., & Ninfa, A. J. (2003). Genetic and Biochemical Analysis of Phosphatase Activity of Escherichia coli NRII (NtrB) and Its Regulation by the PII Signal Transduction Protein. *Journal of Bacteriology*, *185*(4), 1299. https://doi.org/10.1128/JB.185.4.1299-1315.2003

Podust, L. M., Ioanoviciu, A., & Ortiz De Montellano, P. R. (2008). 2.3 Å X-ray structure of the heme-bound GAF domain of sensory histidine kinase DosT of Mycobacterium tuberculosis. *Biochemistry*, *47*(47), 12523–12531. https://doi.org/10.1021/BI8012356/SUPPL_FILE/BI8012356_SI_001.PDF

Qin, L., Cai, S., Zhu, Y., & Inouye, M. (2003). Cysteine-scanning analysis of the dimerization domain of EnvZ, an osmosensing histidine kinase. *Journal of Bacteriology*, *185*(11), 3429–3435. https://doi.org/10.1128/JB.185.11.3429-3435.2003

Rabin, R. S., & Stewart, V. (1992). Either of two functionally redundant sensor proteins, NarX and NarQ, is sufficient for nitrate regulation in Escherichia coli K-12. *Proceedings of the National Academy of Sciences*, *89*(18), 8419–8423. https://doi.org/10.1073/PNAS.89.18.8419

Regelmann, A. G., Lesley, J. A., Mott, C., Stokes, L., & Waldburger, C. D. (2002). Mutational Analysis of the Escherichia coli PhoQ Sensor Kinase: Differences with the Salmonella enterica Serovar Typhimurium PhoQ Protein and in the Mechanism of Mg2+ and Ca2+ Sensing. *Journal of Bacteriology*, *184*(19), 5468. https://doi.org/10.1128/JB.184.19.5468-5478.2002

Reiersen, H., & Rees, A. R. (2001). The hunchback and its neighbours: proline as an environmental modulator. *Trends in Biochemical Sciences*, *26*(11), 679–684. https://doi.org/10.1016/S0968-0004(01)01957-0

Reinelt, S., Hofmann, E., Gerharz, T., Bott, M., & Madden, D. R. (2003). The structure of the periplasmic ligand-binding domain of the sensor kinase CitA reveals the first extracellular pas domain. *Journal of Biological Chemistry*, *278*(40), 39189–39196. https://doi.org/10.1074/JBC.M305864200/ASSET/60165F0D-9117-46F6-9374-C9CE79089CE8/MAIN.ASSETS/GR5.JPG

Rismondo, J., Große, C., & Nies, D. H. (2023a). The Sensory Histidine Kinase CusS of Escherichia coli Senses Periplasmic Copper Ions. *Microbiology Spectrum*, *11*(2). https://doi.org/10.1128/SPECTRUM.00291-23/ASSET/C82EB217-978F-4B4F-9A73-D6DE1900A976/ASSETS/IMAGES/MEDIUM/SPECTRUM.00291-23-F005.GIF

Rismondo, J., Große, C., & Nies, D. H. (2023b). The Sensory Histidine Kinase CusS of Escherichia coli Senses Periplasmic Copper Ions. *Microbiology Spectrum*, *11*(2). https://doi.org/10.1128/SPECTRUM.00291-23

Robin, A. Y., Cobessi, D., Curien, G., Robert-Genthon, M., Ferrer, J. L., & Dumas, R. (2010). A New Mode of Dimerization of Allosteric Enzymes with ACT Domains Revealed by the Crystal Structure of the Aspartate Kinase from Cyanobacteria. *Journal of Molecular Biology*, *399*(2), 283–293. https://doi.org/10.1016/J.JMB.2010.04.014

Rogov, V. V., Rogova, N. Y., Bernhard, F., Koglin, A., Löhr, F., & Dötsch, V. (2006). A New Structural Domain in the Escherichia coli RcsC Hybrid Sensor Kinase Connects Histidine Kinase and Phosphoreceiver Domains. *Journal of Molecular Biology*, *364*(1), 68–79. https://doi.org/10.1016/J.JMB.2006.07.052

Rowe, J. J., Ubbink-Kok, T., Molenaar, D., Konings, W. N., & Driessen, A. J. M. (1994). NarK is a nitrite-extrusion system involved in anaerobic nitrate respiration by Escherichia coli. *Molecular Microbiology*, *12*(4), 579–586. https://doi.org/10.1111/J.1365-2958.1994.TB01044.X

Rowsell, E. H., Smith, J. M., Wolfe, A., & Taylor, B. L. (1995). CheA, CheW, and CheY are required for chemotaxis to oxygen and sugars of the phosphotransferase system in Escherichia coli. *Journal of Bacteriology*, *177*(20), 6011–6014. https://doi.org/10.1128/JB.177.20.6011-6014.1995

Saita, E., Abriata, L. A., Tsai, Y. T., Trajtenberg, F., Lemmin, T., Buschiazzo, A., Dal Peraro, M., de Mendoza, D., & Albanesi, D. (2015). A coiled coil switch mediates cold sensing by the thermosensory protein DesK. *Molecular Microbiology*, *98*(2), 258–271. https://doi.org/10.1111/MMI.13118

Scheu, P. D., Witan, J., Rauschmeier, M., Graf, S., Liao, Y. F., Ebert-Jung, A., Basché, T., Erker, W., & Unden, G. (2012). CitA/CitB Two-Component System Regulating Citrate Fermentation in Escherichia coli and Its Relation to the DcuS/DcuR System In Vivo. *Journal of Bacteriology*, *194*(3), 636. https://doi.org/10.1128/JB.06345-11

Schmidt, N. W., Grigoryan, G., & DeGrado, W. F. (2017). The accommodation index measures the perturbation associated with insertions and deletions in coiled-coils: Application to understand signaling in histidine kinases. *Protein Science : A Publication of the Protein Society*, *26*(3), 414. https://doi.org/10.1002/PRO.3095

Schniederberend, M., Zimmann, P., Bogdanov, M., Dowhan, W., & Altendorf, K. (2010). Influence of K+-dependent membrane lipid composition on the expression of the kdpFABC operon in Escherichia coli. *Biochimica et Biophysica Acta*, *1798*(1), 32–39. https://doi.org/10.1016/J.BBAMEM.2009.10.002

Sen, H., Aggarwal, N., Ishionwu, C., Hussain, N., Parmar, C., Jamshad, M., Bavro, V. N., & Lund, P. A. (2017). Structural and Functional Analysis of the Escherichia coli Acid-Sensing Histidine Kinase EvgS. *Journal of Bacteriology*, *199*(18), e00310-17. https://doi.org/10.1128/JB.00310-17

Song, Y., Peisach, D., Pioszak, A. A., Xu, Z., & Ninfa, A. J. (2004). Crystal structure of the C-terminal domain of the two-component system transmitter protein nitrogen regulator II (NRII; NtrB), regulator of nitrogen assimilation in Escherichia coli. *Biochemistry*, *43*(21), 6670–6678. https://doi.org/10.1021/BI049474R

Stephenson, K., & Hoch, J. A. (2001). PAS-A domain of phosphorelay sensor kinase A: A catalytic ATP-binding domain involved in the initiation of development in Bacillus subtilis. *Proceedings of the National Academy of Sciences*, *98*(26), 15251–15256. https://doi.org/10.1073/PNAS.251408398

Stewart, V., & Chen, L. L. (2010). The S helix mediates signal transmission as a HAMP domain coiled-coil extension in the NarX nitrate sensor from Escherichia coli K-12. *Journal of Bacteriology*, *192*(3), 734–745. https://doi.org/10.1128/JB.00172-09

Stock, A. M., Robinson, V. L., & Goudreau, P. N. (2000). *TWO-COMPONENT SIGNAL TRANSDUCTION*.

Strelkov, S. V., & Burkhard, P. (2002). Analysis of α-helical coiled coils with the program TWISTER reveals a structural mechanism for stutter compensation. *Journal of Structural Biology*, *137*(1–2), 54–64. https://doi.org/10.1006/jsbi.2002.4454

Suskiewicz, M. J., Hajdusits, B., Beveridge, R., Heuck, A., Vu, L. D., Kurzbauer, R., Hauer, K., Thoeny, V., Rumpel, K., Mechtler, K., Meinhart, A., & Clausen, T. (2019). Structure of McsB, a protein kinase for regulated arginine phosphorylation. *Nature Chemical Biology*, *15*(5), 510–518. https://doi.org/10.1038/S41589-019-0265-Y

Szczepaniak, K., Bukala, A., Da Silva Neto, A. M., Ludwiczak, J., & Dunin-Horkawicz, S. (2021). A library of coiled-coil domains: from regular bundles to peculiar twists. *Bioinformatics (Oxford, England)*, *36*(22–23), 5368–5376. https://doi.org/10.1093/BIOINFORMATICS/BTAA1041

Taher, R., & de Rosny, E. (2021). A structure-function study of ZraP and ZraS provides new insights into the two-component system Zra. *Biochimica et Biophysica Acta. General Subjects*, *1865*(3). https://doi.org/10.1016/J.BBAGEN.2020.129810

Tetsch, L., & Jung, K. (2009). The regulatory interplay between membrane-integrated sensors and transport proteins in bacteria. *Molecular Microbiology*, *73*(6), 982–991. https://doi.org/10.1111/J.1365-2958.2009.06847.X

Thompson, J. D., Higgins, D. G., & Gibson, T. J. (1994). CLUSTAL W: improving the sensitivity of progressive multiple sequence alignment through sequence weighting, position-specific gap penalties and weight matrix choice. *Nucleic Acids Research*, *22*(22), 4673–4680. https://doi.org/10.1093/NAR/22.22.4673

Trajtenberg, F., Imelio, J. A., Machado, M. R., Larrieux, N., Marti, M. A., Obal, G., Mechaly, A. E., & Buschiazzo, A. (2016). Regulation of signaling directionality revealed by 3D snapshots of a kinase: Regulator complex in action. *ELife*, *5*(DECEMBER2016). https://doi.org/10.7554/ELIFE.21422

Tschauner, K., Hörnschemeyer, P., Müller, V. S., & Hunke, S. (2014). Dynamic Interaction between the CpxA Sensor Kinase and the Periplasmic Accessory Protein CpxP Mediates Signal Recognition in E. coli. *PLOS ONE*, *9*(9), e107383. https://doi.org/10.1371/JOURNAL.PONE.0107383

Urano, H., Umezawa, Y., Yamamoto, K., Ishihama, A., & Ogasawara, H. (2015). Cooperative regulation of the common target genes between H2O2-sensing yedvw and Cu2+-sensing cussr in Escherichia coli. *Microbiology (United Kingdom)*, *161*(4), 729–738. https://doi.org/10.1099/MIC.0.000026

Urano, H., Yoshida, M., Ogawa, A., Yamamoto, K., Ishihama, A., & Ogasawara, H. (2017). Cross-regulation between two common ancestral response regulators, HprR and CusR, in Escherichia coli. *Microbiology (United Kingdom)*, *163*(2), 243–252. https://doi.org/10.1099/MIC.0.000410

van der Weel, L., As, K. S., Dekker, W. J. C., van den Eijnden, L., van Helmond, W., Schiphorst, C., Hagen, W. R., & Hagedoorn, P. L. (2019). ZraP, the most prominent zinc protein under zinc stress conditions has no direct role in in-vivo zinc tolerance in Escherichia coli. *Journal of Inorganic Biochemistry*, *192*, 98–106. https://doi.org/10.1016/J.JINORGBIO.2018.12.013

Veevers, R., & Hayward, S. (2019). Methodological improvements for the analysis of domain movements in large biomolecular complexes. *Biophysics and Physicobiology*, *16*, 328–336. https://doi.org/10.2142/BIOPHYSICO.16.0_328

Verhamme, D. T., Arents, J. C., Postma, P. W., Crielaard, W., & Hellingwerf, K. J. (2001). Glucose-6-phosphate-dependent phosphoryl flow through the Uhp two-component regulatory system. *Microbiology*, *147*(12), 3345–3352. https://doi.org/10.1099/00221287-147-12-3345

Wahlgren, W. Y., Claesson, E., Tuure, I., Trillo-Muyo, S., Bódizs, S., Ihalainen, J. A., Takala, H., & Westenhoff, S. (2022). Structural mechanism of signal transduction in a phytochrome histidine kinase. *Nature Communications 2022 13:1*, *13*(1), 1–8. https://doi.org/10.1038/s41467-022-34893-3

Wang, C., Sang, J., Wang, J., Su, M., Downey, J. S., Wu, Q., Wang, S., Cai, Y., Xu, X., Wu, J., Senadheera, D. B., Cvitkovitch, D. G., Chen, L., Goodman, S. D., & Han, A. (2013). Mechanistic insights revealed by the crystal structure of a histidine kinase with signal transducer and sensor domains. *PLoS Biology*, *11*(2). https://doi.org/10.1371/JOURNAL.PBIO.1001493

Wanner, B. L., & Chang, B. D. (1987). The phoBR operon in Escherichia coli K-12. *Journal of Bacteriology*, *169*(12), 5569–5574. https://doi.org/10.1128/JB.169.12.5569-5574.1987

Weston, L. A., & Kadner, R. J. (1987). Identification of uhp polypeptides and evidence for their role in exogenous induction of the sugar phosphate transport system of Escherichia coli K-12. *Journal of Bacteriology*, *169*(8), 3546–3555. https://doi.org/10.1128/JB.169.8.3546-3555.1987

Wilke, K. E., Francis, S., & Carlson, E. E. (2015). Inactivation of multiple bacterial histidine kinases by targeting the ATP-binding domain. *ACS Chemical Biology*, *10*(1), 328–335. https://doi.org/10.1021/CB5008019/SUPPL_FILE/CB5008019_SI_001.PDF

Wirtz, L., Eder, M., Schipper, K., Rohrer, S., & Jung, H. (2020). Transport and kinase activities of CbrA of Pseudomonas putida KT2440. *Scientific Reports*, *10*(1), 5400. https://doi.org/10.1038/S41598-020-62337-9

Woolfson, D. N., Mortishire-Smith, R. J., & Williams, D. H. (1991). Conserved positioning of proline residues in membrane-spanning helices of ion-channel proteins. *Biochemical and Biophysical Research Communications*, *175*(3), 733–737. https://doi.org/10.1016/0006-291X(91)91627-O

Wright, J. S., Olekhnovich, I. N., Touchie, G., & Kadner, R. J. (2000). The histidine kinase domain of UhpB inhibits UhpA action at the Escherichia coli uhpT promoter. *Journal of Bacteriology*, *182*(22), 6279–6286. https://doi.org/10.1128/JB.182.22.6279-6286.2000

Wuichet, K., Cantwell, B. J., & Zhulin, I. B. (2010). Evolution and phyletic distribution of two-component signal transduction systems. *Current Opinion in Microbiology*, *13*(2), 219. https://doi.org/10.1016/J.MIB.2009.12.011

Yamamoto, K., Hirao, K., Oshima, T., Aiba, H., Utsumi, R., & Ishihama, A. (2005). Functional characterization in vitro of all two-component signal transduction systems from Escherichia coli. *The Journal of Biological Chemistry*, *280*(2), 1448–1456. https://doi.org/10.1074/JBC.M410104200

Yoshida, T., Phadtare, S., & Inouye, M. (2007). Functional and structural characterization of EnvZ, an osmosensing histidine kinase of E. coli. *Methods in Enzymology*, *423*, 184–202. https://doi.org/10.1016/S0076-6879(07)23008-3

Zhang, H., Chen, X., Nolan, L. K., Zhang, W., & Li, G. (2019). Identification of Host Adaptation Genes in Extraintestinal Pathogenic Escherichia coli during Infection in Different Hosts. *Infection and Immunity*, *87*(12), e00666-19. https://doi.org/10.1128/IAI.00666-19

Zhang, Z., & Hendrickson, W. A. (2010). Structural Characterization of the Predominant Family of Histidine Kinase Sensor Domains. *Journal of Molecular Biology*, *400*(3), 335–353. https://doi.org/10.1016/J.JMB.2010.04.049

Zhang, Z., Liu, Q., & Hendrickson, W. A. (2014). Crystal structures of apparent saccharide sensors from histidine kinase receptors prevalent in a human gut symbiont. *The FEBS Journal*, *281*(18), 4263–4279. https://doi.org/10.1111/FEBS.12904

Zhou, Y. F., Nan, B., Nan, J., Ma, Q., Panjikar, S., Liang, Y. H., Wang, Y., & Su, X. D. (2008). C4-Dicarboxylates Sensing Mechanism Revealed by the Crystal Structures of DctB Sensor Domain. *Journal of Molecular Biology*, *383*(1), 49–61. https://doi.org/10.1016/J.JMB.2008.08.010

Zhu, Y., Dou, Q., Du, L., & Wang, Y. (2023). QseB/QseC: a two-component system globally regulating bacterial behaviors. *Trends in Microbiology*, *31*(7), 749–762. https://doi.org/10.1016/J.TIM.2023.02.001/ASSET/DCB659EB-8172-4445-8A27-2ACC32465A3C/MAIN.ASSETS/GR2.JPG

Zientz, E., Bongaerts, J., & Unden, G. (1998). Fumarate regulation of gene expression in Escherichia coli by the DcuSR (dcuSR genes) two-component regulatory system. *Journal of Bacteriology*, *180*(20), 5421–5425. https://doi.org/10.1128/JB.180.20.5421-5425.1998

Zoetendal, E. G., Smith, A. H., Sundset, M. A., & Mackie, R. I. (2008). The BaeSR two-component regulatory system mediates resistance to condensed tannins in Escherichia coli. *Applied and Environmental Microbiology*, *74*(2), 535–539. https://doi.org/10.1128/AEM.02271-07/SUPPL_FILE/TABLE_S3.DOC